N.I.

PURDUE UNIVERSITY
Purdue Research Foundation
Lafayette, Indiana

Improved Fluid Dynamics Similarity, Analysis and Verification

Final Report - Part I

SIMILARITY STUDIES OF DISCHARGE OF LIQUIDS FROM CONTAINERS THROUGH ORIFICES AND TUBES

by

A. R. Mulukutla, E. R. F. Winter
R. J. Schoenhals

Purdue University — Science, Technology, Agriculture

School of Mechanical Engineering
Heat Transfer Laboratory

Improved Fluid Dynamics Similarity, Analysis and Verification

Final Report - Part I

SIMILARITY STUDIES OF DISCHARGE OF LIQUIDS FROM CONTAINERS THROUGH ORIFICES AND TUBES

by

A. R. Mulukutla, E. R. F. Winter
R. J. Schoenhals

Improved Fluid Dynamics Similarity, Analysis and Verification

Final Report-Part I

SIMILARITY STUDIES OF DISCHARGE OF LIQUID FROM CONTAINERS THROUGH ORIFICES AND TUBES

Submitted by

School of Mechanical Engineering
Purdue University
Lafayette, Indiana

to

NATIONAL AERONAUTICS AND SPACE ADMINISTRATION
George C. Marshall Space Flight Center
Applied Mechanical Research Branch
Propulsion Division
Propulsion and Vehicle Engineering Laboratory
Huntsville, Alabama

Period Covered: June 29, 1965 - June 28, 1968

Principal Investigators: E. R. F. Winter and R. J. Schoenhals

Contracting Officer's Representatives: Hugh M. Campbell
William E. Dickson
Carl G. Fritz

Contract Number: NAS 8-20222
Control Number: DCN 1-5-52-01195-01 (1F) & S1 (1F)

Authors: A. R. Mulukutla
E. R. F. Winter
R. J. Schoenhals

June 1968

ABSTRACT

A study of transient discharge of liquids from containers through orifices and tubes is described. The investigation was conducted with special attention being devoted to the development of proper scaling procedures and similarity relationships. The instantaneous dimensionless mass flow rate was obtained as a function of six other dimensionless parameters.

Analyses based on one-dimensional flow models yielded functional relationships for the dependence of the dimensionless mass flow rate (or alternately the dimensionless liquid height in the container) on the other pertinent parameters obtained from dimensional analysis. Both discharge through an orifice and through a tube were considered. Analyses based on the assumption of quasi-steady flow, and neglecting inertia effects, yielded simple mathematical solutions which were readily evaluated. However, these solutions become inaccurate as the ratio of the container cross-sectional area to the discharge area is decreased. Improved analyses, which properly account for inertia effects, yielded second order non-linear differential equations describing the dynamics of the process. Numerical solutions of these equations were obtained with a Fourth-Order Runge-Kutta method by means of digital computation. A closed form solution was also obtained for the case of transient

discharge through an orifice with a constant discharge coefficient. In reality, the discharge coefficient for discharge through an orifice and the friction factor for discharge through a tube both vary during a transient discharge process due to continuous changes in Reynolds number. However, it was found that when the Reynolds number is of the order of 1000 or larger, predictions of acceptable engineering accuracy can be easily obtained by assuming the discharge coefficient or friction factor, respectively, to be constant throughout the entire process. For the case of discharge through a tube, a closed form solution in terms of elementary functions was obtained for the situation in which the external pressure drop is much greater than the initial hydrostatic head in the container. Limits of validity for the various analyses were determined.

Finally, experiments were conducted in ranges where the inertia effects were significant using two different entrance geometries for the discharge tube entrance (rounded and sharp-edged entrance). A closed circuit Stop-Action TV system was used for recording and read-out of experimental data. The resulting measurements were evaluated in terms of the similarity parameters obtained from dimensional analysis, and were also compared with the analytical predictions.

These evaluations and comparisons establish the validity of the scaling procedures developed and substantiate the ranges of accuracy for the various simplified analytical models. The techniques used and the resulting similarity relationships obtained can be applied to liquid fuel rocket technology and in other areas where rapid discharge of liquids is encountered.

TABLE OF CONTENTS

LIST OF TABLES

LIST OF FIGURES

Figure | Page

Figure | Page

NOMENCLATURE

A	Cross-sectional Area of Container
a	Cross-sectional Area of Discharge Tube
$B(p,q)$	Beta Function
$B_x(p,q)$	Incomplete Beta Function
C_c	Contraction Coefficient
C_D	Discharge Coefficient
C_D	Drag Coefficient (in Chapter 2 only)
C_v	Velocity Coefficient
C_1, C_2, C_3	Coefficients in a Differential Equation (Defined in equation (C5d))
D	Diameter of Container
d	Diameter of Discharge tube
F	Function
F_f	Frictional Force
f	Darcy-Weisbach Friction Factor
G	Function
g	Effective Gravitational Acceleration
H	Initial Height of Liquid in Container
$I_x(p,q)$	$\frac{B_x(p,q)}{B(p,q)}$
K	Entrance Loss Coefficient
L	Length of Discharge Tube
L	Characteristic Length of Ship (in Chapter 2 only)

$\dot{m}$	Mass Flow Rate
$\dot{m}^*$	Dimensionless Mass Flow Rate, $\dfrac{\dot{m}}{\rho\left(\frac{\pi D^2}{4}\right)\frac{1}{\beta}\sqrt{2gH}}$
N	Coefficient in a Differential Equation (Defined in equation (6.14b))
P_1	Pressure at the Top of Liquid in Container
P_1'	Pressure at the Entrance to the Tube
P_2	Discharge Pressure
ΔP	External Pressure Drop (P_1-P_2)
p	Argument of Beta and Incomplete Beta Functions
Q	Coefficient in a Differential Equation (Defined in equation (6.14b))
q	Argument of Beta and Incomplete Beta Functions
R	Coefficient in a Differential Equation (Defined in equation (6.14b))
Re	Reynolds number
r	Radius of Rounding for Tube Entrance, $\frac{d}{4}$ (Figure 7.5)
s	A Dummy Variable
t	Time Elapsed After Initiation of Discharge
t^*	Dimensionless Time, $\dfrac{t}{\beta\sqrt{\frac{2H}{g}}}$
t_t	Total Discharge Time
t_t^*	Dimensionless Total Discharge Time
u	$y^{*(\alpha-1)}$
V	Velocity of Ship (in Chapter 2 only)
V_1	Velocity of Liquid in Container
V_2	Velocity of Liquid Discharge
x	Limit of Integral in Incomplete Beta Function
y	Liquid Height in Container

y^*	Dimensionless Liquid Height, $\frac{y}{H}$
$\dot{y}^*$	$\frac{dy^*}{dt^*}$
α	β^2
β	$\sqrt{(\frac{A}{a})^2 - 1}$
Γ	Gamma Function
ζ	$(\frac{dy^*}{dt^*})^2$
θ	Angle of Inclination of Discharge Tube
μ	Viscosity of Liquid
ν	Kinematic Viscosity of Liquid
π_n	Dimensionless Ratios ($n = 1, 2 \ldots 7$)
π_n'	Modified Dimensionless Ratios
ρ	Density of Liquid
τ	Wall Shear Stress
ψ	Fineness Coefficient

CHAPTER 1

INTRODUCTION

The advent of the space age has accentuated the need for larger and more powerful rockets. As the thrust developed by a liquid propellant rocket is increased, the supply mass flow rates of the fuel (e.g. LH_2 or RP1) and oxidizer (e.g. LOX) have to be increased. Since full scale testing of such large liquid fuel and oxidizer supply systems is expensive and time consuming, it is desirable to ascertain the performance of a large system in advance of its construction. In order to evaluate the soundness of a particular design, it is appropriate to test scaled down laboratory models. It is most desirable to express the results in terms of appropriate dimensionless parameters so that they are independent of the size of the system considered as well as the particular fluid tested. The present investigation was undertaken to examine the possibility of scale model testing (from a fluid dynamic viewpoint) of such systems.

In order to duplicate the behavior of a large system with a corresponding smaller laboratory model, it is required that complete similarity be achieved. This can sometimes be accomplished if fairly simple processes are involved. However, the task of attaining complete similarity becomes increasingly difficult for complex systems (see Figure 1.1) in which a number of physical phenomena all occur simultaneously and interact with each other. In the case of liquid propellant systems, heat is sometimes transferred which can stratify the liquid and cause

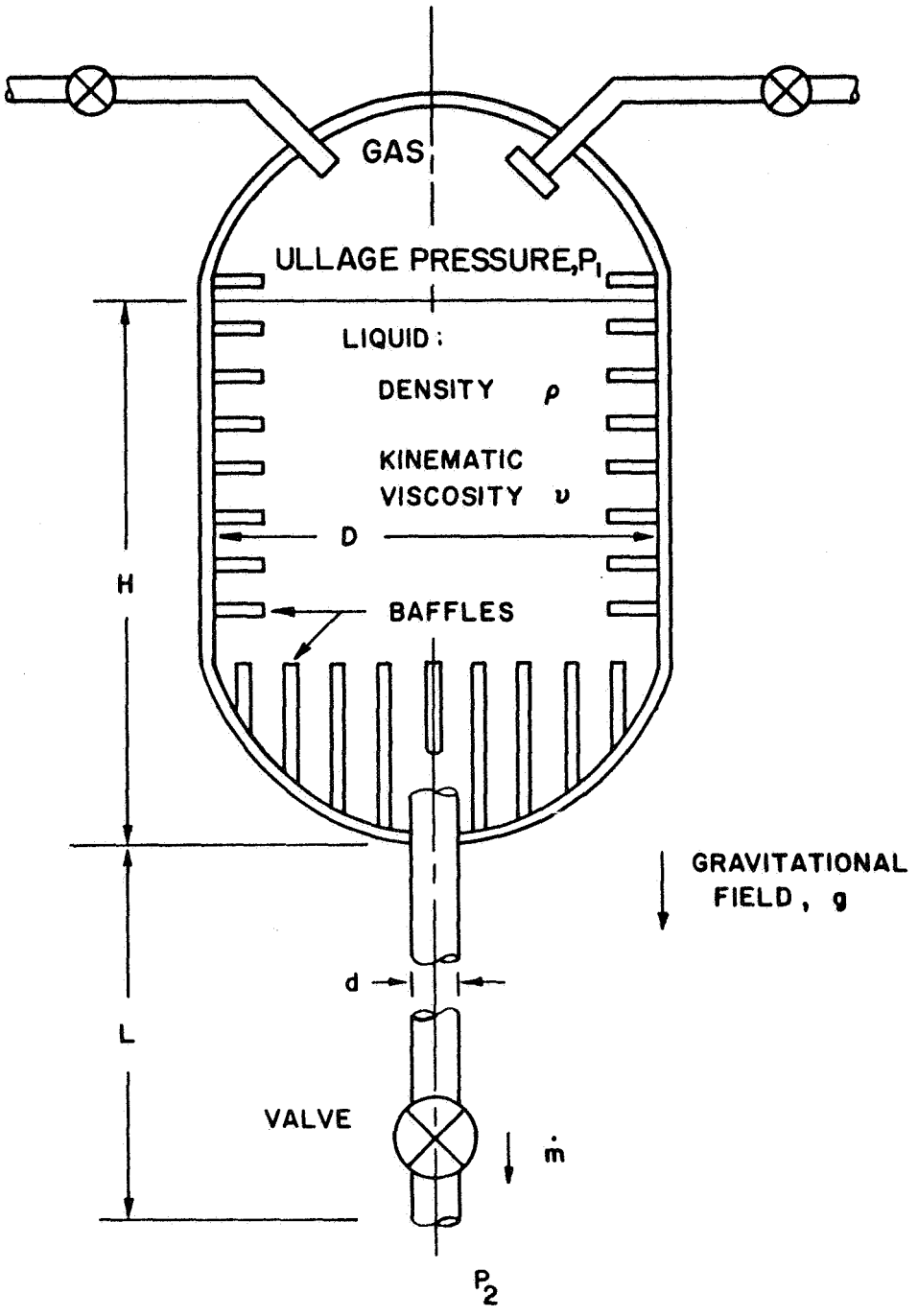

Figure 1.1. Illustration of a Typical Liquid Discharge System in a Liquid Propellant Rocket

evaporation at the gas-liquid interface. This evaporation, in turn, can effect the ullage pressure (pressure above the liquid surface) in the container. If the pressure in the supply line falls below the saturation vapor pressure, cavitation can occur resulting in two-phase flow. It is very difficult to simulate all these effects, simultaneously, in the testing of a scale model. Thus for complex situations, where exact simulation may not be attainable, it is frequently desirable that the phenomena be separated and studied individually. This not only allows an intensive study of a particular aspect but also facilitates a systematic procedure for obtaining large numbers of experimental measurements rapidly and easily. Here it is important to ascertain the limitations of the laboratory simulation and to formulate a laboratory program which minimizes these limitations as much as possible. It should be emphasized that laboratory scale model testing, however exhaustive it may be, is only a precursor to the testing of a prototype. Full scale testing can bring out certain unexpected features of operational behavior. If it does, then further study may be required to establish confidence in the existing system or to determine the necessary changes which will eliminate any of these features which are found undesirable.

This investigation was conducted with a view toward the various practical aspects of liquid propellant supply systems as described above. In order to facilitate the analytical and experimental portions of the research, and simultaneously focus attention on the important physical effects involved, a simplified configuration (Figure 1.2) was chosen for detailed study. Further, only single-phase constant density flow was treated with heat transfer and cavitation phenomena being omitted from consideration. The work reported here comprised an engineering study of

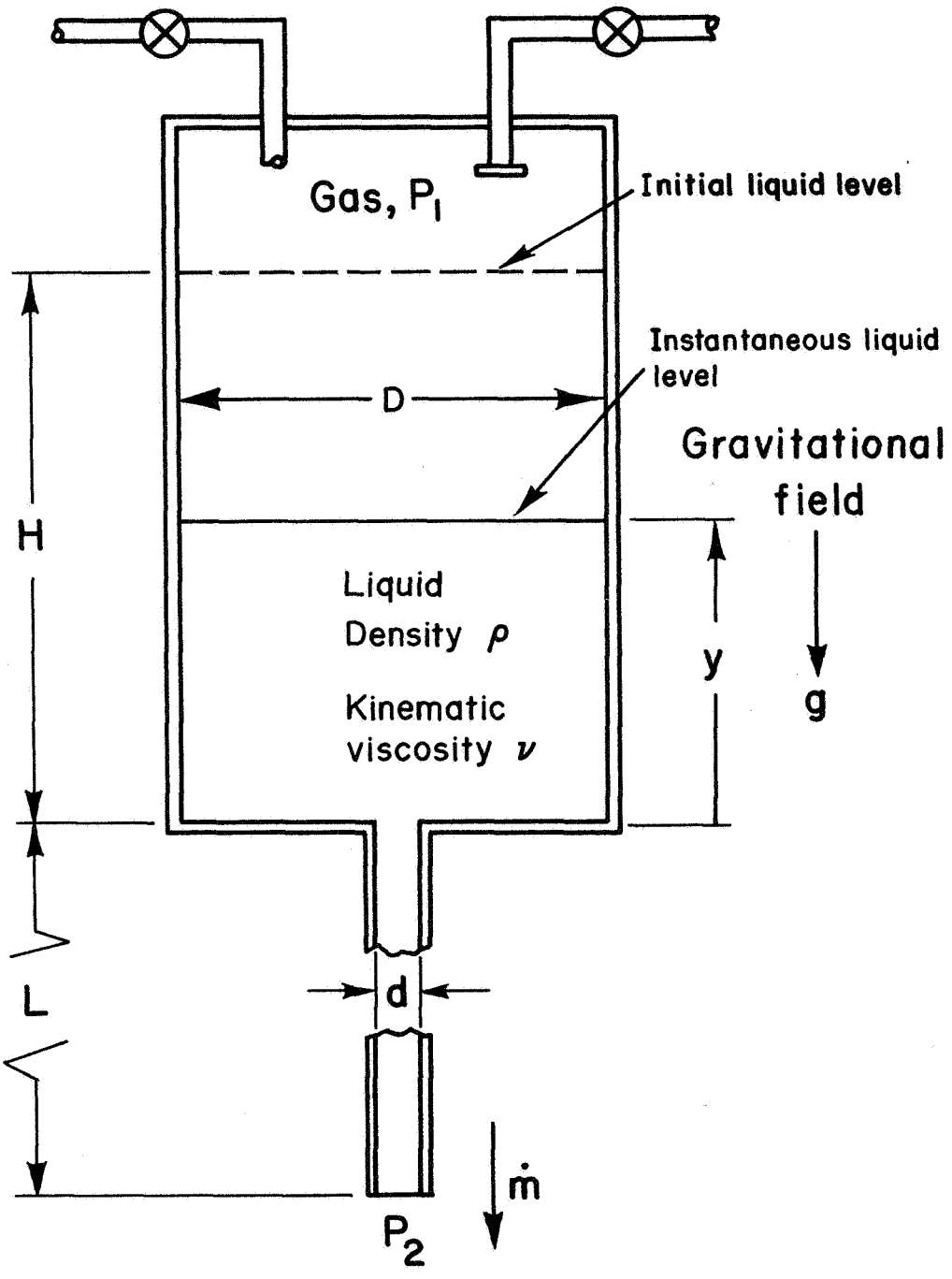

Figure 1.2. Simplified Geometry Used for Analytical and Experimental Studies

transient flow during discharge of a liquid which is initially at rest in a container. The problem is of interest not only in rocketry, but also in many other areas of technology. One example is associated with the rapid transfer of liquids in automated food processing operations having very high production rates. Other examples have to do with liquid transfer in large water supply systems, pumping of petroleum from tankers and rapid movement of water in the case of fire fighting equipment. In most of these situations the pressure above the liquid surface in the supply container is increased in order to increase the mass flow rate. Structural and weight considerations set practical limits on the range of available ullage pressures in the container, however. Another method of increasing the mass flow rate is to increase the cross-sectional area of the discharge stream in relation to that of the container. It is known that a decrease in the ratio of container cross-sectional area to discharge area does not increase the mass flow rate proportionately. Below some value of this ratio local inertia effects play an important part in the transient discharge process and the results obtained from analyses based on quasi-steady flow tend to be erroneous. For this reason considerable attention was directed toward such transient flows in the present investigation, and toward establishing limits of validity for the various types of analyses.

It is clear that the modeling procedures outlined previously (Figure 1.1) can be carried out effectively in general only if the dimensionless similarity parameters have been obtained and if the relationships between them have been roughly established, perhaps by means of approximate analytical techniques or from previously obtained experimental measurements. The second point is very important if exact similarity cannot be achieved.

In this case attempts should be made to maintain similarity with respect to the parameters which are dominant, and should be sacrificed only with respect to those parameters which are known to have a minor effect within the range of operation considered. In order to effect some progress toward these broad and general objectives, the procedure outlined below was followed in treating the system shown in Figure 1.2.

(a) The dimensionless similarity parameters were obtained by means of dimensional analysis.

(b) The physical effects pertaining to the problem of gravity and pressure driven discharge of liquids were studied.

(c) Analytical results, based on approximate physical models, were derived and solutions were expressed in terms of the similarity parameters obtained. Since the bulk average mass flow rate is of primary interest, the analytical models were based on one-dimensional flow because they were the simplest from a mathematical viewpoint and because experiments showed that they yield results of acceptable engineering accuracy. A consideration of transient discharge through an orifice provided the range in which the inertial effects in the container become predominant. Thus both discharge through an orifice and through a tube were considered.

(d) Finally, experimental measurements were made in order to verify the significance and importance of the similarity parameters obtained, and to establish the validity and limitations associated with the approximate analytical solutions. Since the results should be independent of the working liquid when expressed in dimensionless form, water was used in experiments

since it was inexpensive, readily available, and safe and easy to handle.

The details of each of the above sub-studies are contained in the chapters that follow.

The results of the investigation are expected to be useful for:

1. obtaining a better understanding of the dimensionless similarity parameters associated with some of the fluid dynamics phenomena occurring in single-phase liquid discharge systems;
2. providing relationships for the dependence of mass flow rate on various other parameters, at least approximately;
3. developing experimental techniques for laboratory scale model testing;
4. and suggesting improved techniques that may facilitate future similarity investigations in related fields.

Before proceeding with the presentation of details of this study a brief Survey of Literature, related to this research, is given in the following Chapter.

CHAPTER 2

SURVEY OF LITERATURE

The performance of a liquid fuel rocket depends, among other things, on the rate of supply of fuel and oxidizer to the rocket engine. Scaling of rocket engines has been discussed by Penner (Ref. 1), who indicated that scaling of chemical reactors with complete similarity is not possible. For liquid fuel rocket engines, scaling with loss of geometric and dynamic similarity was considered. For small scale units, Penner's analysis suggests a reasonable approach to the interpretation of experimental data. It was concluded that once the relationship between the various parameters has been established from a large number of experiments, rational scaling to larger units should be possible. The present investigation is mainly limited to a consideration of the supply rates of fuel or oxidizer to the engine.

The discharge of containers through orifices and pipes has been studied for many years by hydraulic engineers (Ref. 2), whose main aim was the design of water supply systems. Pure gravity discharge is encountered in such designs and Bernoulli's Equation, with empirical corrections for the viscous and geometric effects, yields reasonably accurate results for the times and rates of discharge (Ref. 3, 4). Many of the modeling techniques developed by hydraulic engineers were concerned with river dams, spillways, open channel flows, etc., and little attention has been paid to the problem of rapid discharge of containers (Ref. 5).

One of the most powerful methods for dealing with such problems is dimensional analysis. This technique yields the similarity parameters involved, through an application of Buckingham's π-Theorem (Ref. 6), in that it groups the pertinent variables into appropriate dimensionless parameters. Sometimes it may appear (from dimensional analysis alone) that conflicting requirements must be satisfied for scaling from which it may be prematurely concluded that no scaling is possible at all. For example, in ship motion (Ref. 7), for geometrically similar hull shapes the dimensionless drag coefficient (C_D) is a function of fineness coefficient (ψ), Froude number ($\frac{V^2}{gL}$) and Reynolds number ($\frac{\rho VL}{\mu}$). This implies that for C_D to be same for two geometrically similar hull shapes, ψ, Froude number and Reynolds number must be the same. To keep $\frac{V^2}{gL}$ constant, the velocity must decrease with a decrease in model size, whereas to keep $\frac{\rho VL}{\mu}$ the same V must increase with decreasing model size, if the same fluid is used. However, the practical possibility of scaling tests for ship hulls stems from the fact that the drag can be separated into two parts, one depending on the Reynolds number and the other on the fineness coefficient and the Froude number. Thus, even though complete similarity is not achieved in its entirety, it is possible in this case to break the problem into two parts and to maintain similarity in each of these two parts.

There is another problem. Sometimes it is very difficult to match one of the non-dimensional parameters. A case in point involves the Reynolds number in wind tunnel testing of aircraft models (Ref. 8, 9). In such instances, the models are tested at a Reynolds number which is different from the full scale one, and the results are extrapolated using some known behavior. Thus it can be seen, that though dimensional analysis gives the dimensionless parameters involved, it does not give the

form of dependence among these parameters. Neither can it predict which of the parameters are significant and which of them can be neglected. Hence, dimensional analysis should be supplemented by experiment, experience, and mathematical analysis wherever possible, to make scale model testing feasible and meaningful.

Flanigan and Putnam (Ref. 10) discuss the principles of similitude in fluid flow and classify modeling programs into four general categories as

(a) diagnostic

(b) predictive

(c) developmental

(d) basic

As was suggested in their paper, the application of modeling to practical problems usually involves more than one category. The problem of scaling and testing distorted models for valid scale model work was discussed by Ezra (Ref. 11). Various methods for distinguishing the independent and dependent similarity parameters and finding the relationships between them were suggested. Methods for scale model work, even when one or more independent parameters cannot be scaled and when there is no knowledge of mathematical relationships between the independent and dependent variables, were given by Ezra. In short, the problem treated in this report involves a twofold attempt to:

(i) match the relevant non-dimensional parameters for scaled down and full scale rocket propellant containers so that the non-dimensional mass flow coefficient remains the same, and

(ii) determine its variation with each of the other dimensionless parameters.

The problem at hand is that of modeling the discharge of a liquid. In the most general terms, two-phase flow of a stratified liquid, with cavitation and heat transfer, through multiple outlets from a single tank can occur. In addition, the effective gravitational field may vary in general. The processes involved are very complicated, with numerous effects to be taken into account. For instance, the investigations of Roudebush and Mandell (Ref. 12) and Nein and Thompson (Ref. 13) clearly indicate the complicated nature of an apparently simple problem of pressurizing a tank containing a cryogenic liquid. Clark (Ref. 14) has reviewed the literature regarding the various problems (pressurization, stratification, and interfacial phenomena) involved with large rocket propellant tank systems. Fischer (Ref. 15) presented the conditions for similarity for two-phase flows with simultaneous heat transfer. He concludes that for two two-phase flows to be similar not only the characteristic Reynolds, Euler and Froude numbers for the individual phases must be the same in the two flows, but also the density and the dynamic viscosity ratios for the two phases in both flows must be the same.

Many problems connected with single phase discharge through orifices and flow through tubes have been studied. For instance, Rouse and Abul-Fetouh (Ref. 16) have calculated pressure distributions for irrotational flow through circular orifices. Saad and Oliver (Ref. 17) and Lubin and Springer (Ref. 18) carried out theoretical and experimental investigations for discharge of a container through an orifice. The flow in the entrance region ('calming length') of a tube was studied theoretically by Schiller for laminar flow (Ref. 19) and by Latzko for turbulent flow (Ref. 20). Nikuradse and Kirsten have given experimental results for these problems (reported in Ref. 21). Szymansky (Ref. 22) studied the flow establishment

in an infinitely long pipe subjected to a sudden pressure gradient. The results of these investigations (References 16 through 22) are discussed in some detail in Chapter 4, where the one-dimensionality of flow through orifices and tubes is examined.

Recent textbooks on fluid mechanics (Refs. 4 and 23), however, have discussed the problem of unsteady discharge of a container through an orifice. There the unsteady flow equation is simplified for final integration (to obtain the total efflux time), with the assumption that the discharge area is small in comparison with the container area, thereby excluding the effects of local acceleration. Bird, Stewart and Lightfoot (Ref. 24) give the correction for the total efflux time, necessary in case of constant cross-section vertical tanks with large discharge openings (in comparison with that of the tank) in the form of a definite integral. Winter and Schoenhals (Ref. 25 and 26) have reported a numerical solution of the unsteady energy equation, for the case of discharge through an orifice. Sestak, Jezek and Jirsak (Ref. 27) at about the time this work was being completed gave an analytical solution to the same problem. These are discussed in later sections of the report.

In summary, it can be said that although there have been numerous investigations with regard to individual phenomena, further attention is needed with respect to the modeling of rapid discharge of a liquid from a container, taking inertia effects into account. This is the aim of the present investigation the results of which are reported in the following chapters of this report.

CHAPTER 3

DIMENSIONAL ANALYSIS

In this chapter dimensional analysis results are given along with a discussion of the relative importance of various dimensionless parameters in different situations. The details of the method of obtaining the dimensionless parameters are presented in Appendix A.

The system illustrated in Figure 1.2 is considered. For this system, both the discharge rate, $\dot{m}$, and the instantaneous liquid height, y, will be discussed. In the experimental portion of the investigation it was found that the height of the liquid could be measured more conveniently than the mass flow rate. It can be noted that $(-\frac{dy}{dt})$ corresponds to the velocity of liquid in the container and thus the mass flow rate is given by $\rho A(-\frac{dy}{dt})$, where A is the cross-sectional area of the container.

The instantaneous liquid height, y, and the mass flow rate, $\dot{m}$, during the transient discharge process should in general be dependent on the variables listed below:

SYMBOL	VARIABLE	DIMENSIONS
t	time elapsed from initiation of discharge	T
Physical Dimensions of the System		
D	container diameter	L
d	diameter of discharge tube	L
L	discharge tube length	L

H	initial height of the liquid in container	L
Imposed Forces		
ΔP	external pressure drop, $(P_1 - P_2)$	$ML^{-1}T^{-2}$
g	effective gravitational acceleration	LT^{-2}
Fluid Properties		
ρ	density of liquid	ML^{-3}
ν	kinematic viscosity of liquid	L^2T^{-1}

The instantaneous liquid height, y, and the instantaneous mass flow rate, $\dot{m}$, are given by

$$y = y\ (t,\ D,\ d,\ L,\ H,\ \Delta P,\ g,\ \rho,\ \nu) \tag{3.1a}$$

$$\dot{m} = \dot{m}\ (t,\ D,\ d,\ L,\ H,\ \Delta P,\ g,\ \rho,\ \nu) \tag{3.1b}$$

Use of Buckingham's π-Theorem (Ref. 6) and the repeated variable technique (Ref. 28) results in the following dimensionless parameters (See Appendix A)[1]:

$\frac{y}{H}$ dimensionless liquid height

$\frac{\dot{m}}{\rho\ (\frac{\pi D^2}{4})\ \frac{1}{\beta}\ \sqrt{2gH}}$ dimensionless mass flow rate

[1]The numerical constants in the various ratios and the geometric parameter β, defined by $\beta^2 = (A/a)^2 - 1$ and appearing in the dimensionless time and dimensionless mass flow rate, were introduced only for convenience in interpretation.

$\frac{t}{\beta\sqrt{\frac{2H}{g}}}$ dimensionless time

$\frac{D}{d}$ ratio of diameters

$\frac{L}{d}$ discharge tube length to diameter ratio

$\frac{L}{H}$ ratio of tube length to initial liquid height in container

$\frac{\Delta P/\rho g}{H}$ ratio of pressure head to initial liquid head in container

$\frac{d\sqrt{2gH}}{\nu}$ characteristic Reynolds number for flow through discharge tube.

Use of these parameters makes it possible to relate the dimensionless liquid height and the dimensionless mass flow rate respectively by

$$\frac{y}{H} = F\left(\frac{t}{\beta\sqrt{\frac{2H}{g}}}, \frac{\Delta P/\rho g}{H}, \frac{d\sqrt{2gH}}{\nu}, \frac{L}{H}, \frac{D}{d}, \frac{L}{d}\right) \tag{3.2a}$$

$$\frac{\dot{m}}{\rho\left(\frac{\pi D^2}{4}\right)\frac{1}{\beta}\sqrt{2gH}} = G\left(\frac{t}{\beta\sqrt{\frac{2H}{g}}}, \frac{\Delta P/\rho g}{H}, \frac{d\sqrt{2gH}}{\nu}, \frac{L}{H}, \frac{D}{d}, \frac{L}{d}\right) \tag{3.2b}$$

Equations (3.2a) and (3.2b) indicate that, for a system of arbitrary geometry, the dimensionless liquid height and the dimensionless mass flow rate are in general dependent on six dimensionless parameters. The exact nature or form of dependence cannot be assessed from dimensional analysis alone.

For a set of geometrically similar systems, only a single characteristic dimension is required to specify the size of a particular system. If geometric similarity is maintained, the ratios $\frac{D}{d}$, and $\frac{L}{d}$ are constants and they cease to be variable parameters. Hence, if any one of the three lengths D, d, or L is fixed, the other two are automatically determined. Thus, for geometrically similar systems equations (3.2a) and (3.2b) reduce to

$$\frac{y}{H} = F\left(\frac{t}{\beta\sqrt{\frac{2H}{g}}}, \frac{\Delta P/\rho g}{H}, \frac{d\sqrt{2gH}}{\nu}, \frac{L}{H}\right) \tag{3.3a}$$

$$\frac{\dot{m}}{\rho\left(\frac{\pi D^2}{4}\right)\frac{1}{\beta}\sqrt{2gH}} = G\left(\frac{t}{\beta\sqrt{\frac{2H}{g}}}, \frac{\Delta P/\rho g}{H}, \frac{d\sqrt{2gH}}{\nu}, \frac{L}{H}\right) \tag{3.3b}$$

Additionally, if the liquid geometry in the container is the same at the start of the discharge process, the ratio $\frac{L}{H}$ also is a constant. Thus, for all systems having similar initial geometry for both the container and the liquid, equations (3.3a) and (3.3b) further simplify to

$$\frac{y}{H} = F\left(\frac{t}{\beta\sqrt{\frac{2H}{g}}}, \frac{\Delta P/\rho g}{H}, \frac{d\sqrt{2gH}}{\nu}\right) \tag{3.4a}$$

$$\frac{\dot{m}}{\rho\left(\frac{\pi D^2}{4}\right)\frac{1}{\beta}\sqrt{2gH}} = G\left(\frac{t}{\beta\sqrt{\frac{2H}{g}}}, \frac{\Delta P/\rho g}{H}, \frac{d\sqrt{2gH}}{\nu}\right) \tag{3.4b}$$

It should be noted that the results given in equations (3.3a), (3.3b), (3.4a) and (3.4b) are quite general. They would apply even for the complicated configuration shown in Figure 1.1, if similarity is maintained

with respect to the baffle geometry and valve setting, so long as the flow is single-phase and heat transfer and surface tension effects are not important.

As mentioned previously, this is all the information that can be obtained from dimensional analysis. The proper forms for the functions F and G have to be obtained by considering the physics and mathematics of the problem. It is the endeavour of the next few chapters to consider these and establish the relationship between the dimensionless liquid height (alternately the dimensionless mass flow rate) and the dimensionless time, and to investigate its dependence on the various other parameters indicated above.

CHAPTER 4

PHYSICAL DESCRIPTION OF TRANSIENT LIQUID DISCHARGE

The physical effects pertaining to the problem of gravity and pressure driven discharge of liquids from containers are described in this chapter to facilitate an overall understanding of the process. Figure 1.2 illustrates the system studied. Forces act on the liquid to produce acceleration during the discharge process. The various kinds of forces, and the corresponding two types of acceleration that result from the action of these forces, are indicated in the following table.

Table 4.1: Physical Effects

Forces		Acceleration
Boundary Forces		
Gravity Forces	Produce →	Convective Acceleration
Forces due to External Pressure Drop	Produce →	Local Acceleration
Viscous Forces		

The boundary forces (forces perpendicular to the walls) are sufficient to prevent the liquid from moving normal to the boundaries, the structure being considered rigid. The downward gravity force and the external pressure drop (from top to the bottom of the fluid column) contribute to downward acceleration of the liquid, while viscous forces

impede this acceleration. Convective acceleration is associated with the change in velocity of a fluid particle as it travels from a region of one velocity into a region having a different velocity. Thus, convective acceleration can be produced even if the flow is steady. Local acceleration of the fluid is associated with the time varying, or transient, condition of the flow. This acceleration component, at any point in the system, is equal to the time rate of change of velocity at that point. The two acceleration contributions, when added together at a particular point in the system, give the actual acceleration of the fluid particle passing through that point at a specific instant of time. In each of the analyses which are presented in later sections of the report the physical effects accounted for are indicated, and errors produced by omitting certain physical effects are evaluated.

In the analytical treatment of the problem the flow was assumed to be one-dimensional. This assumption can be justified on the basis of theoretical and experimental results obtained by previous investigators. Rouse and Abul-Fetouh (Ref. 16) conclude that for steady irrotational flow through an axially symmetric orifice, changes in velocity and pressure due to convective acceleration are confined to a region of about 1 diameter (of the orifice) upstream and downstream of the orifice in the limiting case of very small values of $\frac{d}{D}$. This region of influence decreases with increasing values of $\frac{d}{D}$. Further, the pressure distribution across the cross-section of the orifice itself is nearly uniform. Saad and Oliver (Ref. 17) found that draining of a tank through an orifice produces oscillations of the free surface. Experimentally, they observed that drainage generated a damped oscillation when $\frac{H}{D} = 0.125$. When $\frac{H}{D} > 0.25$ the oscillatory amplitude was too small to be experimentally

detected even with high speed photography, which was in conformity with their theory. Experimental results of Lubin and Springer (Ref. 18) indicate that a dip in the surface does not begin to form until $\frac{y}{d} \approx 0.5$. These results indicate that the flow in the container is one-dimensional except for a limited region near the orifice and it remains so until the liquid height in the container is of the order of the diameter of the orifice. The two dimensional aspects of the flow were not investigated in the present study.

If the junction between the container and the discharge tube attached to it is smoothly rounded, the velocity at the entrance to the tube is nearly uniform (Ref. 4). The flow development in the entrance region of a tube, when the velocity at the entrance itself is uniform, has been investigated by many researchers. For steady laminar flow Schiller (Ref. 19) approximated the actual velocity variation with an assumed slug flow, constant velocity profile near the center of the pipe and with two tangent portions of a parabola near the wall. The analytical results predicted the entrance length to be 57.5d at a Reynolds number of 2000. This is the point where the two parabolas coalesce and the central core of uniform flow vanishes. Nikuradse's experiments (Ref. 21) indicate a smaller entrance length of 20d. But at about 10d from the entrance the ratio of local velocity (at any radial location) to the mean velocity varies from 1.45 at the center of the pipe to 1.0 at a distance of 0.1d from the wall (see Figure 13 in Ref. 21). For turbulent flow Latzko (Ref. 20) obtained the entrance length to be 10d at a Reynolds number of 10^4. However, this length is too short according to the experiments by Kirsten (Ref. 21) and by Nikuradse (Ref. 21) who found the entrance length to be greater than 50d and 25d respectively. The entrance length appears to be a very weak function of the Reynolds number for

turbulent flow. The velocity profiles obtained by Nikuradse (see Figure 25 in Ref. 21) indicate that at 12.5d from the entrance the ratio of local to mean velocity varies only between 1.15 at the center of the pipe and 0.9 at a distance of 0.05d from the wall. The preceeding results all apply only to a steady flow through the tube.

Szymanski (Ref. 22) studied the unsteady situation, i.e. flow establishment in an infinitely long pipe subjected to a sudden pressure gradient at time t = 0. The laminar flow profile does not achieve its fully developed parabolic shape until a time $t \approx 0.125\ d^2/\nu$. In terms of the dimensionless parameters obtained in Chapter 3 this yields $t^* = 2.5$ when $\beta = 10$, $\frac{L}{d} = 5$, $\frac{L}{H} = 1$ and $\frac{d\sqrt{2gH}}{\nu} = 2000$. In the laminar flow regime the ratio of instantaneous local velocity to the final steady state center line velocity varies from 0 to 0.2 at $t^* = 0.25$ (for values of the other parameters given above), the velocity profile being flat over most of the tube during the transient acceleration period. If the same analysis were assumed to hold for larger Reynolds numbers t^* would be about 10 when $\frac{d\sqrt{2gH}}{\nu} = 10^5$. This would not be expected to be accurate for turbulent flow, but this result is cited here to indicate a probable order of magnitude for the turbulent flow situation. These times are considerably longer than the times required for complete discharge of a container through a tube with the previously mentioned geometry ($t^* \approx 0.5$). Therefore, it can be seen that the assumption of one-dimensional flow is reasonable for transient discharge of a container through an orifice or through a tube (when $1 < \frac{L}{d} \leq 10$ for the tube) for the purpose of calculating the flux and time rate of change of momentum and energy respectively. However, when the entrance to the discharge tube is sharp-edged, there is a flow separation and reattachment in the entrance region.

This destroys the one-dimensionality of the flow. Even so, the analyses may be taken to be valid by introducing a loss in head, as is done in classical studies.

Reiterating, the problem studied is that of modeling single-phase discharge of a liquid which is initially at rest in a container. The instantaneous mass flow rate during the transient discharge process and its dependence on the geometry of the system, pressure drop, effective gravitational field and properties of the fluid are of primary interest. Particular attention is devoted to the inertial effects associated with increasing the ratio of cross-sectional area of discharge to that of the container.

In the following chapters various analyses are carried out which vary in complexity, in the geometry associated with the system being studied, and in the physical effects which are accounted for. The liquid is considered to be incompressible for all of the cases studied. For each situation the simplest possible analysis is carried out first and the additional complexities are subsequently added so that the relative magnitude of each physical effect can be illustrated for various operating ranges.

CHAPTER 5

LIQUID DISCHARGE THROUGH AN ORIFICE

Quasi-Steady Flow in the Absence of Viscous Effects for Zero Pressure Drop

Consider the system shown in Figure 5.1 which represents a special case of that shown in Figure 1.2, that is, the case of $\frac{L}{d} = 0$. For the initial study of this system the pressure drop, $(P_1 - P_2)$, is omitted, while viscous and local acceleration effects are neglected. This is the simplest possible situation for discharge of a liquid from a container and is presented here to illustrate how the dimensionless liquid height, mass flow rate and time (given in Chapter 3) arise naturally. The physical effects accounted for are indicated below.

Table 5.1: Physical Effects

Forces		Fluid Acceleration	
[x]	Boundary Forces	[ ]	Local Acceleration
[x]	Gravity Forces		
[ ]	Forces due to External Pressure Drop	[x]	Convective Acceleration
[ ]	Viscous Forces		

The analysis associated with the above conditions is based on a one-dimensional model and assumes a quasi-steady type flow (since local

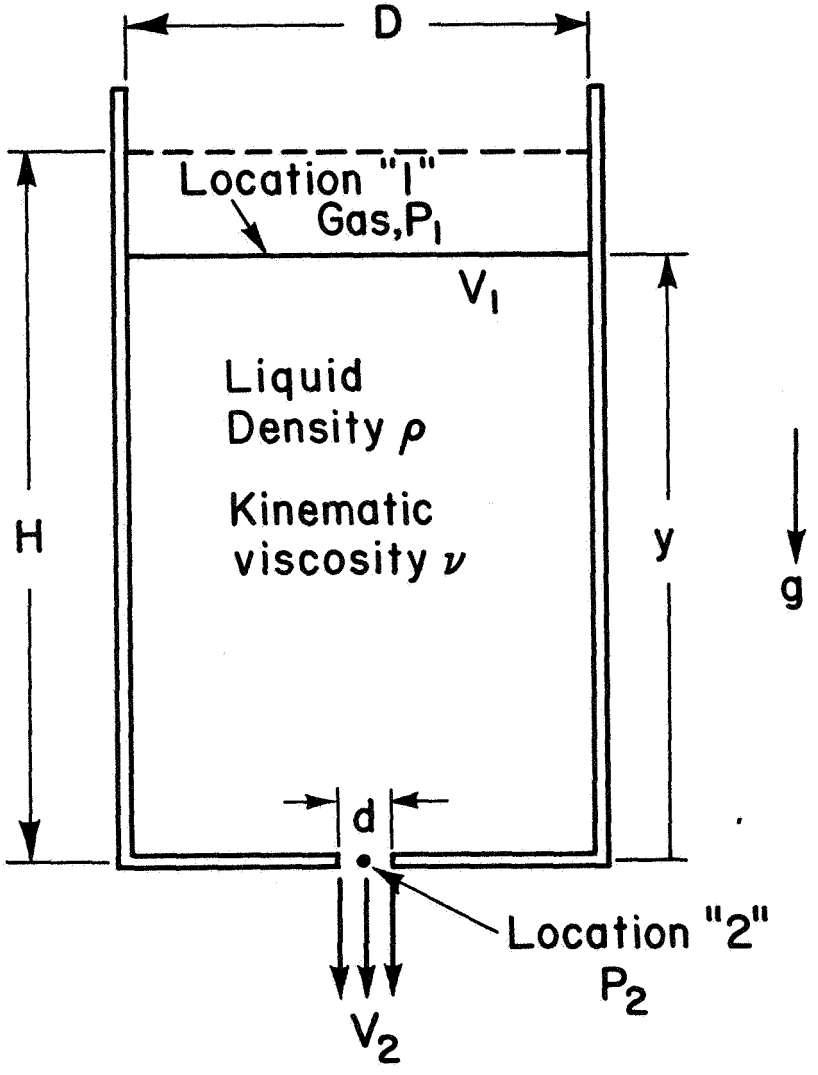

Figure 5.1. Geometry and Coordinate System for Analysis of Liquid Discharge Through an Orifice

acceleration is neglected). The details of the analysis are given in Appendix B. The results, which yield the dimensionless liquid height and dimensionless mass flow rate as functions of dimensionless time, are

$$\frac{y}{H} = \left[1 - \frac{t}{\beta\sqrt{\frac{2H}{g}}}\right]^2 \tag{5.1}$$

and

$$\frac{\dot{m}}{\rho\left(\frac{\pi D^2}{4}\right)\frac{1}{\beta}\sqrt{2gH}} = \left[1 - \frac{t}{\beta\sqrt{\frac{2H}{g}}}\right] \tag{5.2}$$

New variables t^*, y^* and m^* are defined as

$$t^* = \frac{t}{\beta\sqrt{\frac{2H}{g}}}$$

$$y^* = \frac{y}{H} \tag{5.3}$$

and

$$\dot{m}^* = \frac{\dot{m}}{\rho\left(\frac{\pi D^2}{4}\right)\frac{1}{\beta}\sqrt{2gH}} = -\frac{1}{2}\frac{dy^*}{dt^*}$$

These are substituted into equations (5.1) and (5.2) which then reduce to simple forms. Thus,

$$y^* = (1 - t^*)^2 \tag{5.4}$$

and

$$\dot{m}^* = (1 - t^*) \tag{5.5}$$

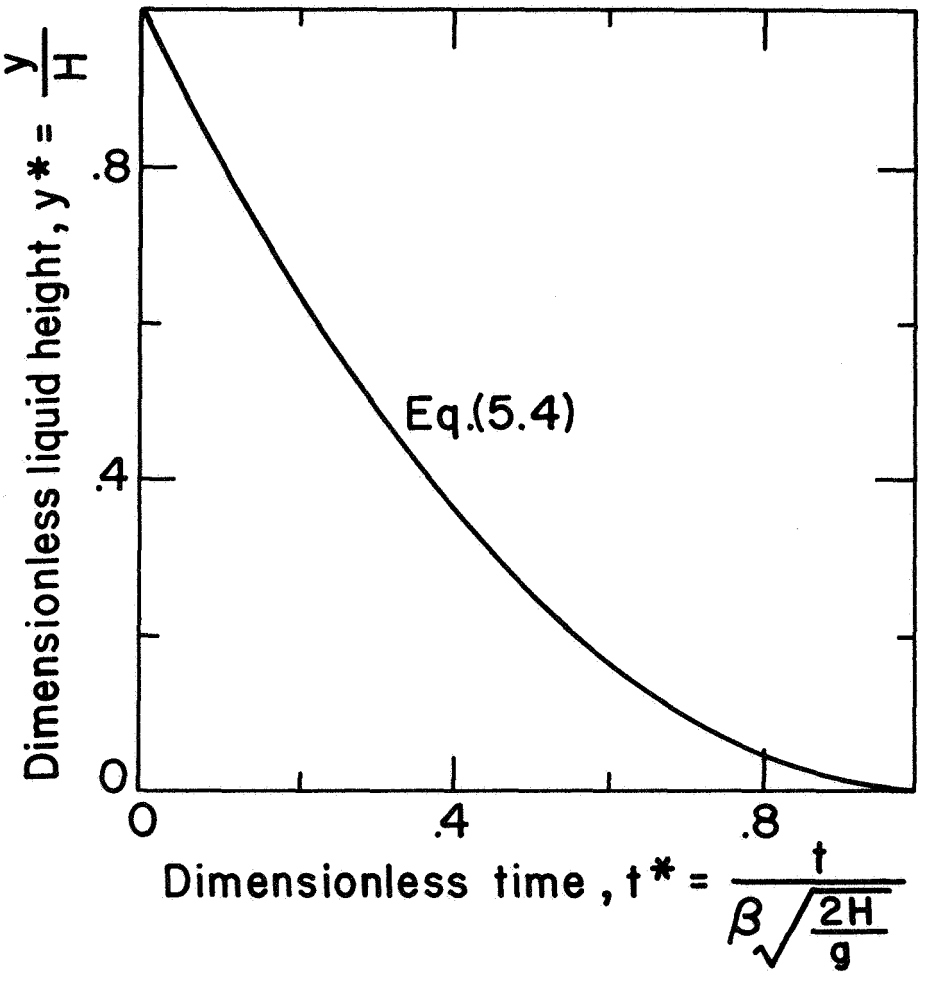

Figure 5.2. Variation of Liquid Height with Time from Analysis Based on Quasi-Steady Flow in the Absence of Viscous Effects for Zero Pressure Drop

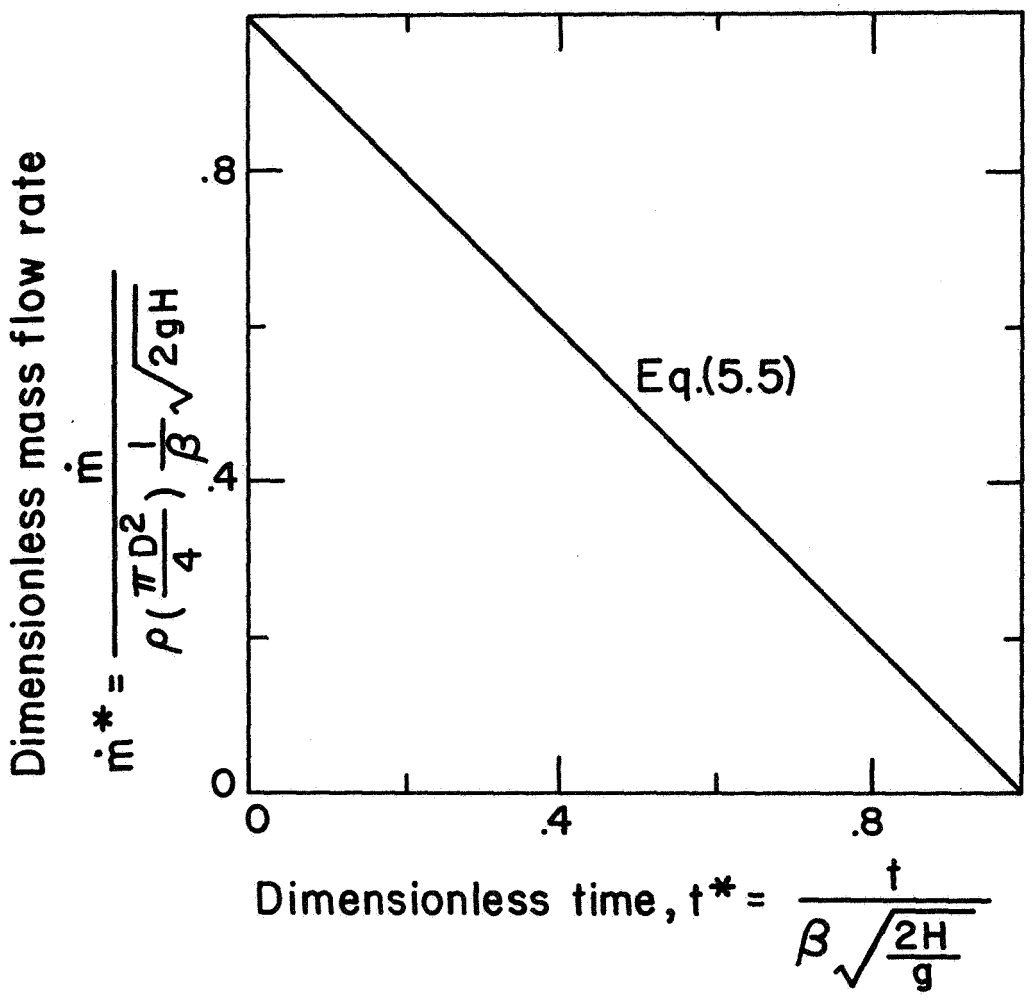

Figure 5.3. Variation of Mass Flow Rate with Time from Analysis Based on Quasi-Steady Flow in the Absence of Viscous Effects for Zero Pressure Drop

It is now apparent as to why the initial π-factors obtained in dimensional analysis were modified to include the numerical constants and the factor β. According to equations (3.4a) and (3.4b), for systems which are similar with respect to geometry and initial liquid height, y^* and $\dot{m}^*$ are unique functions of only t^*, when viscous effects and external pressure drop are neglected. Equations (5.4) and (5.5) give the functional relationships. These results are represented graphically in Figures 5.2 and 5.3, which show that the dimensionless liquid height decreases parabolically and the dimensionless mass flow rate linearly with dimensionless time. The latter result is associated with the drop-off in the hydrostatic head (which corresponds to the gravitational driving potential) as liquid is removed from the container. Further, the analysis gives the total discharge time for emptying a container through an orifice at its bottom as $\beta\sqrt{\frac{2H}{g}}$.

It is interesting to note that when the instantaneous liquid height, y, mass flow rate, $\dot{m}$, and the time elapsed since initiation of the discharge process, t, are non-dimensionalized as indicated in equations (5.3), the graphs y^* vs. t^* and $\dot{m}^*$ vs. t^* become universal with respect to β.

Transient Flow through an Orifice in the Absence of Viscous Effects for Zero Pressure Drop

The process studied and described in this thesis involves the behavior of a liquid, initially at rest, when it is discharged from a container. This implies that the initial flow rate (at $t = 0$) must be zero. Although the actual flow rate may in reality rise very rapidly with time, the inertia of the fluid prevents acceleration to the maximum flow rate in zero time (as indicated in Figure 5.3). On this basis the model

analyzed in the previous section is physically unacceptable, at least for small values of time. During this initial time period local acceleration effects, not considered in the previous analysis, are appreciable when the fluid accelerates from rest. An analysis which considers these aspects is given in this section. The physical effects accounted for are indicated below.

Table 5.2: Physical Effects

Forces		Fluid Acceleration	
[x]	Boundary Forces	[x]	Local Acceleration
[x]	Gravity Forces		
[ ]	Forces due to External Pressure Drop	[x]	Convective Acceleration
[ ]	Viscous Forces		

In the analysis considered here transient flow conditions are treated, and local acceleration effects are accounted for. The system analyzed is shown in Figure 5.1. For simplicity the flow is assumed to be one dimensional. It is convenient in this case to apply conservation of energy to a control volume surrounding the fluid remaining in the container at any given instant of time. For this control volume conservation of energy gives

$$\left[\begin{array}{c}\text{Rate of increase of}\\ \text{fluid energy in the}\\ \text{C.V.}\end{array}\right] + \left[\begin{array}{c}\text{Net rate}\\ \text{of energy}\\ \text{outflow}\end{array}\right] = \left[\begin{array}{l}\text{Rate of work done}\\ \text{on the fluid by}\\ \text{pressure forces at}\\ \text{boundaries where}\\ \text{fluid motion occurs.}\end{array}\right] \quad (5.6)$$

where both potential and kinetic energies must be accounted for. When expressed in terms of symbols this relation becomes

$$\frac{d}{dt}\left[(\rho Ay)g\,\frac{y}{2} + (\rho Ay)\,\frac{V_1^2}{2}\right] + \left[(\rho aV_2)\,\frac{V_2^2}{2}\right] = \left[P_1AV_1 - P_2aV_2\right] \quad (5.7)$$

Since P_2 is chosen equal to P_1 for this analysis and since $AV_1 = aV_2$ from continuity, the net rate of work done by the external pressure forces (given by the right hand side of the above equation) is zero. Inserting $V_1 = -(\frac{dy}{dt})$ and $V_2 = -(\frac{A}{a}\,\frac{dy}{dt})$ makes it possible, after some manipulation, to rewrite equation (5.7) as

$$\frac{d^2y}{dt^2} = -g + \frac{\beta^2(\frac{dy}{dt})^2}{2y} \quad (5.8)$$

where $\beta^2 = [(\frac{A}{a})^2 - 1]$. Notice that if $a = A$, $\beta^2 = 0$, and the physical system reduces to the case of a fluid cylinder of constant area A. For this situation equation (5.8) gives the acceleration as $d^2y/dt^2 = -g$.

In general $\frac{dy}{dt} = 0$ at $t = 0$ (zero initial discharge flow rate), and local acceleration effects dominate. Equation (5.8) shows that $d^2y/dt^2 \approx (-g)$ for small values of time when $\frac{dy}{dt}$ is negligibly small. However, once $\frac{dy}{dt}$ becomes sufficiently large the convective acceleration effect, as indicated by the value of $[\beta^2(dy/dt)^2]/2y$ in equation (5.8), increases and the local acceleration effect, as indicated by d^2y/dt^2, decreases in magnitude.

For large values of β, ($a \ll A$), the local acceleration effect diminishes very rapidly when $\frac{dy}{dt}$ is still quite small. Once the local acceleration effect becomes negligible, equation (5.8) predicts $\frac{dy}{dt} = -\frac{1}{\beta}\sqrt{2gy}$ in agreement with the result given in equation (B.4) for quasi-steady flow.

Equation (5.8) can be expressed in dimensionless form as

$$\frac{d^2y^*}{dt^{*2}} = -2\beta^2 \left[1 - \frac{1}{4y^*}\left(\frac{dy^*}{dt^*}\right)^2\right] \qquad (5.9)$$

The above differential equation was solved by means of digital computer calculations. The resulting numerical solutions of equation (5.9) are given in Figure 5.4 for various β values. The dimensionless mass flow rate values were obtained from the same program and are given in Figure 5.5.

The above description includes the inertia of the fluid as associated with the time varying, or transient, condition of the flow in the absence of viscous effects for zero pressure drop. The fluid is at rest initially, and all of the curves exhibit a zero discharge velocity and mass flow rate at t = 0. For small discharge openings ($a \ll A$ and $\beta \gg 1$) the flow accelerates rapidly, with respect to the total discharge time, and the system behavior, after the initial brief period of acceleration, closely approximates that predicted previously (Figures 5.2 and 5.3). For larger discharge openings the flow is considerably retarded over relatively longer times due to the inertia of the fluid during its initial period of acceleration. However, the predicted total discharge times are, for all practical purposes, fairly independent of β except in the range where β decreases to values smaller than 2. Even though the fluid inertia retards the flow initially for these situations, it also has the effect of maintaining the flow rate at higher values during the deceleration period so that the overall discharge time is almost unaffected.

Figures 5.4 and 5.5 can be used to ascertain the range of usefulness of the results given in Figures 5.2 and 5.3 which do not account for

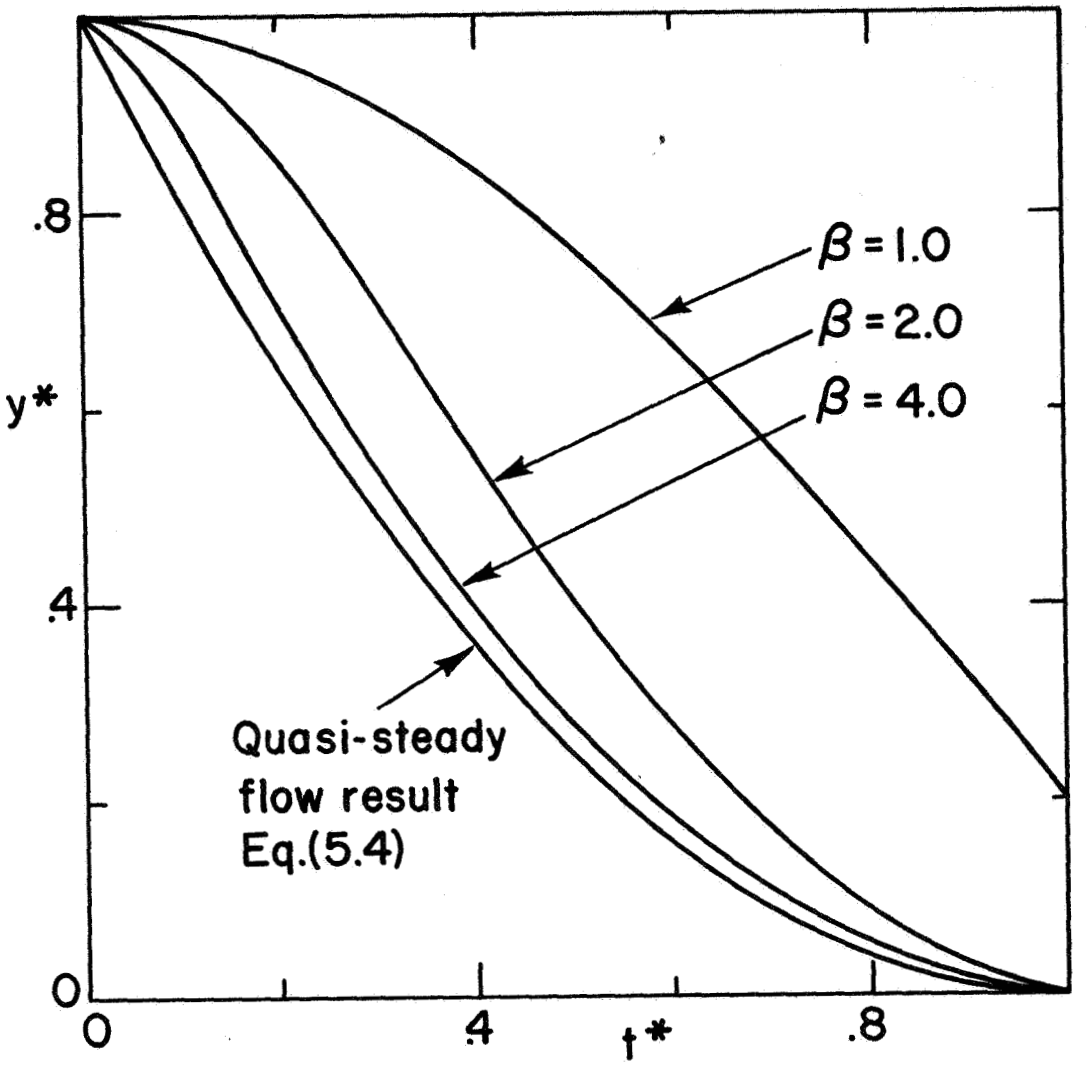

Figure 5.4. Variation of Liquid Height with Time from Analysis Based on Transient Flow in the Absence of Viscous Effects for Zero Pressure Drop

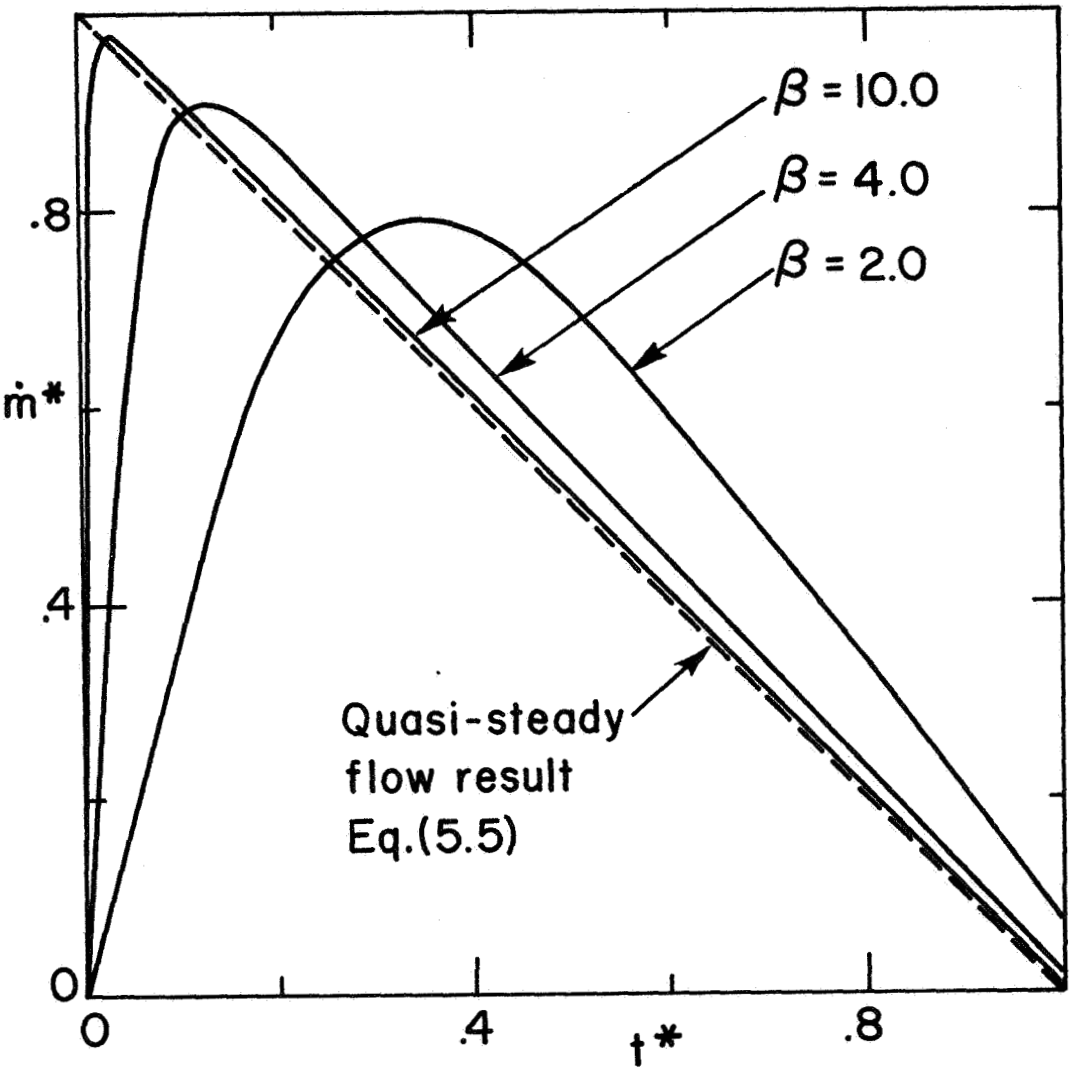

Figure 5.5. Variation of Mass Flow Rate with Time from Analysis Based on Transient Flow in the Absence of Viscous Effects for Zero Pressure Drop

local acceleration effects. For many typical situations (where $\beta >> 1$) predictions based on the quasi-steady flow model (Figures 5.2 and 5.3) are quite adequate for engineering purposes. Figures 5.4 and 5.5 show that although the inertia effect tends to retard the discharge initially, there is very little overall effect on the height versus time curve or total dimensionless discharge time unless β is small, that is, unless the discharge area, a, is of the same order of magnitude as the container area, A.

The results given in Figures 5.4 and 5.5 have been reported previously (Ref. 25, 26). Shortly thereafter, Sestak et al. (Ref. 27) gave an analytical solution for equation (5.9) in terms of Complete and Incomplete Beta Functions. This solution gives plots identical with those given in Figures 5.4 and 5.5 (this will be illustrated in the next section). These results apply for ideal discharge only, i.e. when viscous and stream contraction effects are not taken into account. However, in actual situations these effects should be considered. In the following section this aspect is considered.

Transient Discharge Through an Orifice Taking Viscous and Contraction Effects into Account

In each of the analyses considered thus far viscous effects have been neglected. Also, it has been assumed that the streamlines are all perpendicular to the cross-sectional area at the location of the opening (Ref. 4). Under certain conditions, which depend, in general, on geometry and on a Reynolds number associated with the flow, the discharge stream may contract to a smaller diameter as shown in Figure 5.7. For this situation the streamlines at the discharge opening are not all

perpendicular to the cross-sectional area of the opening. At the location where the streamlines do become perpendicular to the cross section, the area of the stream is somewhat reduced. Both viscous effects (Figures 5.6 and 5.7) and the contraction effects (Figure 5.7) tend to make the discharge rates smaller than those predicted for ideal flow (Figure 5.5). They are accounted for in a conventional manner (Ref. 3) and are now superimposed upon the treatment yielding the results given in the previous section. The corresponding physical model is based on the description below.

Table 5.3: Physical Effects

Forces		Fluid Acceleration	
[x]	Boundary Forces	[x]	Local Acceleration
[x]	Gravity Forces		
[ ]	Forces due to External Pressure Drop	[x]	Convective Acceleration
[x]	Viscous Forces		

In the analysis which follows fluid local acceleration effects are taken into account. The physical effects indicated above are all accounted for, at least approximately. The retardation of the flow is specified by means of a velocity coefficient, C_v, and a contraction coefficient, C_c (see Ref. 3). The reduction in flow rate due to both effects is specified in terms of a discharge coefficient, C_D, which is the product of C_v and C_c. Typical values of these coefficients (obtained from Ref. 4), which are valid for large β values are indicated in

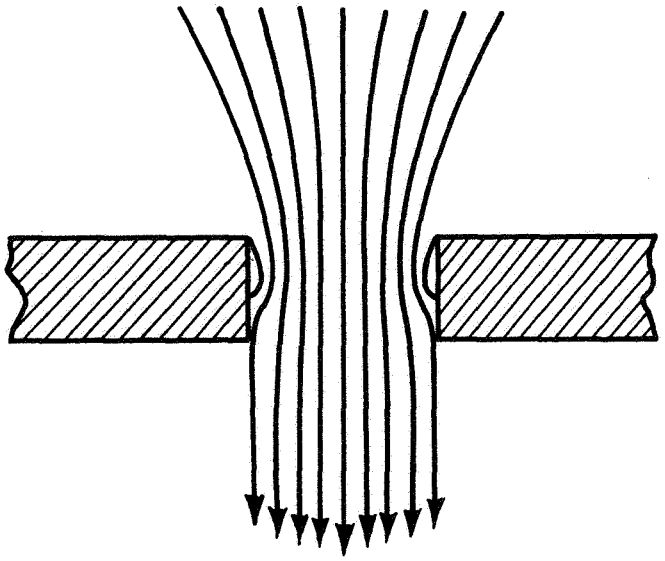

$C_V = 0.82$

$C_C = 1.00$

$C_D = 0.82$

Figure 5.6. Discharge with Viscous Effects Without Contraction (Ref. 4)

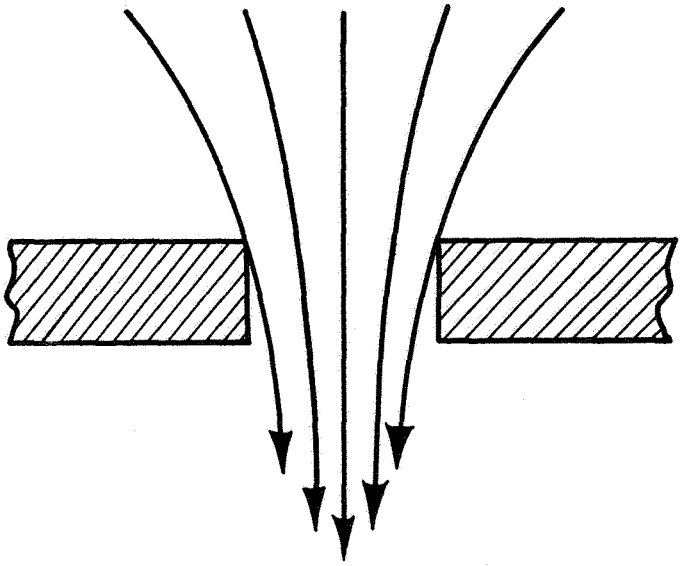

$C_V = 0.98$

$C_C = 0.61$

$C_D = 0.60$

Figure 5.7. Discharge with Viscous Effects With Contraction (Ref. 4)

Figures 5.6 and 5.7.

The equation for ideal discharge of fluids from a container is

$$\frac{d^2y^*}{dt^{*2}} = -2\beta^2 \left[1 - \frac{1}{4y^*} \left(\frac{dy^*}{dt^*}\right)^2\right] \tag{5.9}$$

Rearrangement of the terms makes it possible to write equation (5.9) as

$$\frac{d^2y^*}{dt^{*2}} - \frac{\beta^2}{2y^*} \left(\frac{dy^*}{dt^*}\right)^2 = -2\beta^2 \tag{5.10}$$

Since

$$\frac{d^2y^*}{dt^{*2}} = \frac{d}{dt^*} \left(\frac{dy^*}{dt^*}\right) = \frac{dy^*}{dt^*} \cdot \frac{d}{dy^*} \left(\frac{dy^*}{dt^*}\right) = \frac{1}{2} \frac{d}{dy^*} \left(\frac{dy^*}{dt^*}\right)^2 \tag{5.11}$$

equation (5.10) can be written as

$$\frac{d\zeta}{dy^*} - \frac{\beta^2}{y^*} \zeta = -4\beta^2 \tag{5.12a}$$

where

$$\zeta = \left(\frac{dy^*}{dt^*}\right)^2 \tag{5.12b}$$

After multiplying throughout by the integrating factor

$$e^{-\int \frac{\beta^2}{y^*} dy^*} = e^{-\beta^2 \ln y^*} = y^{*-\beta^2},$$

equation (5.12a) can be written as

$$\frac{d}{dy^*} \left(\zeta\, y^{*-\beta^2}\right) = -4\beta^2\, y^{*-\beta^2} \tag{5.13}$$

Integration of the above equations gives

$$\zeta\, y^{*(-\beta^2)} \Big|_{\substack{y^*=y^* \\ \zeta=\zeta}}^{\substack{y^*=1 \\ \zeta=0}} = -4\beta^2 \int_1^{y^*} y^{*(-\beta^2)}\, dy^*$$

or

$$\zeta\, y^{*(-\beta^2)} = -\frac{4\beta^2}{-\beta^2+1}\, y^{*(-\beta^2+1)} \Big|_1^{y^*}$$

$$= -\frac{4\beta^2}{-\beta^2+1}\left[y^{*(-\beta^2+1)} - 1\right]$$

Therefore

$$\zeta = \left(\frac{dy^*}{dt^*}\right)^2 = \frac{4\beta^2}{\beta^2-1}\left[y^* - y^{*\beta^2}\right]$$

So

$$\frac{dy^*}{dt^*} = -\left(\frac{4\beta^2}{\beta^2-1}\right)^{\frac{1}{2}}\left[y^* - y^{*\beta^2}\right]^{\frac{1}{2}} \tag{5.14}$$

The negative sign is chosen because y^* decreases with increasing t^*. The discharge coefficient is defined by the equation

$$\dot{m}_{actual} = C_D\, \dot{m}_{ideal} \tag{5.15}$$

where $\dot{m}$'s represent mass flow rates. Thus for the case of discharge of a container through an orifice, when viscous and stream contraction effects are taken into account equations (5.14) and (5.15) can be combined to yield

$$\frac{dy^*}{dt^*} = - C_D \cdot \left(\frac{4\beta^2}{\beta^2-1}\right)^{\frac{1}{2}} \left[y^* - y^{*(\beta^2)}\right]^{\frac{1}{2}} \tag{5.16a}$$

or, writing $\beta^2 = \alpha$ for convenience,

$$\frac{dy^*}{dt^*} = - C_D \left(\frac{4\alpha}{\alpha-1}\right)^{\frac{1}{2}} \cdot y^{*\frac{1}{2}} \left(1 - y^{*\alpha-1}\right)^{\frac{1}{2}} \tag{5.16b}$$

In equation (5.16b) C_D varies with Reynolds number and thus is a function of $\frac{dy^*}{dt^*}$ and t^*. In certain practical cases of interest, however, C_D can be taken to be constant. The validity of the assumption of a constant C_D and the discrepancies arising out of it are discussed later. With C_D constant equation (5.16b) can be integrated further to obtain t^* as a function of y^* as follows. Integration of equation (5.16b) between $t^* = 0$ and $t^* = t^*$ gives

$$\int_0^{t^*} dt^* = \frac{1}{C_D} \left(\frac{\alpha-1}{4\alpha}\right)^{\frac{1}{2}} \int_{y^*}^{1} y^{*-\frac{1}{2}} \left(1 - y^{*\alpha-1}\right)^{-\frac{1}{2}} dy^*$$

Substitution of $y^{*(\alpha-1)} = u$ in the integral on the right hand side yields

$$t^* = \frac{1}{C_D} \left(\frac{\alpha-1}{4\alpha}\right)^{\frac{1}{2}} \int_{y^{*(\alpha-1)}}^{1} u^{-\frac{1}{2(\alpha-1)}} (1-u)^{-\frac{1}{2}} \cdot \frac{1}{\alpha-1} u^{\frac{2-\alpha}{\alpha-1}} du$$

$$= \frac{1}{C_D} \left[\frac{1}{4\alpha(\alpha-1)}\right]^{\frac{1}{2}} \int_{y^{*(\alpha-1)}}^{1} u^{\frac{3-2\alpha}{2(\alpha-1)}} (1-u)^{-\frac{1}{2}} du \tag{5.17}$$

The integral in equation (5.17) can be expressed in terms of well known Beta and incomplete Beta functions, as Sestak et al. (Ref. 27) have done.

From the definitions of Beta function, B(p,q) and incomplete Beta function $B_x(p,q)$ (Ref. 29)

$$\int_x^1 s^{p-1} (1-s)^{q-1} ds = B(p,q) - B_x(p,q)$$

$$= B(p,q) [1 - I_x(p,q)] \tag{5.18}$$

So equation (5.17) can be written as

$$t^* = \frac{1}{C_D} \left[\frac{1}{4\alpha(\alpha-1)}\right]^{\frac{1}{2}} \int_{y^{*\alpha-1}}^1 u^{\frac{1}{2(\alpha-1)} - 1} (1-u)^{\frac{1}{2} - 1} du$$

Thus

$$t^* = \frac{1}{C_D} \left[\frac{1}{4\alpha(\alpha-1)}\right]^{\frac{1}{2}} B\left(\frac{1}{2(\alpha-1)}, \frac{1}{2}\right)$$

$$\left[1 - I_{y^*(\alpha-1)} \left(\frac{1}{2(\alpha-1)}, \frac{1}{2}\right)\right] \tag{5.19}$$

The result given by equation (5.19) reduces to the solution given by Sestak et al. (Ref. 27) for the case of ideal discharge of fluids where there are no viscous and contraction effects and the discharge coefficient is 1.0. It can be observed that the actual time taken to reach any particular height since the initiation of discharge is increased with respect to the ideal solution by a factor $\frac{1}{C_D}$. This means that the total discharge time also is increased by $(\frac{1}{C_D})$. Of course, the above analysis assumes that the factor C_D is a constant throughout the period of discharge. The limitations of such an assumption are discussed in the following section. The results are essentially the same as those shown in Figures 5.4 and 5.5, with the abscissa changed to read (C_D t*) instead of t* and ordinate for mass flow rate changed to read ($\frac{1}{C_D}$ $\dot{m}$*) instead

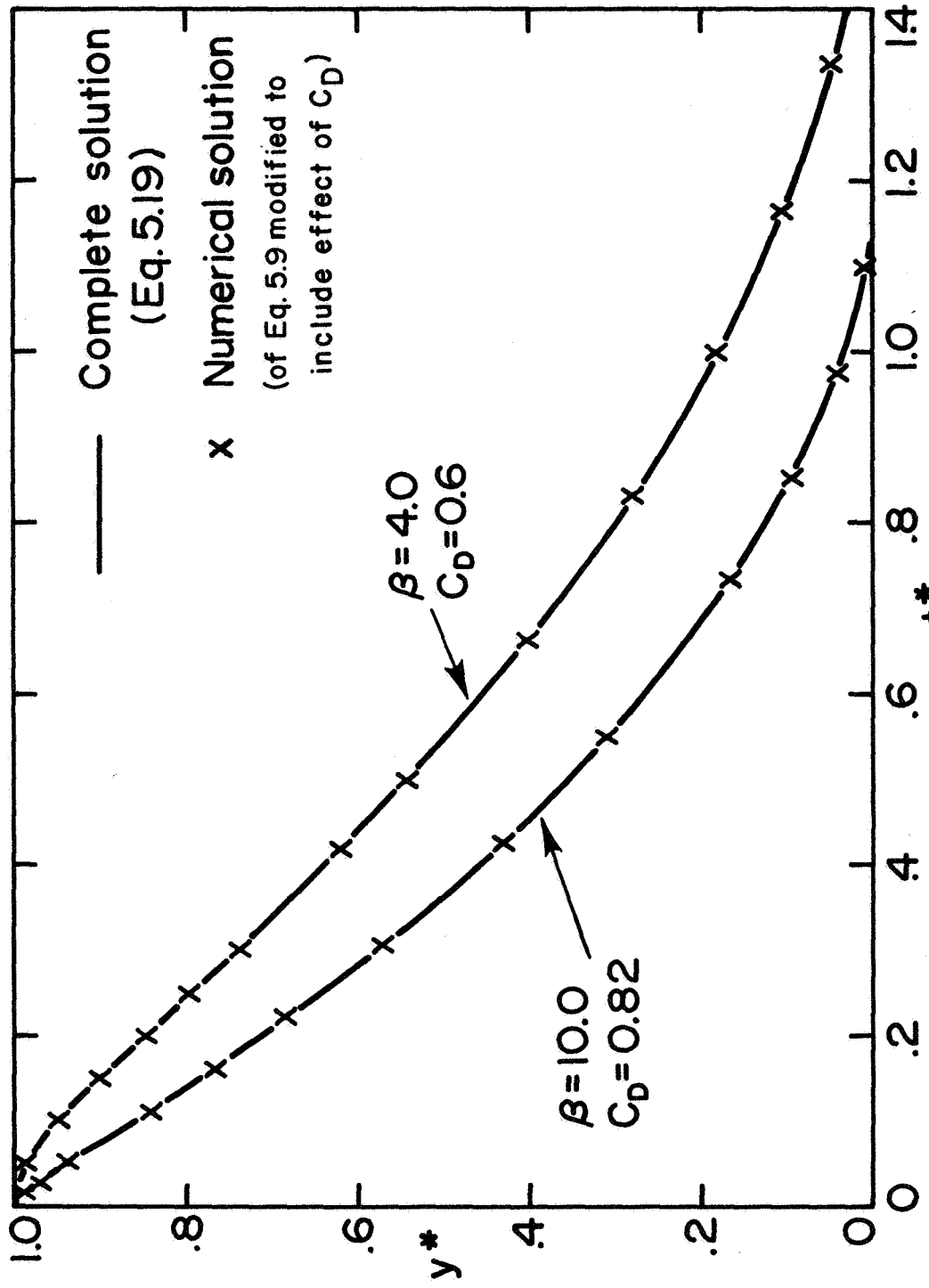

Figure 5.8. Variation of y* with t* as predicted by the Complete Solution and Comparison with the Numerical Solution of the Differential Equation for Transient Discharge Through an Orifice

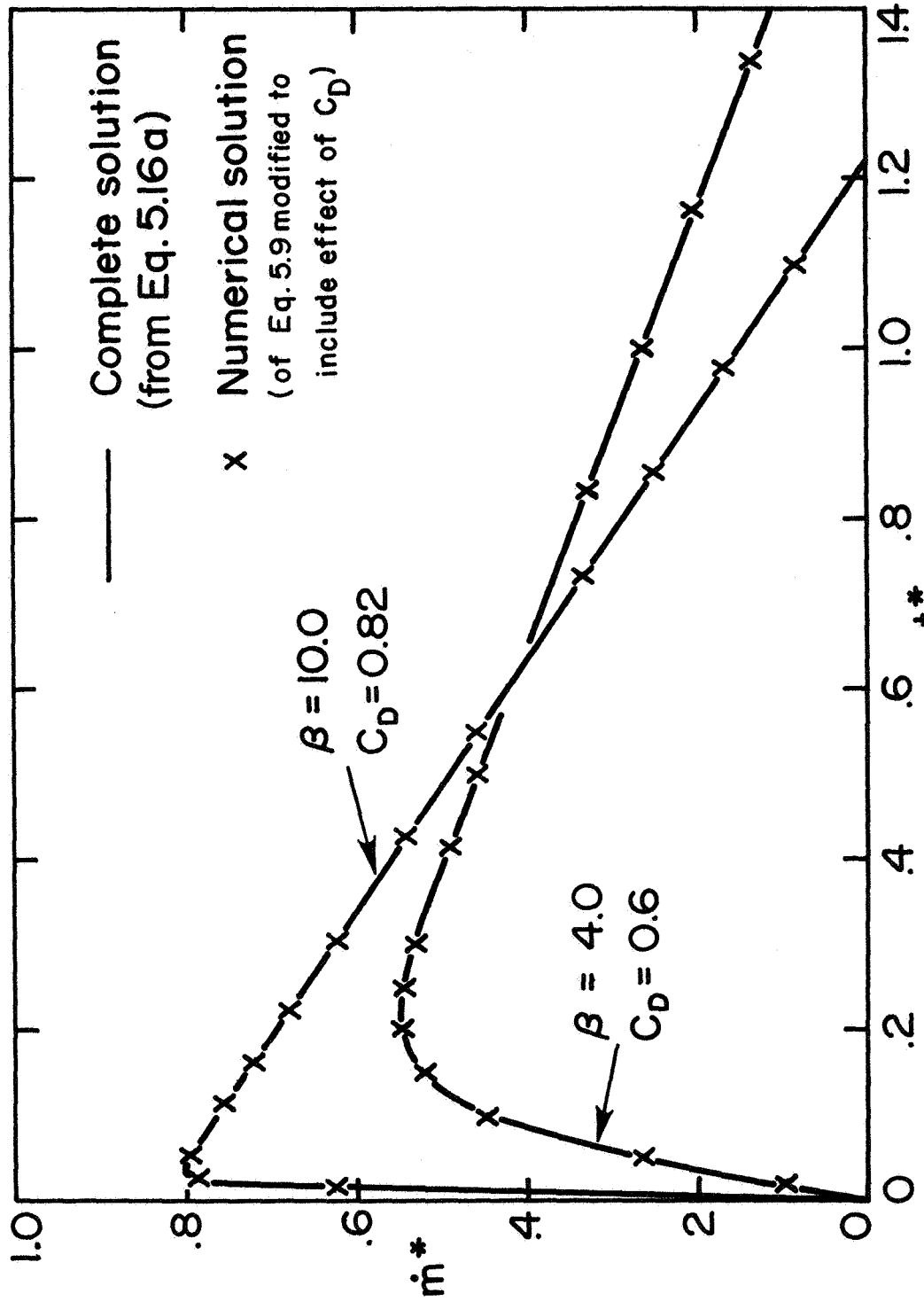

Figure 5.9. Variation of $\dot{m}^*$ with t^* as predicted by the Complete Solution and Comparison with the Numerical Solution of the Differential Equation for Transient Discharge Through an Orifice

of $\dot{m}^*$. A program for obtaining numerical results from equation (5.19) is presented in Appendix D. In this program the Beta function was evaluated using the well known formula (Ref. 29), $B(x,y) = \frac{\Gamma(x)\,\Gamma(y)}{\Gamma(x+y)}$, and the incomplete Beta function was approximated (Ref. 30) by Soper's formula

$$B_x(p,q) = \int_0^x x^{p-1}\,(1-x)^{q-1}\,dx \approx \frac{x^p}{(p+1)(p+2)}\left[\frac{2}{p} - 1 + 4\left(1-\frac{x}{2}\right)^{q-1} + p(1-x)^{q-1}\right]$$

The computations have been carried out on the CDC 6500 computer. Figures 5.8 and 5.9 illustrate that the numerical solution of the differential equation (5.9), modified to include the effects of geometry and viscosity (the t^* scale expanded by a factor $\frac{1}{C_D}$ and $\dot{m}^*$ scale reduced by a factor C_D), and the complete solution given in equations (5.19) and (5.16a) are identical. The total time for discharge, obtained by substituting $y^* = 0$ in equation (5.19), is given by

$$t_t^* = \frac{1}{C_D}\left[\frac{1}{4\alpha(\alpha-1)}\right]^{\frac{1}{2}} B\left(\frac{1}{2(\alpha-1)}\,,\,\frac{1}{2}\right) \qquad (5.19a)$$

Discussion of the Discharge Coefficient, C_D

It is appropriate at this point to include a discussion of the discharge coefficient C_D, since it is typically used whenever orifice discharge is encountered. If the quasi-steady analysis is modified to include effects of external pressure drop, of geometry and of viscosity, equations (5.4) and (5.5) become

$$y^* = 1 - 2\sqrt{1 + \frac{\Delta P}{\rho g H}}\,(C_D t^*) + (C_D t^*)^2 \qquad (5.20)$$

and

$$\dot{m}^* = C_D \left[\sqrt{1 + \frac{\Delta P}{\rho g H}} - C_D t^* \right] \tag{5.21}$$

Variations of y^* and $\dot{m}^*$ with respect to t^* as given by the above equations are shown in Figures 5.10 and 5.11, to illustrate the retardation effect produced by $C_D < 1$ for two different values of $\frac{\Delta P}{\rho g H}$.

In the previous analyses it was assumed, implicitly, that the discharge coefficient is a constant throughout the discharge process. Such an assumption yields good predictions, as will be shown, but there are certain limitations.

Figure 5.12 shows the variation of C_D with Reynolds number (based on total head), as given by Vennard (Ref. 31), which is applicable to quasi-steady flow conditions when $y/d > 5$ and for $\frac{D}{d} >> 1$. When $y/d \approx 1$ or smaller, the lowering of the liquid surface into the vicinity of the outlet obviously causes considerable variation in the fluid streamline pattern at the exit. Thus, for small values of y/d some deviation from the C_D curve of Figure 5.12 can be expected. Since $(\frac{y}{d}) = (\frac{H}{d}) \cdot (\frac{y}{H})$, this implies that even when $\frac{d\sqrt{2gH}}{\nu}$, $\frac{y}{H}$, and $\frac{\Delta P}{\rho g H}$ are held constant, various values of C_D can be obtained by varying $\frac{H}{d}$ in the operating range where $(\frac{H}{d}) \cdot (\frac{y}{H})$ is small. Also, the curve of Figure 5.12 applies only if $\frac{D}{d} >> 1$. When d is large, approaching the value of D, the cylindrical container wall effects the streamline pattern in the vicinity of the outlet, so that C_D varies with $\frac{D}{d}$ in general. This can be expected on the basis of C_D values obtained for flow through an orifice in a tube full of liquid (Figure 5.13), a situation which is not quite the same as the case discussed here, but is somewhat similar.

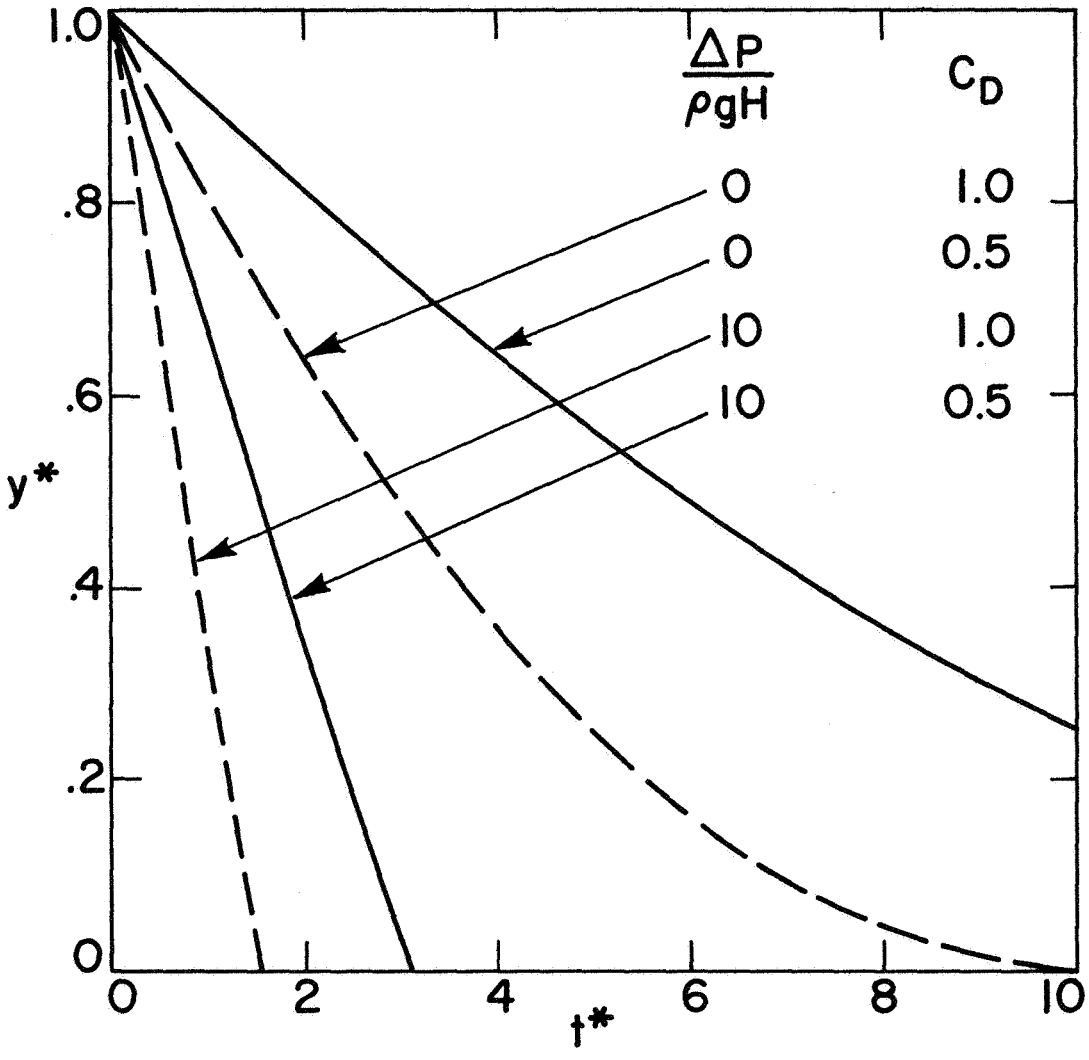

Figure 5.10. Variation of Liquid Height with Time from Analysis Based on Quasi-Steady Flow in the Presence of Viscous Effects for Non-Zero Pressure Drop, Equation (5.20)

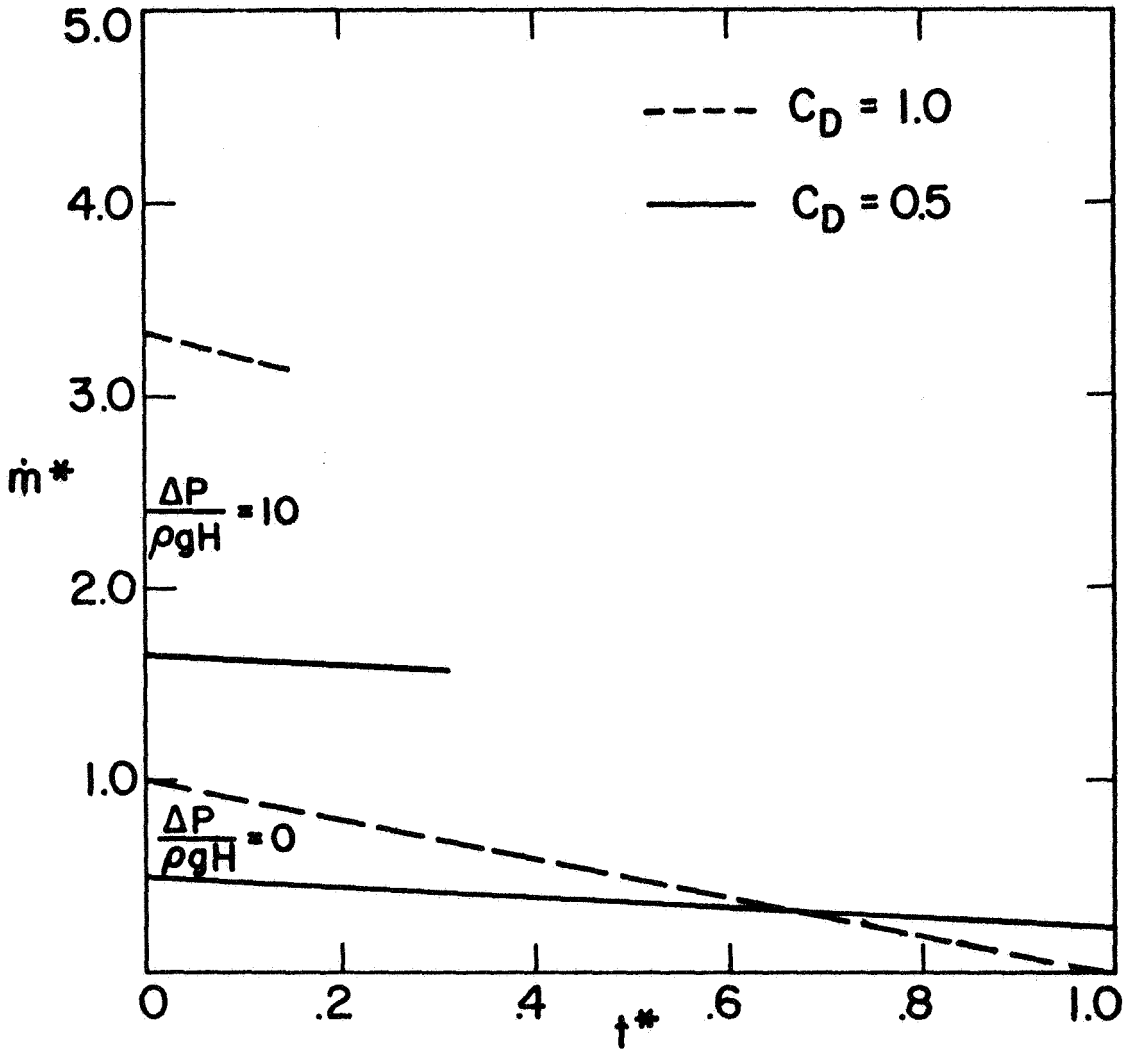

Figure 5.11. Variation of Mass Flow Rate with Time from Analysis Based on Quasi-Steady Flow Including Viscous Effects for Non-Zero Pressure Drop, Equation (5.21)

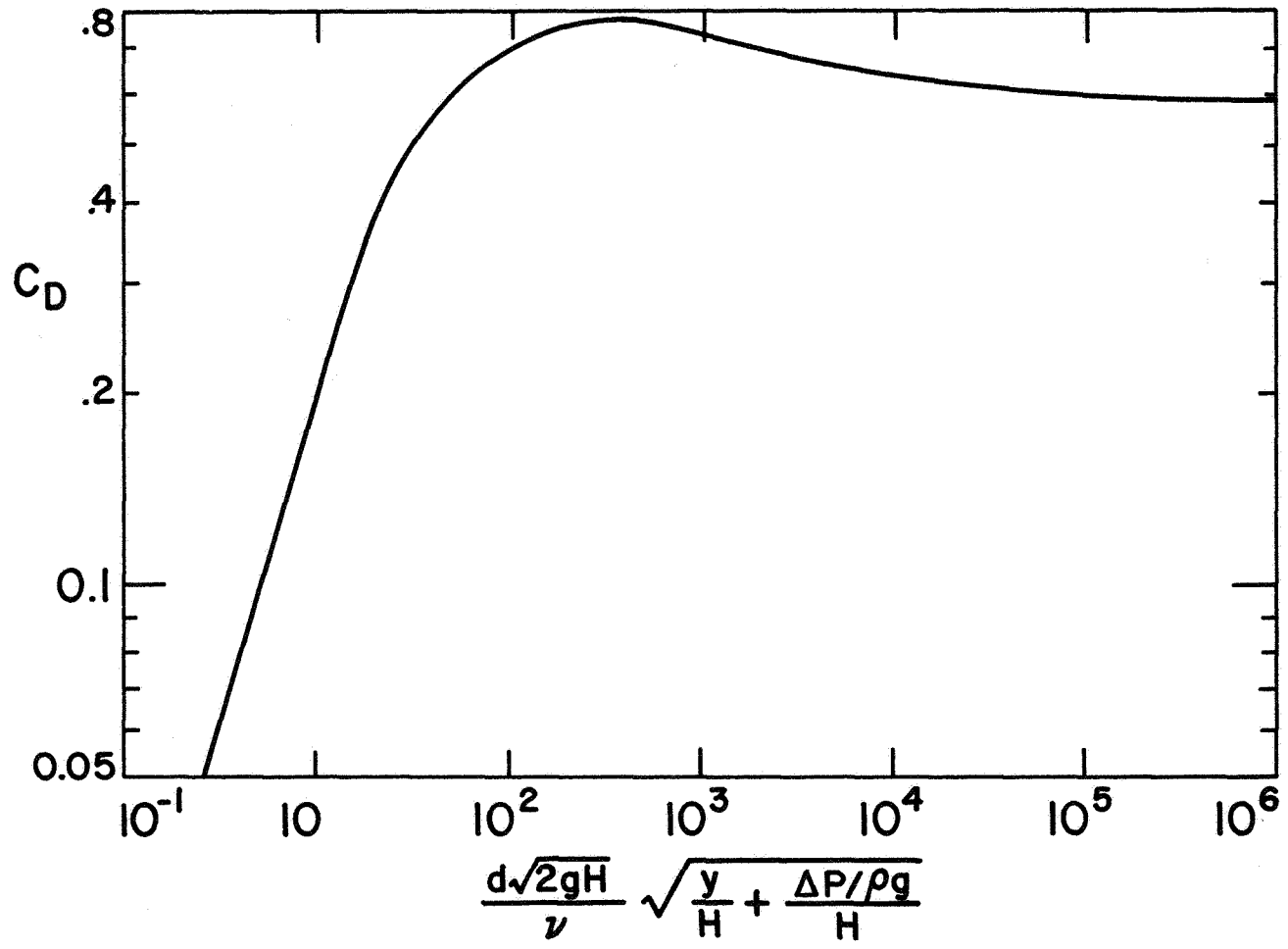

Figure 5.12. Variation of Discharge Coefficient for y/d > 5 and D/d >> 1 from Ref. 31 for Steady Flow Situations

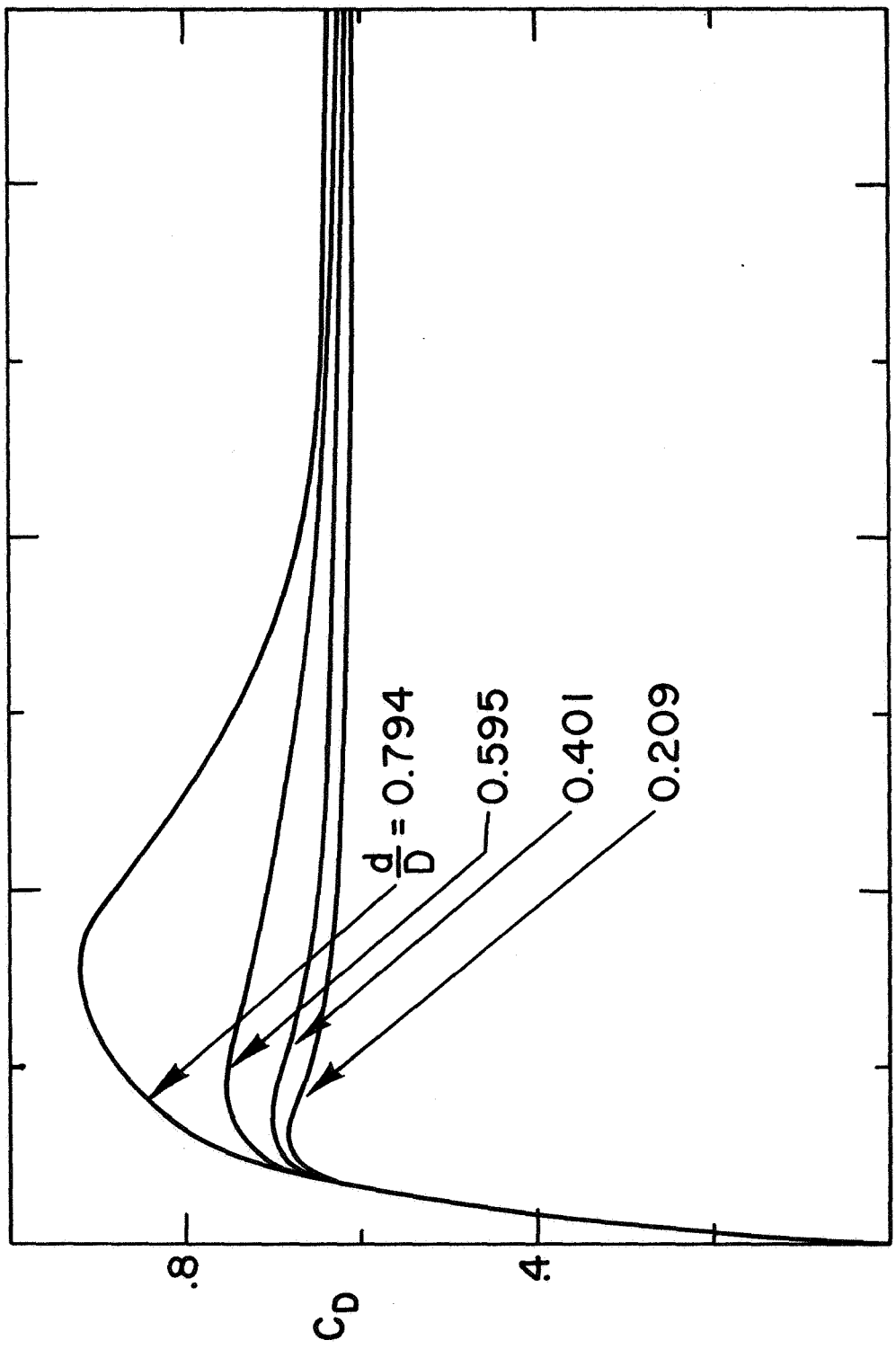

Figure 5.13. Variations of Discharge Coefficient for Flow Through an Orifice in Tube (Ref. 32)

On the basis of the discussion above, it is clear that C_D is somewhat dependent on $\frac{H}{d}$ and $\frac{D}{d}$ in addition to the dimensionless ratios appearing in the abscissa of Figure 5.12. Therefore, all of the dimensionless parameters given initially in equations (3.2a) and (3.2b) are appropriately included in the results given by equations (5.19) through (5.21).[1] However, the results given by the above equations are not exact in general since C_D was assumed constant throughout the discharge period in their derivation. In reality C_D may be expected to vary somewhat with time as y decreases (Figure 5.12). Despite this fact, use of a constant C_D value for an entire transient run can be expected to produce reasonably accurate results in many typical situations where $\frac{d\sqrt{2gH}}{\nu}\sqrt{\frac{y}{H}+\frac{\Delta P}{\rho g H}}$ remains somewhat above 10^4 throughout most of the discharge period (Figure 5.12). In this case C_D is very close to 0.6 during most of the process (provided that $\frac{H}{d} >> 1$), except for possible changes in C_D occurring at the very end of the process ($\frac{y}{d} \approx 1$, or smaller) brought about by an alteration of the flow pattern as the liquid surface is lowered into the region of the exit (Ref. 18).

To illustrate the effect of the variation of C_D with Reynolds number on the discharge process, the curve in Figure 5.12 was approximated by a series of straight lines. In all the cases discussed below the instantaneous Reynolds number was calculated and the corresponding C_D value was used in performing a step by step integration to obtain the curves for y^* vs. t^* and $\dot{m}^*$ vs. t^*. Further, $\frac{\Delta P}{\rho g H}$ was taken to be zero, because this situation gives the greatest variation in Reynolds number and hence in C_D. Figure 5.14 shows the variation of Reynolds number (abscissa of Figure

[1] Note that $L/d = 0$ in this treatment, while $a/A = (d/D)^2$ and $\beta = \sqrt{(D/d)^4 - 1}$.

5.12) with dimensionless time for quasi-steady discharge through an orifice, for two values of the ratio $\frac{d\sqrt{2gH}}{\nu}$, 10^5 and 10^3 respectively. Figures 5.15 and 5.16 illustrate the variation of y* vs. t* and $\dot{m}^*$ vs. t*. The solid lines were calculated assuming the discharge coefficient (C_D), evaluated at the initial Reynolds number, to be constant for the entire run. The + marks indicate the results of the step by step integration procedure for the situation in which C_D varies with Reynolds number (as given in Figure 5.14). It is evident that there is very little difference between the two sets of results for these ranges of $\frac{d\sqrt{2gH}}{\nu}$ (10^3 and above). However, it is worth noting that when $\frac{d\sqrt{2gH}}{\nu} = 10^5$ (curves ① in Figures 5.15 and 5.16) a slight increase in discharge rate is discernable, due to an increase of C_D in the range from 0.6 to 0.75. Figures 5.17 through 5.19 illustrate these results for transient flow, where the Reynolds number varies from zero to a maximum and then decreases to zero. Note that unlike in the quasi-steady flow case (where the Reynolds number is based on the ideal discharge velocity), the Reynolds number is calculated using the instantaneous discharge velocity. The trends are identical with those obtained for quasi-steady flow. Therefore, when $\frac{d\sqrt{2gH}}{\nu}$ is 10^3 or higher predictions can be made using the C_D evaluated at $\frac{d\sqrt{2gH}}{\nu}$ (from Fig. 5.12) without incurring significant errors.

In the lower ranges of $\frac{d\sqrt{2gH}}{\nu}$ (100 and below) C_D drops from 0.75 to zero. In this situation viscous effects become highly dominant. Figure 5.20 shows the variation of Re (abscissa of Figure 5.12) with t* for quasi-steady flow when $\frac{d\sqrt{2gH}}{\nu} = 50.0$. Figures 5.21 and 5.22 illustrate the effect of variation of C_D with Re on y* vs. t* and $\dot{m}^*$ vs. t* respectively. Again, the solid lines were computed by using the initial C_D value for the entire run. A constant C_D gives a linear variation of $\dot{m}^*$

with t* (see equation 5.21). It is evident from Figure 5.22 that a constant C_D (appropriately evaluated at a lower Re) cannot predict the variations correctly for the entire run. Figures 5.23 through 5.25 represent similar results for the case of transient flow when $\beta = 4.0$ and $\frac{d\sqrt{2gH}}{\nu} = 100$. In this situation, it is interesting to note that the discharge process takes a long time to get started because of the low value of C_D (in the range from zero to 0.05) when Reynolds number is very small. Therefore, in cases where $\frac{d\sqrt{2gH}}{\nu}$ is less than 100 (i.e. for highly viscous flow and/or with low initial heads) the strong variations in C_D with Re cause predictions from equations (5.19) through (5.21) to be quite inaccurate. Thus, a word of caution is in order with respect to the ability of equations (5.19) through (5.21) to predict the actual discharge behavior in certain operating ranges.

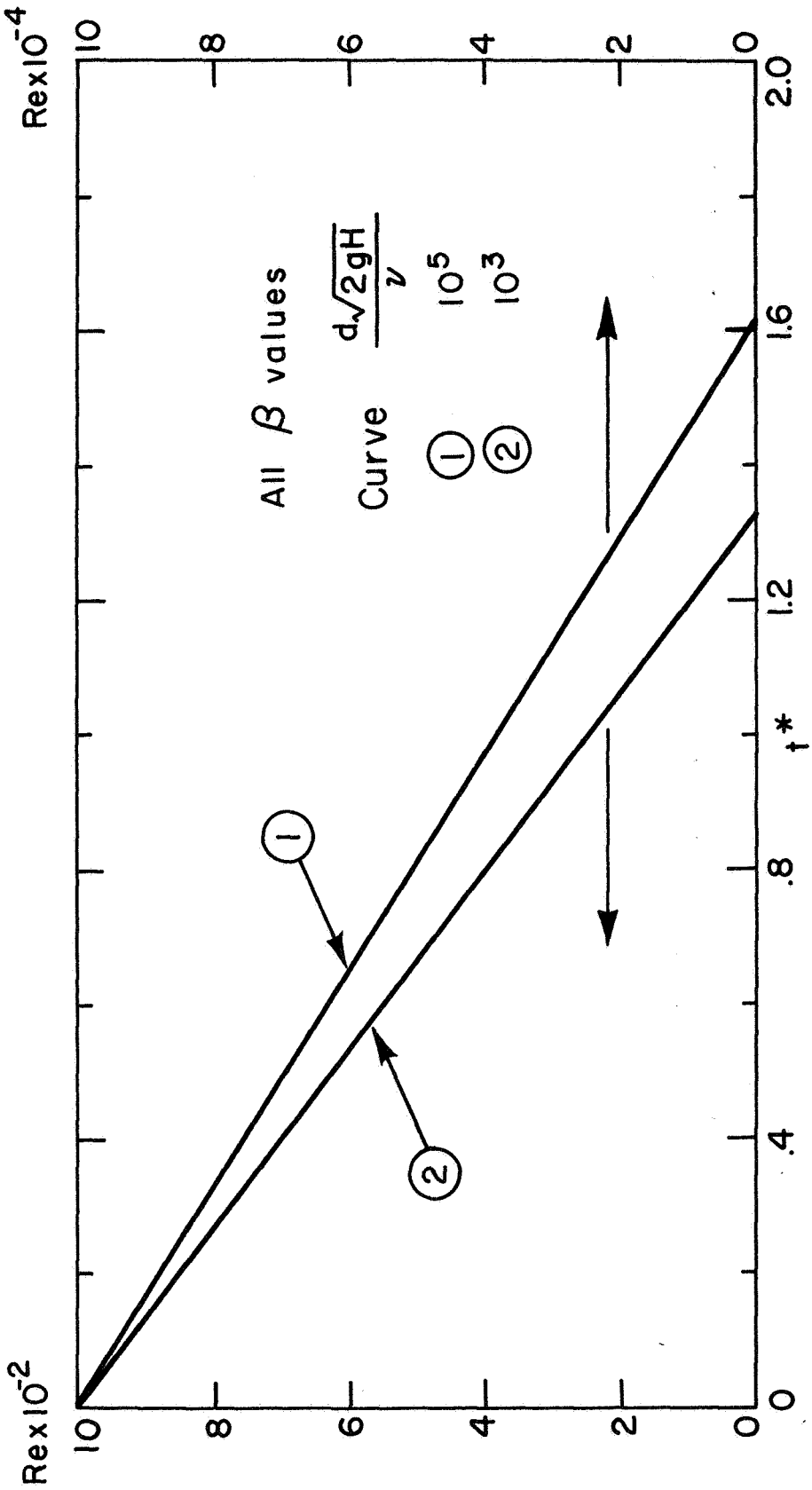

Figure 5.14. Variation of Reynolds Number (Re = $d\sqrt{2gy}/\nu$) with Dimensionless Time (t*) for Discharge Through an Orifice for Two Different Values of $d\sqrt{2gH}/\nu$ (Quasi-Steady Flow Analysis)

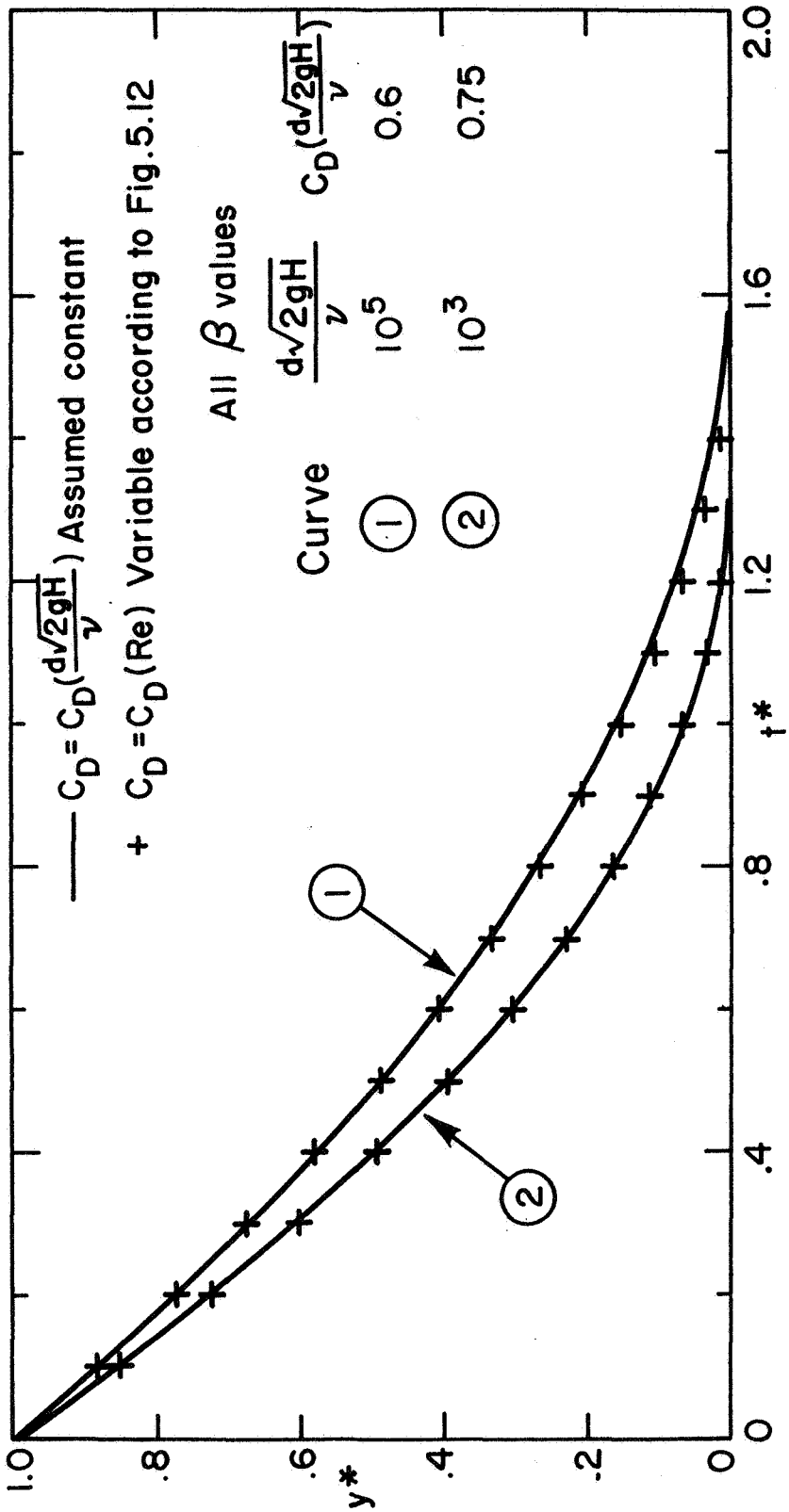

Figure 5.15. Effect of Variation of C_D with Re on y* vs. t* for Discharge Through an Orifice for Two Different Values of $d\sqrt{2gH}/\nu$ (Quasi-Steady Flow Analysis)

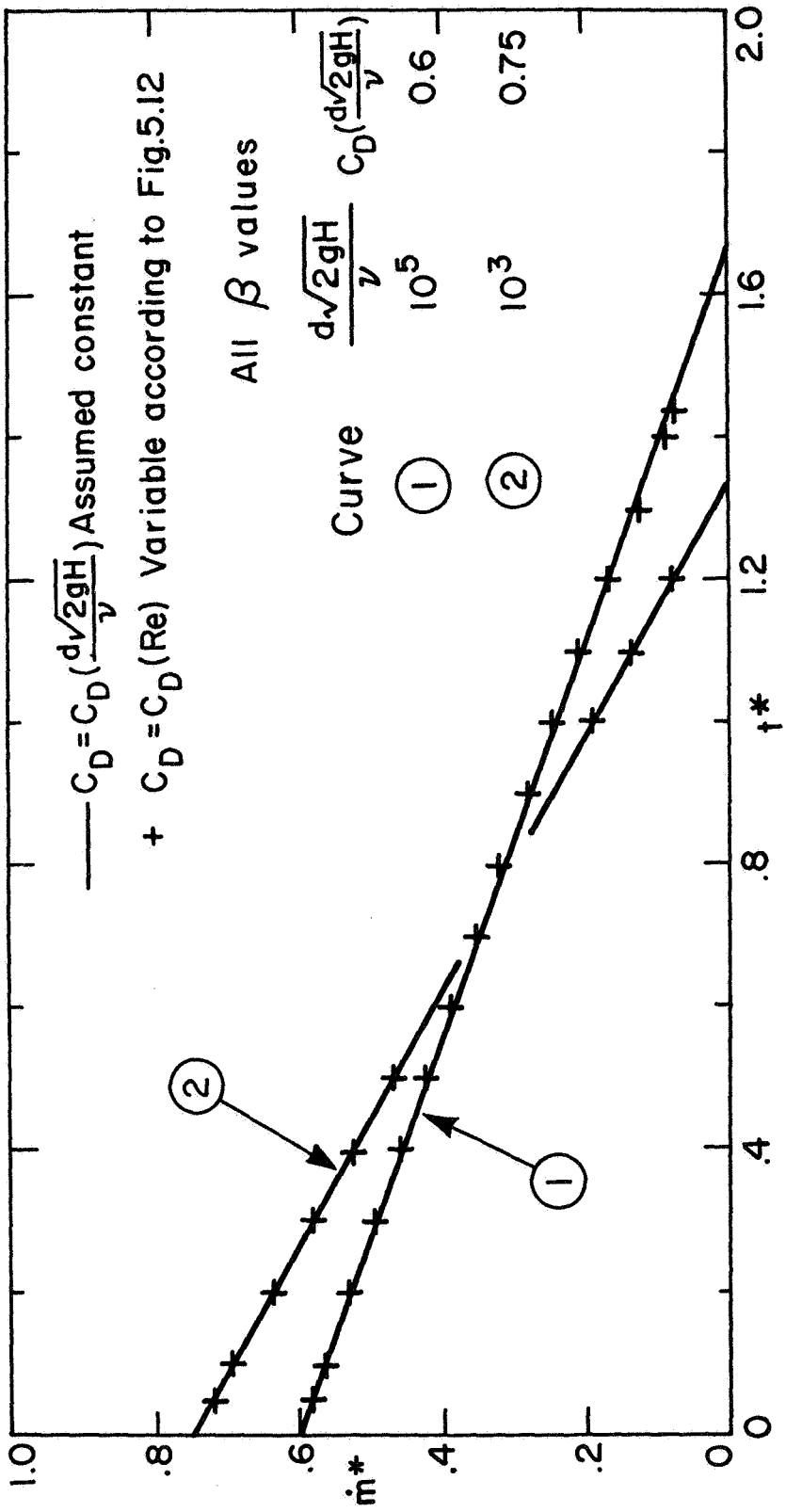

Figure 5.16. Effect of Variation of C_D with Re on $\dot{m}^*$ vs. t^* for Discharge Through an Orifice for Two Different Values of $d\sqrt{2gH}/\nu$ (Quasi-Steady Flow Analysis)

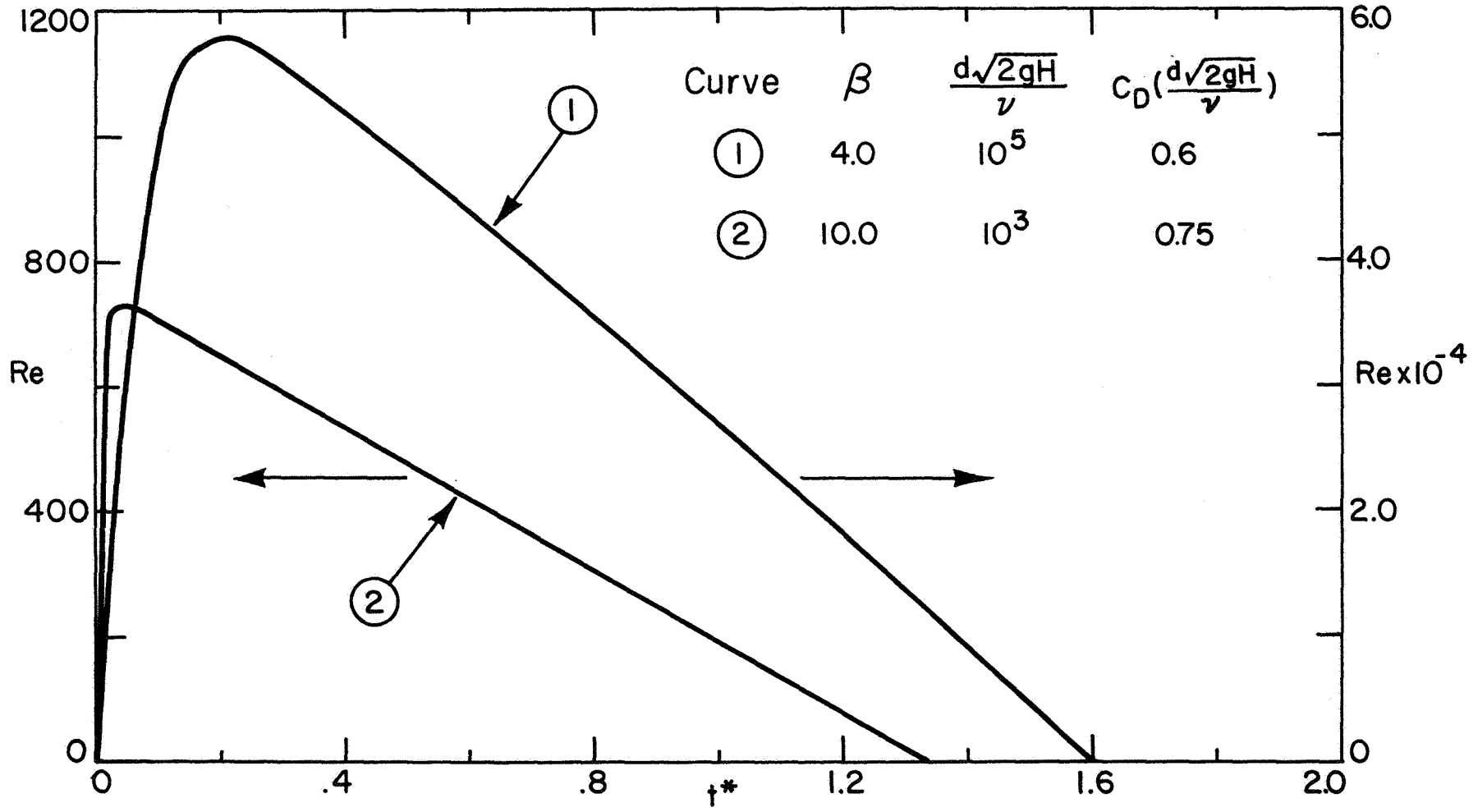

Figure 5.17. Variation of Reynolds Number ($Re = dV_2/\nu$) with Dimensionless Time (t^*) for Discharge Through an Orifice for Two Different Values of $d\sqrt{2gH}/\nu$ (Transient Flow Analysis)

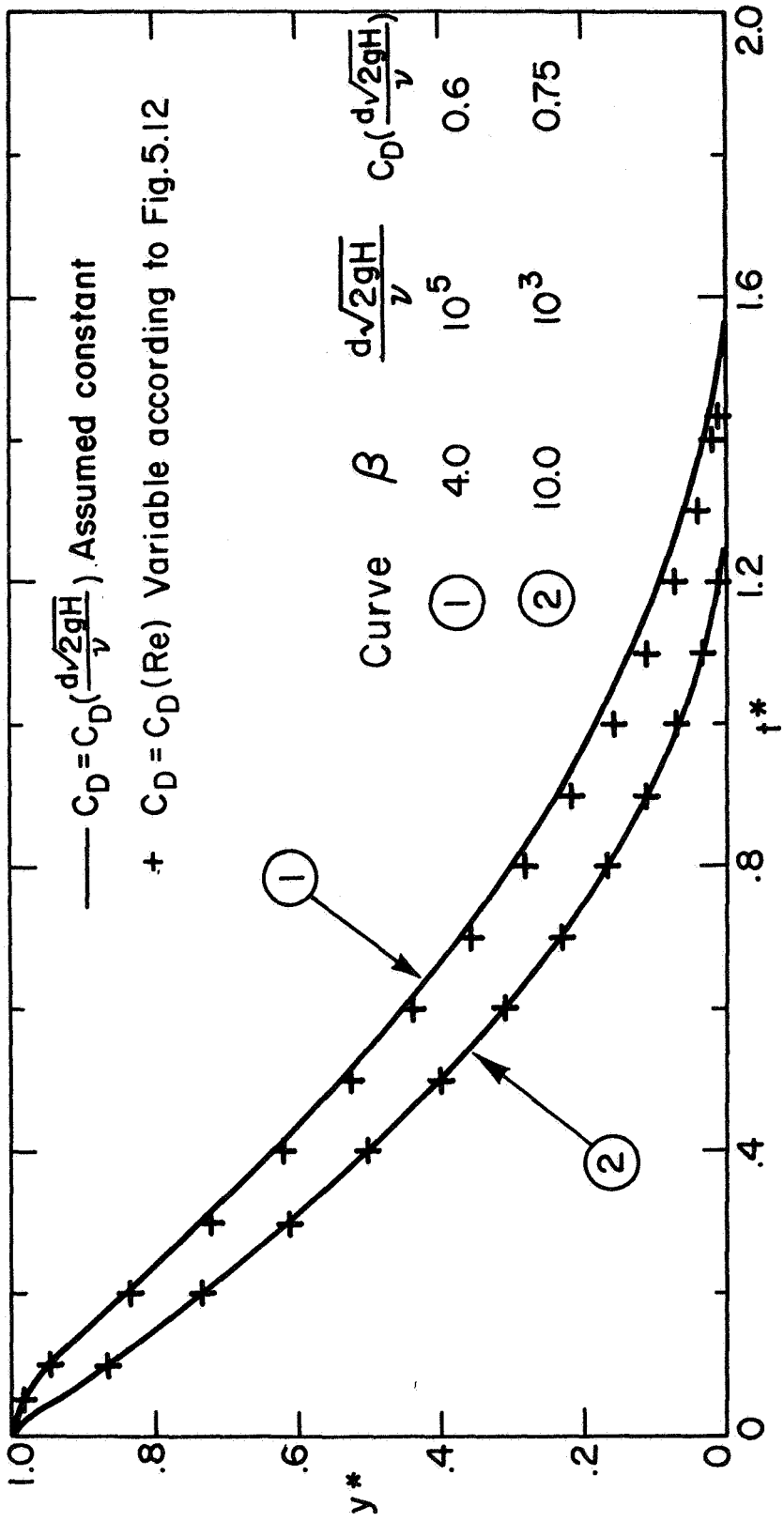

Figure 5.18. Effect of Variation of C_D with Re on y* vs. t* for Discharge Through an Orifice for Two Different Values of $d\sqrt{2gH}/\nu$ (Transient Flow Analysis)

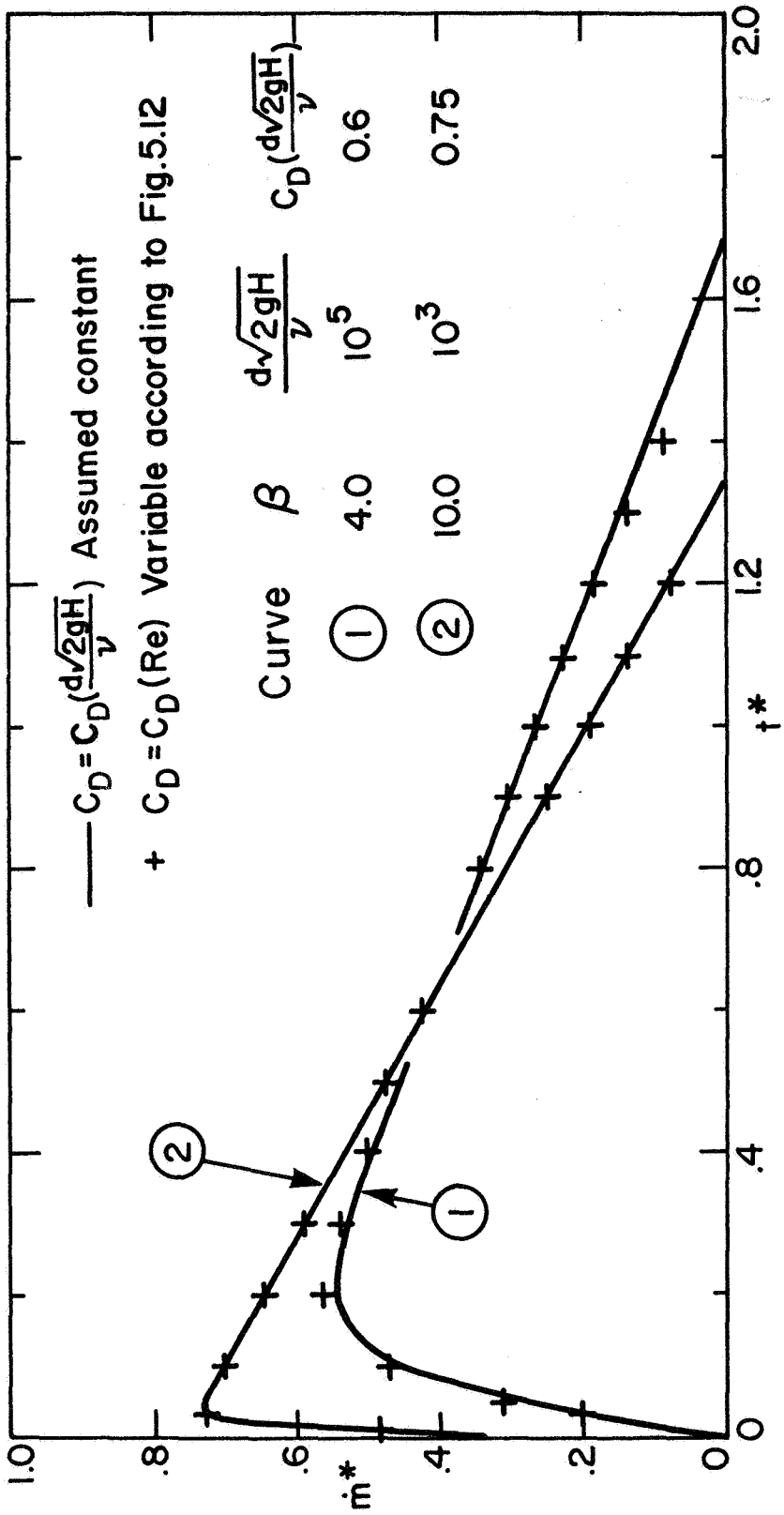

Figure 5.19. Effect of Variation of C_D with Re on $\dot{m}^*$ vs. t^* for Discharge Through an Orifice for Two Different Values of $d\sqrt{2gH}/\nu$ (Transient Flow Analysis)

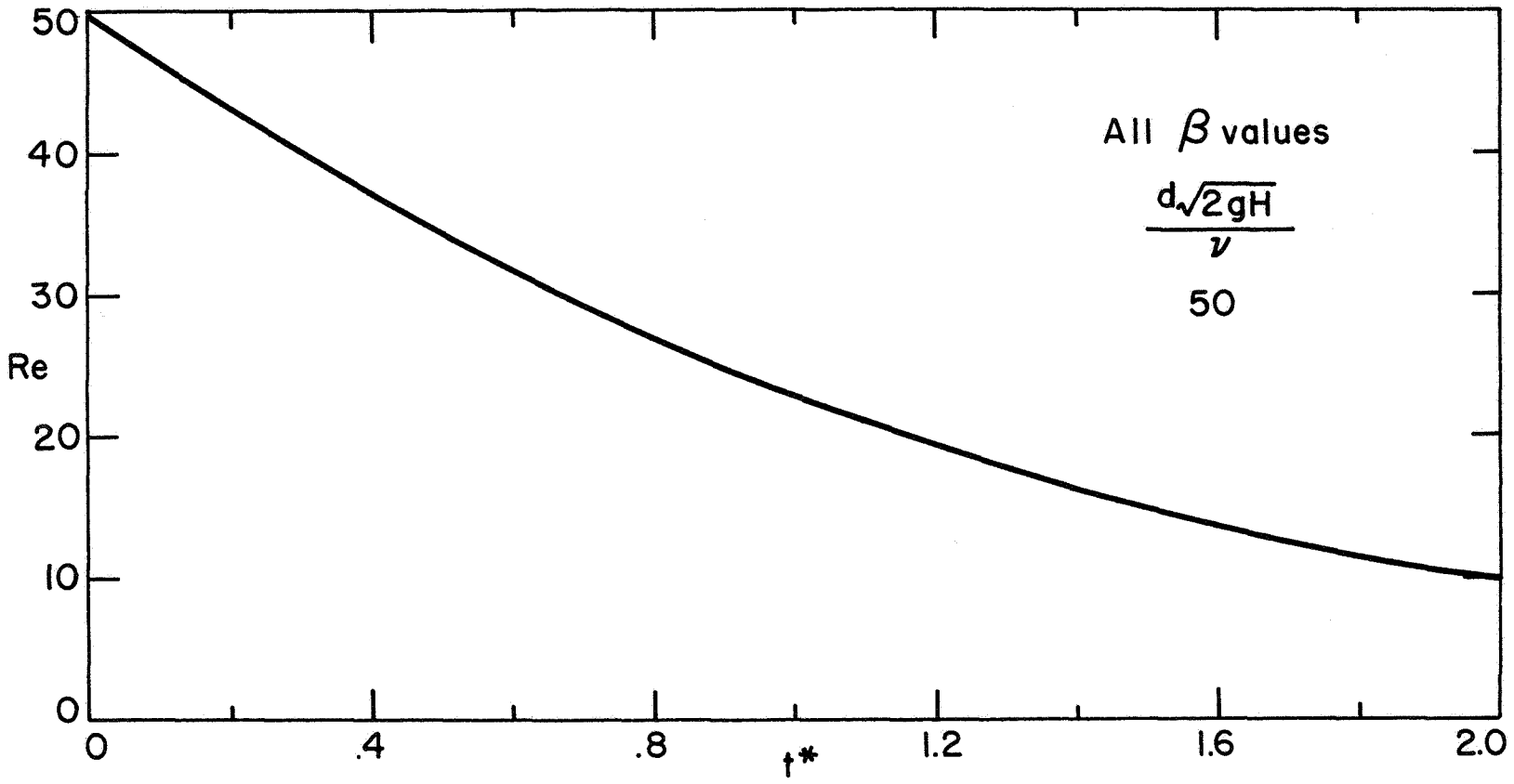

Figure 5.20. Variation of Reynolds Number ($Re = d\sqrt{2gy}/\nu$) with Dimensionless Time (t^*) for Discharge Through an Orifice when $d\sqrt{2gH}/\nu = 50.0$ (Quasi-Steady Flow Analysis)

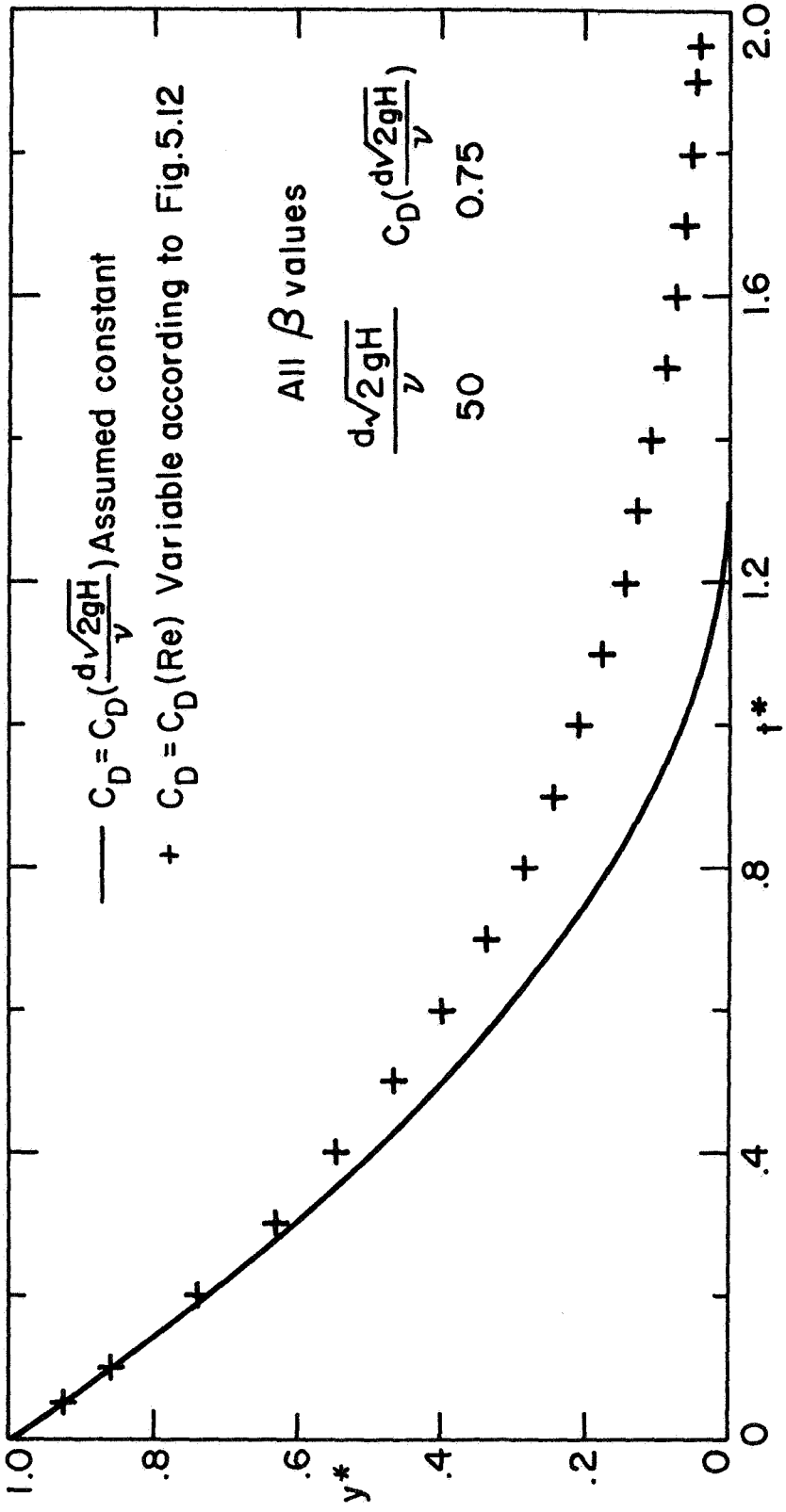

Figure 5.21. Effect of Variation of C_D with Re on y^* vs. t^* for Discharge Through an Orifice when $d\sqrt{2gH}/\nu = 50.0$ (Quasi-Steady Flow Analysis)

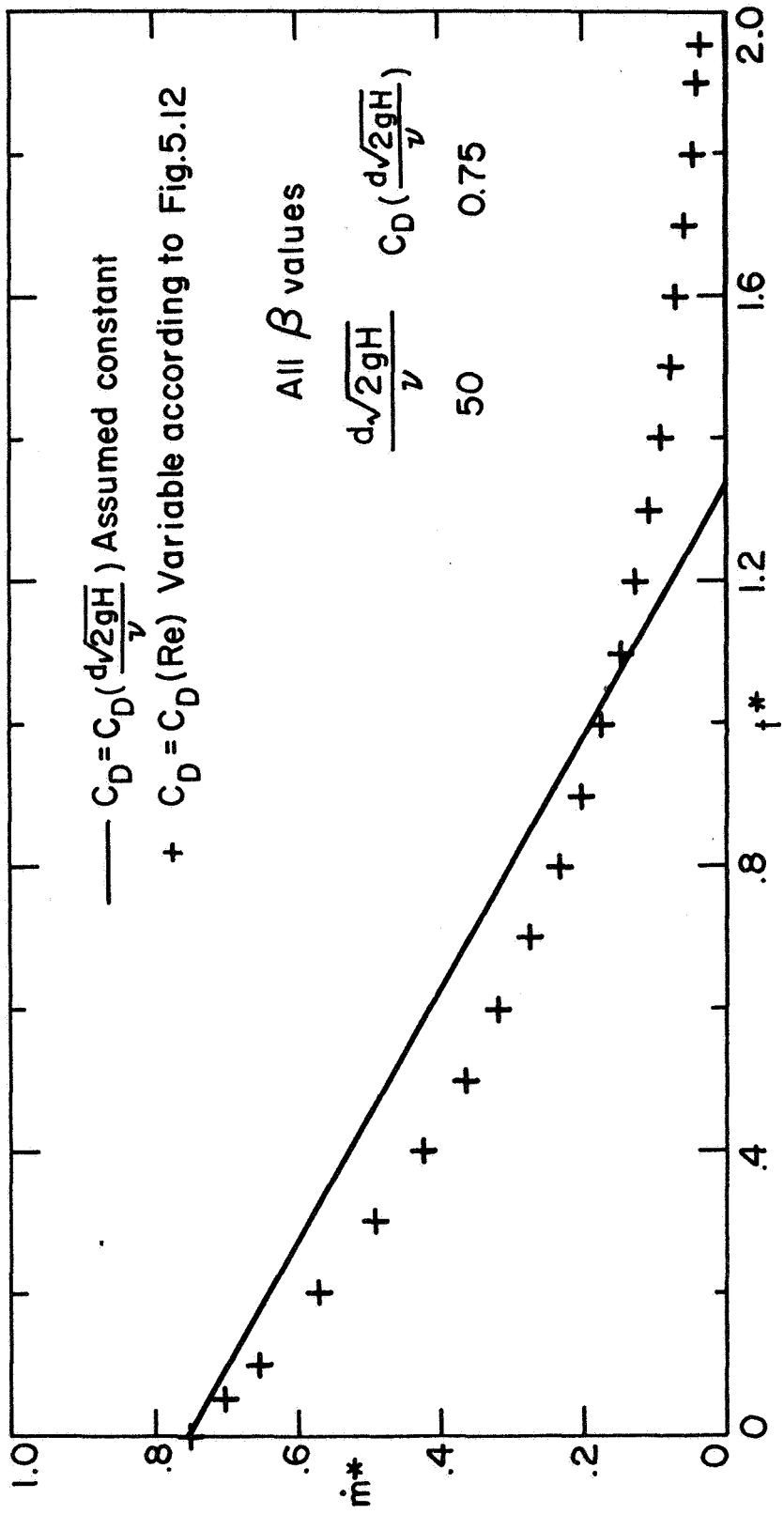

Figure 5.22. Effect of Variation of C_D with Re on $\dot{m}^*$ vs. t^* for Discharge Through an Orifice when $d\sqrt{2gH}/\nu = 50.0$ (Quasi-Steady Flow Analysis)

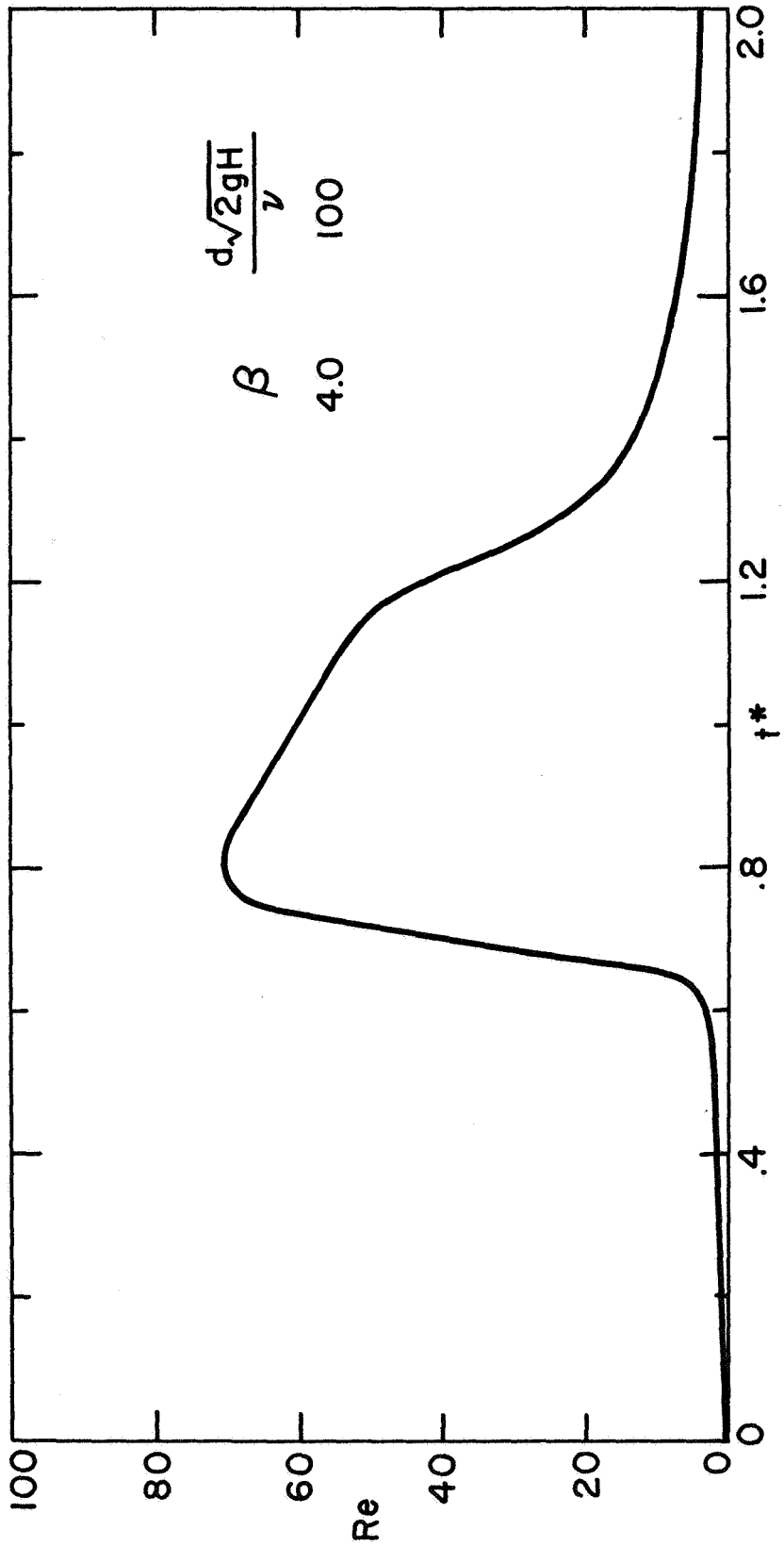

Figure 5.23. Variation of Reynolds Number ($Re = dV_2/\nu$) with Dimensionless Time (t^*) for Discharge Through an Orifice when $d\sqrt{2gH}/\nu = 100.0$ (Transient Flow Analysis)

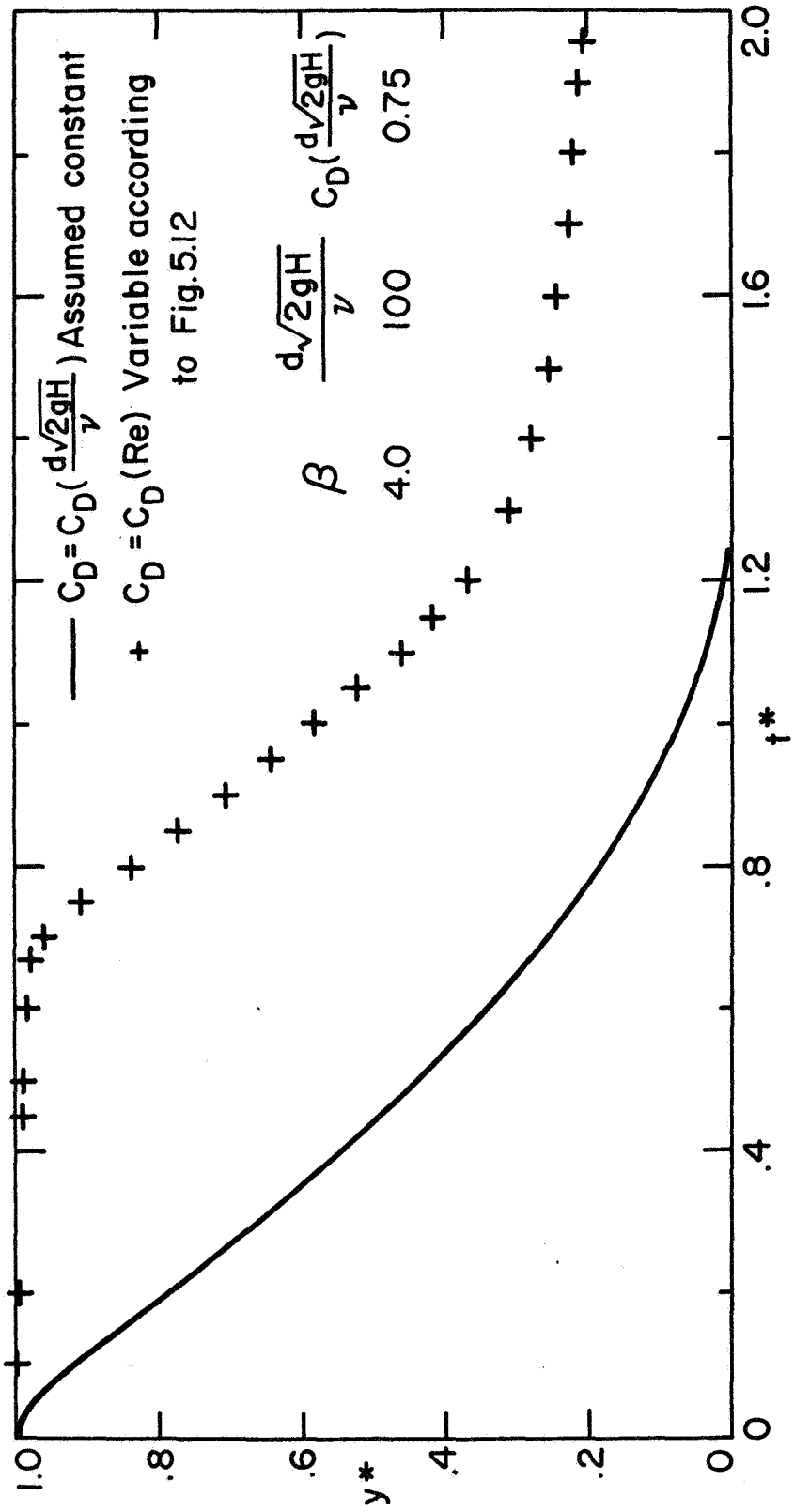

Figure 5.24. Effect of Variation of C_D with Re on y^* vs. t^* for Discharge Through an Orifice when $d\sqrt{2gH}/\nu = 100.0$ (Transient Flow Analysis)

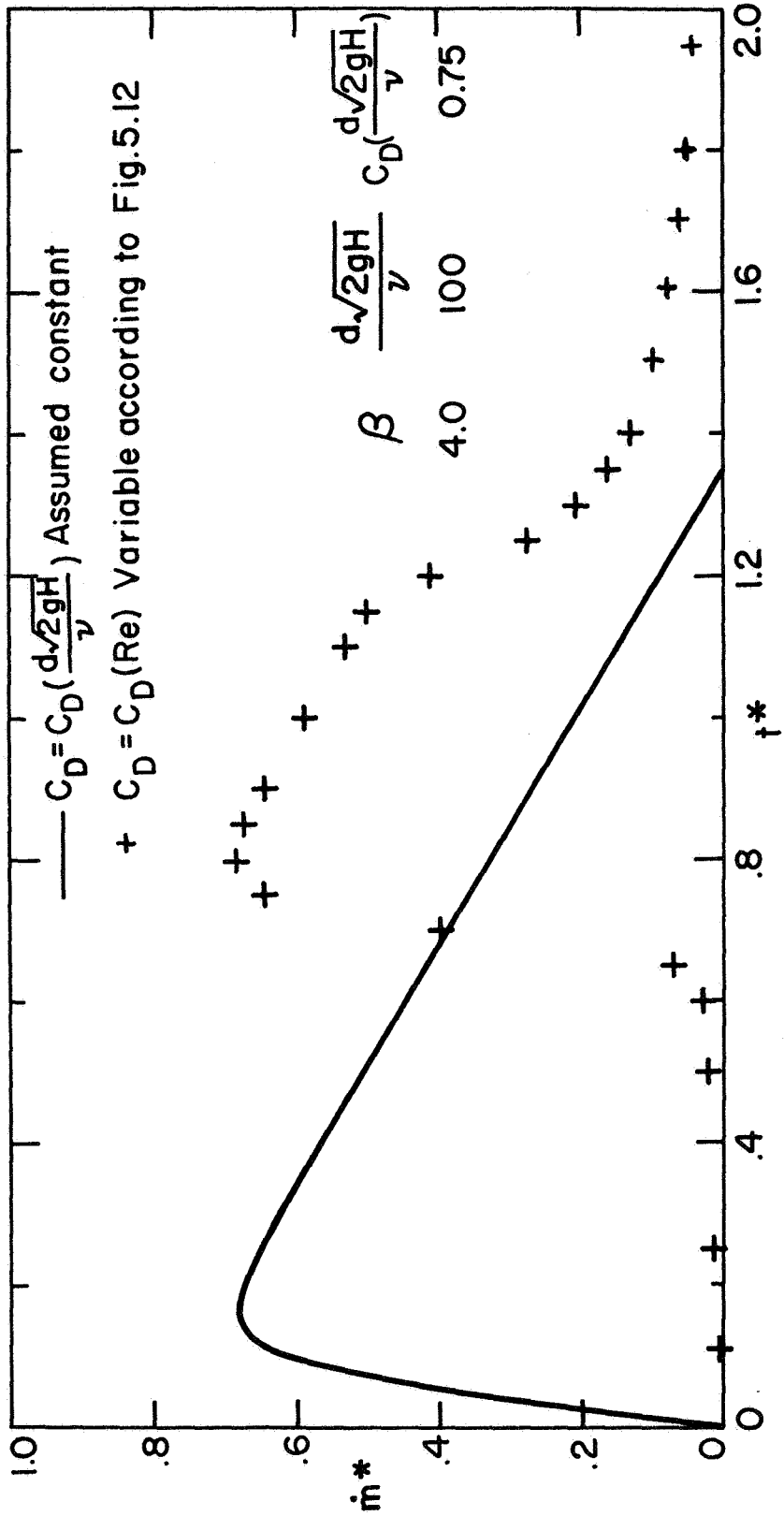

Figure 5.25. Effect of Variation of C_D with Re on $\dot{m}^*$ vs. t^* for Discharge Through an Orifice when $d\sqrt{2gH}/\nu$ = 100.0 (Transient Flow Analysis)

CHAPTER 6

LIQUID DISCHARGE THROUGH A TUBE

Quasi-Steady Discharge Through a Tube

The previously presented analytical results apply to liquid discharge through an opening at the bottom of the container (Figure 5.1) and correspond to the special case of $\frac{L}{d} = 0$. In this section, discharge of a liquid from a container through a tube is considered. The analysis is based on quasi-steady type flow, which accounts for all of the physical effects except those due to local acceleration. It can be recalled that the local acceleration effects were found to be important only if the size of the discharge opening approaches the cross-sectional area of the container ($\beta < 20$). This case, where the local acceleration effects are taken into account, is presented in the next section.

The physical effects associated with the procedure outlined above are summarized in the following table.

Table 6.1: Physical Effects

Forces		Fluid Acceleration	
[x]	Boundary Forces	[ ]	Local Acceleration
[x]	Gravity Forces		
[x]	Forces due to External Pressure Drop	[x]	Convective Acceleration
[x]	Viscous Forces		

The details are presented in Appendix C and the results are discussed herein. According to equations (C7b) and (C8b) the variation of the dimensionless liquid height and the dimensionless mass flow rate with dimensionless time are respectively given by

$$y^* = 1 - \left(\frac{C_2 + C_3}{C_1}\right)^{\frac{1}{2}} t^* + \frac{C_2}{4C_1} t^{*2} \tag{6.1}$$

and

$$\dot{m}^* = \frac{1}{2}\left(\frac{C_2 + C_3}{C_1}\right)^{\frac{1}{2}} - \frac{C_2}{4C_1} t^* \tag{6.2}$$

where C_1, C_2, and C_3 are defined by equations (C5d). These results are presented graphically in Figures 6.1 through 6.12. In all these cases entrance losses were neglected (K = 0) and the results would apply to discharge through tubes with rounded entrances. When there are no friction and entrance effects, i.e. for the case of ideal discharge of fluids, equations (6.1) and (6.2) reduce to

$$y^* = 1 - 2\left(1 + \frac{P_1 - P_2}{\rho g H} + \frac{L}{H}\right)^{\frac{1}{2}} t^* + t^{*2} \tag{6.3}$$

and

$$\dot{m}^* = \left(1 + \frac{P_1 - P_2}{\rho g H} + \frac{L}{H}\right)^{\frac{1}{2}} - t^* \tag{6.4}$$

indicating that both y^* and $\dot{m}^*$ are independent of the parameters β and $\frac{L}{d}$. These results are depicted in Figures 6.1 and 6.2.

Even when the friction factor, f, is not zero variations in β and $\frac{L}{d}$ have only a small effect on the variations of y^* and $\dot{m}^*$ with t^*. According to Figure 6.3 when β is changed from 20 to 1, the change in total

dimensionless discharge time is only about 2.3%. Similarly, when $\frac{L}{d}$ is altered from 1 to 10, total time of discharge[1] is changed by about 2.5% (Figure 6.5). However, Figure 6.7 indicates that when $\frac{L}{H}$ is increased from 0.1 to 1.0 the total discharge time is decreased from 0.667 to 0.405, a change of about 40%. This is due to the smaller quantity of liquid to be discharged from the container. Also, when the external pressure drop $(P_1 - P_2)$ is increased, the mass flow rates are increased and the total discharge times are decreased (Figures 6.9 and 6.10). Figures 6.11 and 6.12 show that an increase in the friction factor, which is in part dependent on the Reynolds number $\frac{d\sqrt{2gH}}{\nu}$, causes a flow retardation, a result that is to be expected. The results presented here were obtained by assuming f to be constant for the entire process. A method for choosing a suitable constant value for f for a given set of experimental conditions is described in Chapter 7.

In general it is seen that when the local acceleration effects are neglected, changing the value of β has very little effect on the instantaneous mass flow rates and the total discharge times. For the case of discharge through an orifice it was shown that even though the total dimensionless discharge time remained essentially constant for $\beta > 2$ the instantaneous mass flow rates were very much different from those predicted by the quasi-steady analysis. Also, these varied considerably with β, the fluid taking more time to accelerate to its maximum velocity when β is decreased. For this reason, an analysis accounting for local acceleration effects is presented in the following section of the report for the case of discharge through a tube.

---

[1] In this discussion total discharge time refers to the dimensionless quantity, $t_t/\beta\sqrt{2H/g}$.

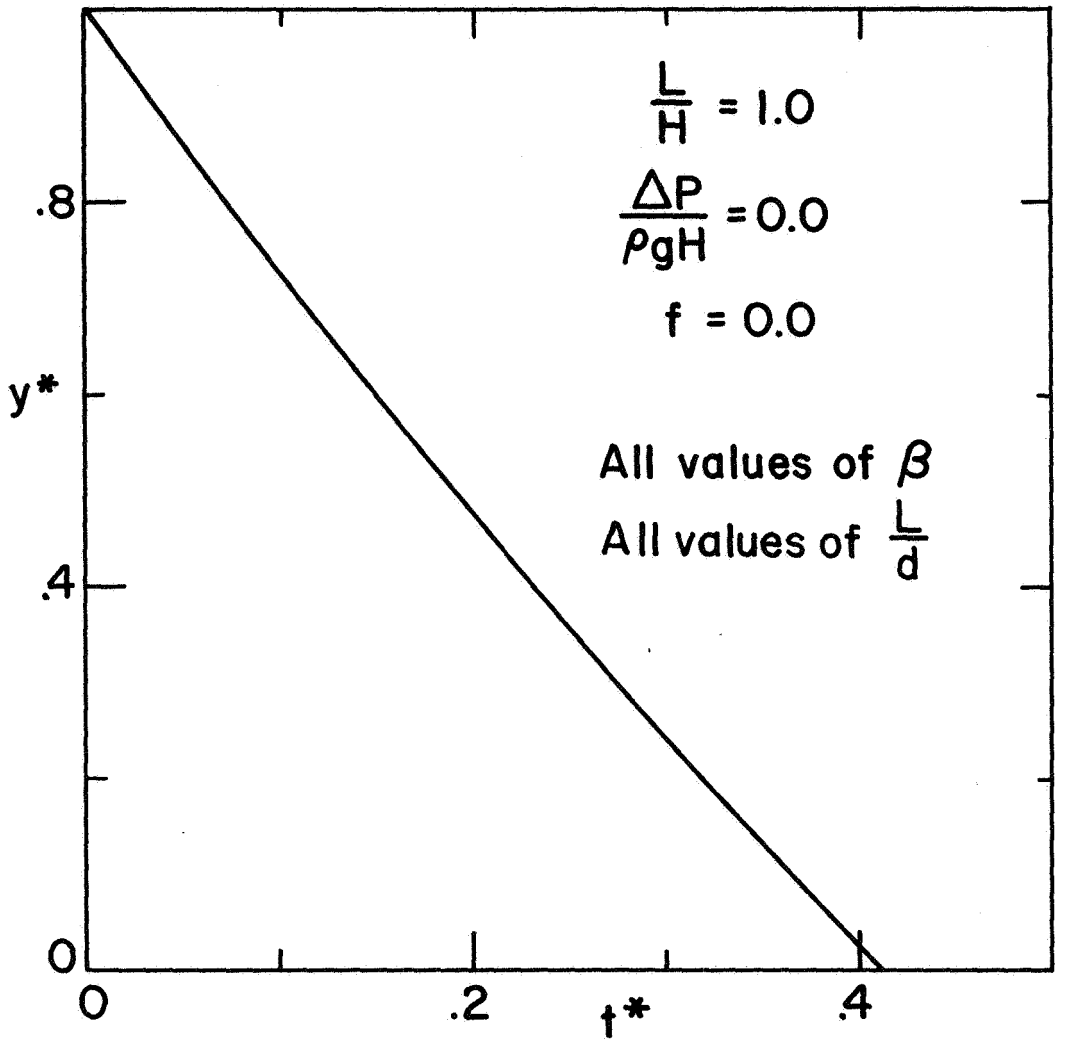

Figure 6.1. Variation of Dimensionless Liquid Height (y*) with Dimensionless Time (t*) for All Values of the Parameters β and L/d when f = 0

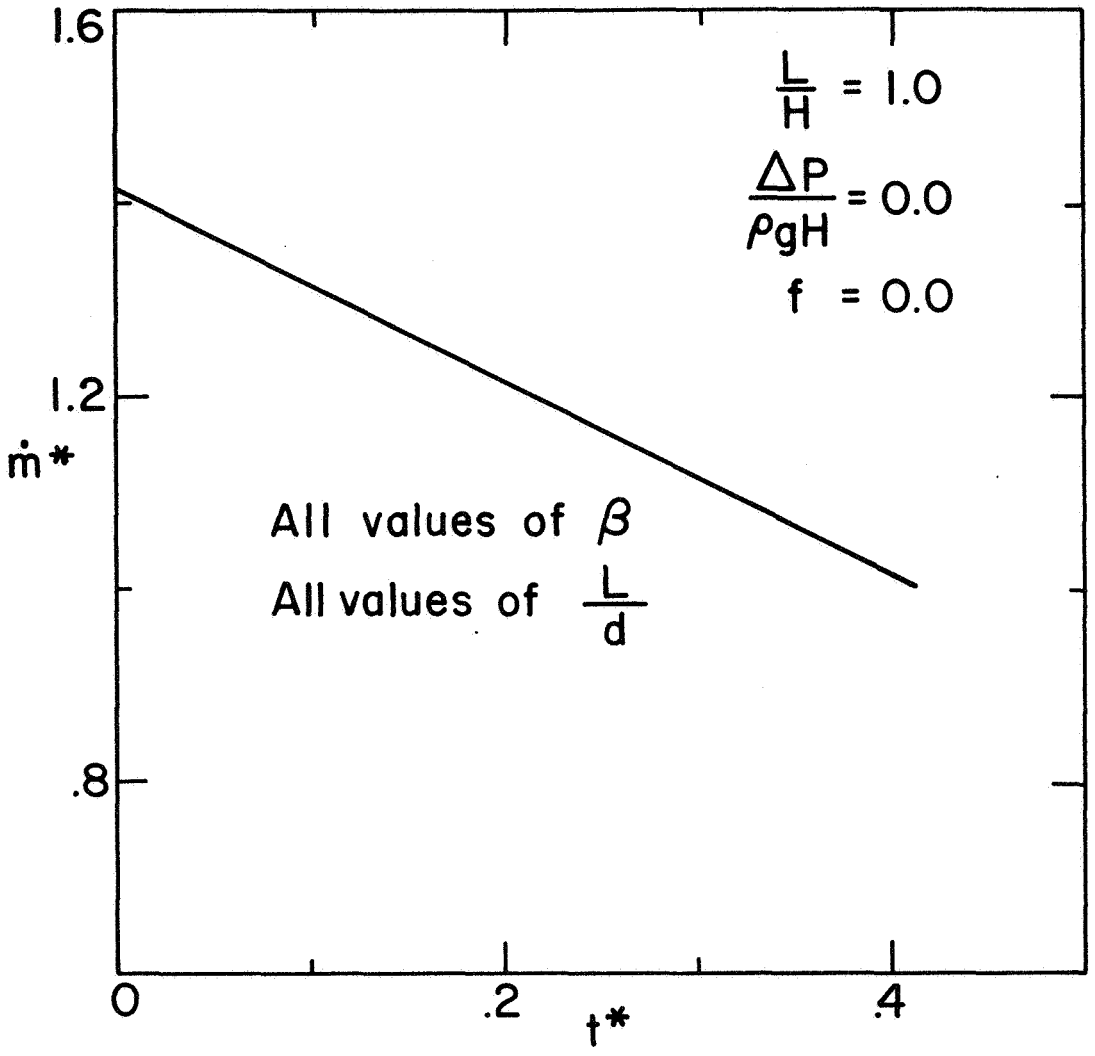

Figure 6.2. Variation of Dimensionless Mass Flow Rate ($\dot{m}^*$) with Dimensionless Time (t^*) for All Values of β and L/d when f = 0

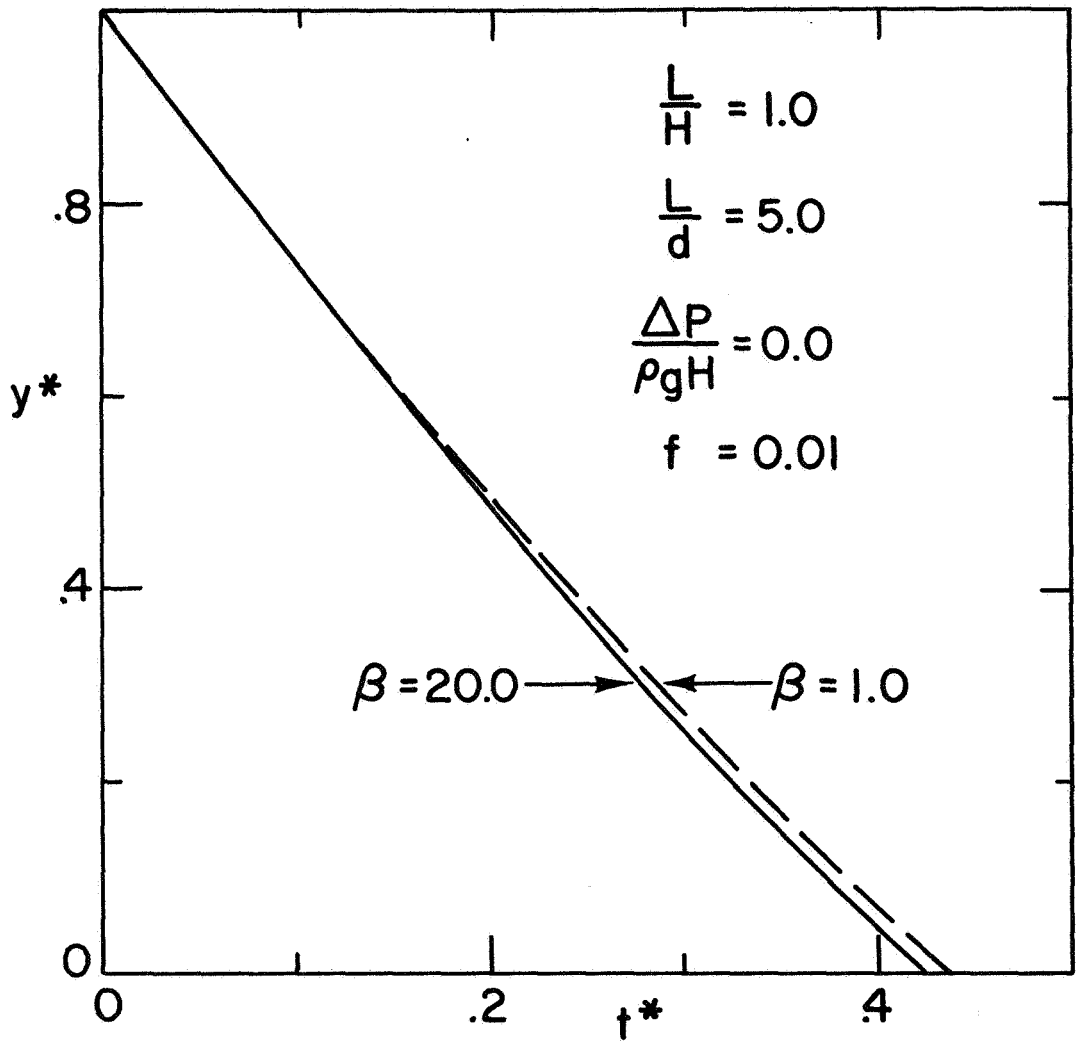

Figure 6.3. Variation of y^* with t^* for Various Values of the Parameter β when Friction Factor $f \neq 0$

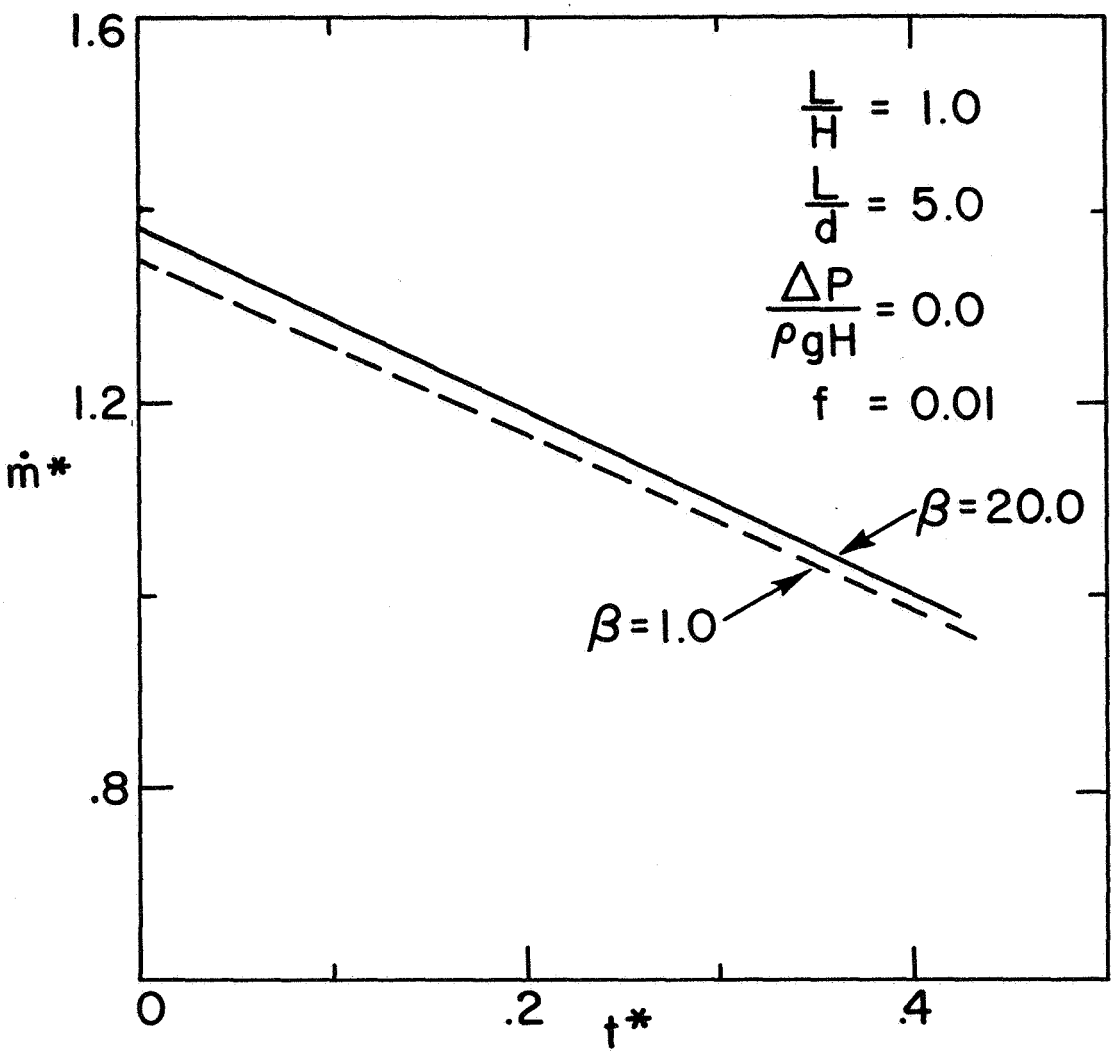

Figure 6.4. Variation of $\dot{m}^*$ with t^* for Various Values of the Parameter β when Friction Factor $f \neq 0$

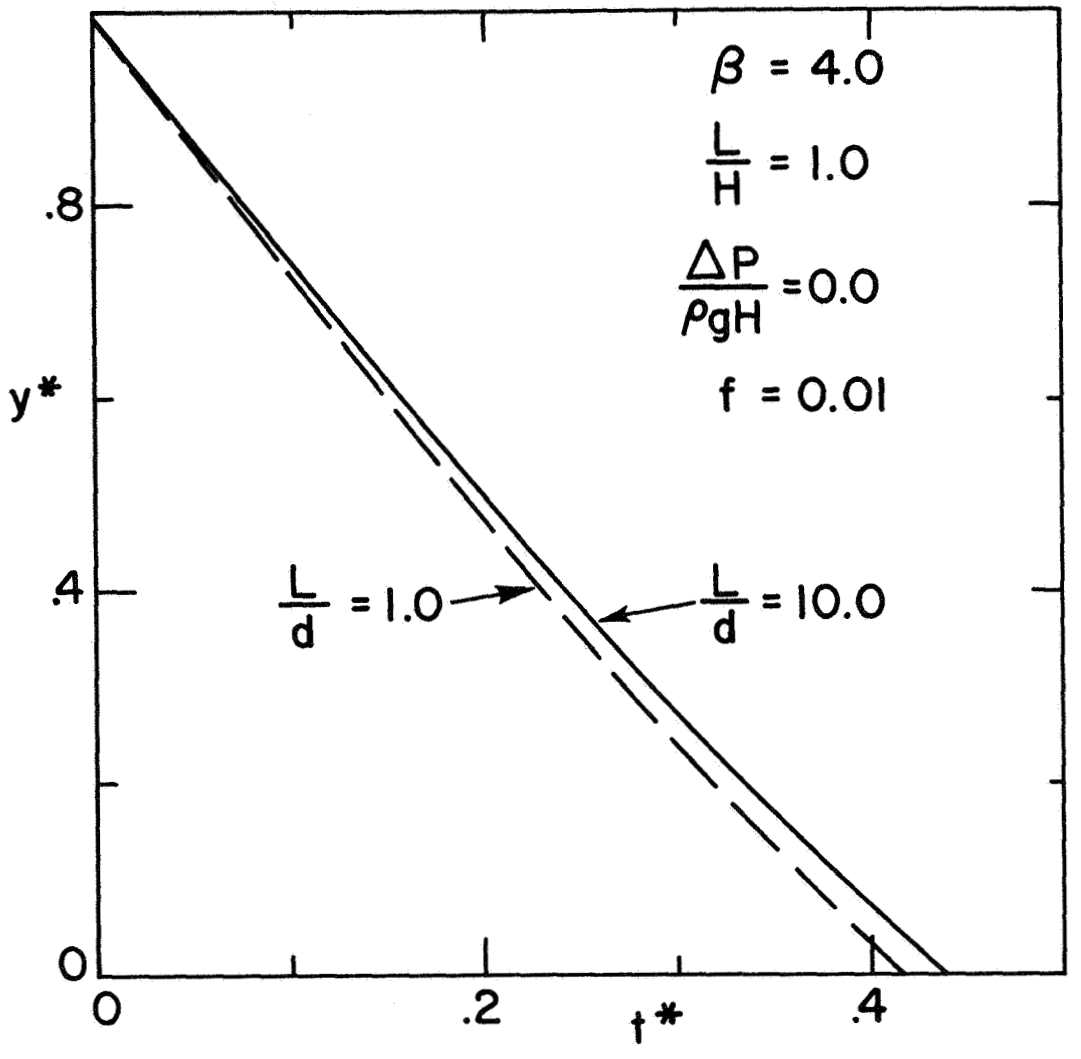

Figure 6.5. Variation of y* with t* for Various Values of the Parameter L/d when f ≠ 0

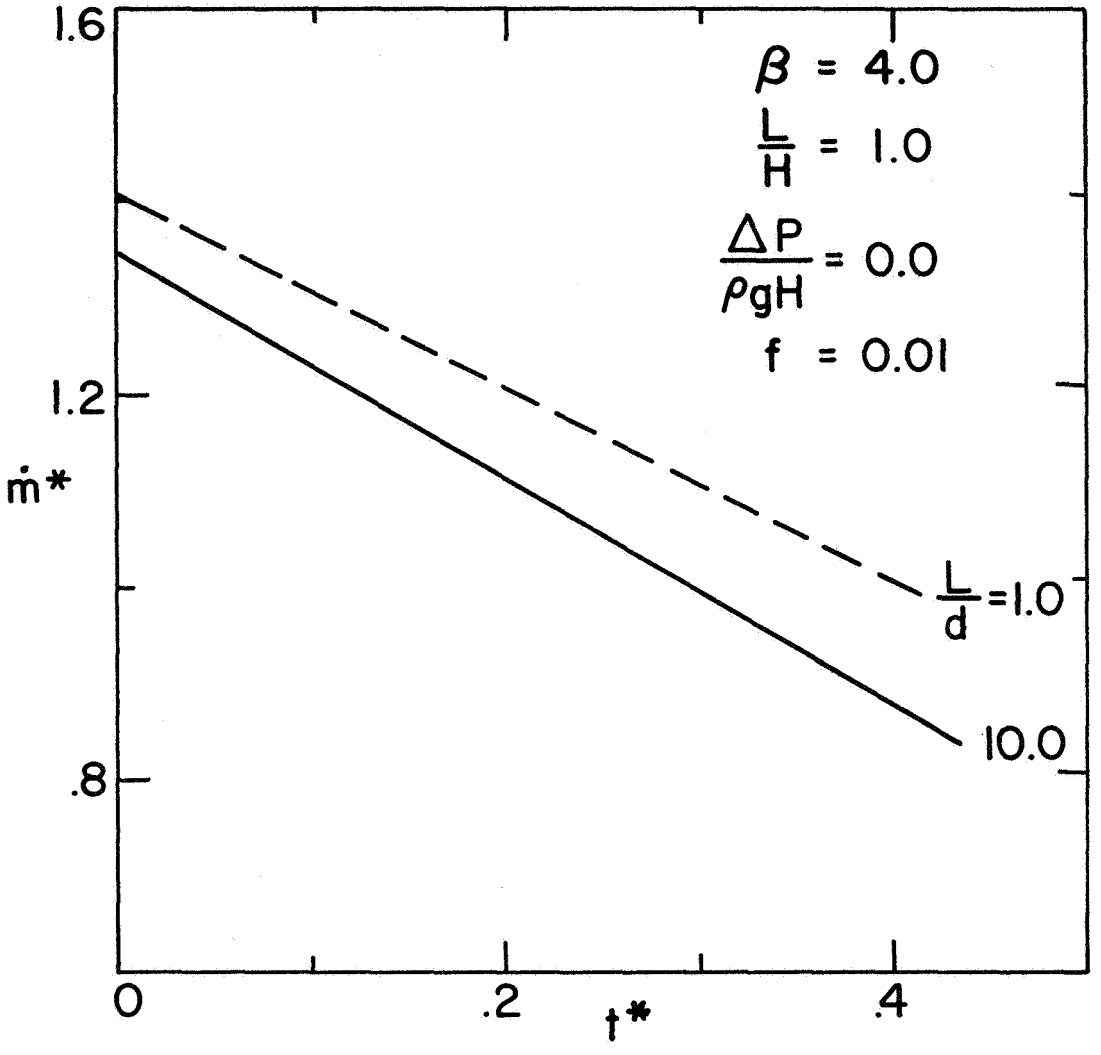

Figure 6.6. Variation of $\dot{m}^*$ with t^* for Various Values of the Parameter L/d when $f \neq 0$

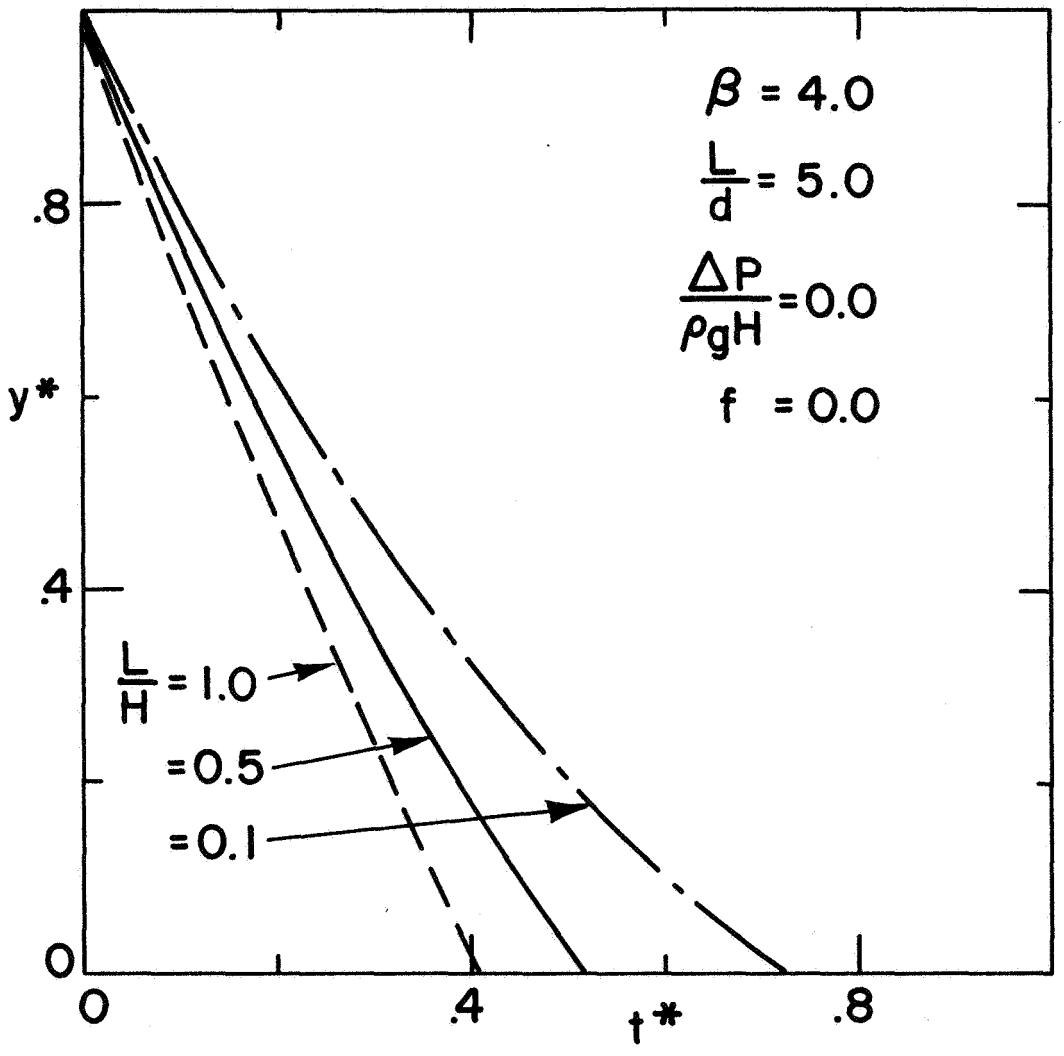

Figure 6.7. Variation of y* with t* for Various Values of the Parameter L/H

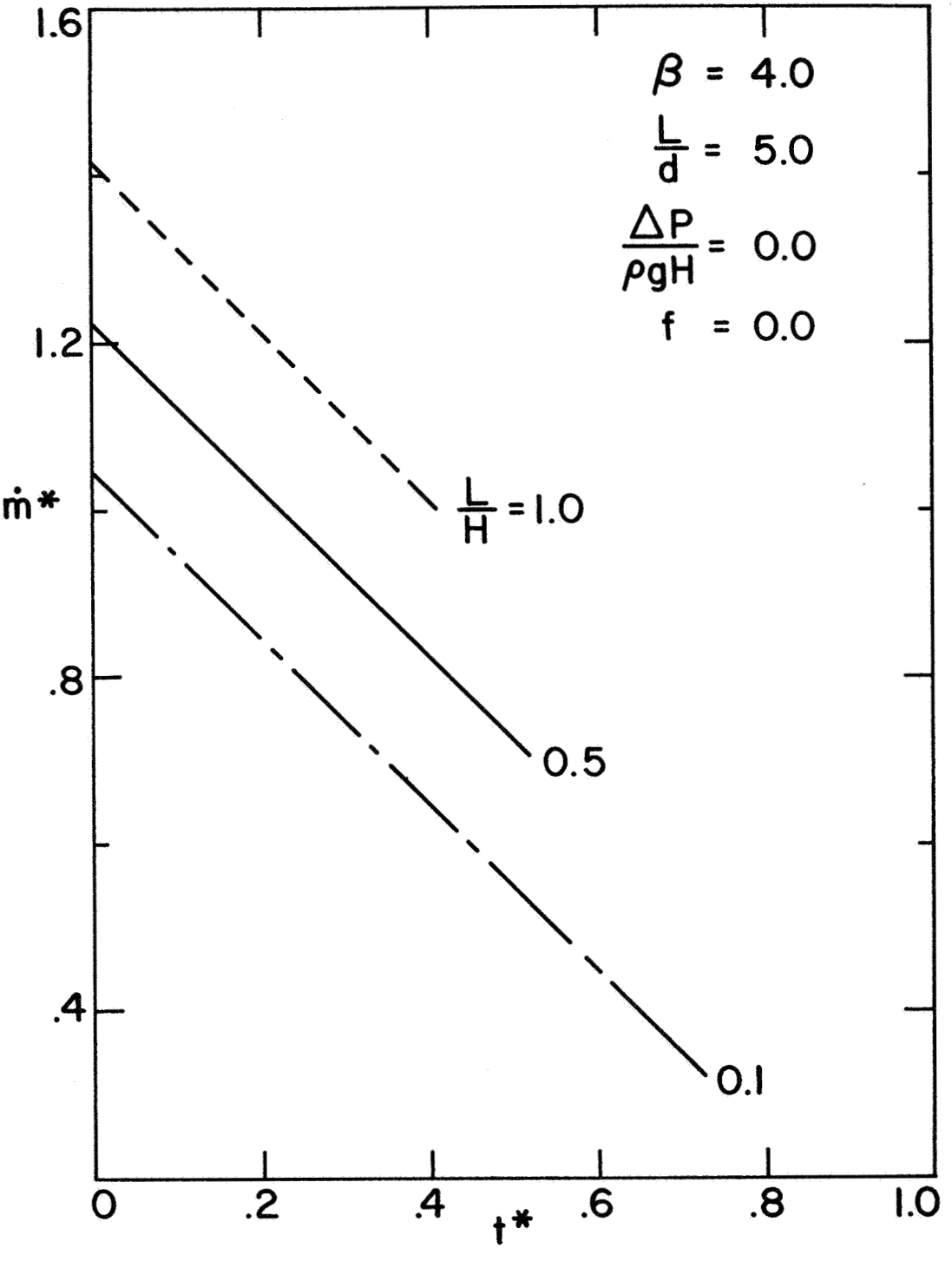

Figure 6.8. Variation $\dot{m}^*$ with t^* for Various Values of the Parameter L/H

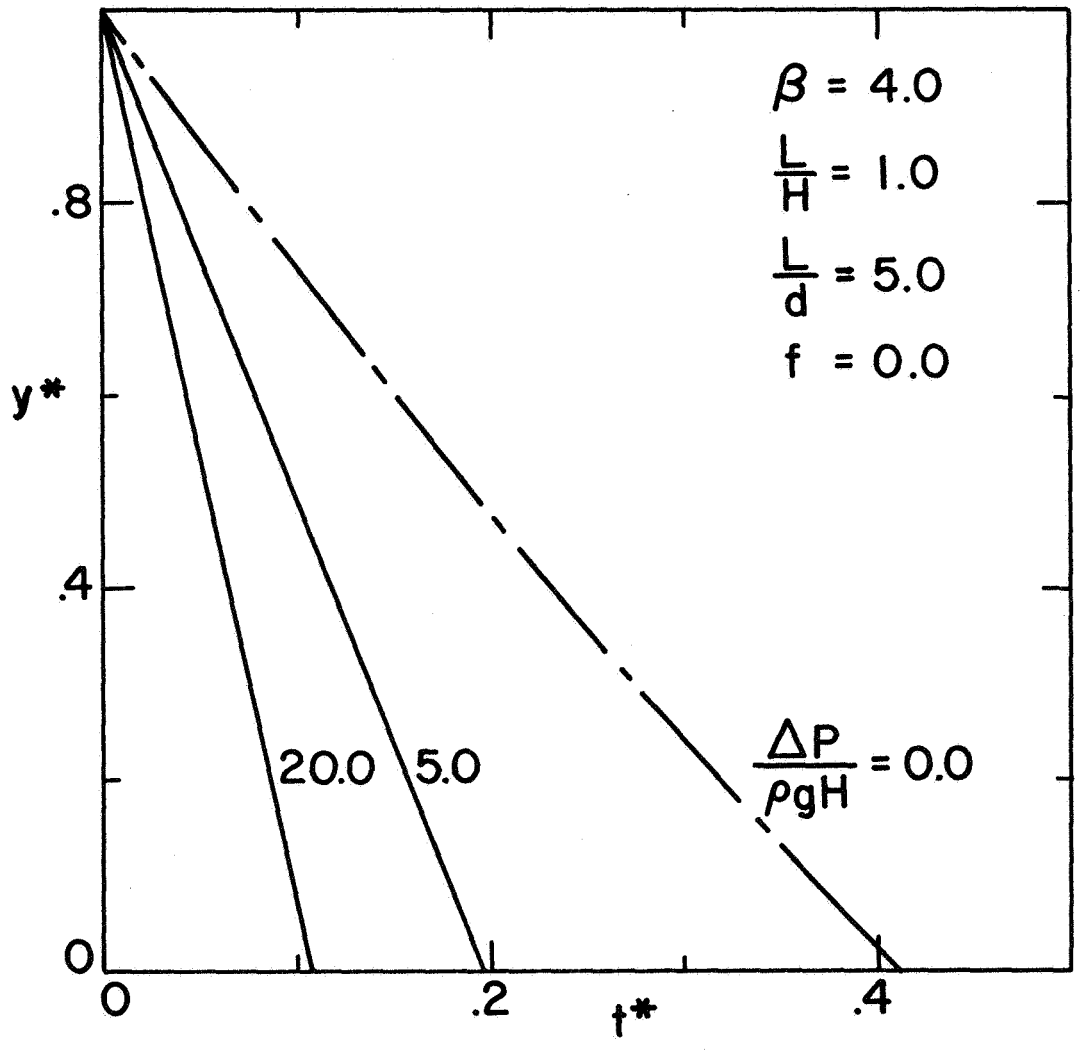

Figure 6.9. Variation of y* with t* for Various Values of the Parameter $\Delta P/\rho gH$

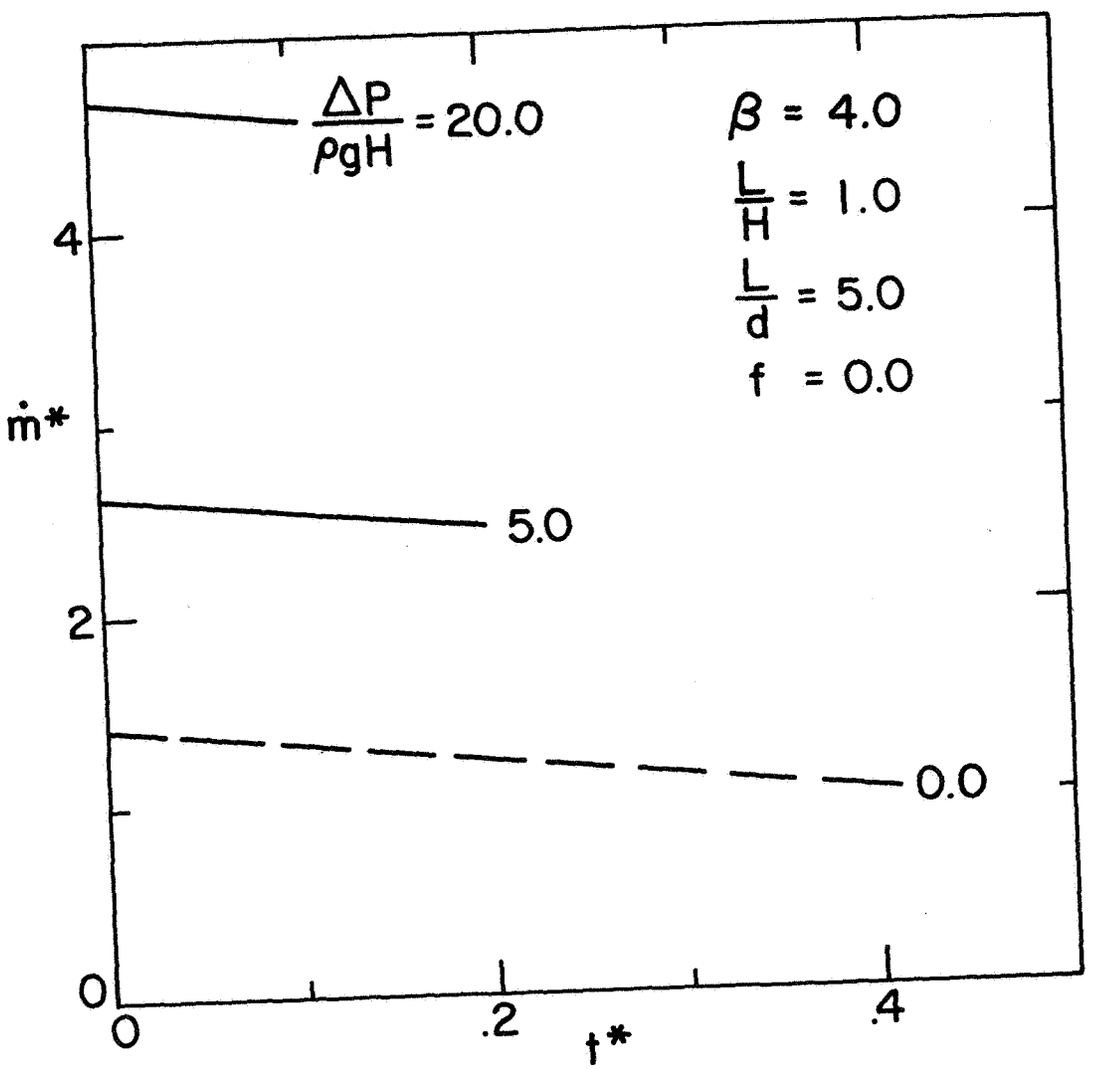

Figure 6.10. Variation of $\dot{m}^*$ with t^* for Various Values of the Parameter $\Delta P/\rho gH$

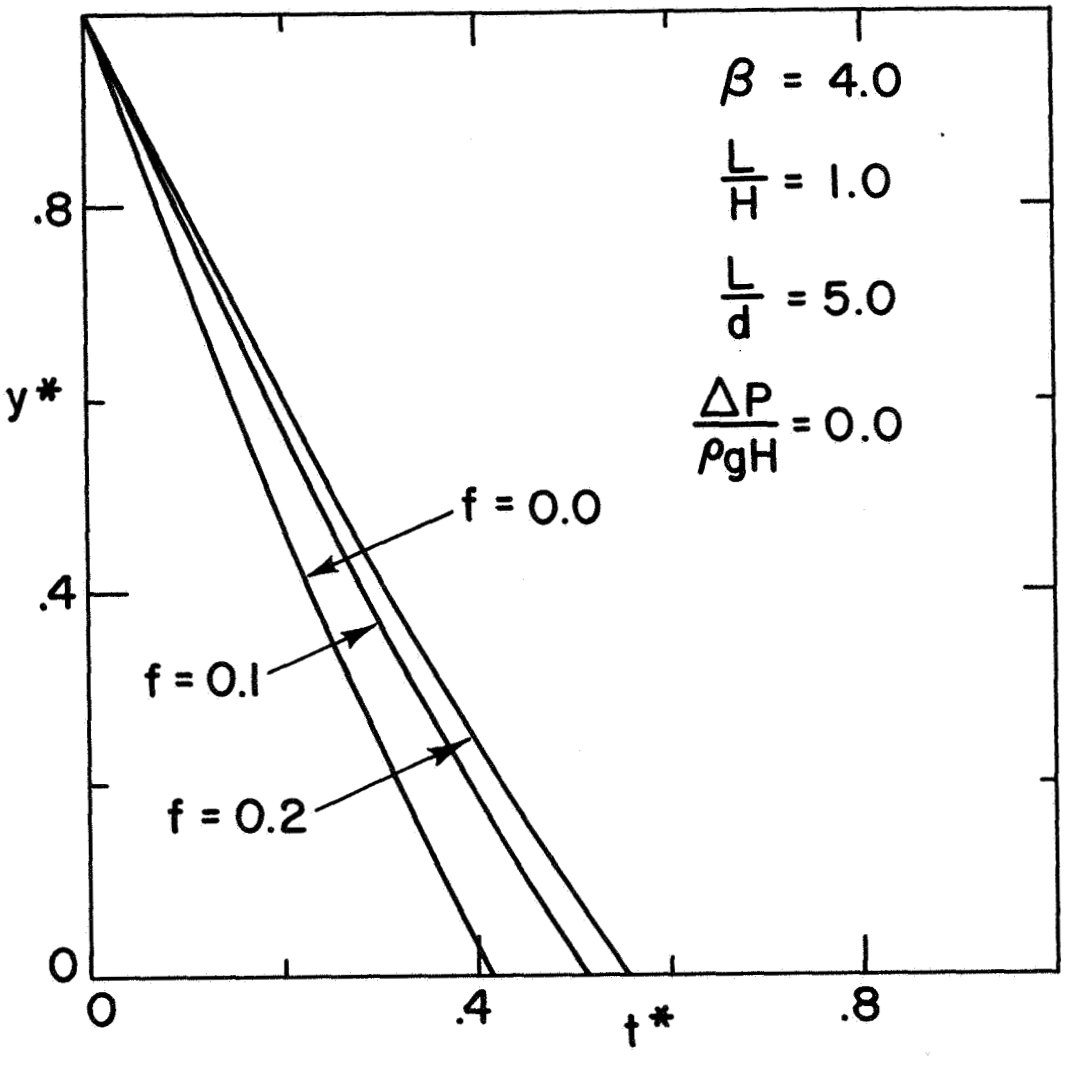

Figure 6.11. Variation of y* with t* for Various Values of the Parameter f

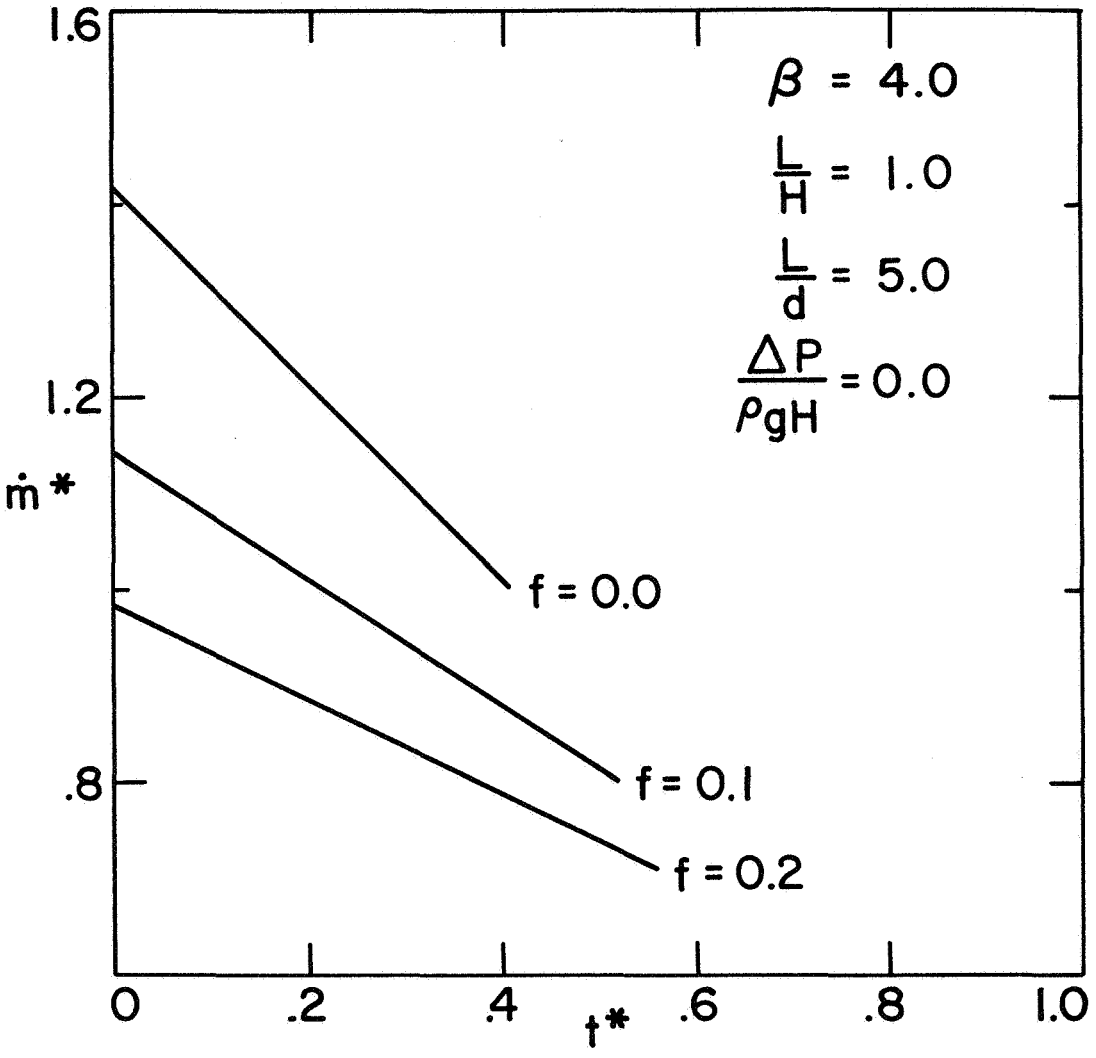

Figure 6.12. Variation of $\dot{m}^*$ with t^* for Various Values of the Parameter f

Transient Discharge Through a Tube

In this section of the report an analysis of transient discharge of a container through a tube, which takes local acceleration effects into account, is presented. Forces due to viscous shear and external pressure drop are also considered. These conditions are summarized in the following table.

Table 6.2: Physical Effects

Forces		Fluid Acceleration	
[x]	Boundary Forces	[x]	Local Acceleration
[x]	Gravity Forces		
[x]	Forces due to External Pressure Drop	[x]	Convective Acceleration
[x]	Viscous Forces		

It is assumed that:

1) the flow is one dimensional
2) the flow is incompressible and single-phase
3) the surface of the fluid is horizontal at all times
4) friction and inertia effects in the container are negligible, so that the pressure at the entrance to the tube is given by Bernoulli's equation.[2]

[2] This assumption is valid only if the discharge tube diameter is small enough, relative to the container diameter, so that the frictional and inertial effects associated with the higher velocity levels in the tube outweigh these same effects for the fluid in the container.

5) the friction coefficient for flow through the tube is constant during the transient flow period.

6) energy dissipation corresponding to entrance losses at the tube inlet are negligible, unless otherwise specified.[3]

Figure 6.13 shows the system configuration at a particular instant of time. The principle of conservation of momentum is applied to the fluid within the control volume shown in dashed lines surrounding the fluid in the tube. Thus,

$$\begin{bmatrix}\text{Rate of increase}\\ \text{of momentum of the}\\ \text{fluid in the C.V.}\end{bmatrix} + \begin{bmatrix}\text{Net Flux of}\\ \text{momentum}\\ \text{out of C.V.}\end{bmatrix} = \begin{bmatrix}\text{Net Force}\\ \text{Acting on}\\ \text{the C.V.}\end{bmatrix} \qquad (6.5)$$

By continuity (since the fluid is incompressible) the mass of fluid entering the control volume, $\rho A(-\frac{dy}{dt})$, is the same as that leaving the volume. Since the tube has a constant cross-sectional area, the instantaneous velocities of inflow and outflow are equal. Hence the net momentum flux across the boundaries of the control volume is zero. By assumptions (4) and (6), the pressure at Q is given by

$$P_1' = P_1 + \rho g y - \frac{1}{2}\rho\beta^2 \left(\frac{dy}{dt}\right)^2 \qquad (6.6)$$

where

$$\beta = \sqrt{\left(\frac{A}{a}\right)^2 - 1}$$

---

[3] Although this assumption is made here for the sake of simplicity in presenting the essential features of the analysis, entrance losses can be taken into account as in the case of Quasi-Steady Discharge through a Tube (See equation (C1)). They were introduced into the calculations made for sharp-edged entrances (See Chapter 7).

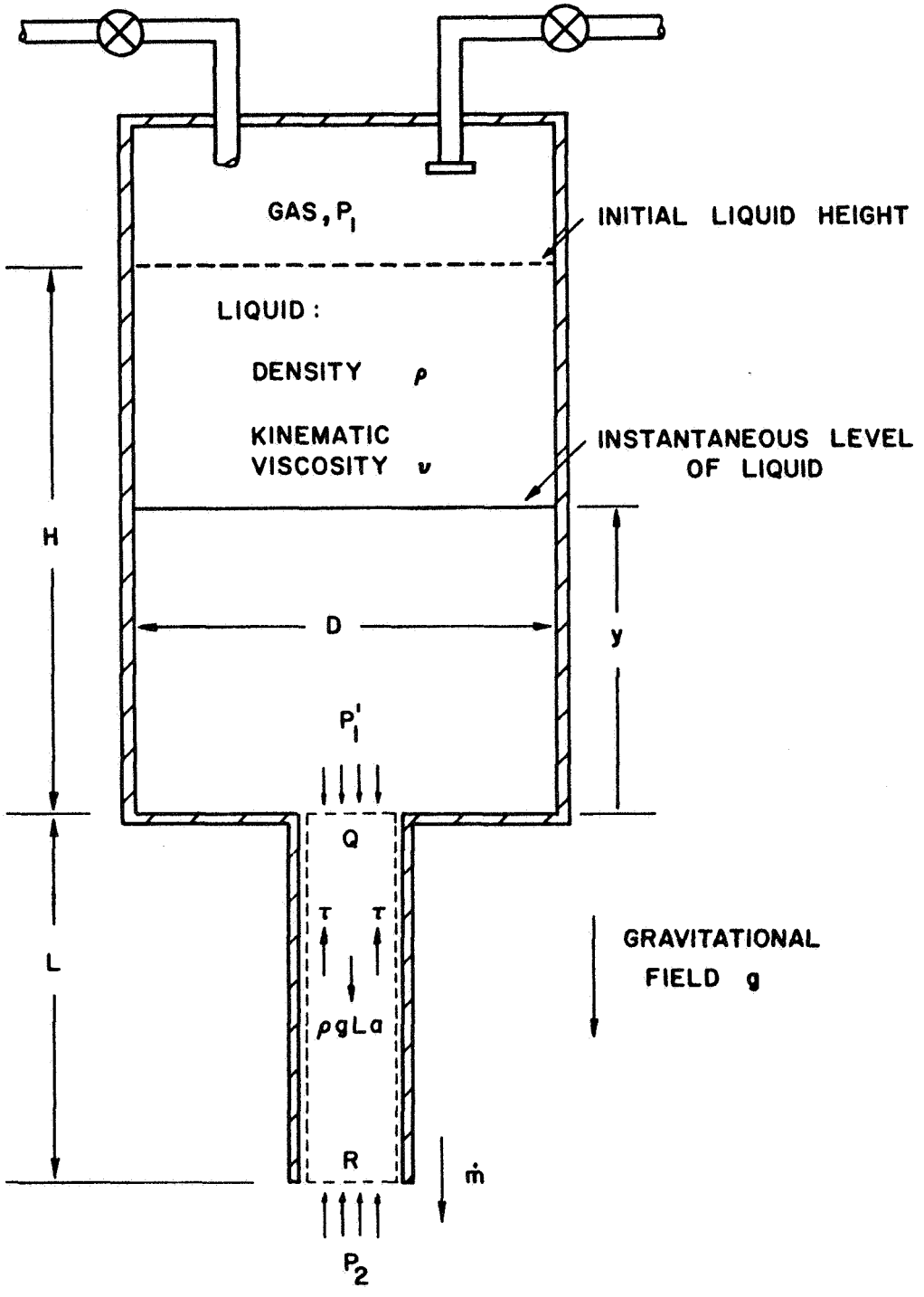

Figure 6.13. System Configuration at Any Instant of Time

The fifth assumption yields the frictional force (Ref. 33) on the control volume as

$$F_f = \tau \cdot \pi d \cdot L = \frac{1}{8} f \rho (-\frac{A}{a} \frac{dy}{dt})^2 \cdot \pi d \cdot L \qquad (6.7)$$

Finally, the momentum of the fluid within the control volume is given by $[\rho aL(-\frac{A}{a} \frac{dy}{dt})]$. The net force on the control volume includes the gravity force ρgaL (i.e., the weight of the fluid). Consideration of this force along with the pressure and viscous forces makes it possible to rewrite equation (6.5) as

$$\frac{d}{dt} [\rho aL(-\frac{A}{a} \frac{dy}{dt})] = [P_1 + \rho gy - \frac{1}{2} \rho \beta^2 (\frac{dy}{dt})^2] a - P_2 a$$
$$- \frac{1}{8} f \cdot \rho \cdot (-\frac{A}{a} \frac{dy}{dt})^2 \cdot \pi d \cdot L + \rho gaL \qquad (6.8)$$

After dividing equation (6.8) by $(-\rho A)$ and rearranging terms, the relationship becomes

$$L \frac{d^2y}{dt^2} - \frac{1}{2} [\beta^2 \frac{a}{A} + f \frac{A}{a} \frac{L}{d}] (\frac{dy}{dt})^2 + g \frac{a}{A} y$$
$$= - [\frac{P_1 - P_2}{\rho} + gL] \frac{a}{A} \qquad (6.9)$$

Equation (6.9) describes the variation of height of the liquid in the container as a function of time for the case of discharge through a tube under the assumptions listed previously. The initial conditions for the problem are $y = H$ and $\frac{dy}{dt} = 0$ at $t = 0$. By introducing the dimensionless time, t^*, and dimensionless liquid height, y^*, as defined by equations (5.3), equation (6.9) is expressed in dimensionless form as

$$\frac{L}{H}\frac{d^2y^*}{dt^{*2}} - \frac{1}{2}\left[\beta^2\frac{a}{A} + f\frac{A}{a}\frac{L}{d}\right]\left(\frac{dy^*}{dt^*}\right)^2 + 2\beta^2\frac{a}{A}y^*$$

$$= -2\left[\frac{P_1-P_2}{\rho gH} + \frac{L}{H}\right]\frac{a}{A}\beta^2 \qquad (6.10)$$

Now the initial conditions become $y^* = 1.0$ and $\frac{dy^*}{dt^*} = 0$ at $t^* = 0$.

It can be shown from equation (6.10) that the dimensionless liquid height, y^*, and the dimensionless mass flow rate, $\dot{m}^*$, are functions of all the dimensionless parameters obtained in Chapter 3. Note that β and $\frac{A}{a}$ are functions of $\frac{D}{d}$. The friction factor, f, which can be obtained from the Moody Chart (Ref. 3), is mainly a function of the characteristic Reynolds number $\frac{d\sqrt{2gH}}{\nu}$ and $\frac{dy^*}{dt^*}$ for the range of conditions studied experimentally in this investigation.[4] This means in general it is also dependent on the other dimensionless parameters $\frac{\Delta P}{\rho gH}$, $\frac{D}{d}$, $\frac{L}{d}$, and $\frac{L}{H}$. For any given geometry the ratios $\frac{L}{H}$, $\frac{A}{a}$, β, $\frac{L}{d}$, f and $\frac{\Delta P}{\rho gH}$ are known and the coefficients for the various derivatives in the above differential equation can be calculated. Equation (6.10) was solved by a Fourth-Order Runge-Kutta method, with the indicated initial conditions, to obtain the dimensionless liquid height and the dimensionless mass flow rate as functions of dimensionless time for various geometries. The numerical integrations were performed on an IBM 7094 computer, and the program is presented in Appendix E. The results are shown in Figures 6.14 through 6.25.

Figures 6.14 and 6.15 show that as β is decreased, the fluid is retarded due to local acceleration effects even when viscous and entrance loss effects are neglected. Decreasing β from 20 to 2 increases the dimensionless discharge time from 0.436 to 0.65 or by about 50%. As the

[4] The results given here were obtained by assuming f to be constant for the entire process. See also "Discussion of the Friction Factor, f" at the end of this Chapter.

discharge area is increased in relation to the container area, the fluid spends more time in accelerating to the maximum discharge rate. When β is increased the results of the present analysis approach those obtained by the quasi-steady type analysis. Even for high β values also the transient analysis gives the initial mass flow rate (at time $t = 0$) as zero, which is a physical fact. However, in this case the fluid accelerates very rapidly to its maximum discharge rate.

Figures 6.16 and 6.17 indicate that when frictional resistance is neglected the parameter $\frac{L}{d}$ has no effect on the discharge process and Figures 6.18 and 6.19 show that even when friction is not zero the influence of $\frac{L}{d}$ is quite small. It can be noted that an increase in $\frac{L}{d}$ from 1 to 10 increases the total discharge time by only about 3%.

As in the case of quasi-steady type flow, variations in the parameter $\frac{L}{H}$ have a large influence on the discharge times, (Figures 6.20 and 6.21). Increasing $\frac{L}{H}$ from 0.1 to 1 decreases the total discharge time by about 28%. It is interesting to note that the curves for the various $\frac{L}{H}$ values cross over. This is due to the fact that for lower values of this parameter, the fluid accelerates faster at the beginning of the discharge process because of the higher initial head. The larger column of fluid, having a higher inertia, requires a greater total time for the discharge.

Figures 6.22 and 6.23 show that for increasing external pressure drop the fluid is discharged faster. Also, the fluid spends a greater percentage of total discharge time in an accelerating condition as $\frac{\Delta P}{\rho g H}$ is increased. For instance, when $\frac{\Delta P}{\rho g H} = 0$ the fluid takes less than 40% of the total time to accelerate to 90% of its peak value. But when $\frac{\Delta P}{\rho g H} = 20$ it takes 50% of the total time.

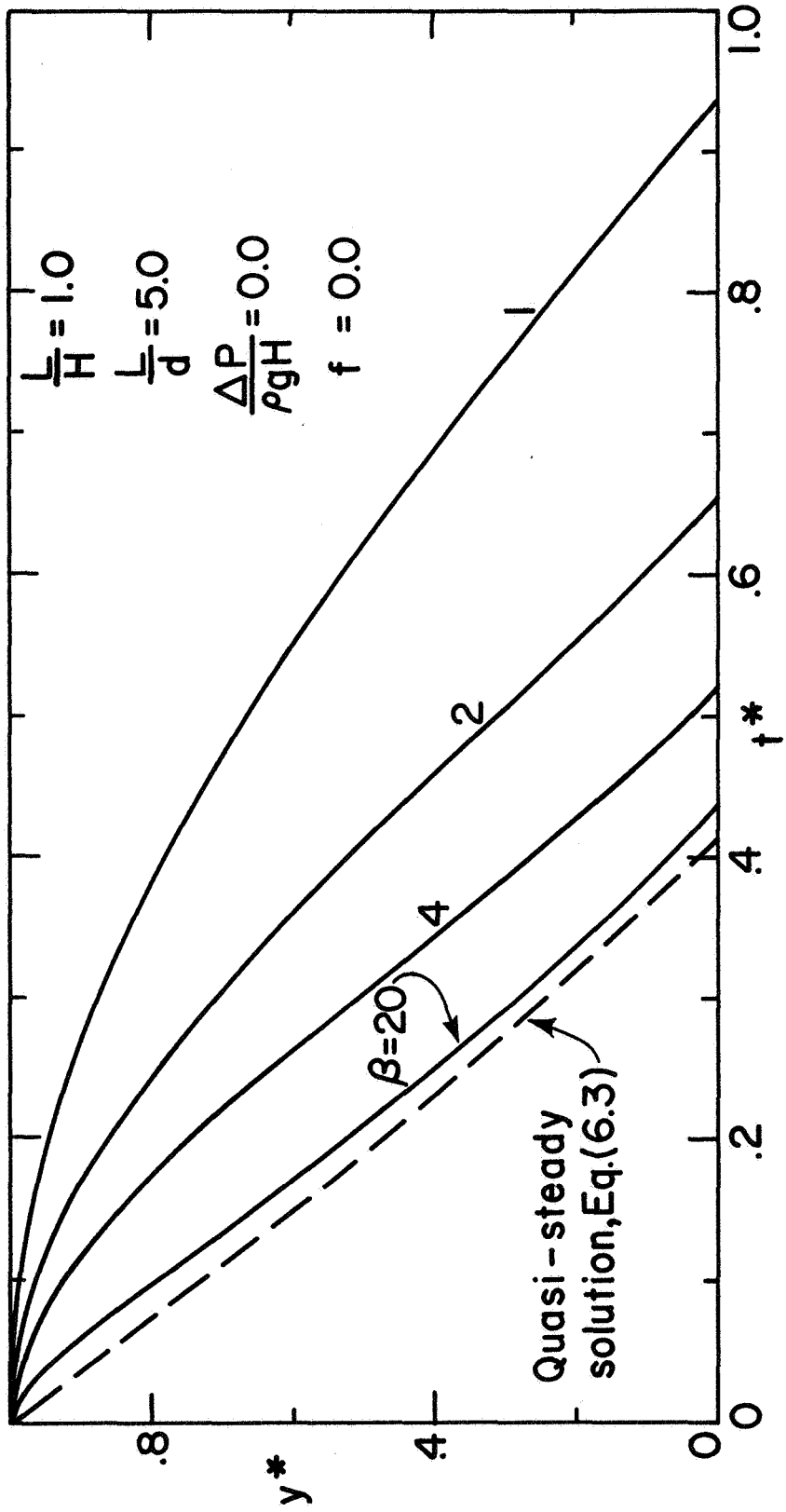

Figure 6.14. Variation of Dimensionless Liquid Height with Dimensionless Time for Various Values of Parameter β

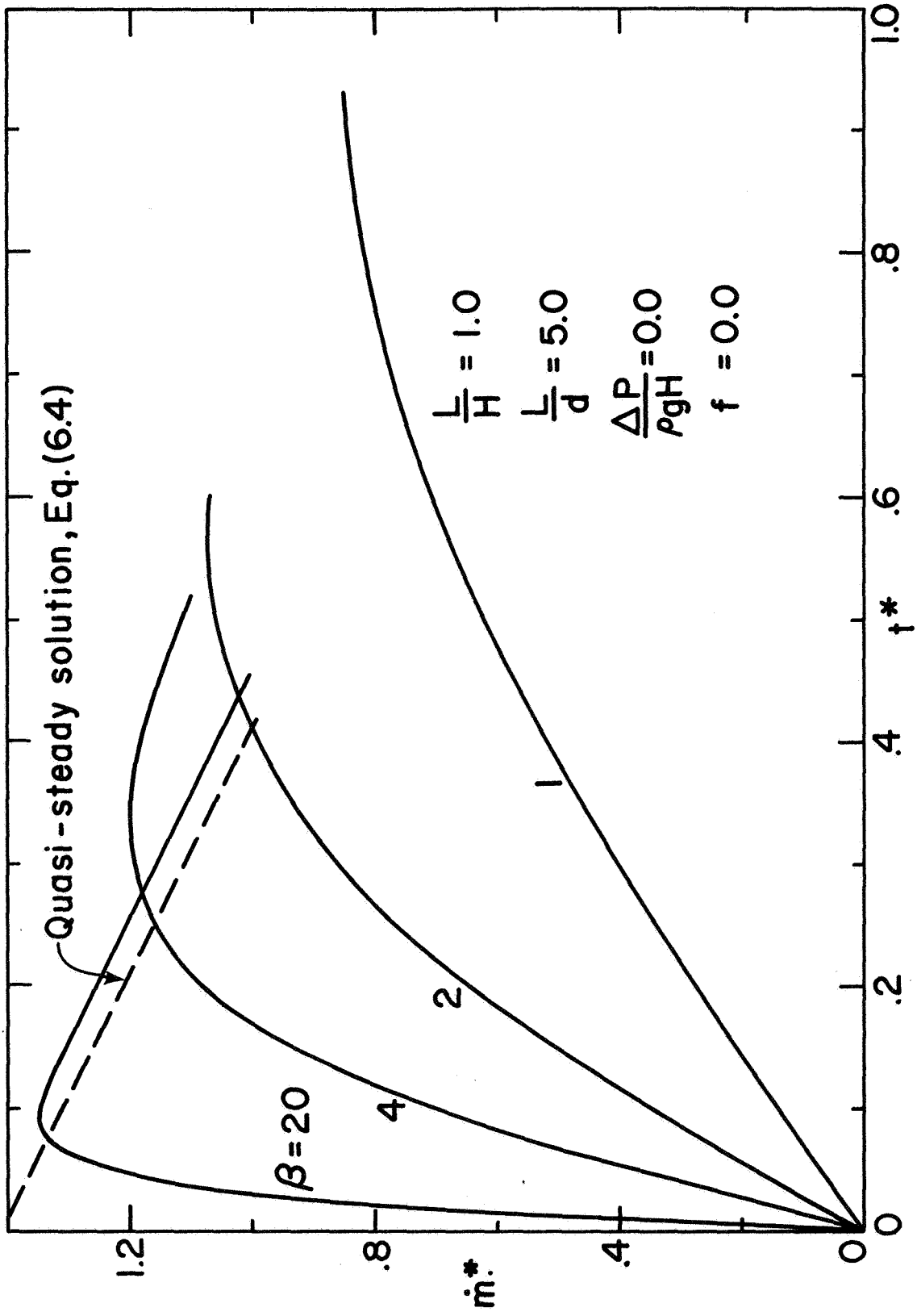

Figure 6.15. Variation of Dimensionless Mass Flow Rate with Dimensionless Time for Various Values of the Parameter β

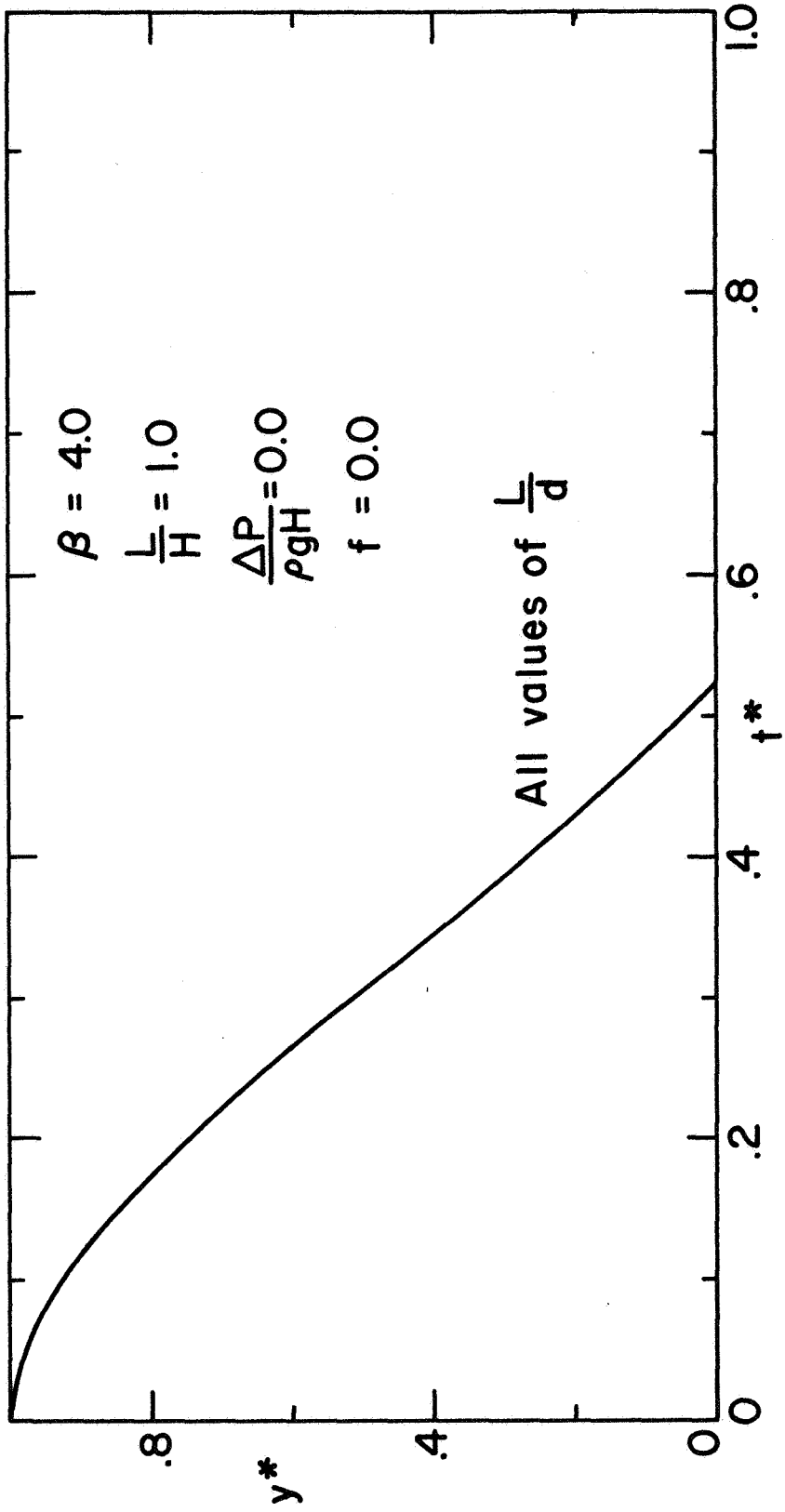

Figure 6.16. Variation of y* with t* for Various Values of the Parameter L/d when f = 0.0

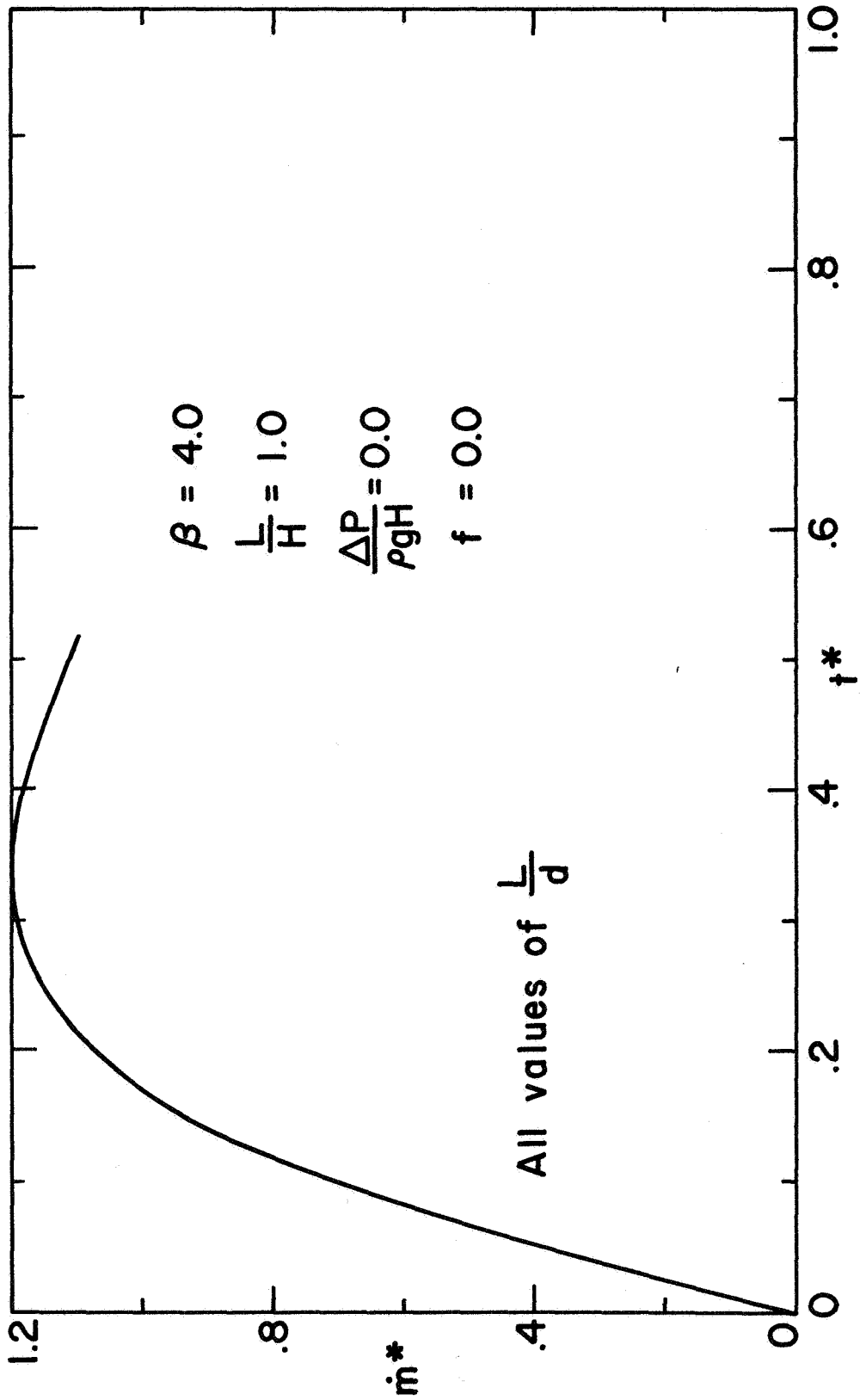

Figure 6.17. Variation of $\dot{m}^*$ with t^* for Various Values of the Parameter L/d when $f = 0.0$

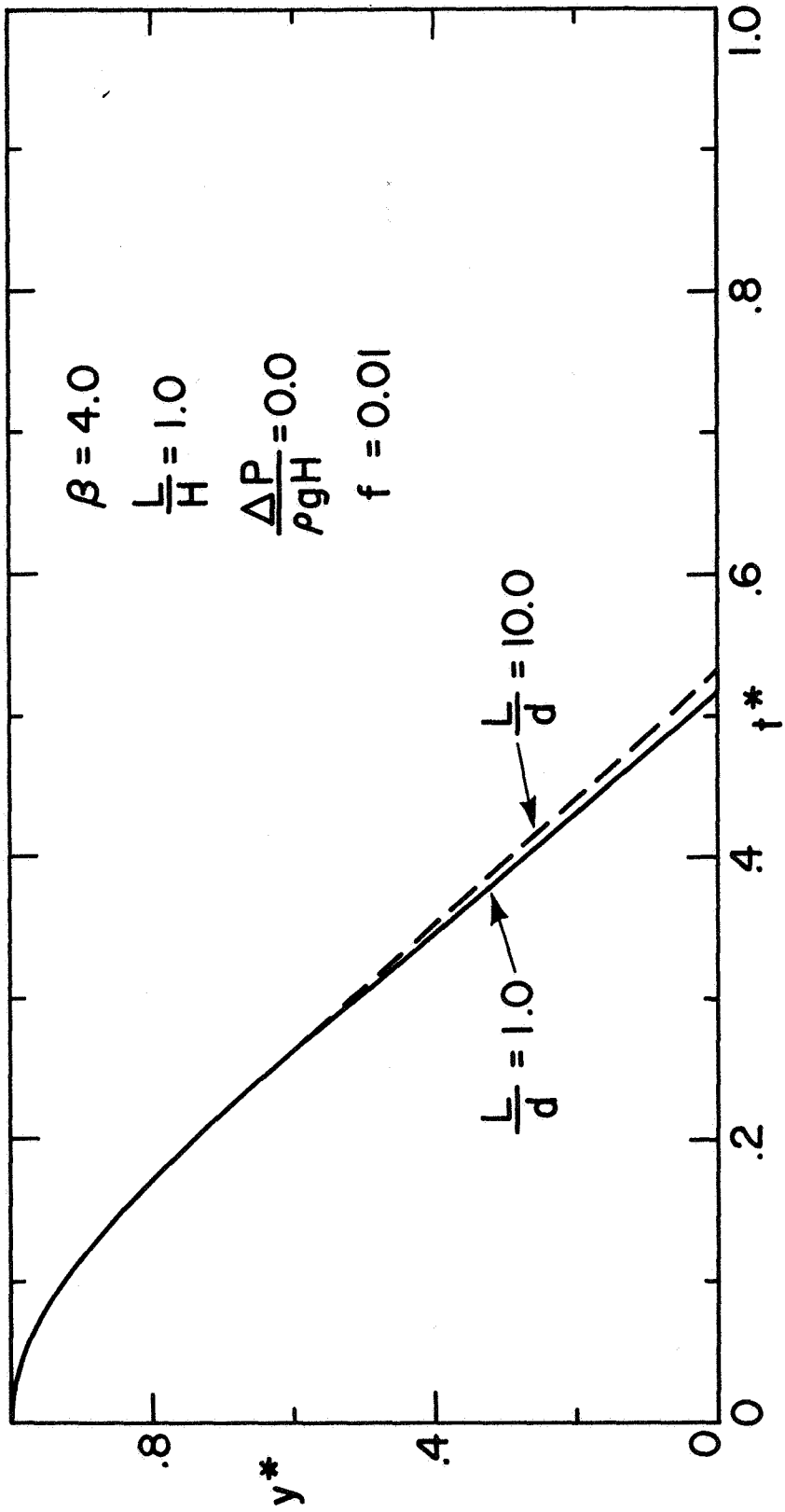

Figure 6.18. Variation of y* with t* for Various Values of the Parameter L/d when f ≠ 0

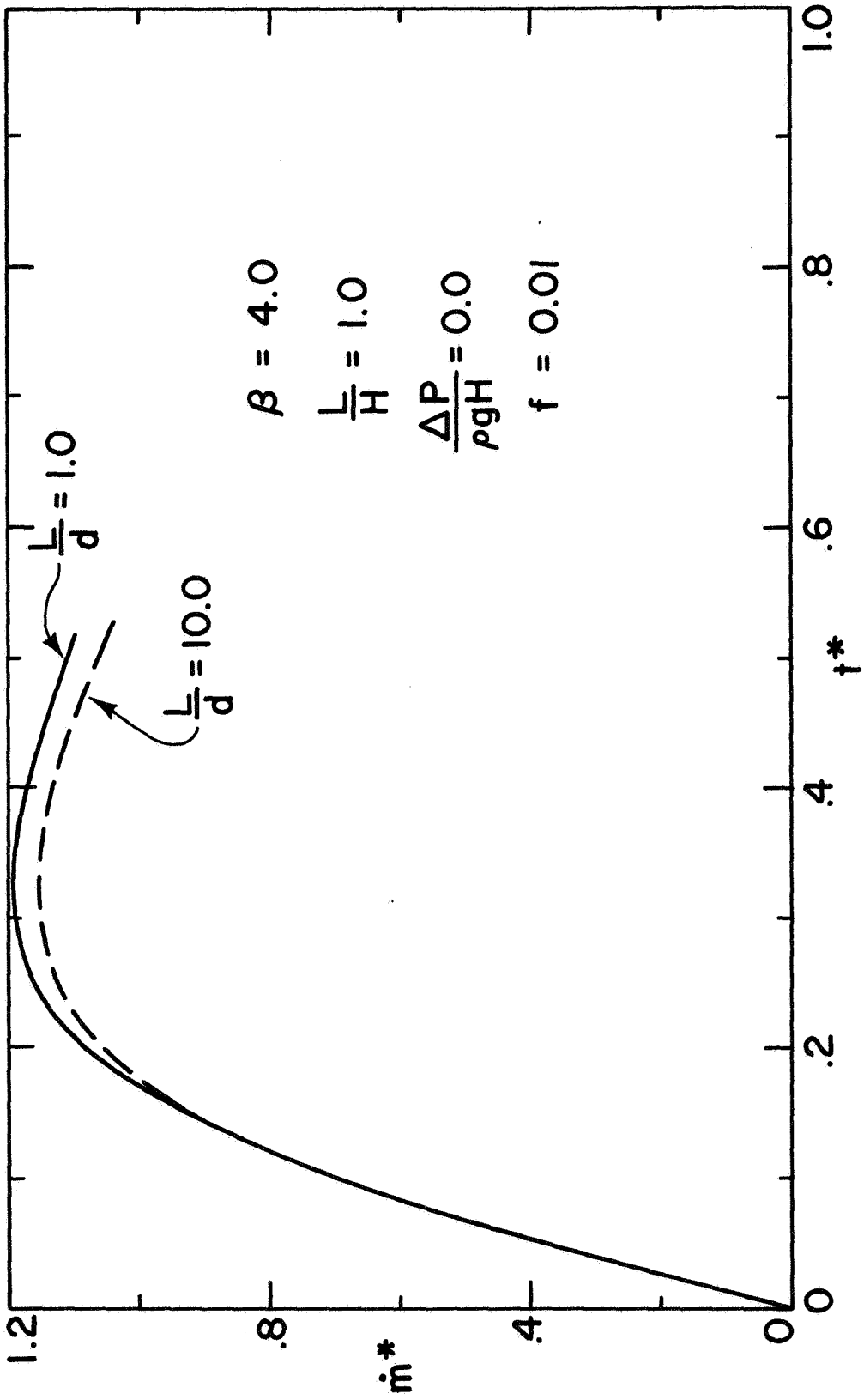

Figure 6.19. Variation of $\dot{m}^*$ with t^* for Various Values of the Parameter L/d when $f \neq 0$

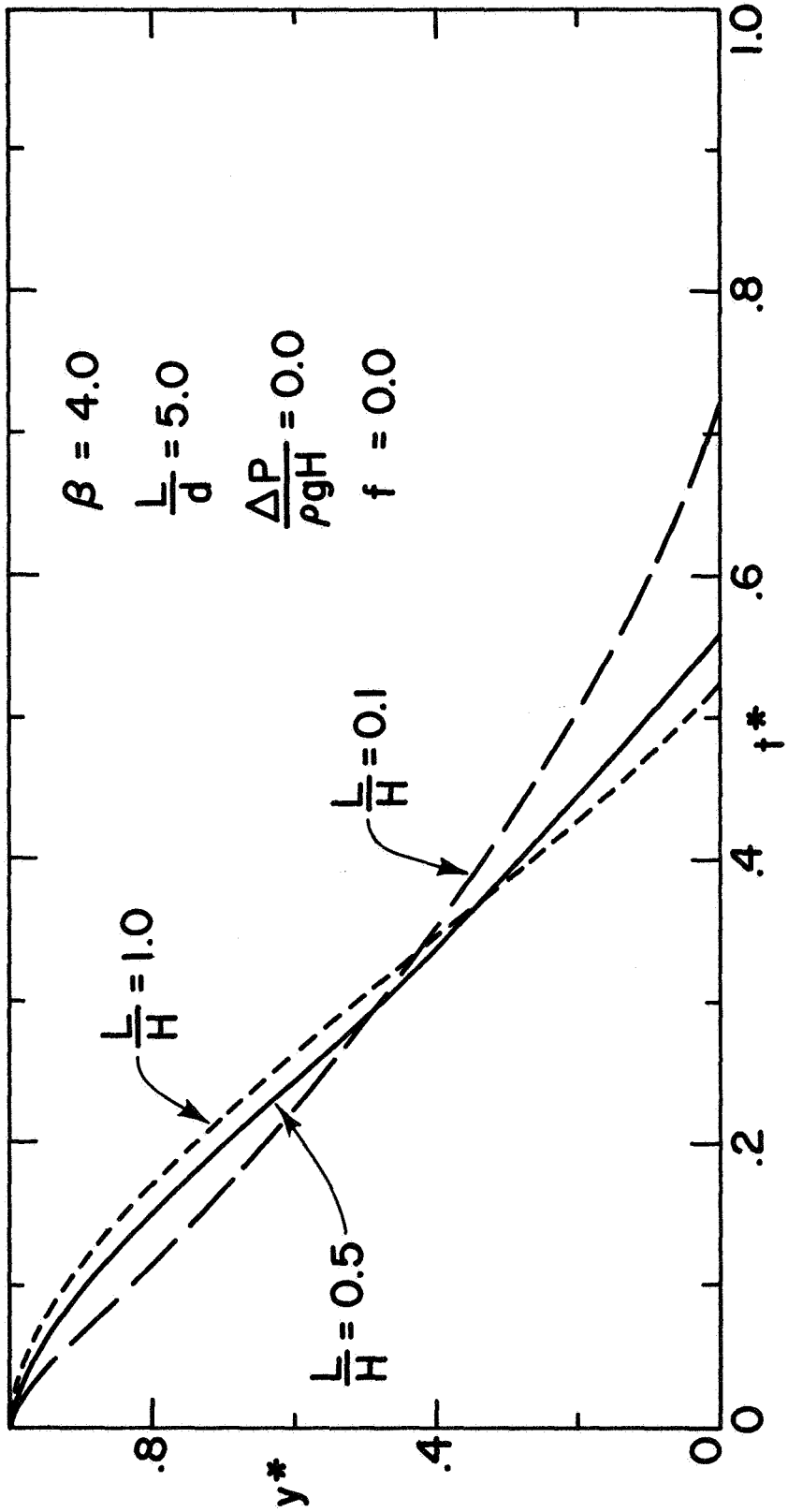

Figure 6.20. Variation of y* with t* for Various Values of the Parameter L/H

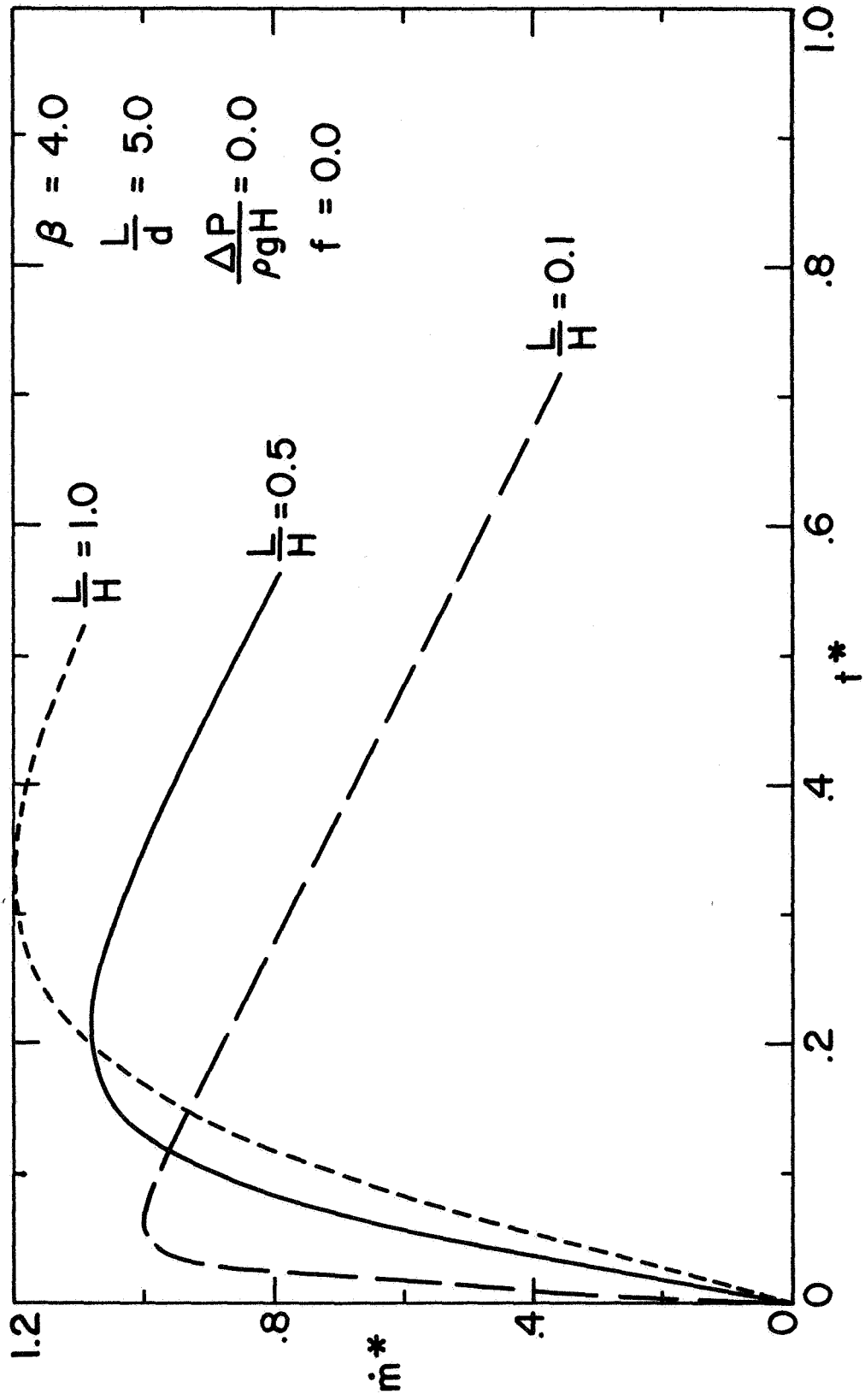

Figure 6.21. Variation of $\dot{m}^*$ with t^* for Various Values of the Parameter L/H

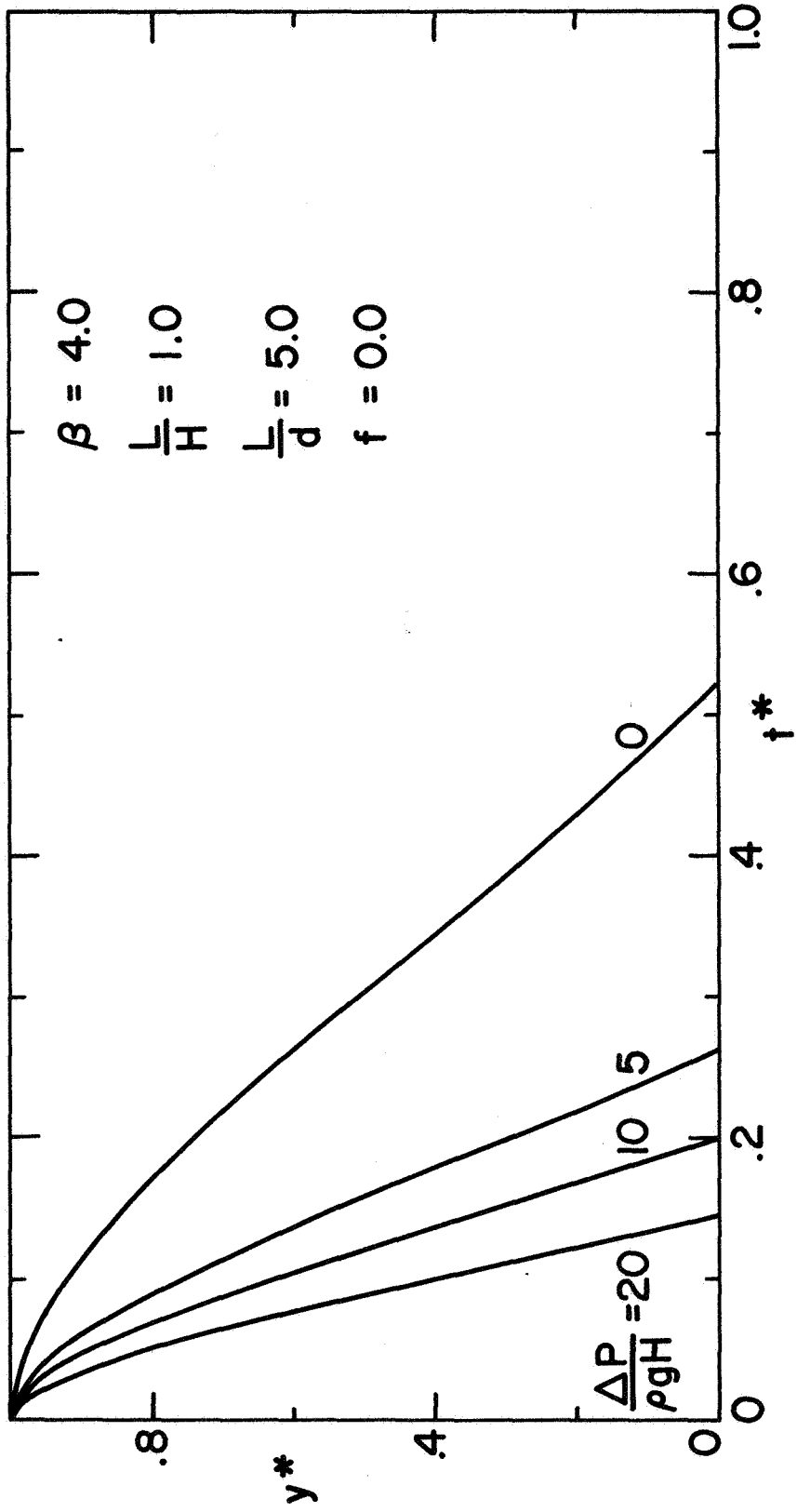

Figure 6.22. Variation of y* with t* for Various Values of the Parameter $\Delta P/\rho gH$

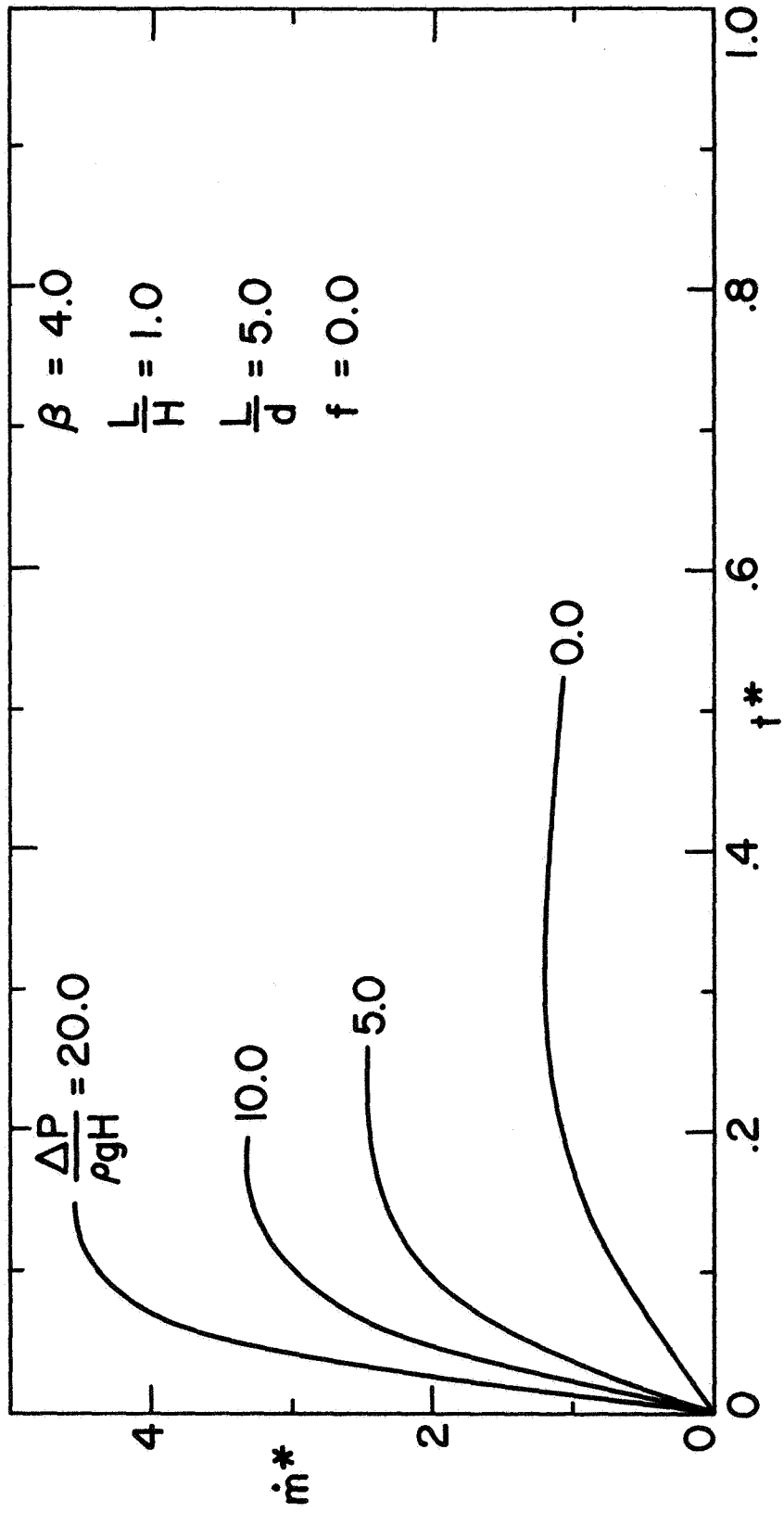

Figure 6.23. Variation of $\dot{m}^*$ with t^* for Various Values of the Parameter $\Delta P/\rho gH$

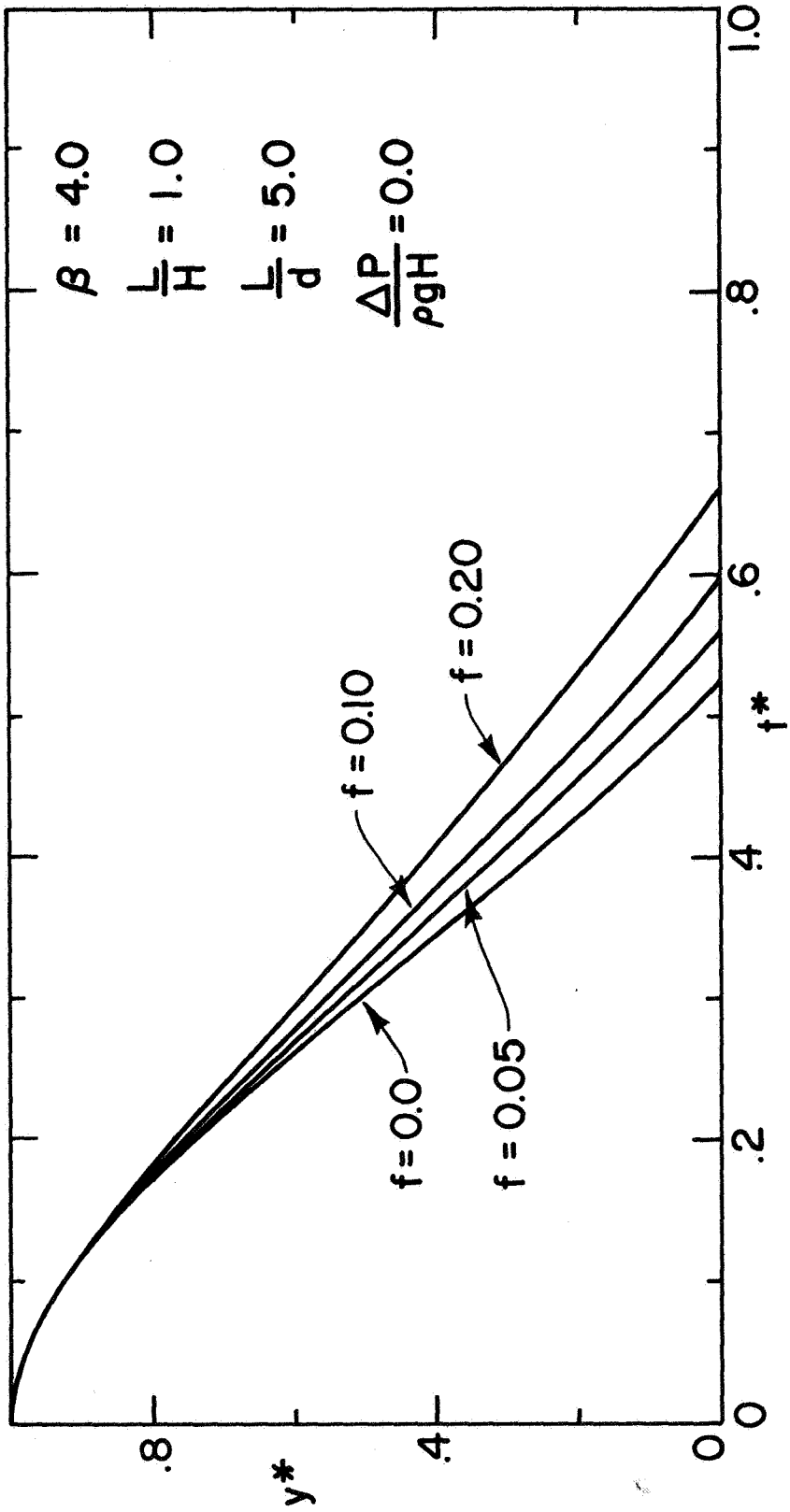

Figure 6.24. Variation of y* with t* for Various Values of the Parameter f

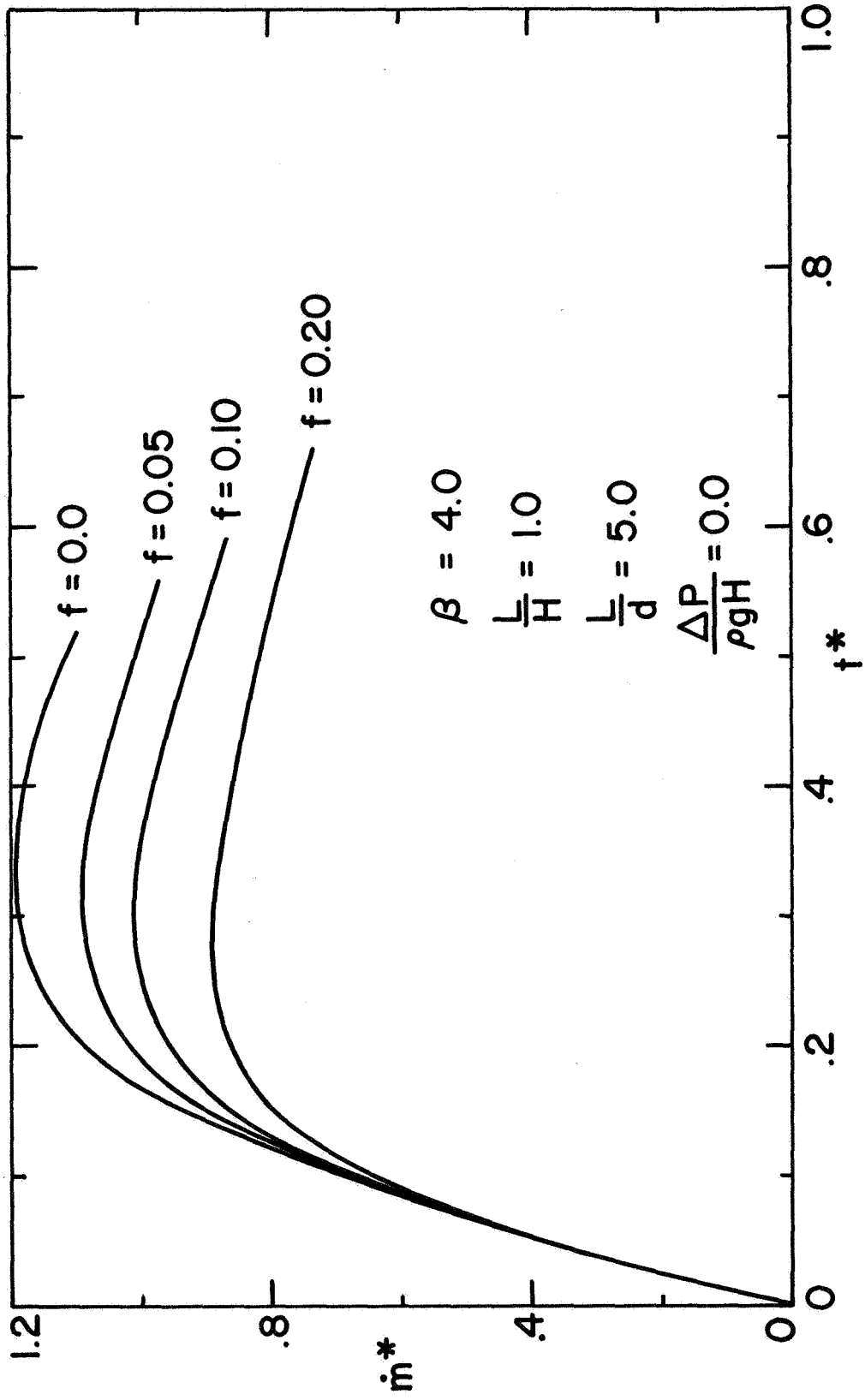

Figure 6.25. Variation of $\dot{m}^*$ with t^* for Various Values of the Parameter f

Finally, Figures 6.24 and 6.25 illustrate the effect of increasing the friction which retards the flow, as was previously mentioned, and can be easily understood on physical grounds.

Transient Discharge Through a Tube for Large External Pressure Drop

A very interesting problem involves pressure driven discharge of a container through a tube. A closed form solution for the governing differential equation in terms of well known elementary functions can be obtained when the external pressure drop, (P_1-P_2), is large in comparison with the hydrostatic head in the container. By transposing terms, equation (6.9) can be written as

$$L\frac{d^2y}{dt^2} - \frac{1}{2}\left[\beta^2\frac{a}{A} + f\cdot\frac{A}{a}\cdot\frac{L}{d}\right]\left(\frac{dy}{dt}\right)^2 = -\left[\frac{P_1-P_2}{\rho} + g(y+L)\right]\frac{a}{A} \qquad (6.11)$$

If the external pressure drop is large compared to the hydrostatic head, then $\frac{P_1-P_2}{\rho} + gL \gg gy$, and equation (6.11) reduces to

$$L\frac{d^2y}{dt^2} - \frac{1}{2}\left[\beta^2\frac{a}{A} + f\cdot\frac{A}{a}\cdot\frac{L}{d}\right]\left(\frac{dy}{dt}\right)^2 = -\left(\frac{P_1-P_2}{\rho} + gL\right)\frac{a}{A} \qquad (6.12)$$

Equation (6.12) can be written in dimensionless form as

$$\left(\frac{L}{H}\right)\frac{d^2y^*}{dt^{*2}} - \frac{1}{2}\left[\beta^2\frac{a}{A} + f\cdot\frac{A}{a}\cdot\frac{L}{d}\right]\left(\frac{dy^*}{dt^*}\right)^2 = -2\beta^2\left(\frac{P_1-P_2}{\rho gH} + \frac{L}{H}\right)\frac{a}{A} \qquad (6.13)$$

If (P_1-P_2) does not vary with time, equation (6.13) can be written as

$$N \frac{d^2y^*}{dt^{*2}} - Q^2 \left(\frac{dy^*}{dt^*}\right)^2 = - R^2 \qquad (6.14a)$$

where

$$N = \frac{L}{H}$$

$$Q^2 = \frac{1}{2} \left[\beta^2 \frac{a}{A} + f \cdot \frac{A}{a} \cdot \frac{L}{d}\right] \qquad (6.14b)$$

and $$R^2 = 2\left(\frac{P_1-P_2}{\rho g H} + \frac{L}{H}\right) \cdot \frac{a}{A} \cdot \beta^2$$

The initial conditions to be applied at $t^* = 0$ are $y^* = 1.0$ and $\frac{dy^*}{dt^*} = 0$. A complete solution can be obtained as follows. By writing $\frac{dy^*}{dt^*} = \dot{y}^*$ and rearranging terms, equation (6.14a) becomes

$$N \frac{d\dot{y}^*}{dt^*} = - (R^2 - Q^2 \dot{y}^{*2}) \qquad (6.15)$$

Since $\dot{y}^*$ is always negative the left hand side of equation (6.15) is negative. Therefore $R^2 > Q^2 \dot{y}^{*2}$. Hence

$$- \frac{1}{N} \int_o^{t^*} dt^* = \int_o^{\dot{y}^*} \frac{d\dot{y}^*}{R^2-Q^2 \dot{y}^{*2}}$$

$$- \frac{1}{N} [t^*]_o^{t^*} = \frac{1}{QR} \left[\text{Tanh}^{-1} \frac{Q\dot{y}^*}{R}\right]_o^{\dot{y}^*}$$

$$- \frac{t^*}{N} = \frac{1}{QR} \text{Tanh}^{-1} \frac{Q\dot{y}^*}{R}$$

Therefore

$$\frac{Q}{R} \dot{y}^* = \text{Tanh} \left(- \frac{QR}{N} t^*\right) = - \text{Tanh} \frac{QR}{N} t^*$$

Hence

$$\frac{dy^*}{dt^*} = -\frac{R}{Q}\,\text{Tanh}\,\left(\frac{QR}{N}\,t^*\right) \tag{6.16}$$

Integrating once again, with the initial condition $y^* = 1$ at $t^* = 0$, gives

$$-\int_1^{y^*} dy^* = \frac{R}{Q}\int_0^{t^*} \text{Tanh}\,\left(\frac{QR}{N}\,t^*\right)\,dt^*$$

$$(1 - y^*) = \frac{R}{Q}\,\frac{N}{QR}\,\ell n\,\left(\text{Cosh}\,\frac{QR}{N}\,t^*\right)$$

Finally, the dimensionless liquid height is given by

$$y^* = 1 - \frac{N}{Q^2}\,\ell n\,\left[\text{Cosh}\,\left(\frac{QR}{N}\,t^*\right)\right] \tag{6.17}$$

Equations (6.17) and (6.16) are presented graphically in Figures 6.26 and 6.27 respectively. These are compared with the numerical solutions for the complete equation (6.10), obtained by the Fourth-Order Runge-Kutta method. Even for $\frac{\Delta P}{\rho g H} = 5.0$, the approximate solution predicts the behaviour of the fluid quite well. As expected, the approximate solution approaches the exact solution as $\frac{\Delta P}{\rho g H}$ is increased.

Figures 6.26 and 6.27 are plotted for $\frac{L}{H} = 1.0$ and $\frac{L}{d} = 5.0$. For obvious reasons the approximation should become better if $\frac{L}{H}$ is increased. But if β and $\frac{L}{d}$ are kept constant and $\frac{L}{H}$ is inordinately increased, the ratio of $\frac{H}{d}$ falls off. This means that the initial height of the liquid in the container is of the order of the discharge diameter or less. In such a case the analysis ceases to be valid owing to the free surface of the liquid dipping into the discharge tube. On the other hand if both $\frac{L}{d}$ and $\frac{L}{H}$ are increased the tubes may become too long for the assumption

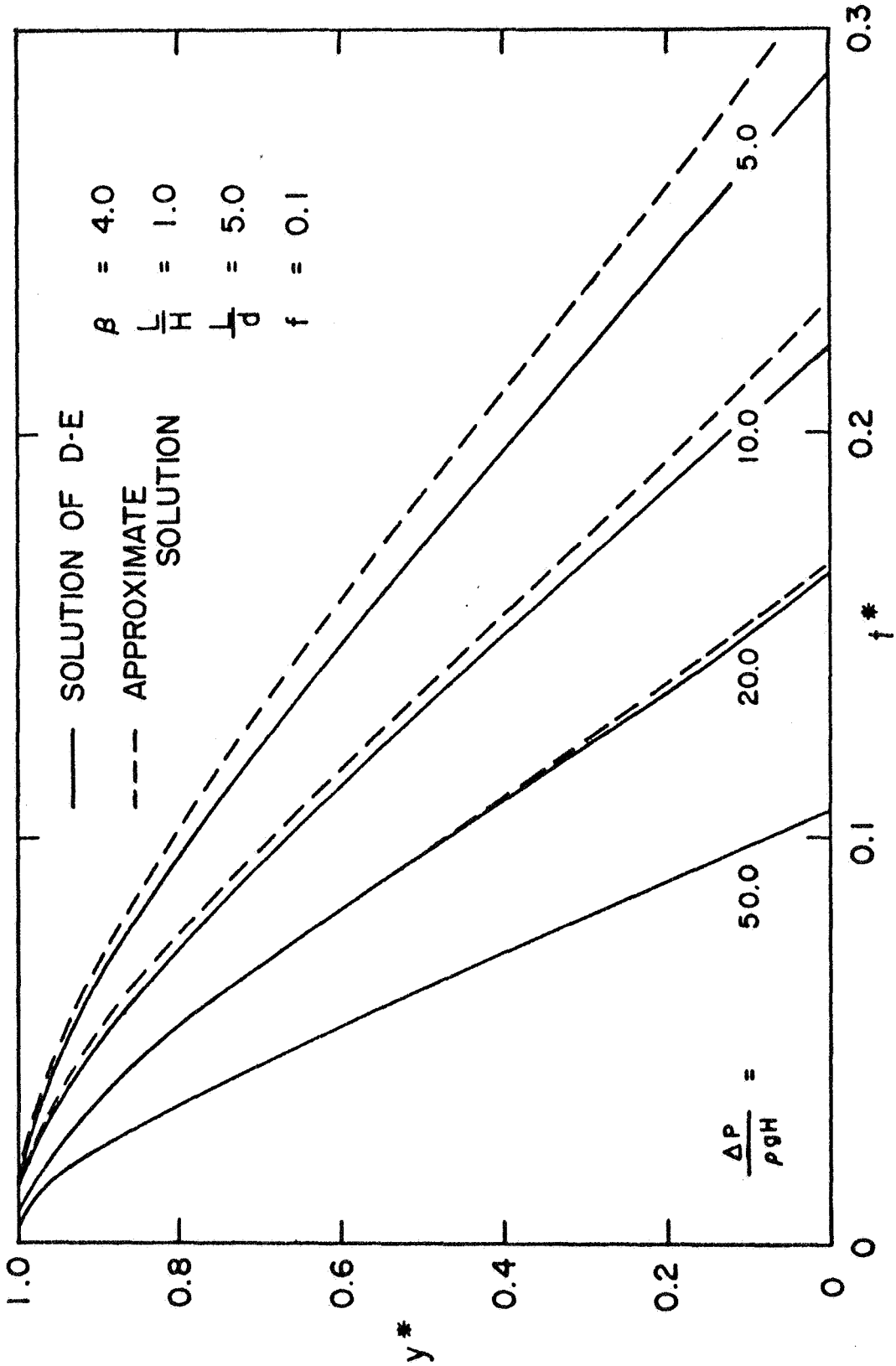

Figure 6.26. Variation of y* with t* as Predicted by Approximate Solution for $[\frac{\Delta P}{\rho g H} + \frac{L}{H}] >> 1.0$ and Comparison with Numerical Solution of the Differential Equation (6.10)

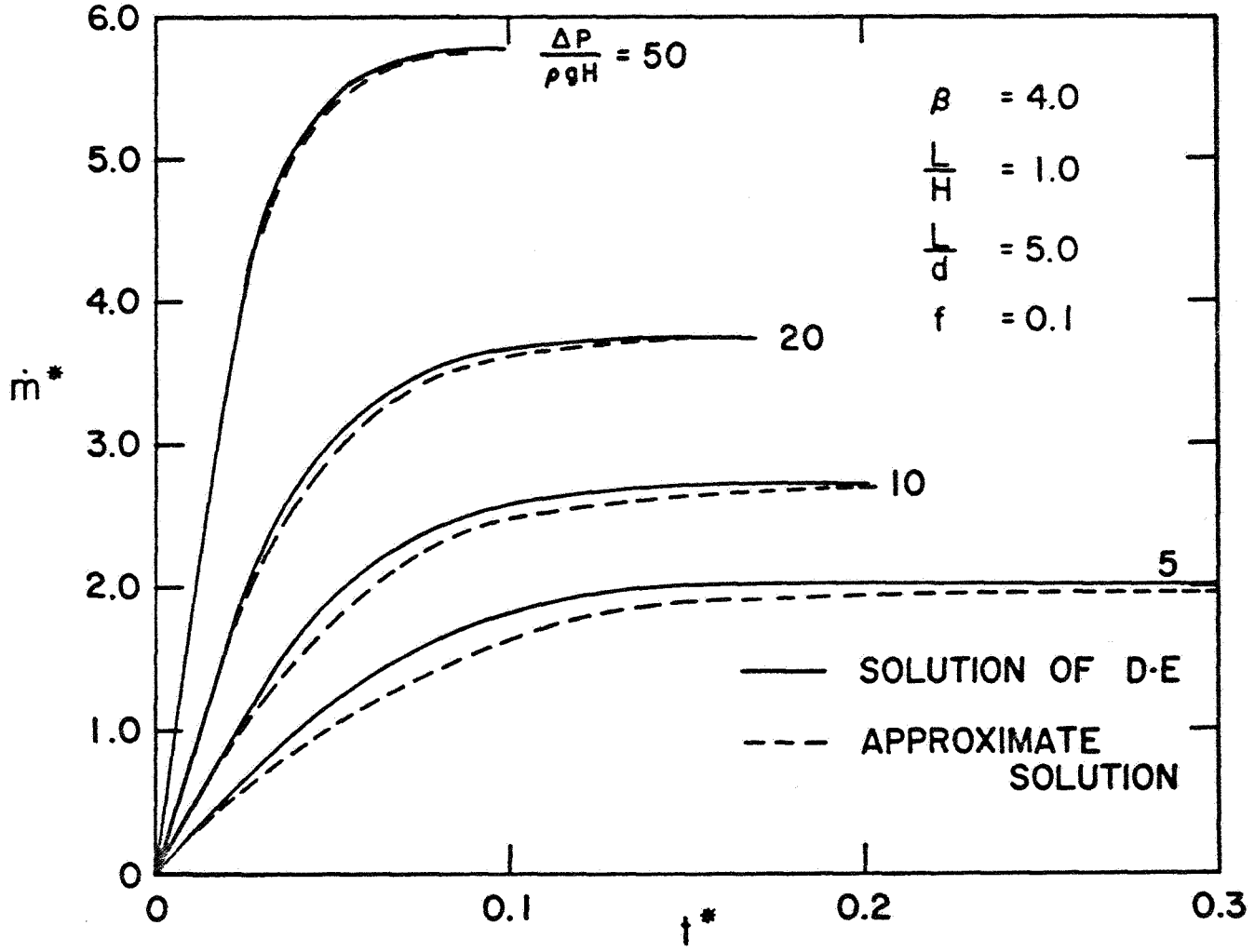

Figure 6.27. Variation of $\dot{m}^*$ with t^* as Predicted by Approximate Solution for $[\frac{\Delta P}{\rho g H} + \frac{L}{H}] >> 1.0$ and Comparison with Numerical Solution of the Differential Equation (6.10)

of one-dimensionality to be valid. Therefore a word of caution is necessary with regard to the ability of equations (6.10) and (6.17) to predict experimental behavior beyond certain ranges of $\frac{L}{H}$ and $\frac{L}{d}$.

Once again, an important difference between the quasi-steady flow analysis and the transient flow analysis is discernable. In the case of quasi-steady flow discharge, when $\frac{\Delta P}{\rho g H}$ is increased $\dot{m}^*$ increases and remains nearly constant at its peak value throughout the period of discharge (see Figure 6.10). But the unsteady flow analysis shows that as $\frac{\Delta P}{\rho g H}$ is increased, the fluid spends a major portion of the total discharge time accelerating from zero to the peak value of the mass flow rate during this period (see Figures 6.23 and 6.27).

Discussion of the Friction Factor, f

The friction factor, f, which is used for flow through tubes, is in general a function of the Reynolds number $(\frac{dV_2}{\nu})$ and the relative roughness of the tube. For smooth tubes, the friction factor is a function of Reynolds number only. Formulae for the variation of friction factor with Reynolds number (for different ranges of Re) for fully developed pipe flow are well known (Ref. 33). In the entrance section where the flow is not fully developed, due to the acceleration imparted to the fluid near the center of the tube, the friction factors have larger values (Refs. 34, 35). However, Weiland and Lowdermilk (Ref. 36) have found experimentally that the average friction factors are not affected by the acceleration in the entrance section when the Reynolds numbers are above 30,000 for tubes with $\frac{L}{d} = 15$.

In obtaining the results for discharge of a container through a tube, the friction factor was assumed to be constant. The range of validity of this assumption for flow under a varying head (quasi-steady and transient) and when the discharge velocity is zero initially (transient) is discussed in this section. The Reynolds number for the flow in the tube is given by $Re = \frac{dV_2}{\nu} = \frac{d[-(A/a)(dy/dt)]}{\nu} = \frac{1}{2}\frac{d\sqrt{2gH}}{\nu}\frac{A}{a}\frac{1}{\beta}(-\frac{dy^*}{dt^*})$. Figure 6.28 shows the variation of Re with t* for two situations for quasi-steady discharge through a tube. Figures 6.29 and 6.30 illustrate the effect of a varying f on y* vs. t* and $\dot{m}^*$ vs. t* respectively. The solid lines were computed using f = 0.015 and assuming it to be constant.[5] The + marks were obtained for the same initial conditions, but accounting for the variation of f with Re. This was accomplished by carrying out a step by step integration of equation (C5b). It can be observed that there is practically no difference between the two solutions. Similar results for the transient flow case, where the Reynolds number varies from zero to a maximum and falls off again, are depicted in Figures 6.31 through 6.33. In these cases the + marks were obtained by means of a step by step integration of equation (6.10). Figure 6.34 shows the variation of Re with t* when $\frac{d\sqrt{2gH}}{\nu} = 2000$. The sudden changes in slope of the curves in the neighborhood of Re = 2000 are due to the flow being assumed to change from turbulent to laminar at that Reynolds number. Figures 6.35 and 6.36 depict the effect of the variation of f with Re (as shown in Figure 6.34) on y* vs. t* and $\dot{m}^*$ vs. t* respectively. In these figures the solid lines were computed using f = 0.035 (as compared to 0.015 in Figures 6.29 and 6.30). Similar results are shown in Figures 6.37 through

[5] For a method of estimating f for a typical situation see Chapter 7.

6.39 for the transient flow case when $\frac{d\sqrt{2gH}}{\nu} = 2000$ to illustrate what happens in the low Reynolds number range. Thus, it can be seen that even though the flow in the tube changes from turbulent to laminar (changing the f vs. Re relationship significantly) the predictions obtained using a constant value for f compare very favorably with those obtained using an f which varies continuously with time in accordance with the instantaneous Reynolds number. It is clear from the illustrations described above that in most ranges of the parameter $\frac{d\sqrt{2gH}}{\nu}$ where the analyses given in the earlier sections of this chapter are valid, a judicious choice of f,[6] taken as constant throughout the discharge process, yields predictions of acceptable engineering accuracy. However, it should be emphasized that this procedure may lead to considerable errors when $\frac{d\sqrt{2gH}}{\nu}$ is somewhat smaller than 2000.

[6]For a method of estimating f for a typical situation see Chapter 7.

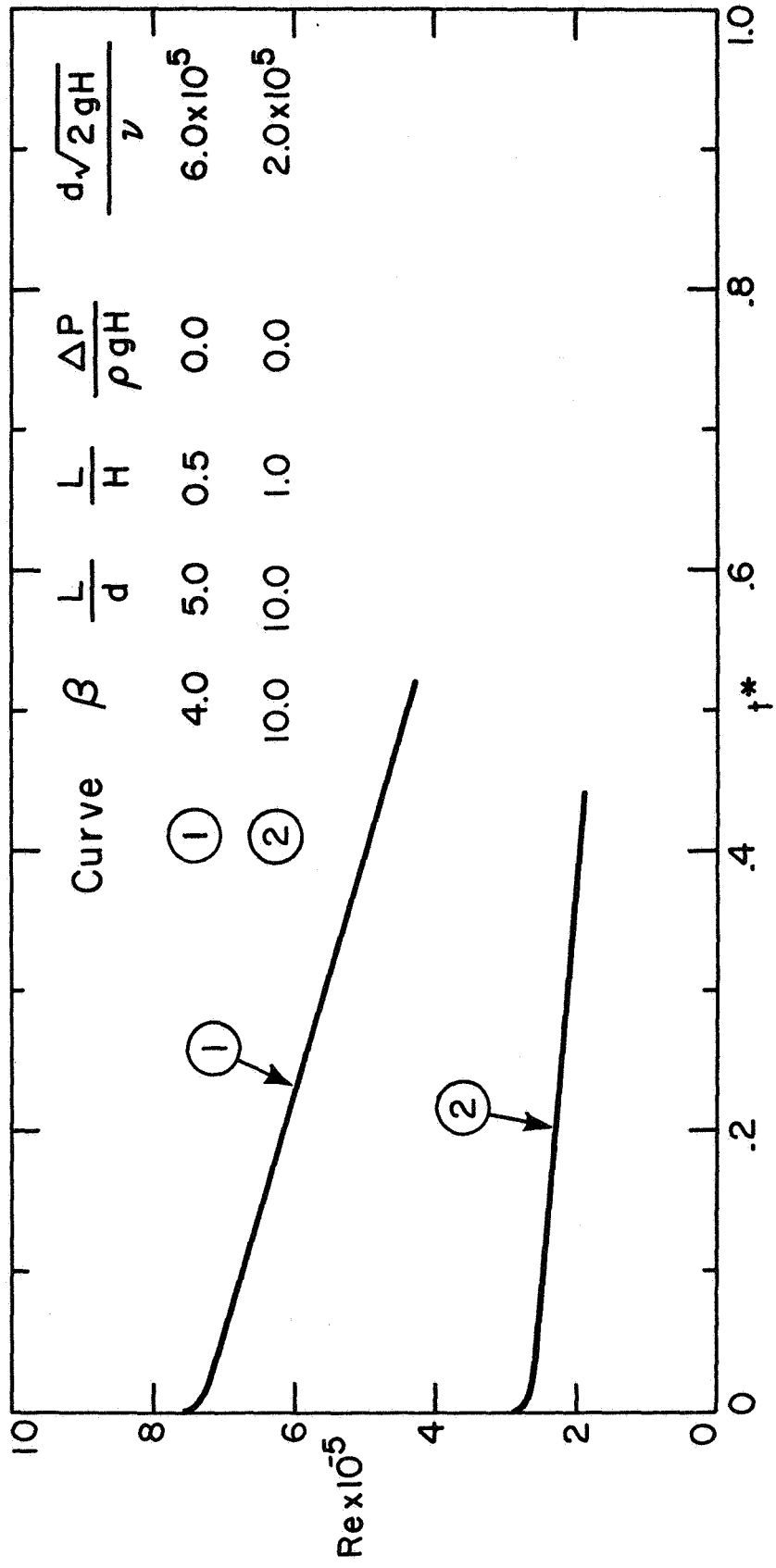

Figure 6.28. Variation of Reynolds Number (Re = dV_2/ν) with Dimensionless Time (t*) for Discharge Through a Tube for Large Values of $d\sqrt{2gH}/\nu$ (Quasi-Steady Flow Analysis)

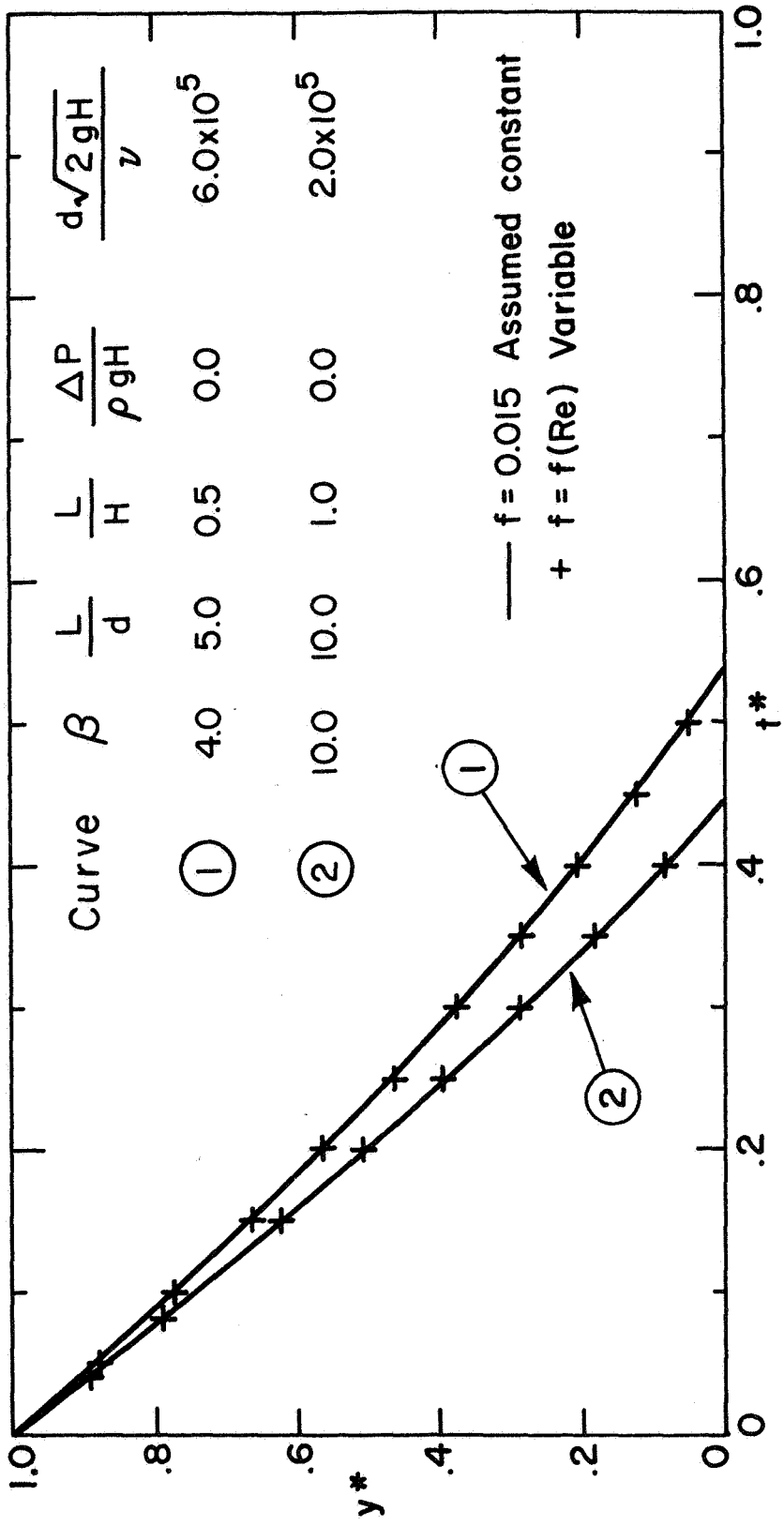

Figure 6.29. Effect of Variation of f with Re on y* vs. t* for Discharge Through a Tube for Large Values of $d\sqrt{2gH}/\nu$ (Quasi-Steady Flow Analysis)

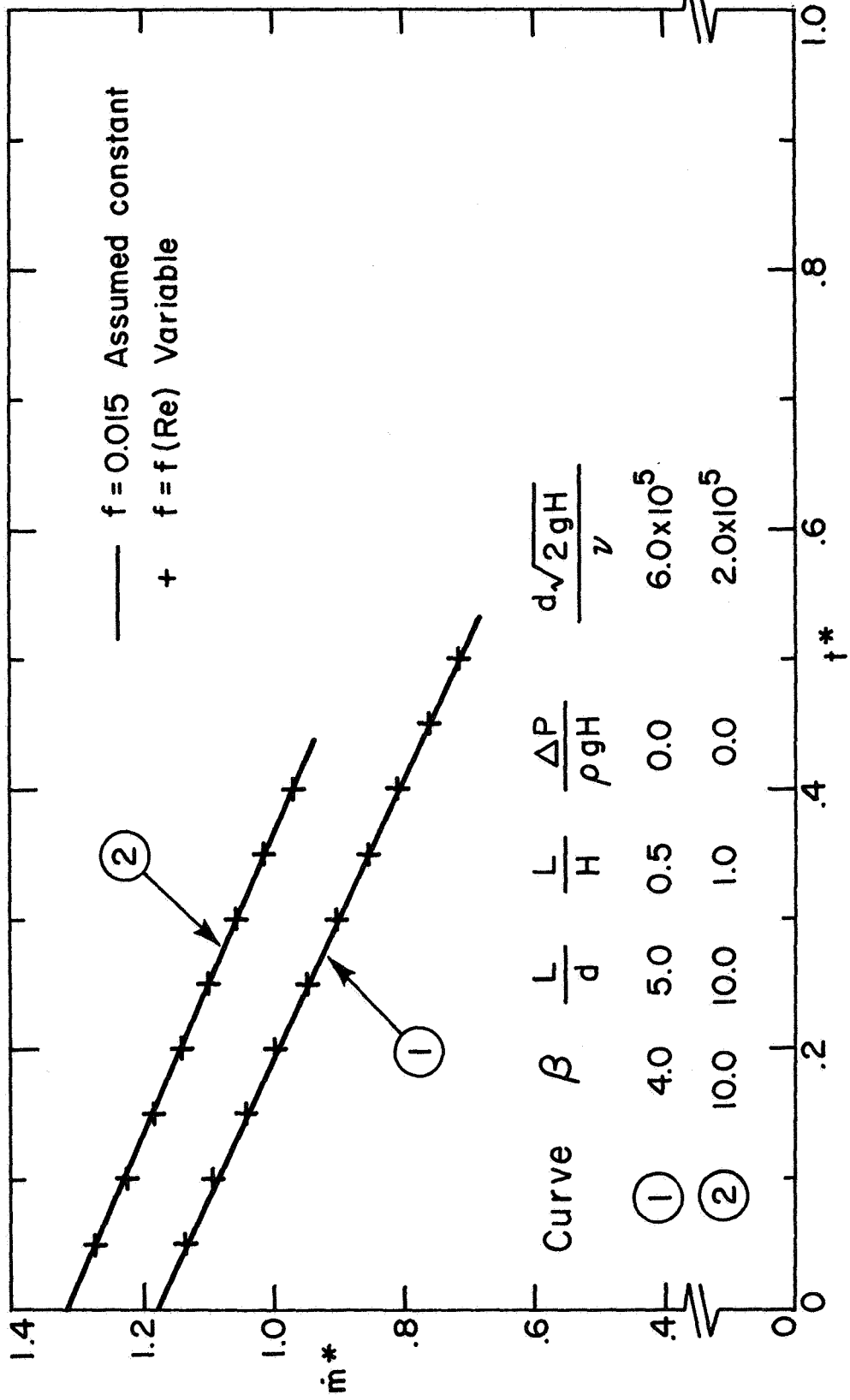

Figure 6.30. Effect of Variation of f with Re on $\dot{m}^*$ vs. t^* for Discharge Through a Tube for Large Values of $d\sqrt{2gH}/\nu$ (Quasi-Steady Flow Analysis)

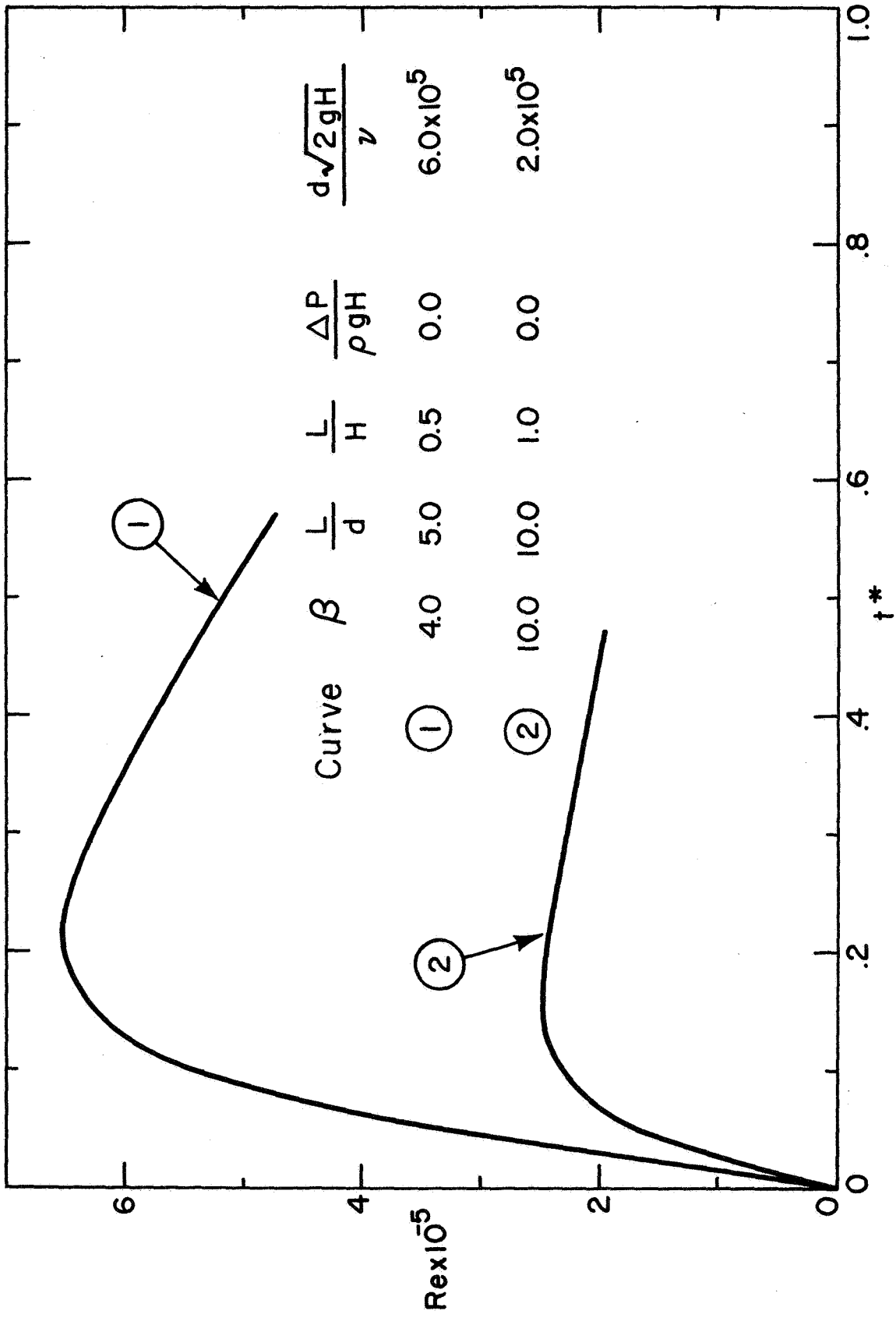

Figure 6.31. Variation of Reynolds Number (Re = dV_2/ν) with Dimensionless Time (t*) for Discharge Through a Tube for Large Values of $d\sqrt{2gH}/\nu$ (Transient Flow Analysis)

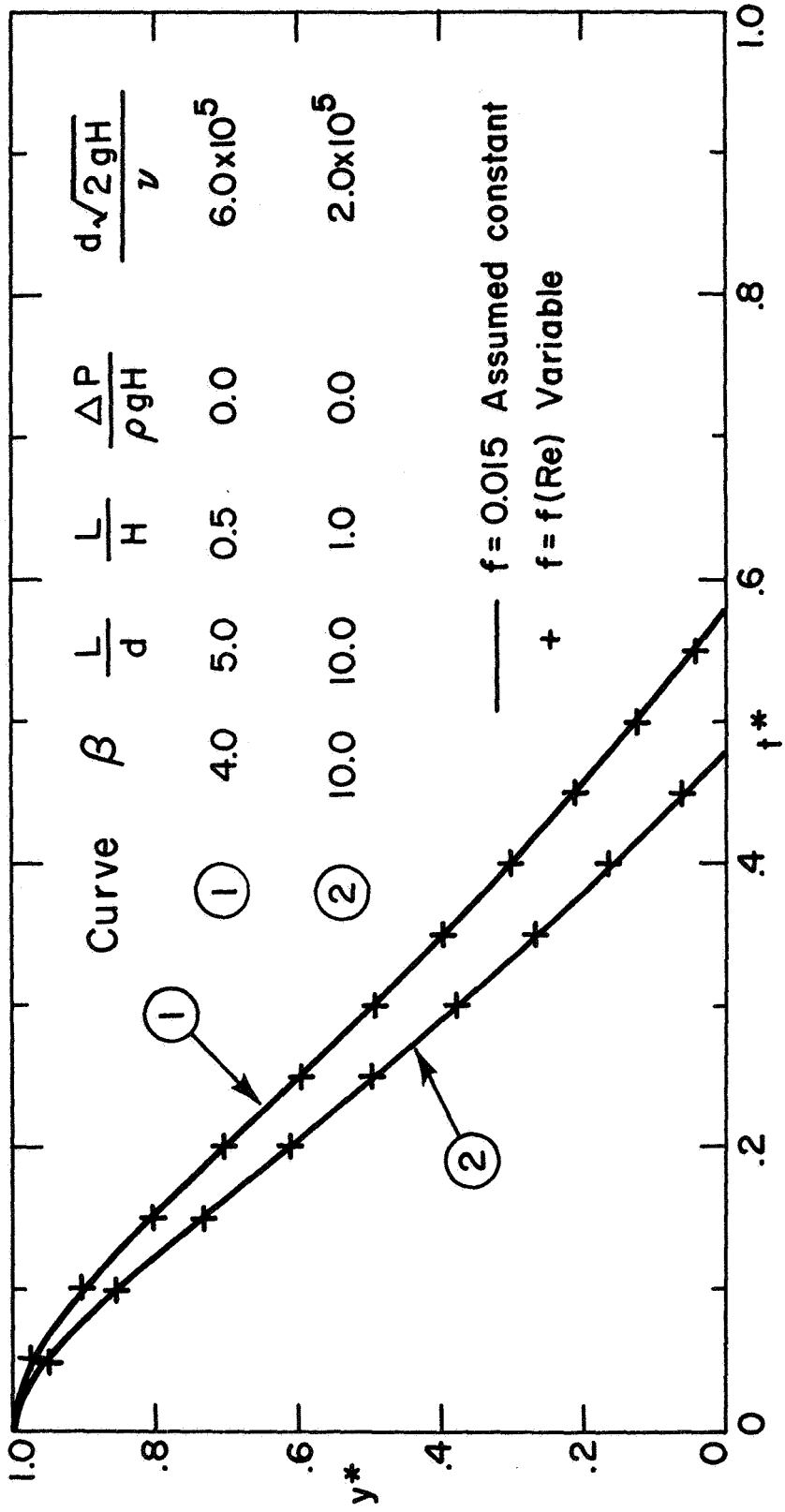

Figure 6.32. Effect of Variation of f with Re on y* vs. t* for Discharge Through a Tube for Large Values of $d\sqrt{2gH}/\nu$ (Transient Flow Analysis)

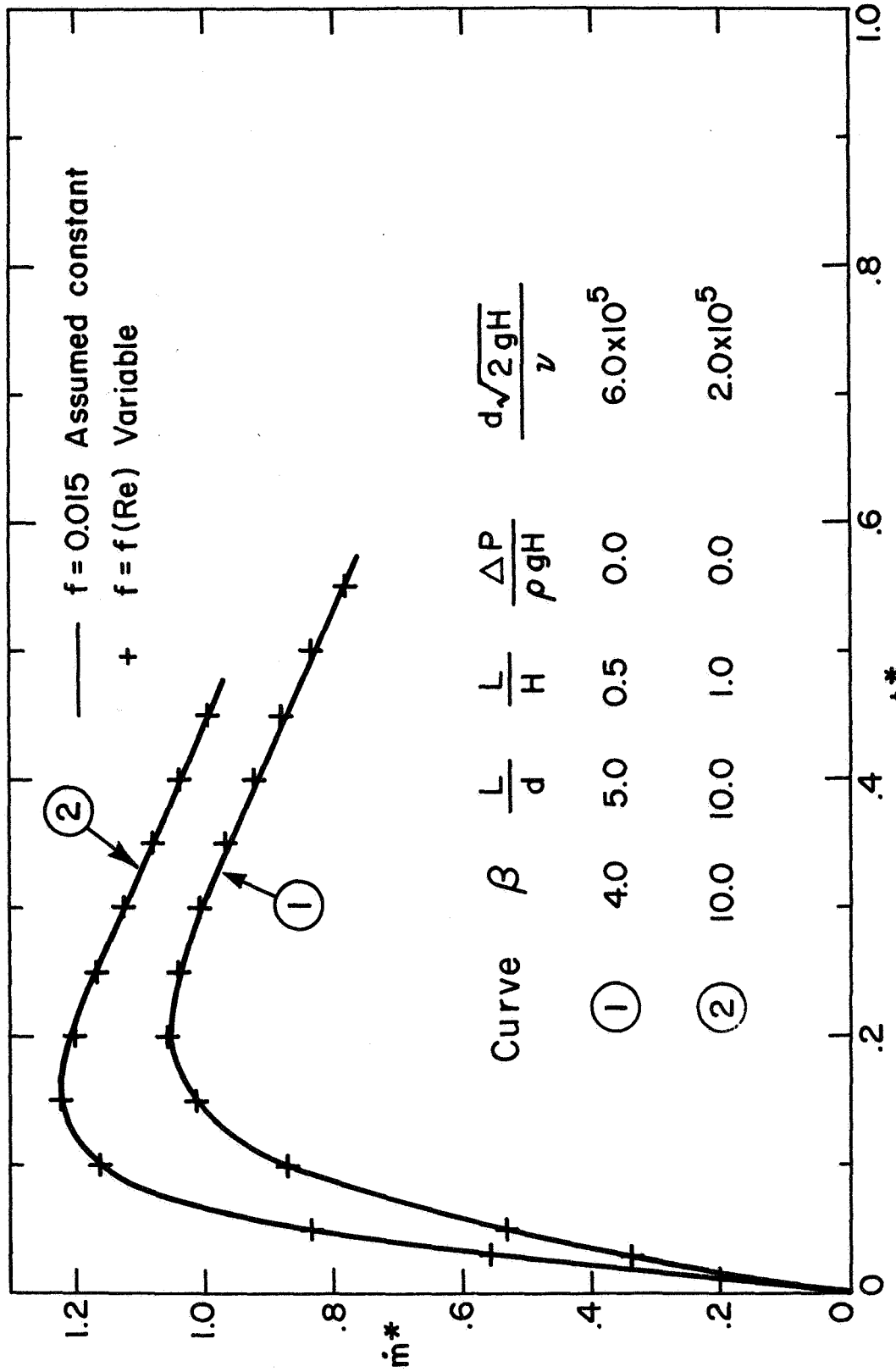

Figure 6.33. Effect of Variation of f with Re on $\dot{m}^*$ vs. t^* for Discharge Through a Tube for Large Values of $d\sqrt{2gH}/\nu$ (Transient Flow Analysis)

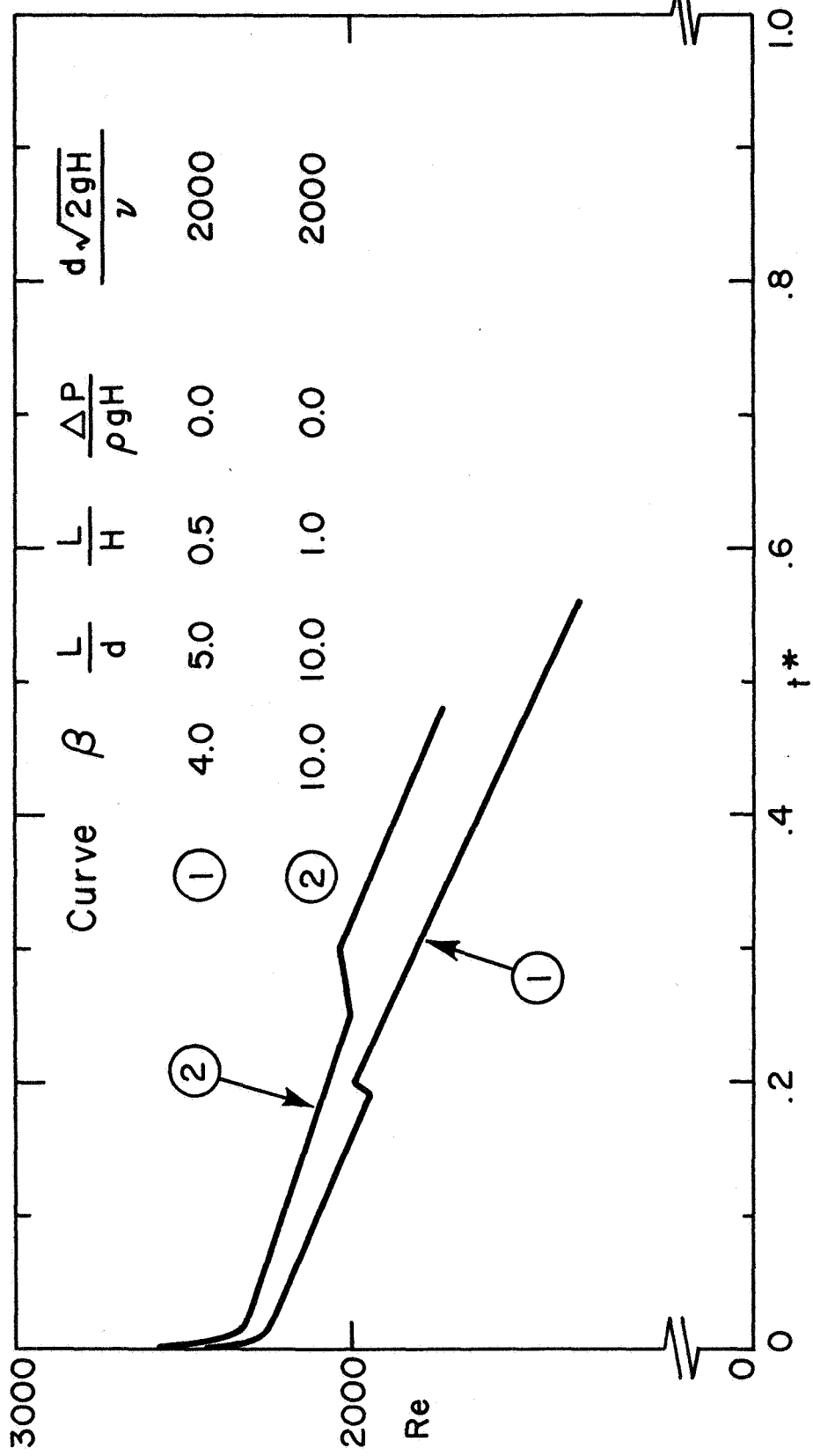

Figure 6.34. Variation of Reynolds Number ($\frac{Re}{d\sqrt{2gH}/\nu} = dV_2/\nu$) with Dimensionless Time (t*) for Discharge Through a Tube when $d\sqrt{2gH}/\nu = 2000$ (Quasi-Steady Flow Analysis)

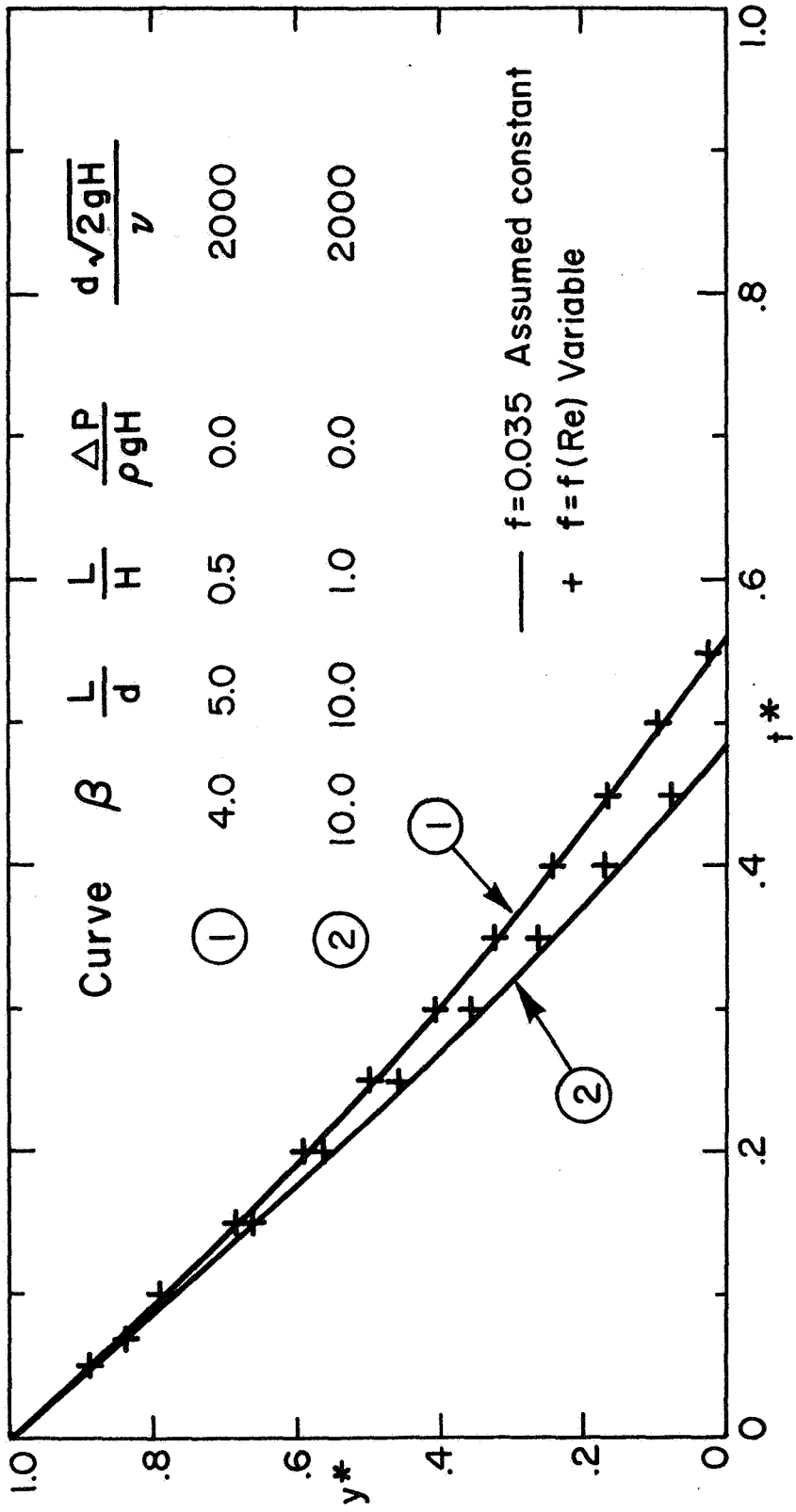

Figure 6.35. Effect of Variation of f with Re on y^* vs. t^* for Discharge Through a Tube when $d\sqrt{2gH}/\nu = 2000$ (Quasi-Steady Flow Analysis)

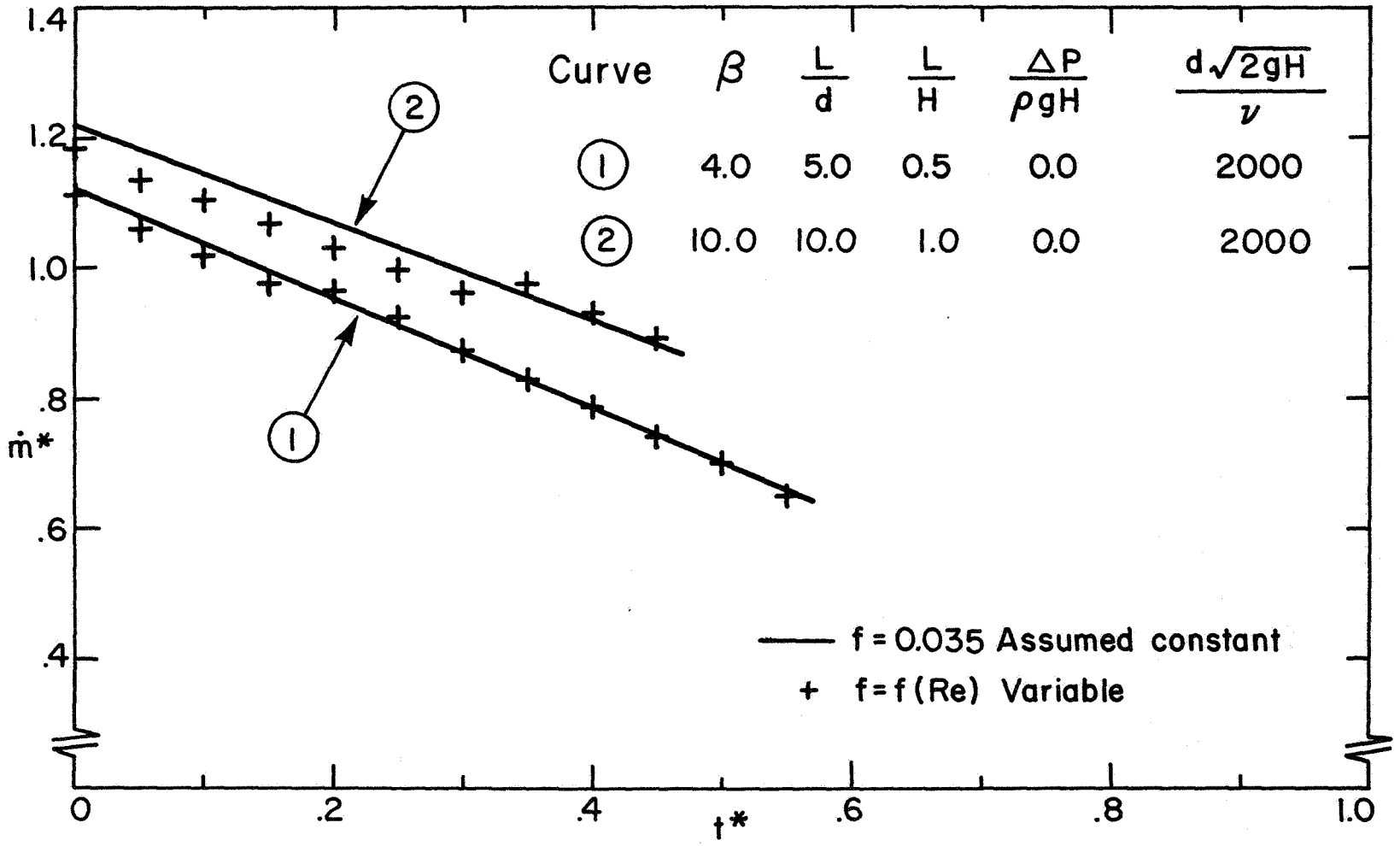

Figure 6.36. Effect of Variation of f with Re on $\dot{m}^*$ vs. t^* for Discharge Through a Tube when $d\sqrt{2gH}/\nu = 2000$ (Quasi-Steady Flow Analysis)

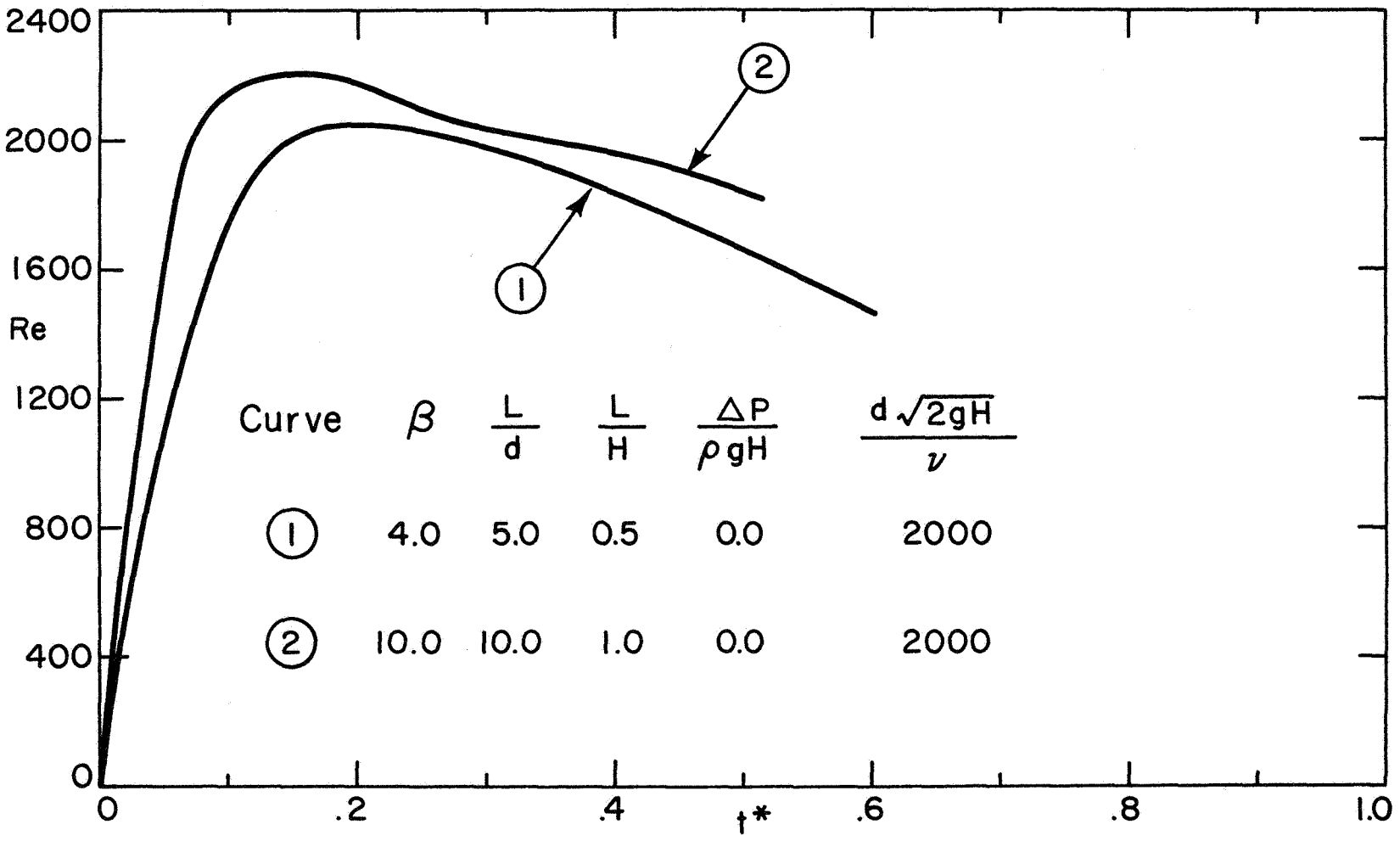

Figure 6.37. Variation of Reynolds Number ($Re = dV_2/\nu$) with Dimensionless Time (t^*) for Discharge Through a Tube when $d\sqrt{2gH}/\nu = 2000$ (Transient Flow Analysis)

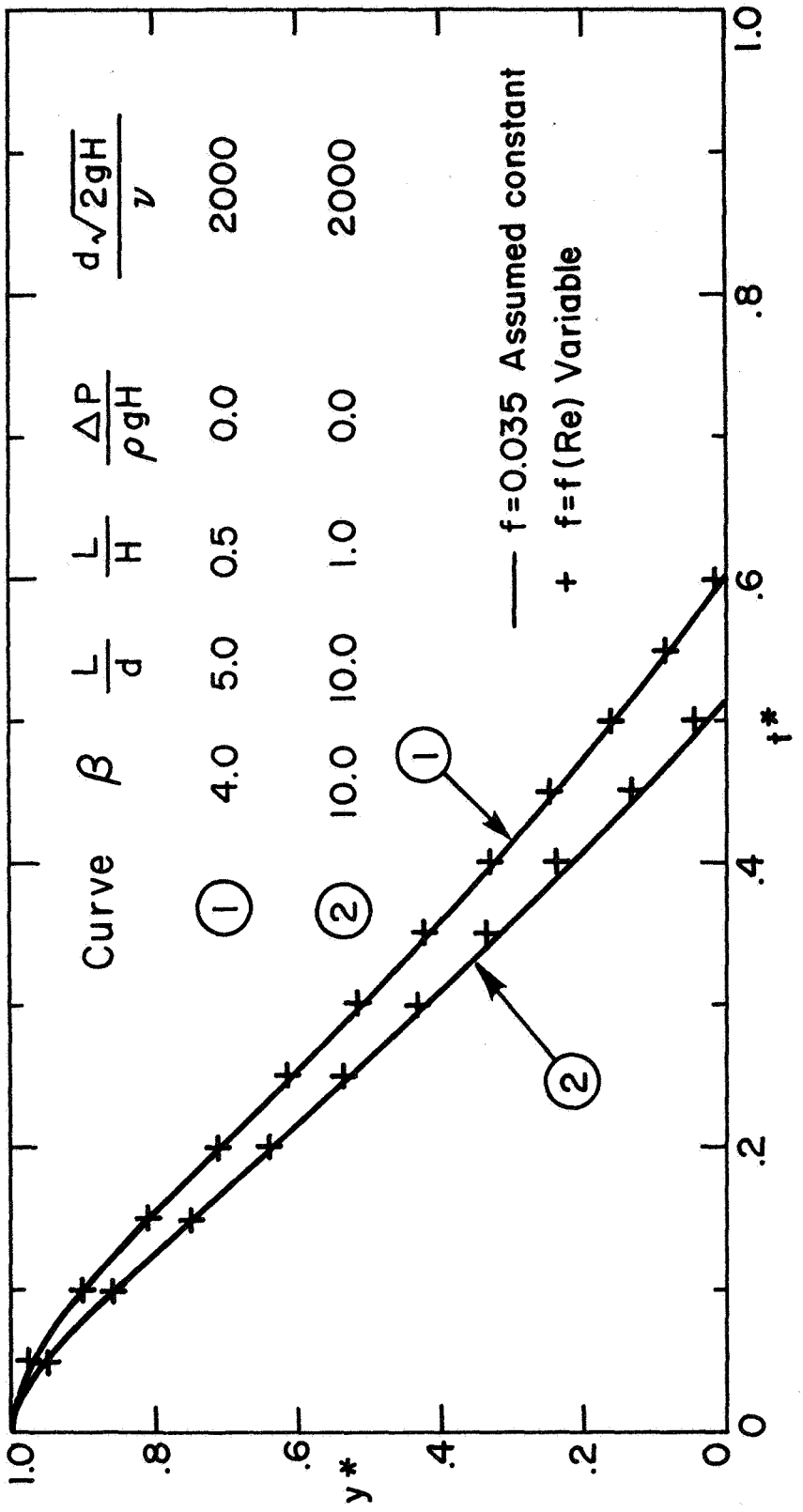

Figure 6.38. Effect of Variation of f with Re on y* vs. t* for Discharge Through a Tube when $d\sqrt{2gH}/\nu$ = 2000 (Transient Flow Analysis)

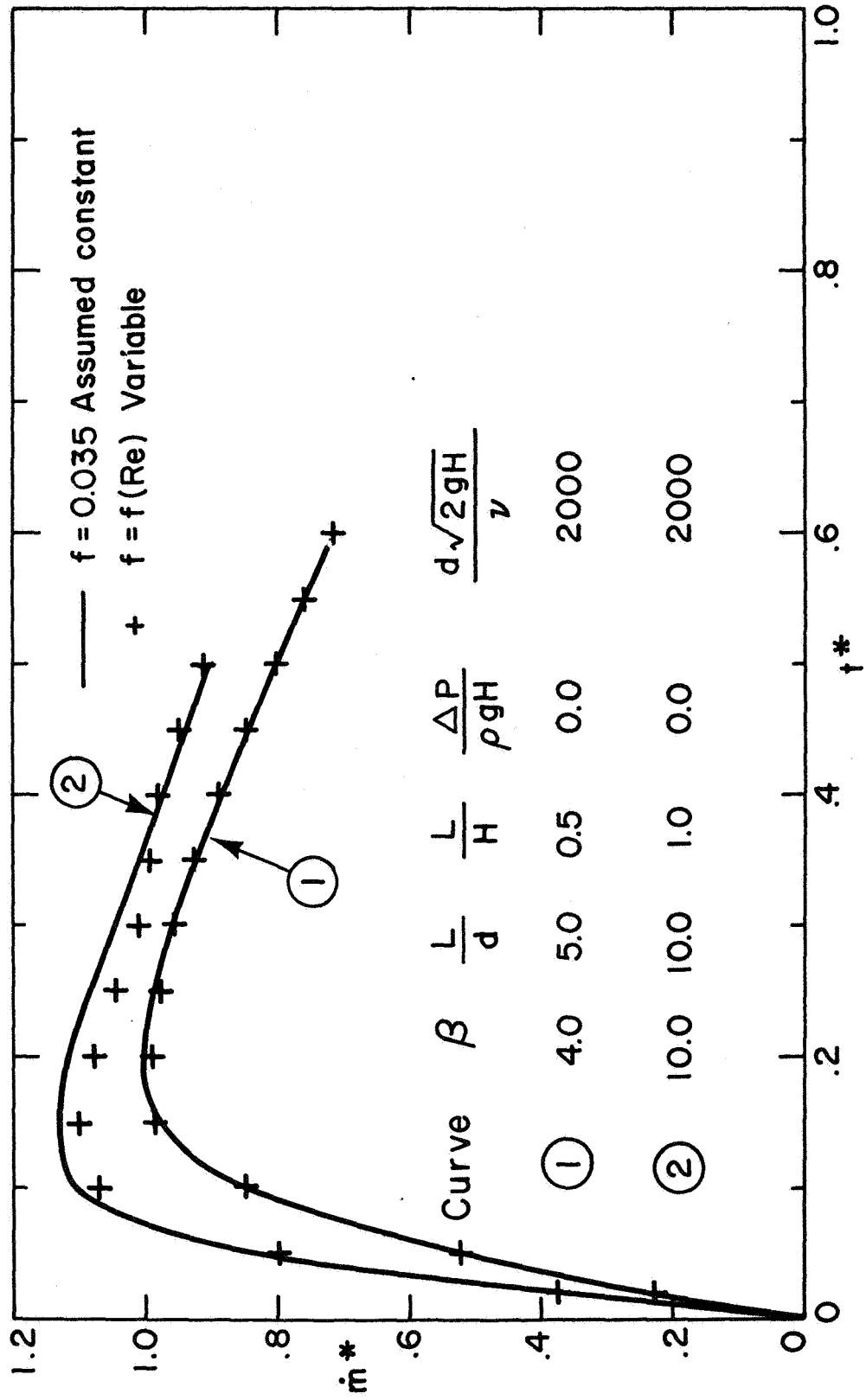

Figure 6.39. Effect of Variation of f with Re on $\dot{m}^*$ vs. t^* for Discharge Through a Tube when $d\sqrt{2gH}/\nu = 2000$ (Transient Flow Analysis)

CHAPTER 7

EXPERIMENTS

Experiments were performed with water using plexiglass containers (Figure 7.1) and tubes (Figure 7.2) to facilitate visual observation and television tape recording (Figures 7.3 and 7.4). The choice of containers and discharge tubes was governed by the sizes of commercially available plexiglass tubes. Table 7.1 gives the diameters of the containers and tubes which were used, along with the corresponding dimensionless ratios characterizing the geometry. Eight different cases are indicated, but only two of these cases yield β-values which are approximately the same (see the first and last entries in Table 7.1). Therefore, these two were used to investigate the effect of changing the size of the system without appreciably altering any of the other pertinent dimensionless parameters.

Due to laboratory space limitations, the container height was restricted to 48". Experiments for discharge through an orifice were conducted using the 5.5" diameter container with a 2.5" sharp-edged hole in the base plate and adapters having 2" and 1.5" holes. For investigation of discharge through a tube, discharge tubes of three different diameters, each with $\frac{L}{d}$ values of 1.1, 5, and 10 were constructed. Two base plates were made to accomodate each of the diameters, one with a rounded entrance as shown in Figure 7.5 and another with a sharp-edged entrance. The rounding of the entry was done according to Powell's specification for a circular arc profile (Ref. 37). Containers of 3 different diameters

Table 7.1. Geometric Parameters Used in Experiments

Container Diameter (in.)	Discharge Diameter (in.)	Area Ratio	β
10.97	5.46	4.03	3.91
10.97	3.95	7.70	7.64
10.97	2.95	13.78	13.74
8.95	5.46	2.68	2.49
8.95	3.95	5.13	5.03
8.95	2.95	9.18	9.12
5.49	3.95	1.93	1.65
5.49	2.95	3.45	3.31

could be adapted to each of the base plates. To summarize, there were 9 tubes, 6 base plates, and 3 containers which made it possible to investigate a large number of different geometries (for discharge through a tube). The containers were centered with respect to the discharge opening by use of an L-square and were held firmly in place by a top plate and 7/16" diameter threaded brass rods. A 3" diameter opening in the top plate was used to fill the container with water. A manually operated gate valve was employed to initiate the discharge. Specially prepared measuring tapes, with markings at 2" intervals, were attached to the containers so that the liquid height could be easily determined to an accuracy of 0.1" from the TV screen. A Standard Timer with a 9" dial was used to record the time. The time resolution was 0.01 sec.

The discharge process was recorded on video-tape, and the instantaneous liquid heights and the corresponding times were read out by means of a closed circuit stop-action TV system. The TV recording system consisted of a Fairchild TC-175 camera equipped with a zoom lens, an Ampex VR-7000 videotape recorder, and a Sony (Model PVJ-3030) 5" video monitor which was mounted on top of the camera to serve as viewfinder. In addition, an Ampex VM-9A portable video monitor was used for playback of the taped data which could be read out easily while operating the tape recorder in the stop-motion mode (Figure 7.4). The camera had a resolution of about 350 lines. In the stop-motion mode of operation the discharge process was examined frame by frame (60 frames/sec.). The time of initiation of discharge ($t = 0$) could be determined to within 0.02 sec. The instantaneous liquid height, y, and the corresponding time, t, were tabulated and non-dimensionalized to yeild the corresponding values of y^* and t^*. Some of these experimental results are presented, along with the appropriate

analytical predictions, in the following chapter. In calculating the analytically predicted curves from equation (6.10) the friction factor, f, was estimated as follows.

The Reynolds number in the tube is given by

$$\frac{d.V_2}{\nu} = \frac{1}{2}\frac{d\sqrt{2gH}}{\nu} \cdot \frac{A}{a} \cdot \frac{1}{\beta}\left(-\frac{dy^*}{dt^*}\right) .$$

$\frac{A}{a} \cdot \frac{1}{\beta} \approx 1$ and the maximum value of $\left(-\frac{1}{2}\frac{dy^*}{dt^*}\right) = \dot{m}^*$ is also of the order of 1.0 (see Figure 6.15). Therefore the maximum value of the Reynolds number for the flow in the tube is of the order of $\frac{d\sqrt{2gH}}{\nu}$. For the transient case, however, since the fluid is initially at rest, the Reynolds number is zero at the start of the discharge process and increases continuously to a peak value of about $\frac{d\sqrt{2gH}}{\nu}$, and again falls off to a lower value (see Figures 6.31 and 6.37). For water at 70°F temperature the kinematic viscosity $\nu = 1 \times 10^{-5}$ ft^2/sec. With the acceleration due to gravity $g = 32.2$ ft/sec^2, the parameter $\frac{d\sqrt{2gH}}{\nu} = 1.93 \times 10^4\ d\sqrt{H}$, where d and H are in inches. Over the entire range of experiments $\frac{d\sqrt{2gH}}{\nu}$ varied from about 2.21×10^5 to 5.8×10^5. In this range the Moody chart (Figure 7.6) shows that the friction factor varies very little, from 0.015 to 0.013. This means the friction factor has a very high value at the start of a run (because Re starts from zero) and decreases to the values indicated above before increasing again. Thus the higher value, f = 0.015, for the friction factor was assumed for the entire range of experiments, for calculating the predicted curves from equation (6.10). As can be seen from Figures 6.32 and 6.33, for this range of Re there is practically no difference between predictions with f = 0.015 assumed constant and those with f varying as a function of Re.

As mentioned in Chapter 6 (see page 80) the entrance losses were neglected in deriving equation (6.10). This is acceptable for tubes with rounded entrances. If entrance losses are introduced (as in the case of Quasi-Steady Discharge through a tube, see equation C1), equation (6.10) is modified as

$$\frac{L}{H}\,\frac{d^2y^*}{dt^{*2}} - \frac{1}{2}\left[\beta^2\,\frac{a}{A} + f\,\frac{A}{a}\,\frac{L}{d} + K\,\frac{A}{a}\right] + 2\beta^2\,\frac{a}{A}\,y^* = -\,2\left[\frac{P_1-P_2}{\rho g H} + \frac{L}{H}\right]\frac{a}{A}\cdot\beta^2 \qquad (7.1)$$

For steady flow through a sudden contraction (Ref. 31) K varies between 0.4 and 0.5 for β-values ranging from 4 to ∞. The higher value of K = 0.5 was used, analogous to the manner in which the friction factor was treated, in the calculations for transient discharge through tubes with sharp-edged entrances.

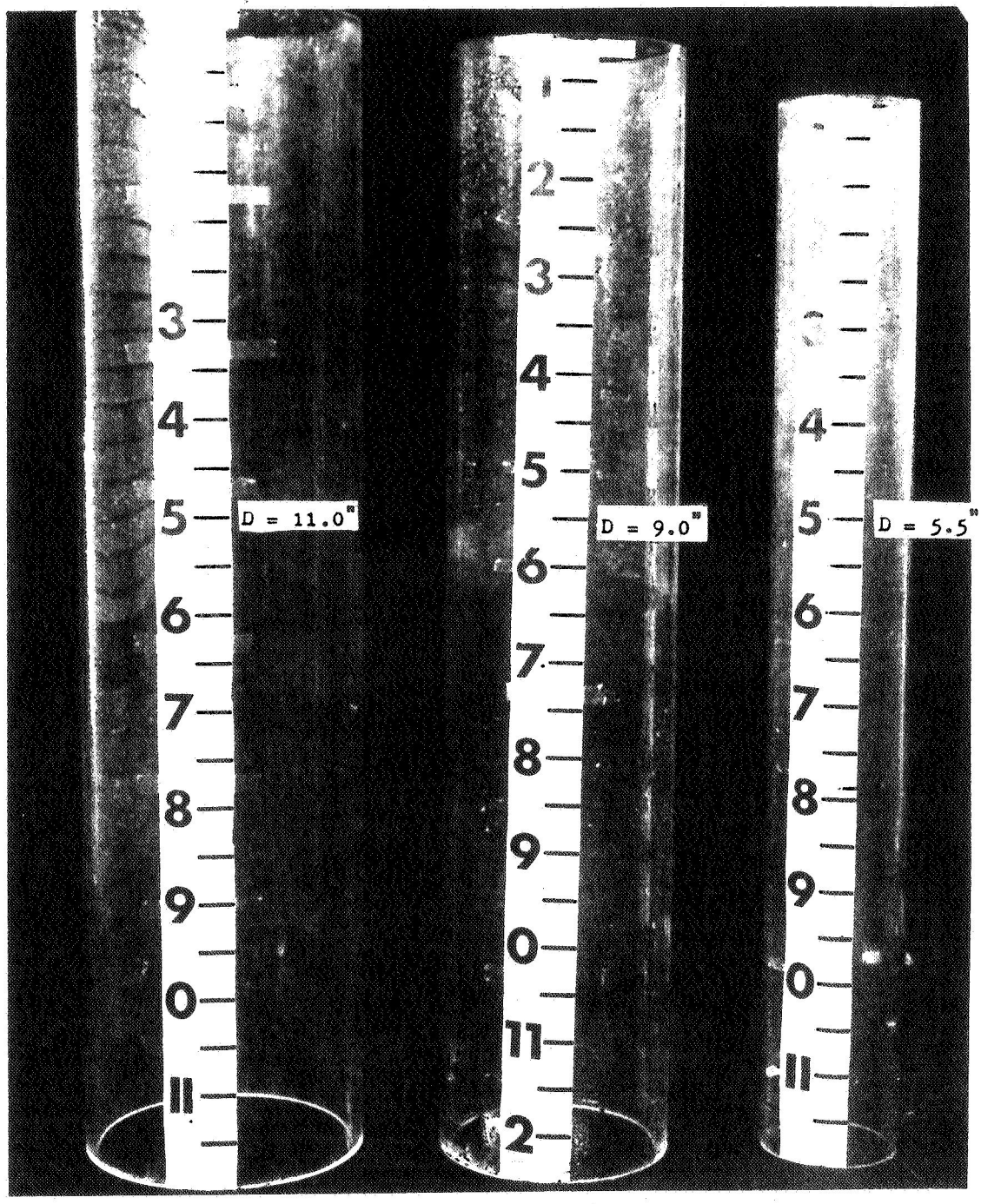

Figure 7.1. Plexiglass Containers

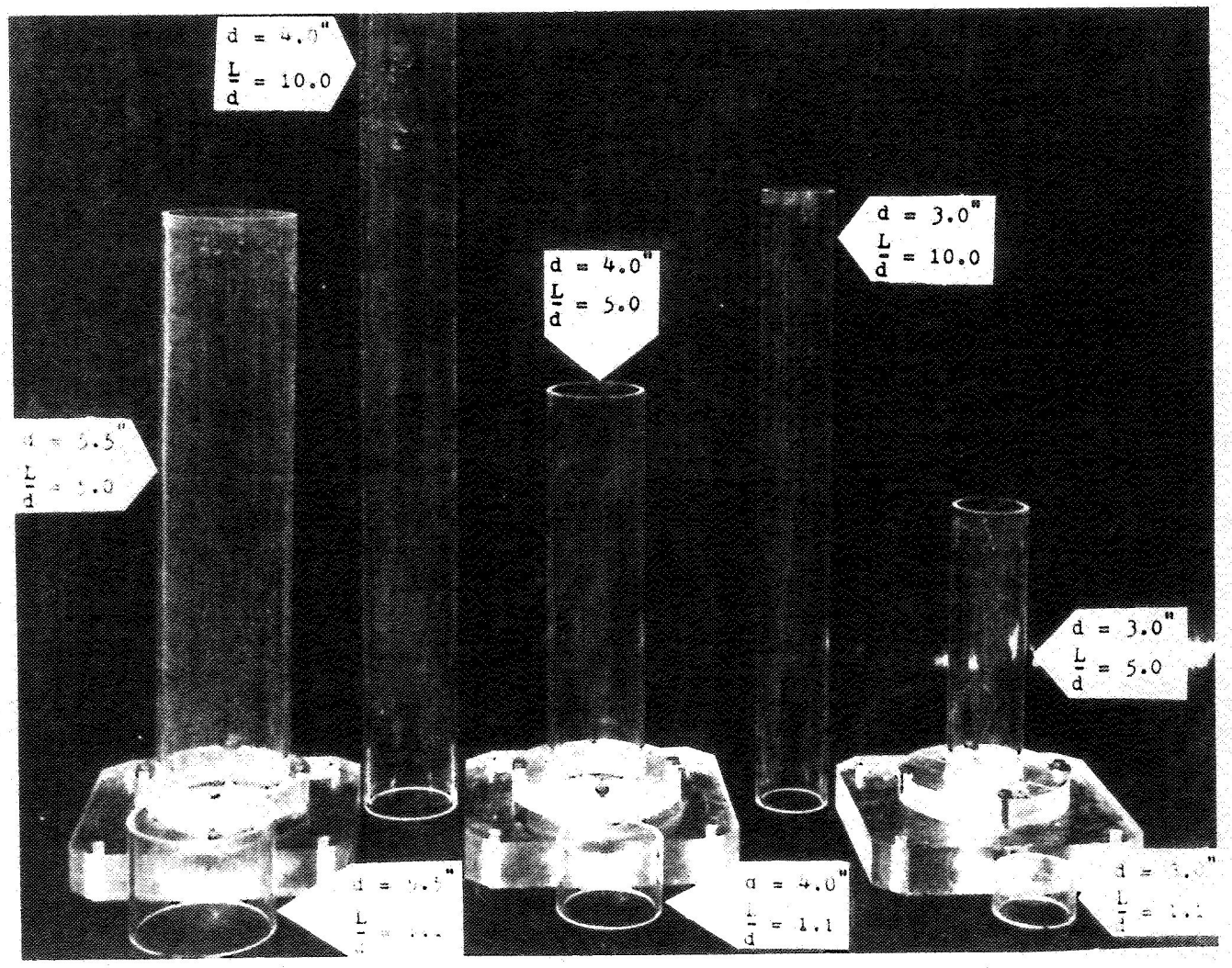

Figure 7.2. Plexiglass Discharge Tubes

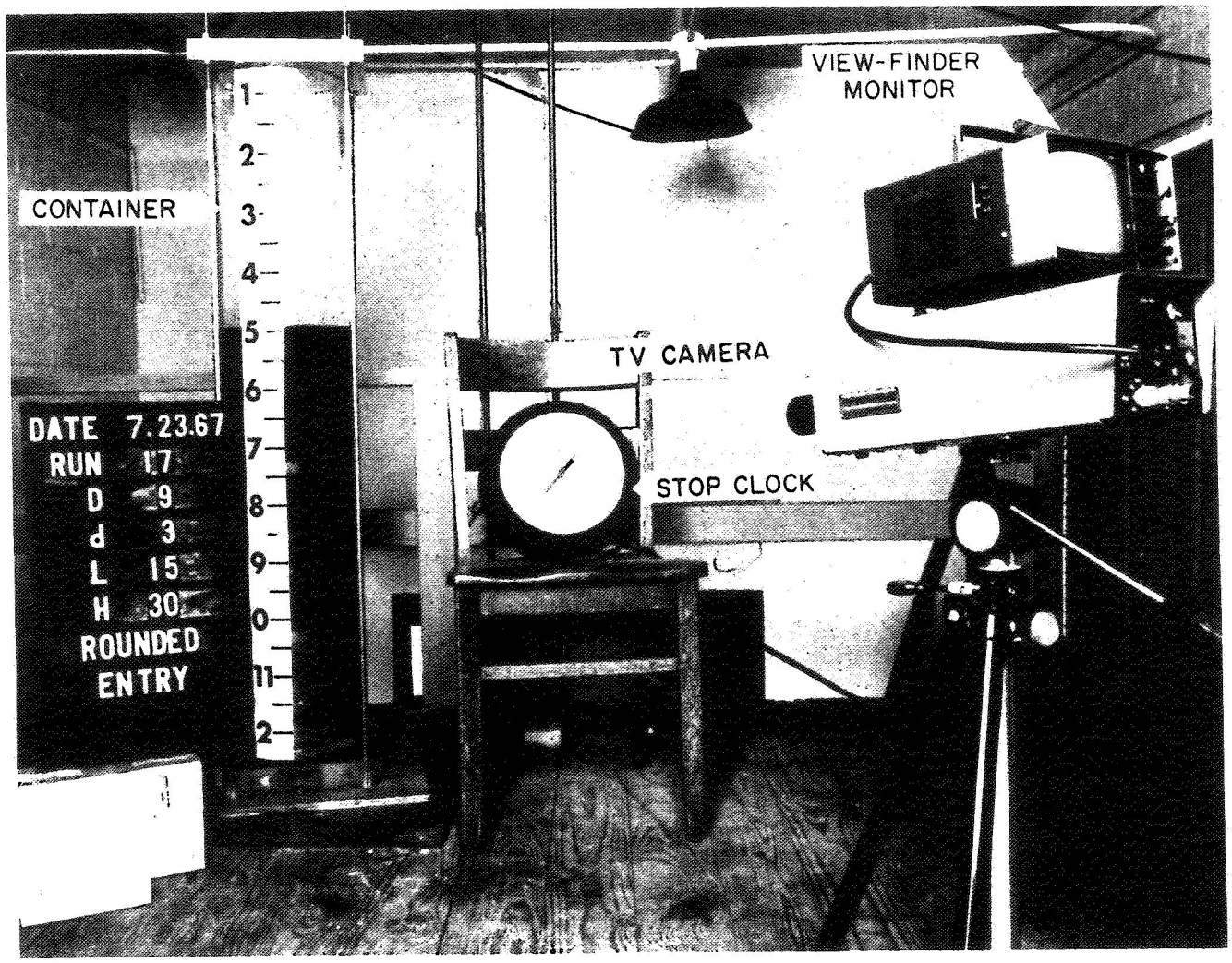

Figure 7.3. Experimental Apparatus

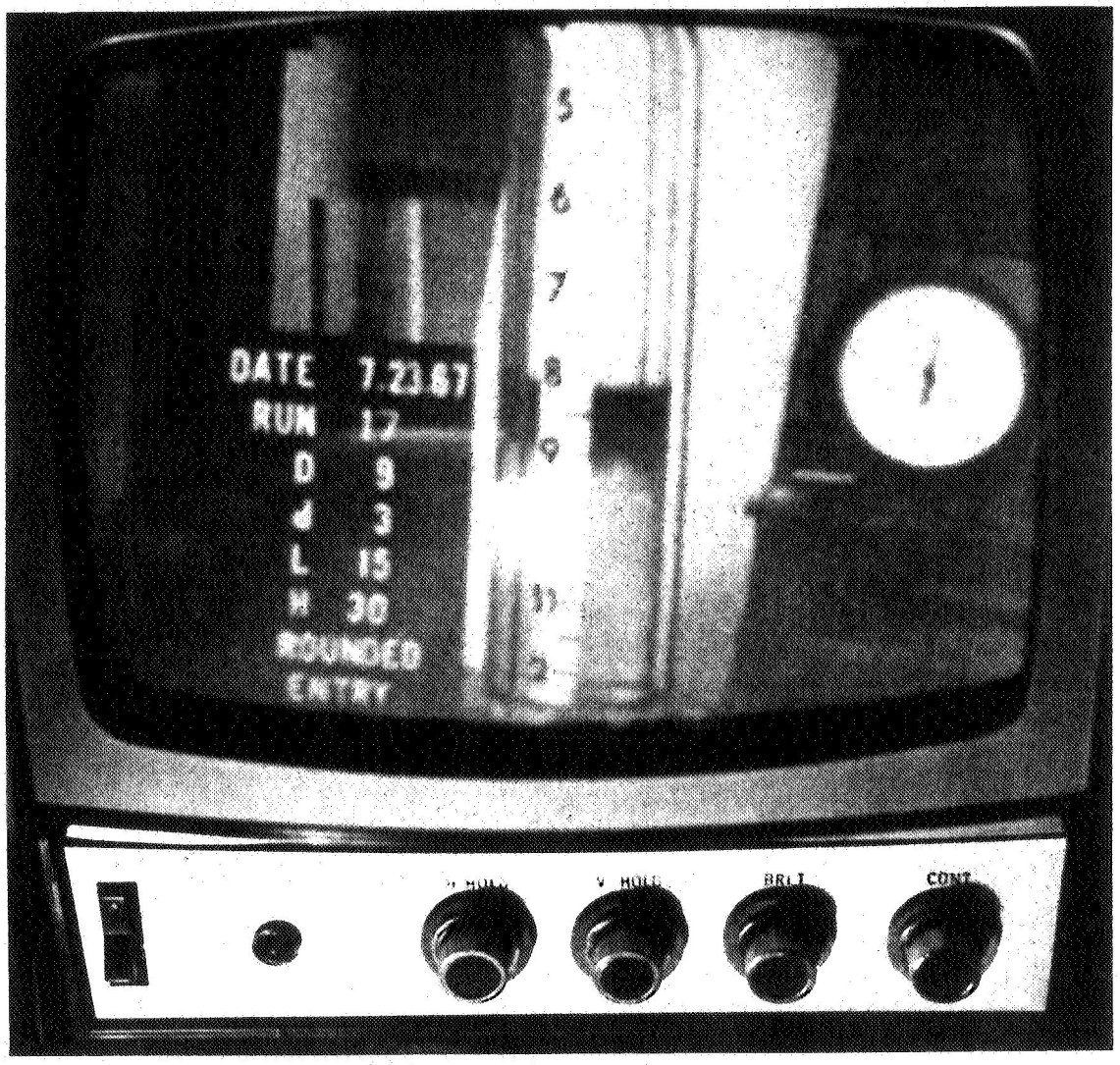

Figure 7.4. Video Tape Monitor in Stop-Motion Mode of Operation

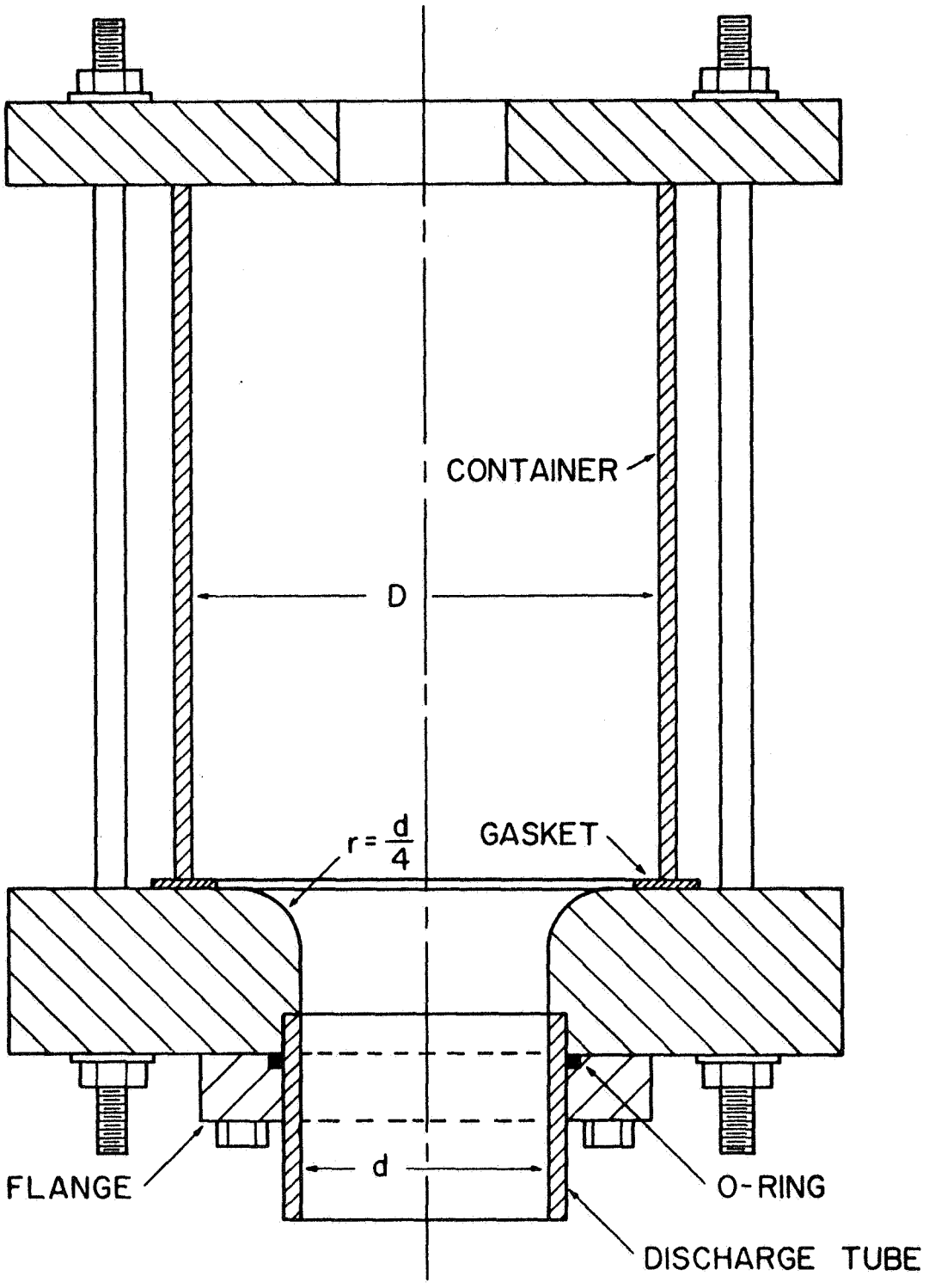

Figure 7.5. Assembly Drawing of Discharge Container

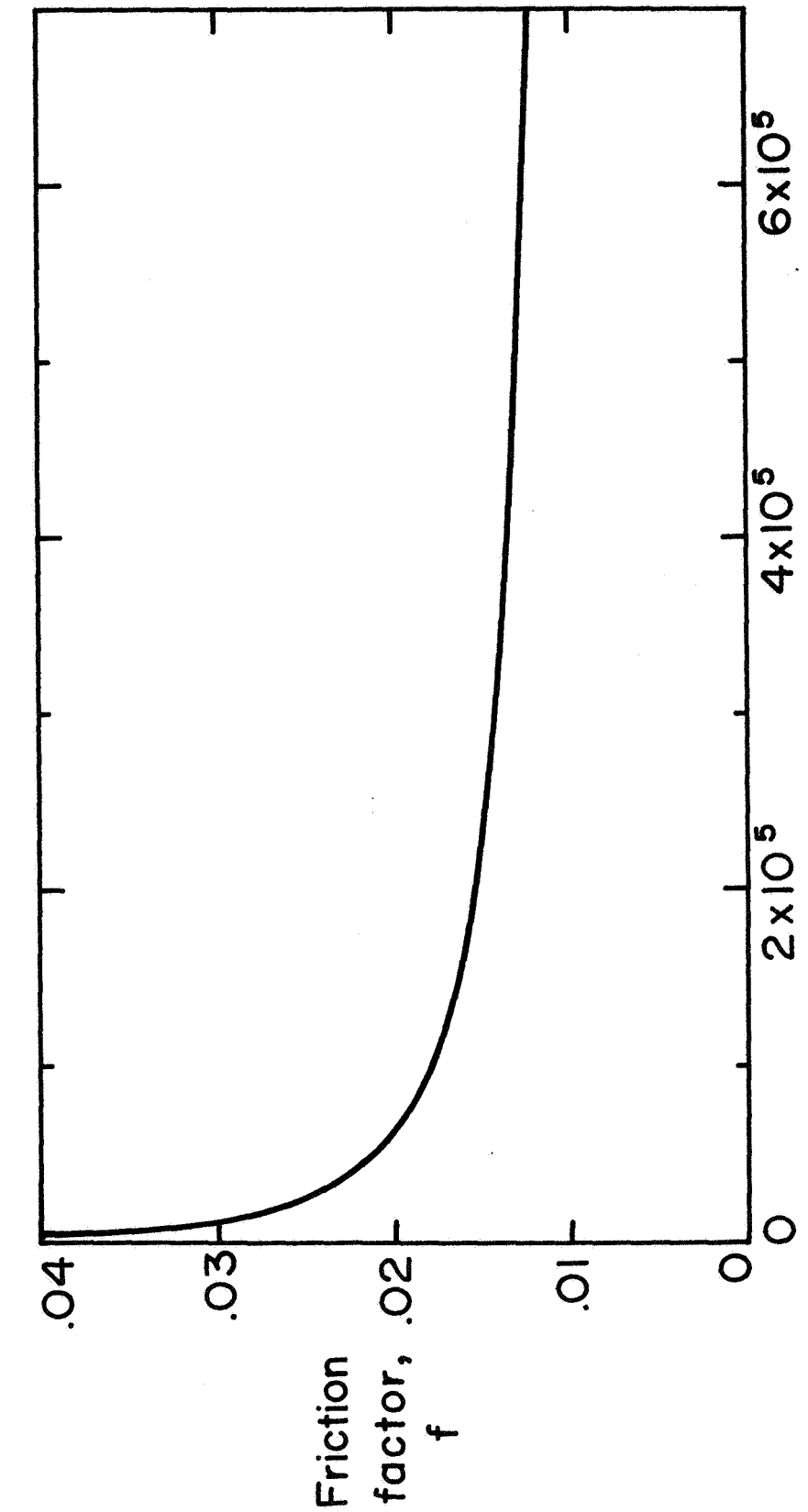

Figure 7.6. Moody Chart (Ref. 3) Giving Dependance of the Smooth Tube Friction Factor on the Reynolds Number.

CHAPTER 8

RESULTS AND CONCLUSIONS

The dimensional analysis for the problem of single-phase discharge of a liquid from a container yielded the instantaneous dimensionless liquid height, $y^* = \frac{y}{H}$, and the dimensionless mass flow rate, $\dot{m}^* = \frac{\dot{m}}{\rho \left(\frac{\pi D^2}{4}\right) \frac{1}{\beta} \sqrt{2gH}}$, respectively as functions of six dimensionless parameters $t/\beta \sqrt{\frac{2H}{g}}$, $\frac{D}{d}$, $\frac{L}{d}$, $\frac{L}{H}$, $\frac{\Delta P}{\rho g H}$ and $\frac{d\sqrt{2gH}}{\nu}$. Heat transfer, cavitation and surface tension effects were not taken into account. Figures 8.1 through 8.3 show measurements that illustrate the correctness of the parameters obtained by the dimensional analysis procedure. Equation (3.2a) indicates that two systems having the same dimensionless parameters $\frac{D}{d}$, $\frac{L}{d}$, $\frac{L}{H}$, $\frac{\Delta P}{\rho g H}$ and $\frac{d\sqrt{2gH}}{\nu}$ should exhibit a single functional relationship between dimensionless liquid height, y^*, and dimensionless time, t^*. The data shown in Figures 8.1 through 8.3 were obtained with two systems of different sizes, but having essentially the same values for 4 of the 5 dimensionless groups just indicated. The fifth parameter, $\frac{d\sqrt{2gH}}{\nu}$, was considerably different for the two systems compared in each figure. It is interesting to note that experiment indicates that the dependence of the y^* vs. t^* relationship on the parameter $\frac{d\sqrt{2gH}}{\nu}$ is very weak, a fact that dimensional analysis alone cannot reveal. Such weak dependence can be expected, however, from the physics of the problem because the effect of varying a Reynolds number is indirect. When the Reynolds number is

changed, the friction factor which determines the resistance to the fluid motion changes. But for the values of $\frac{d\sqrt{2gH}}{\nu}$ indicated (i.e. 2.21×10^5 to 5.8×10^5), f can be assumed constant (see Figures 6.32 and 6.33). The measurements represented by circles were obtained with a 5.5" diameter container, while those indicated by the triangles were obtained with a larger container having a diameter of 11". The two systems were geometrically similar. Two sets of data are shown for each container, and it is apparent that the measurements were essentially reproducible despite the fact that some scatter did result. The data imply that the instantaneous liquid height, y*, is a unique function of the dimensionless time, t*, when the other 4 dominant dimensionless groups are each maintained constant. Most of the discrepancy between two sets of results is attributed to the fact that the two $\frac{D}{d}$ - values were slightly different, being 1.86 in one case and 2.01 in the other. Similar results are depicted in Figures 8.4 through 8.6 for tubes with sharp-edged entrances for this more complex flow situation. This supports the observation made in Chapter 3, that the dimensional analysis results given in equations (3.3a) and (3.4a) are valid if geometrical similarity is maintained and the physical conditions assumed in their derivation are satisfied for the two systems.

An analysis of discharge through an orifice indicated that when the flow is quasi-steady, the dimensionless liquid height and the dimensionless mass flow rate vary parabolically and linearly, respectively, with dimensionless time (see equations 5.4 and 5.5). It is interesting to note that when the instantaneous liquid height, instantaneous mass flow rate and time elapsed since the initiation of discharge are non-dimensionalized as given in equations (5.3), the graphs of y* vs. t* and $\dot{m}$* vs. t*

are universal for this type of discharge. They are independent of the geometric π-factors $\frac{L}{d}$, $\frac{D}{d}$, $\frac{L}{H}$. The total dimensionless time for discharge is always 1.0, indicating that when β is decreased (i.e. when the area of discharge is increased in relation to the container cross-sectional area) the actual discharge time decreases proportionately.

When transient effects are taken into account, equation (5.9) describes the behavior of the liquid height with time for discharge through an orifice in the absence of viscous effects for zero pressure drop. Figures 5.4 and 5.5 respectively illustrate the effect of changing the parameter β on the variations of y^* and $\dot{m}^*$ with t^*. They indicate that, except for very low values of β ($\beta < 4$) and at very small periods of time after the initiation of discharge, the inertia effects are essentially negligible. In the cases where $\beta > 4$ the liquid accelerates rapidly from rest and then very closely follows the quasi-steady solution. A complete solution for equation (5.9) exists, and this solution can be expressed in terms of complete and incomplete Beta functions. This result is given in equation (5.19) for the case where geometric and viscous effects are taken into account (by inclusion of the discharge coefficient, C_D). A comparison of the complete solution with the numerical solution of equation (5.9) obtained by a Fourth Order Runge-Kutta method is given in Figures 5.8 and 5.9 for two different sets of conditions: $\beta = 4$, $C_D = 0.6$ and $\beta = 10$, $C_D = 0.82$. These figures show that the solutions are identical, thus providing some confidence in the numerical techniques employed in their evaluation. The total discharge time for transient discharge of a container through an orifice, given by equation (5.19a), is

$$t_t^* = \left[\frac{1}{4\alpha(\alpha-1)}\right]^{\frac{1}{2}} B\left(\frac{1}{2(\alpha-1)}, \frac{1}{2}\right)$$

and this is only about 1% above that given by the quasi-steady analysis for $\beta = 4$. A comparison of the total discharge times obtained from the two analyses is given in Figure 8.7.

Figures 8.8 through 8.11 depict the experimental results for discharge through an orifice and comparison with theory. In Figure 8.8, the experimental measurements are plotted for three different situations. The difference between the measurements for $\beta = 4.76$ (represented by solid circles) and for $\beta = 7.58$ and 13.65 (represented by the hollow and solid triangles respectively) can be attributed to a difference in the discharge coefficients rather than to a change in β-value. This is apparent from Figures 8.9 to 8.11 where these three sets of data are compared to theoretical predictions. In Figure 8.9 the results for $\beta = 4.76$ are compared with theoretical curves for the same β and the two different values of C_D for orifice flow given in Figures 5.6 and 5.7. This indicates that for flow through orifices, where the thickness of the orifice is not zero (i.e., $L/d \neq 0$) the discharge coefficient C_D lies between 0.6 and 0.82. However, no clear cut method was found for establishing, a priori, the value of C_D for a particular geometry. On the other hand, it would appear from Figures 8.10 and 8.11, where experimental results for $\beta = 7.58$ and 13.65 are compared with theory, that when $\frac{L}{d} \geq 1.0$ the fluid fills the orifice (i.e. the hole in the base plate) and C_D can be taken to be 0.82 (see Figure 5.6). It is contended that these are really cases of discharge through short tubes and that the analysis based on transient flow through a tube should be able to predict the variation of y^* with t^* accurately. The solid lines in Figures 8.10 and 8.11,

which were obtained from equation (7.1) and which account for losses due to a sharp-edged entrance, support this contention.

For the case of discharge through a tube the analysis based on quasi-steady flow (equations 6.1 and 6.2), as well as the analysis taking transient effects into account (equation 6.10), gives the dimensionless liquid height as a function of all the parameters obtained in the dimensional analysis (equation 3.2a). It should be remembered that β is a function of $\frac{D}{d}$ and the friction factor, f, is essentially a function of $\frac{d\sqrt{2gH}}{\nu}$ and $\frac{dy^*}{dt^*}$. However, the quasi-steady analysis indicates that, when the friction factor $f = 0$, there is no effect of changing β, and even when $f \neq 0$ the effect of varying β is essentially negligible. The only parameters which have a significant effect on the discharge process are $\frac{L}{H}$, $\frac{\Delta P}{\rho gH}$ and f. These results from the analysis based on quasi-steady flow have been found to be valid only when β-values are large ($\beta > 20$). The experimental results for this case have been available for some time and are presented in Ref. (25) and (26).

The analysis which takes into account the inertia effects in the tube indicates that β plays a very important role even when friction effects are neglected. Since transient effects in the container were neglected, this analysis is valid only for β-values in the neighborhood of 4 or above. Figures 8.12 through 8.20 depict experimental results for discharge of a container through a tube with a rounded entrance at low β-values ($\beta < 20$). In all these figures the solid and dashed lines were computed by numerical integration of equation (6.10) for the values of the dimensionless parameters indicated. The friction factor, f, was estimated by the method described in Chapter 7 and was assumed to be a constant for the entire transient period. Further, entrance losses were

neglected.

Figure 8.12 shows measurements for 4 different values of β and for two different values of $\frac{L}{H}$ for each, when $\frac{L}{d} = 1.1$. These results indicate that when $\frac{L}{d}$ is small (i.e. approximately 1.0) variations in β and $\frac{L}{H}$ have very little effect on the discharge process. This can be expected from physical reasoning, because the inertia effects in the container are negligible for $\beta > 4$ and the tubes are not sufficiently long to dominate the discharge process. Also, it can be seen from Figure 8.12 that the analysis for orifice flow does not predict the actual behavior accurately (note that the curves for orifice flow assuming transient effects will all lie above the solid line. (See Figure 5.4). On the other hand, equation (6.10) predicts the experimental behavior quite accurately (once again note that the dashed line Figure 8.12 is relatively insensitive to changes in β for the values of other parameters indicated on the figure). This supports the result discussed earlier, that when $\frac{L}{d} \geq 1.0$ the discharge of the container can be treated as if it occurs through a tube rather than an orifice.

When $\frac{L}{d}$ is increased to 5 or 10, changes in β have a pronounced effect, the fluid taking more time for discharging as β is decreased. Figures 8.13 through 8.16 represent the effect of changing β on the variation of y^* with t^* for several values of the other parameters ($\frac{L}{d}$ and $\frac{L}{H}$). It is worth noting that theory (equation 6.10) predicts the experimental behavior reasonably, even for $\beta = 2.49$ (Figure 8.15).

Figures 8.17 and 8.18 show the effect of altering $\frac{L}{d}$ from 5 to 10 for $\beta = 13.74$ and 3.91 respectively. These results suggest that at a particular value of β, variations in $\frac{L}{d}$ have only a limited effect in retarding the flow in the ranges investigated. A glance at equation

(6.10) shows that when f = 0.015 (the value estimated for these experiments), changing $\frac{L}{d}$ from 5 to 10 only slightly alters the coefficient of $(\frac{dy^*}{dt^*})^2$, the one place where this parameter appears. Thus, this result is logical from a theoretical viewpoint.

Figures 8.19 and 8.20 exhibit the effect of altering the parameter, $\frac{L}{H}$. Theoretical curves indicate that for $\frac{L}{H} = 0.5$ the fluid accelerates faster at the beginning of the discharge process than in the case of $\frac{L}{H} = 1.0$, which is due to the larger initial head in the former case. Since the larger column of liquid has a higher inertia, it requires a greater total time for the entire discharge. Although the measurements follow the theoretical curves closely in the latter half, they were not sufficiently precise to pick out the initial cross-over, owing to the very small periods of time (of the order of 0.5 sec.) involved.

Figures 8.21 through 8.29 depict the measurements for the case where the entrance to the discharge tube is sharp-edged, instead of being rounded as illustrated in Figure 7.5. This represents a slightly more complex situation, and it necessitates taking into account the loss in head due to the stream separation at the entrance and subsequent reattachment. The theoretical curves were calculated from equation (7.1), where the entrance loss coefficient, K, is included. The trends are identical with those described above for the case of rounded entrances (K = 0). The discharge process in general is slower because of the loss in head mentioned above.

For the case of pressure driven discharge of a container through a tube, a closed form solution in terms of elementary functions has been found for equation (6.10). This solution (given in equation 6.17) agrees very will with the numerical solution of the complete equation (see

Figures 6.26 and 6.27). In this important case of pressure driven discharge, it is seen that when β-values are low, the fluid spends a major portion of the total discharge time accelerating to the peak value attained during the transient period. No experimental measurements were obtained for $\frac{\Delta P}{\rho pH} > 0$ due to difficulty in fabricating the necessary apparatus and lack of the necessary sensitivity in the recording equipment. These problems are discussed in Chapter 9.

All the analytically predicted variations (the solid and dashed lines in Figures 8.9 through 8.29) were obtained assuming the discharge coefficient C_D or the friction factor f to be constant throughout a transient run. These assumptions are justified by the results presented in Chapters 5 and 6 (Figures 5.14 through 5.25 and 6.28 through 6.39). For discharge through an orifice it was shown that the predictions with a constant C_D (evaluated at $\frac{d\sqrt{2gH}}{\nu}$) and with a C_D varying according to the instantaneous Reynolds number differ little from each other when $\frac{d\sqrt{2gH}}{\nu} \geq 1000$ (Figures 5.18 and 5.19). Similarly, for discharge through a tube predictions assuming a constant friction factor f, chosen judiciously, and those with f varying as a function of instantaneous Reynolds number differ little over most of the ranges of $\frac{d\sqrt{2gH}}{\nu}$ (Figures 6.32, 6.33, 6.38, and 6.39).

In conclusion, it can be said that the scaling procedures developed during this investigation can be used with confidence for predicting the behavior of large liquid discharge systems when the flow is incompressible and single-phase, and when effects of heat transfer can be neglected. The data presented show good agreement between theory and experiment. Hence, the equations developed here can be applied for predicting the mass flow rate and its variation with time. In the following chapter, which

concludes the report, these results are summarized and recommendations are made for further research.

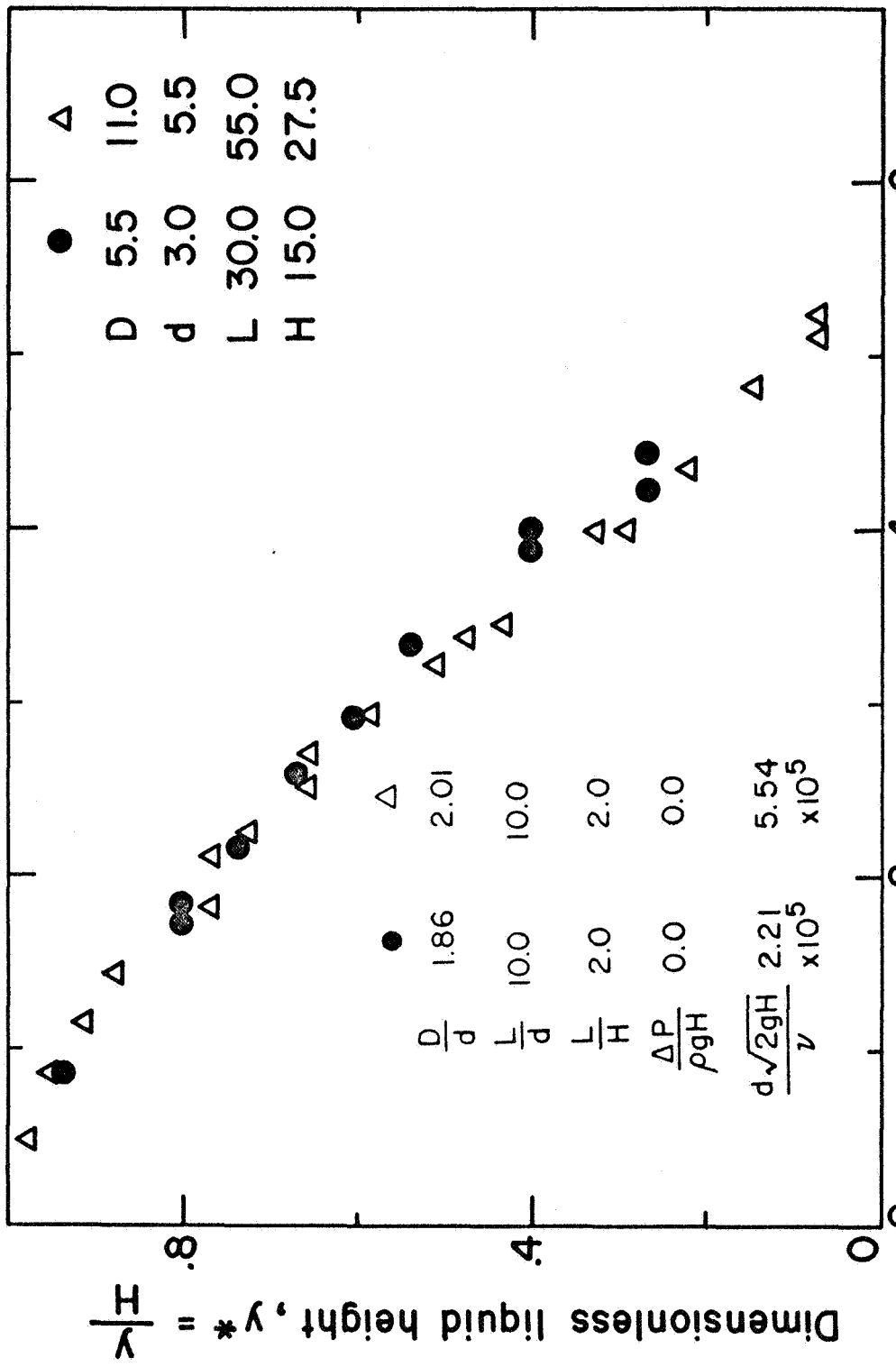

Figure 8.1. Variation of Liquid Height with Time for Two Similar Systems (Rounded Entrance)

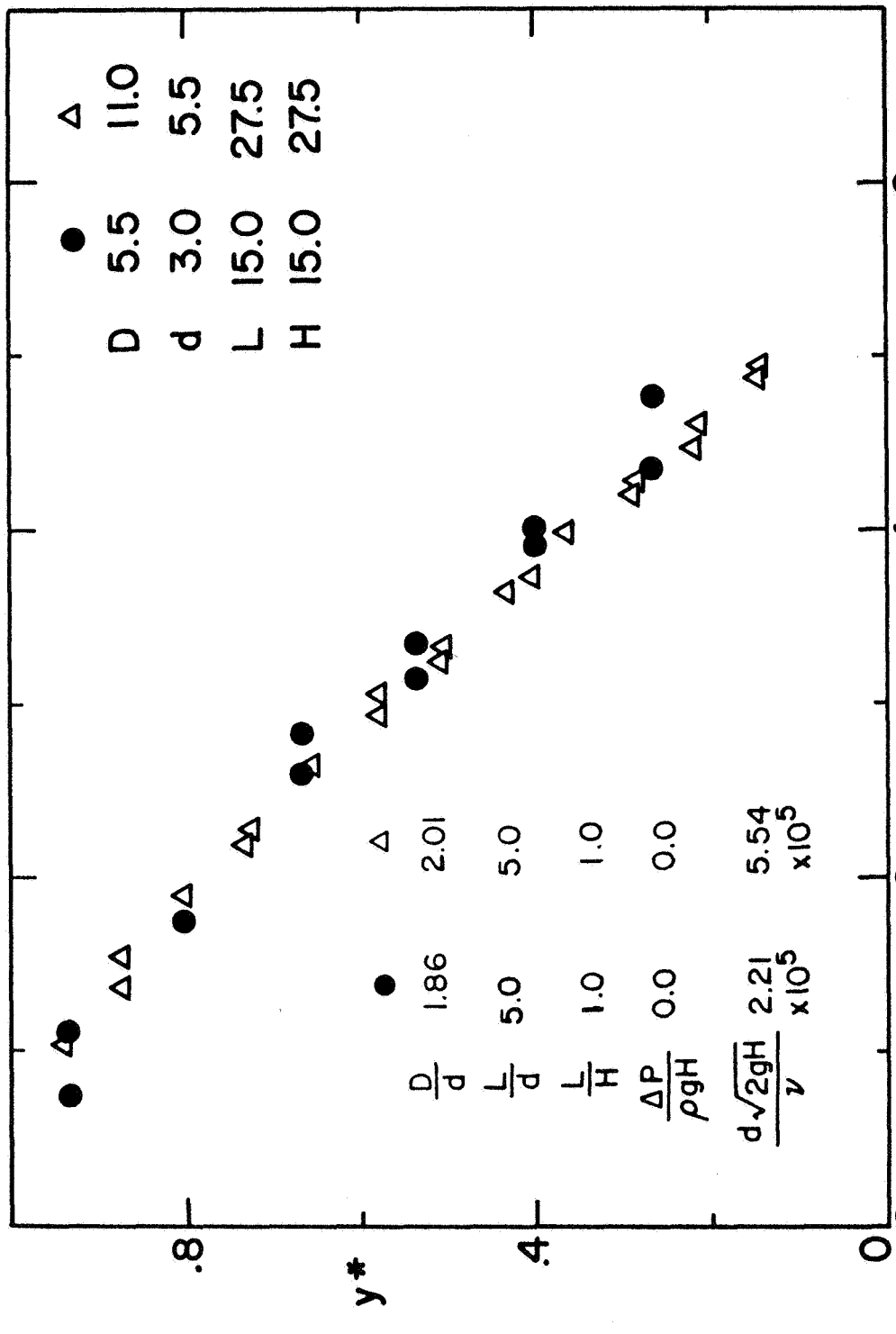

Figure 8.2. Variation of Liquid Height with Time for Two Similar Systems (Rounded Entrance)

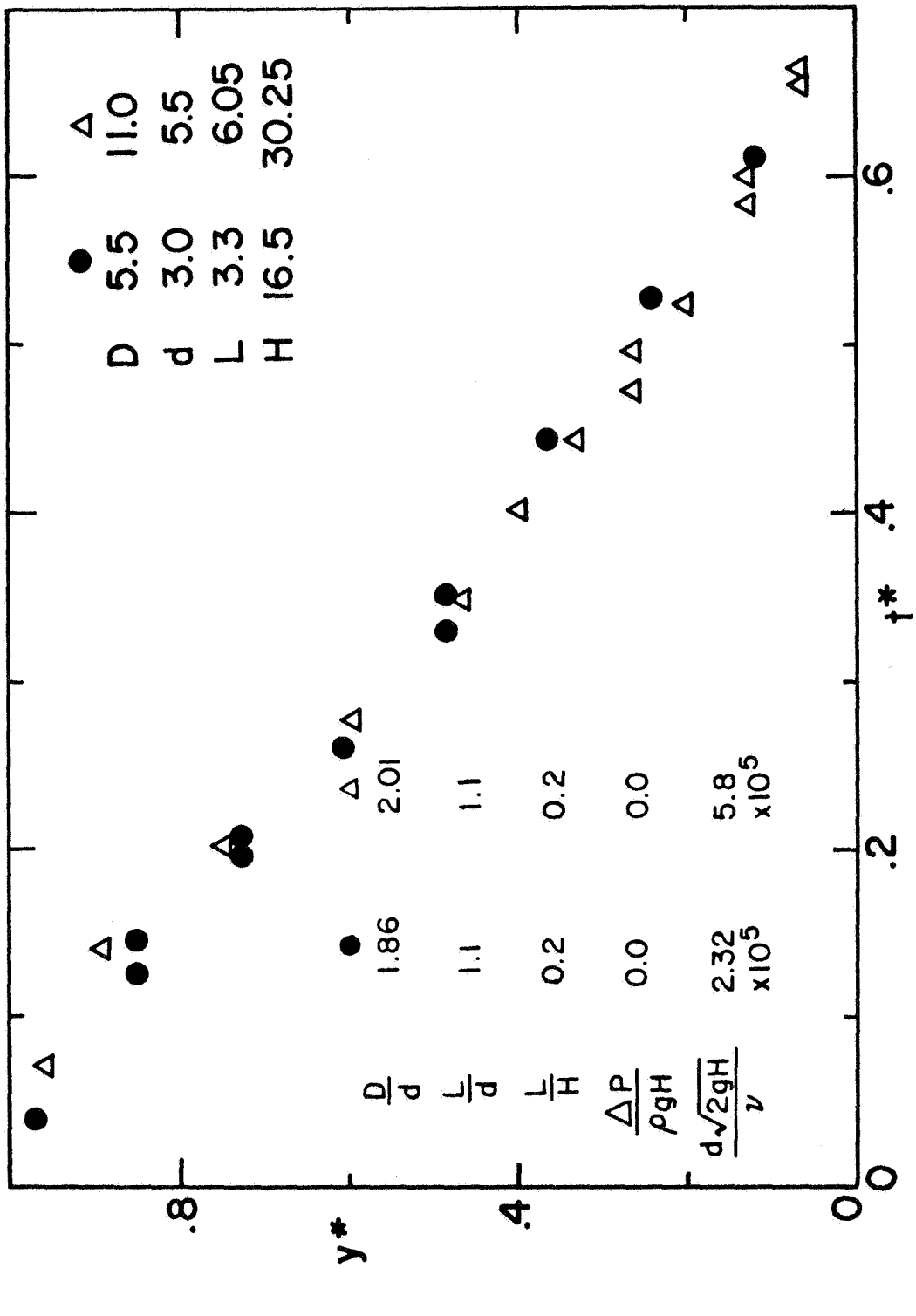

Figure 8.3. Variation of Liquid Height with Time for Two Similar Systems (Rounded Entrance)

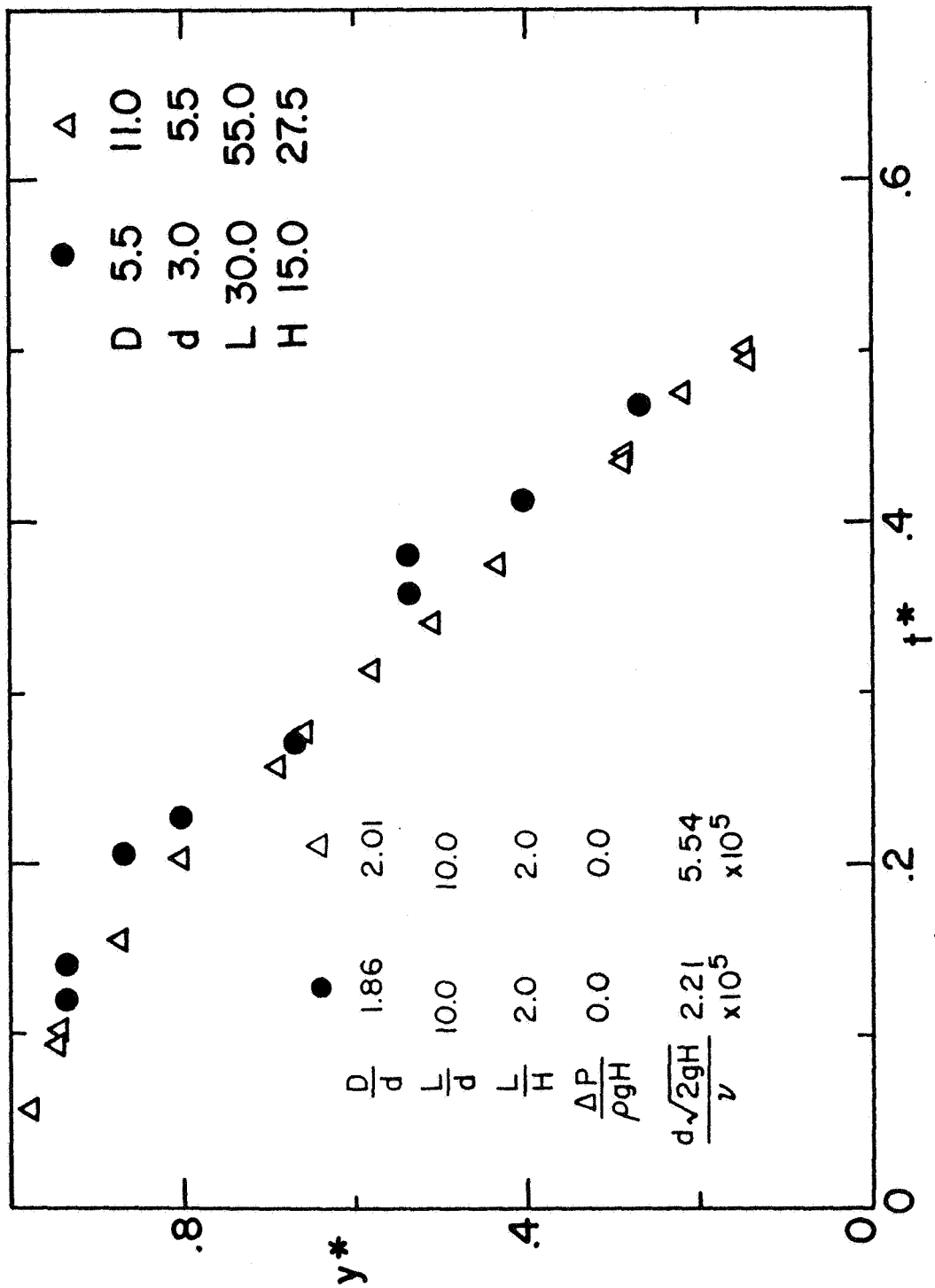

Figure 8.4. Variation of Liquid Height with Time for Two Similar Systems (Sharp-Edged Entrance)

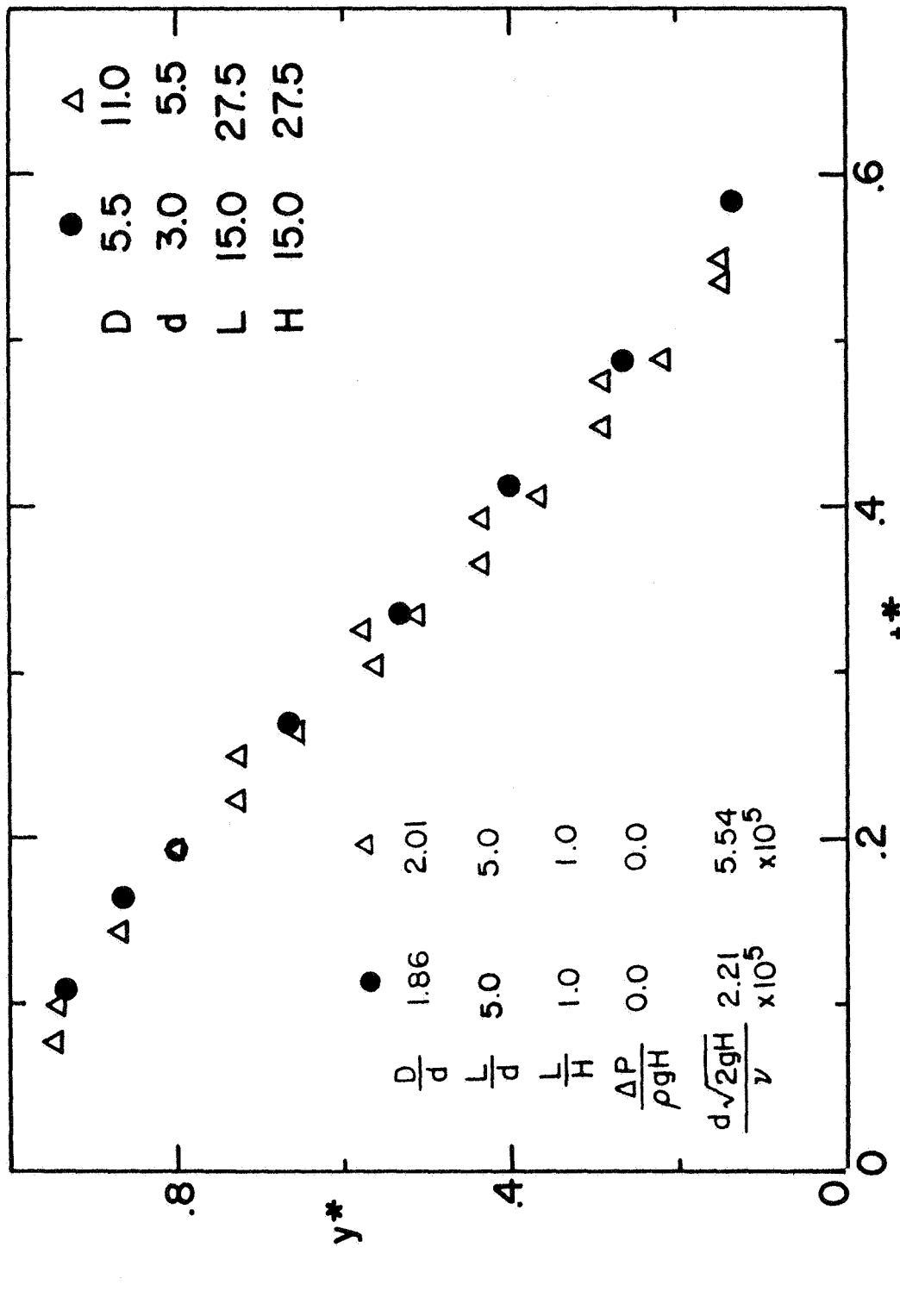

Figure 8.5. Variation of Liquid Height with Time for Two Similar Systems (Sharp-Edged Entrance)

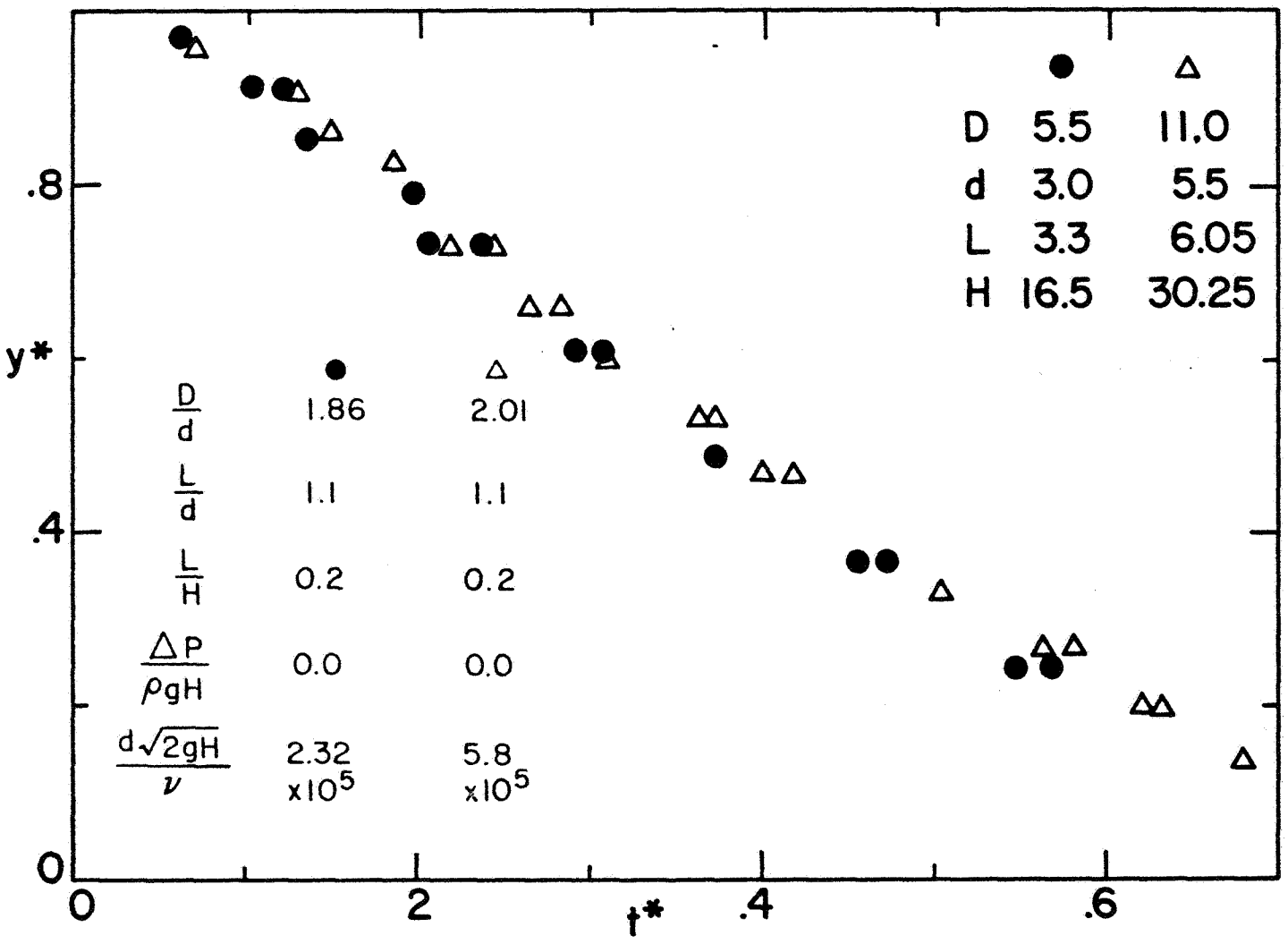

Figure 8.6. Variation of Liquid Height with Time for Two Similar Systems (Sharp-Edged Entrance)

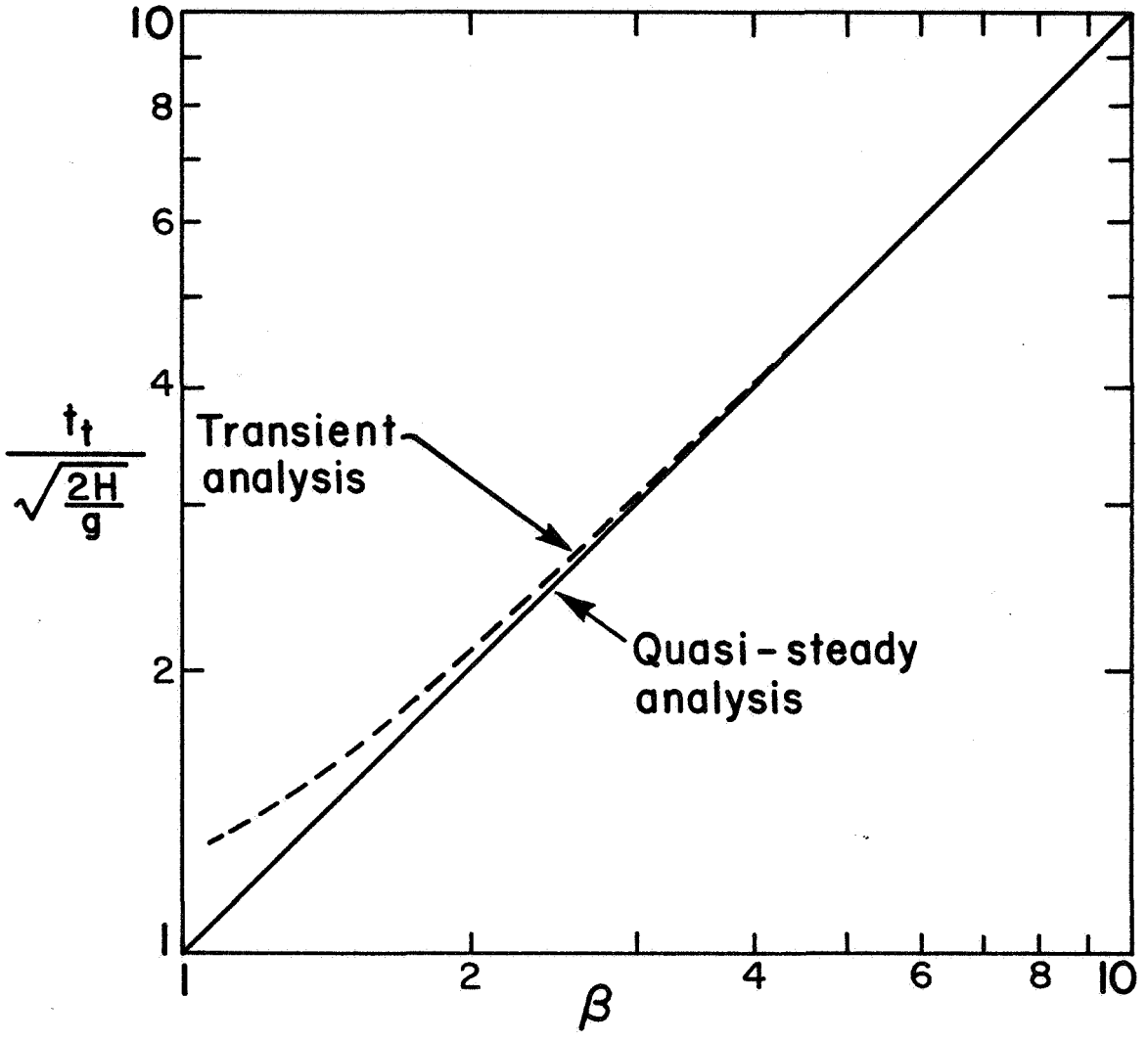

Figure 8.7. Variation of Total Discharge Time with β for Orifice Flow

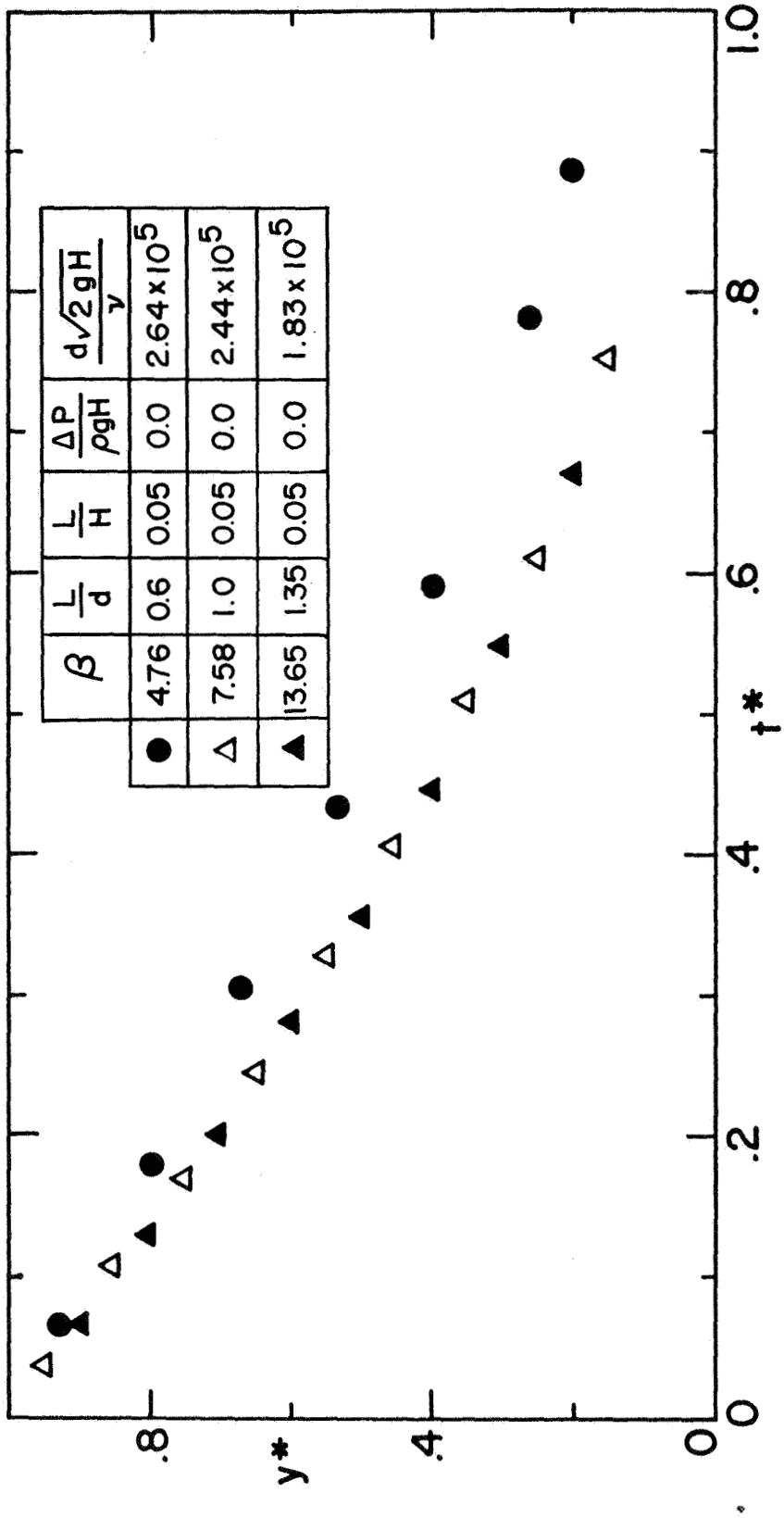

Figure 8.8. Variation of y* with t* for Various Values of the Parameter β (Orifice Flow Measurements)

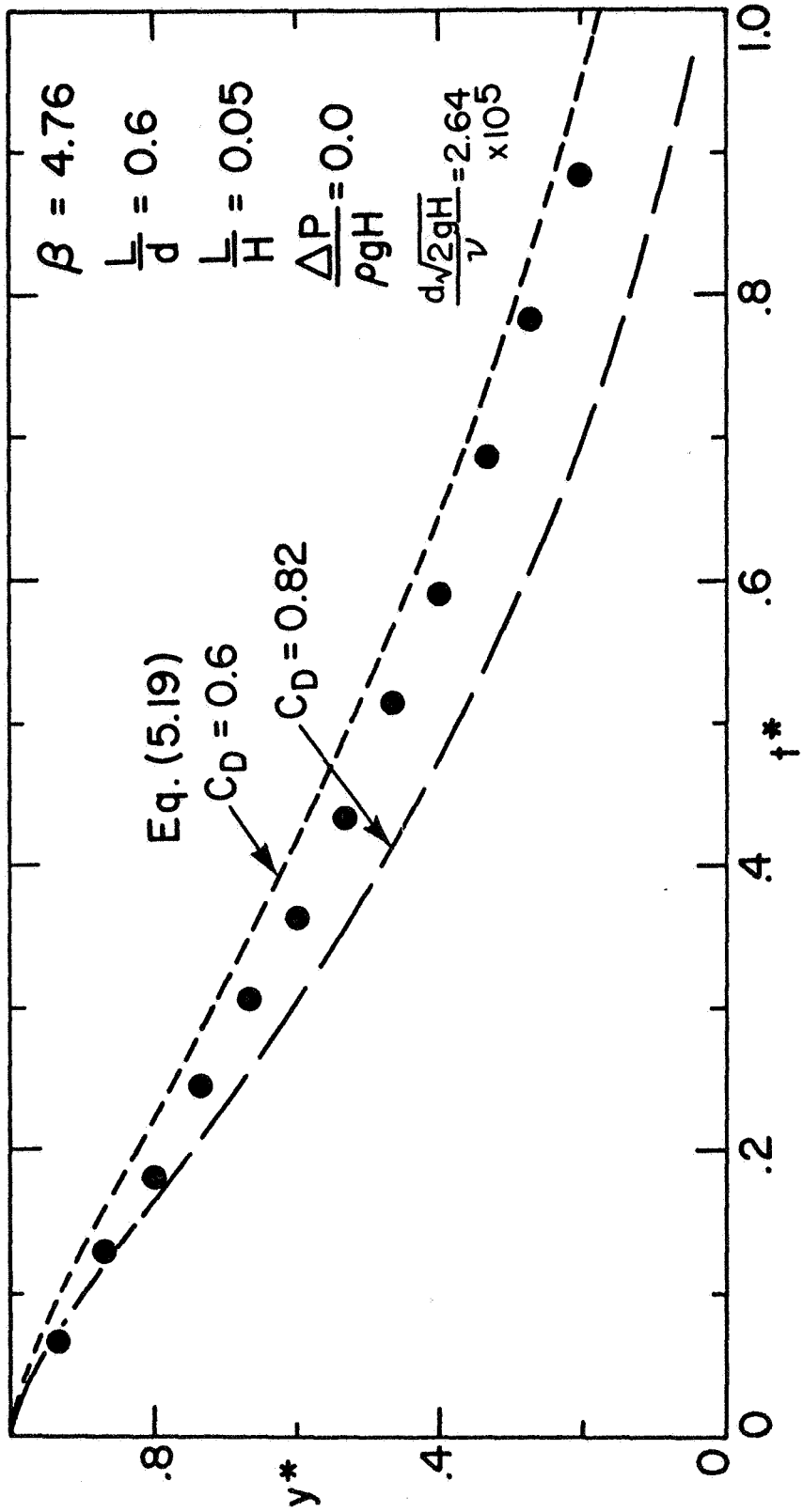

Figure 8.9. Predicted and Measured Results for Orifice Flow (β = 4.76)

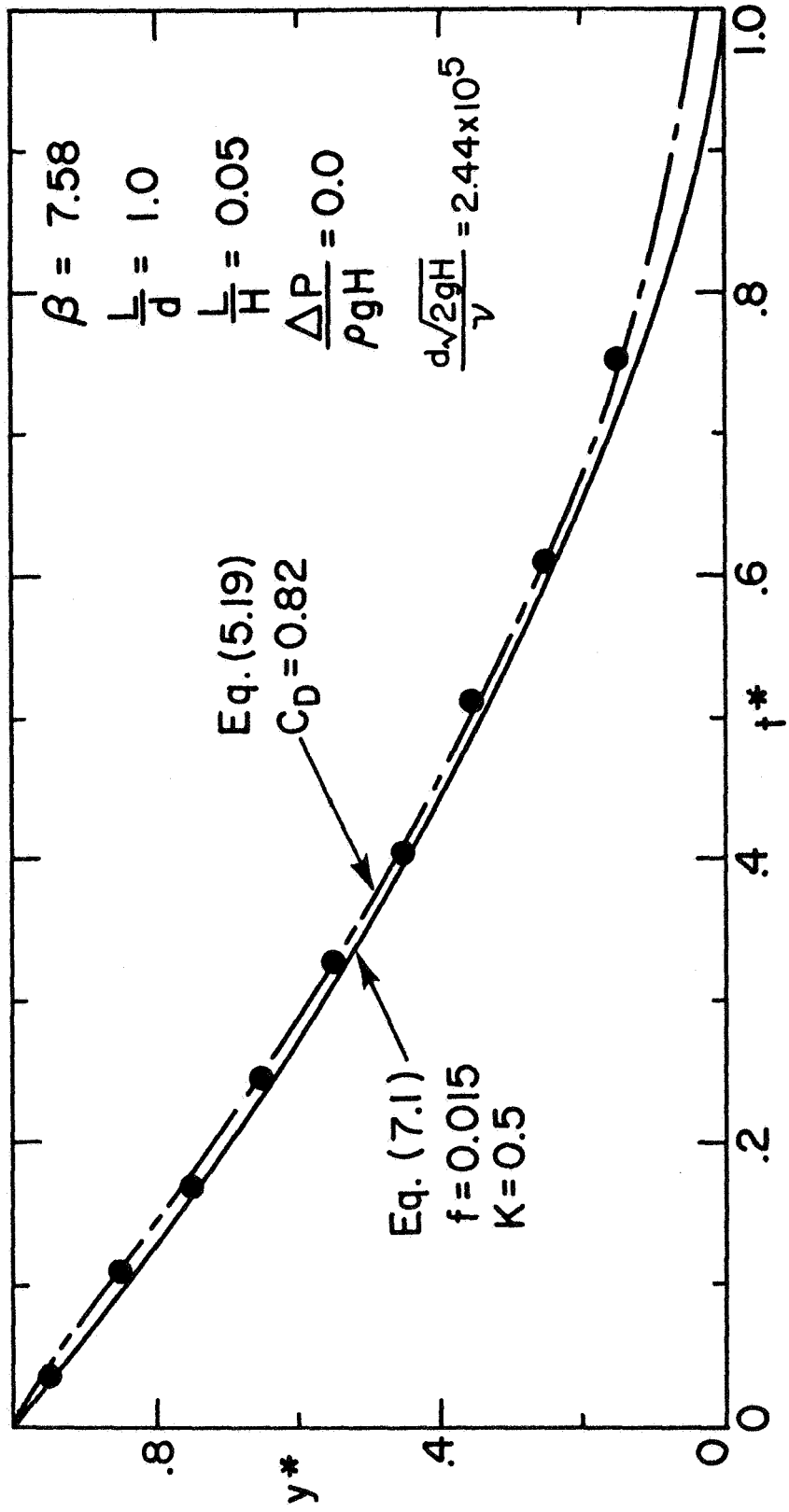

Figure 8.10. Predicted and Measured Results for Orifice Flow (β = 7.58)

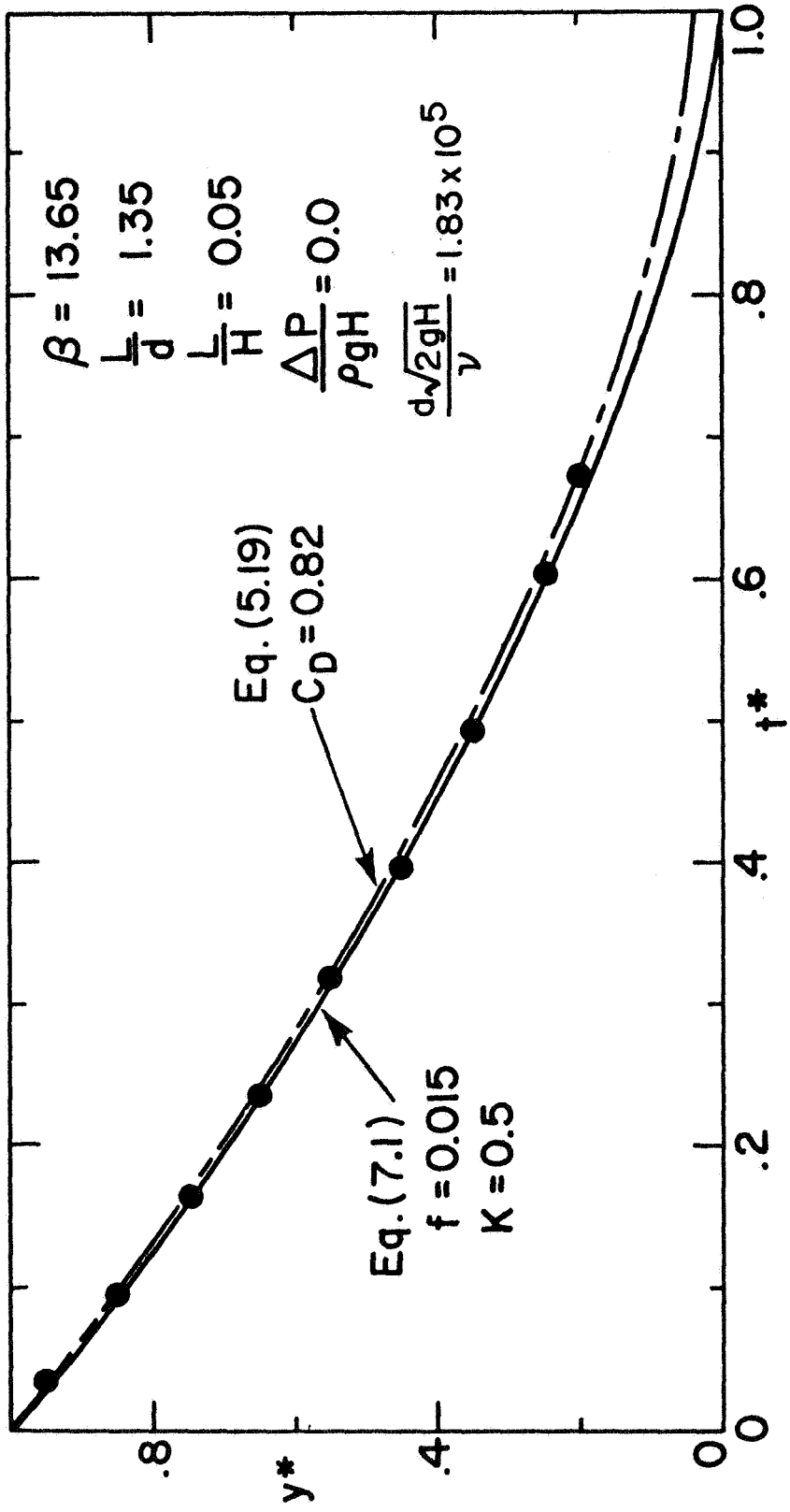

Figure 8.11. Predicted and Measured Results for Orifice Flow (β = 13.65)

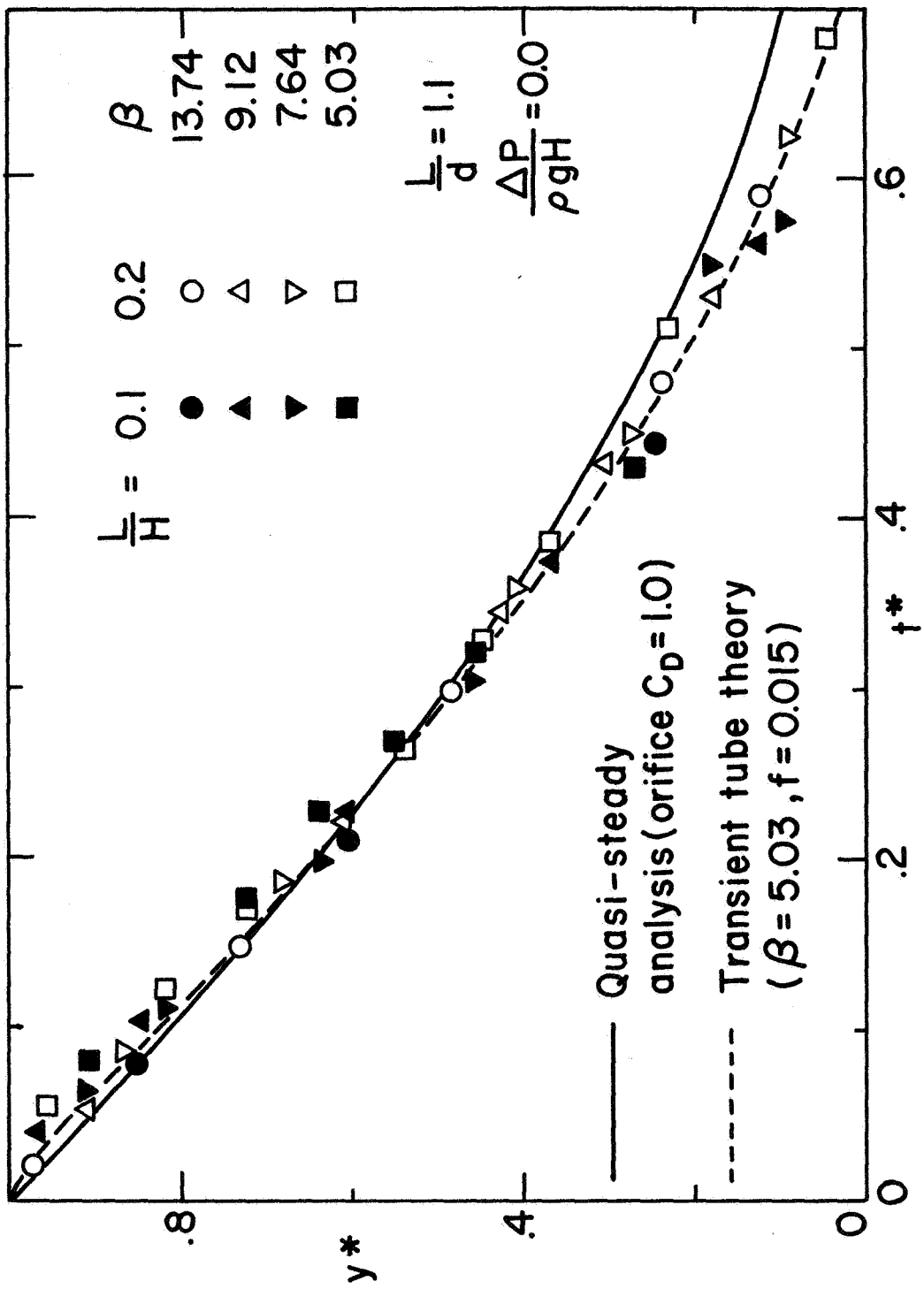

Figure 8.12. Predicted and Measured Results for Various Values of the Parameter β, for Short Tubes (L/d = 1.1, Rounded Entrance)

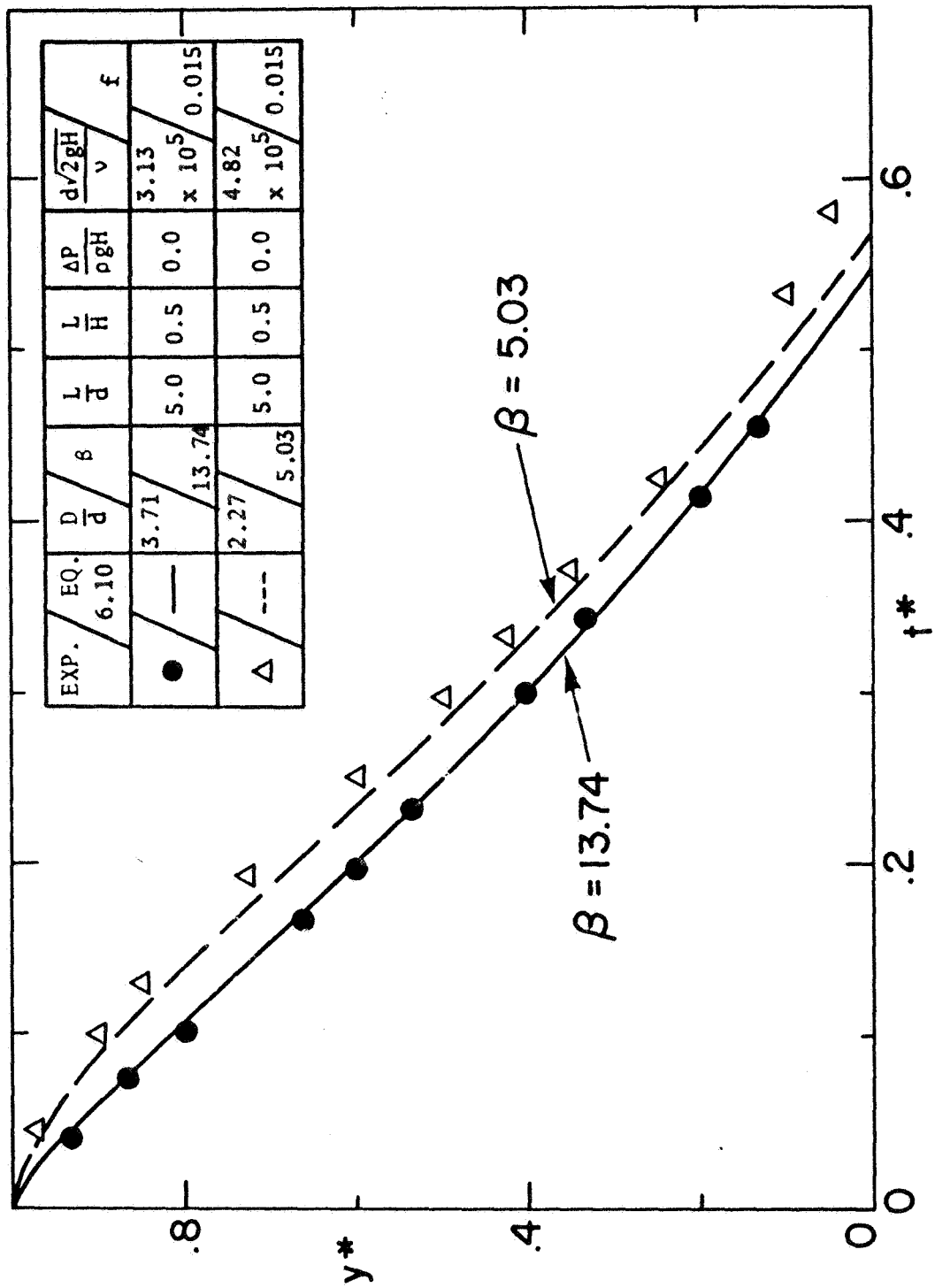

Figure 8.13. Predicted and Measured Results Exhibiting Flow Retardation with Decreasing β (Rounded Entrance)

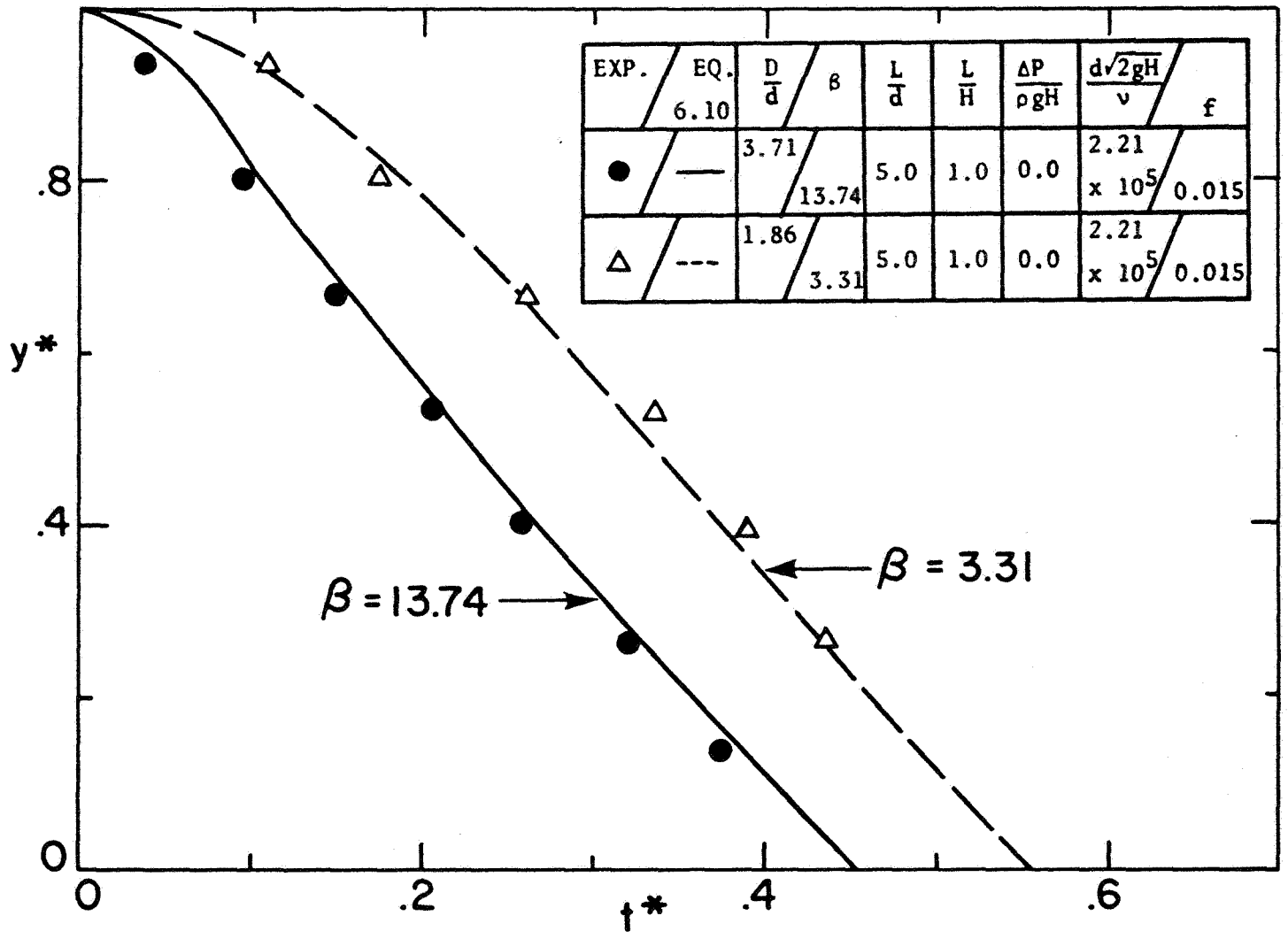

Figure 8.14. Predicted and Measured Results Exhibiting Flow Retardation with Decreasing β (Rounded Entrance)

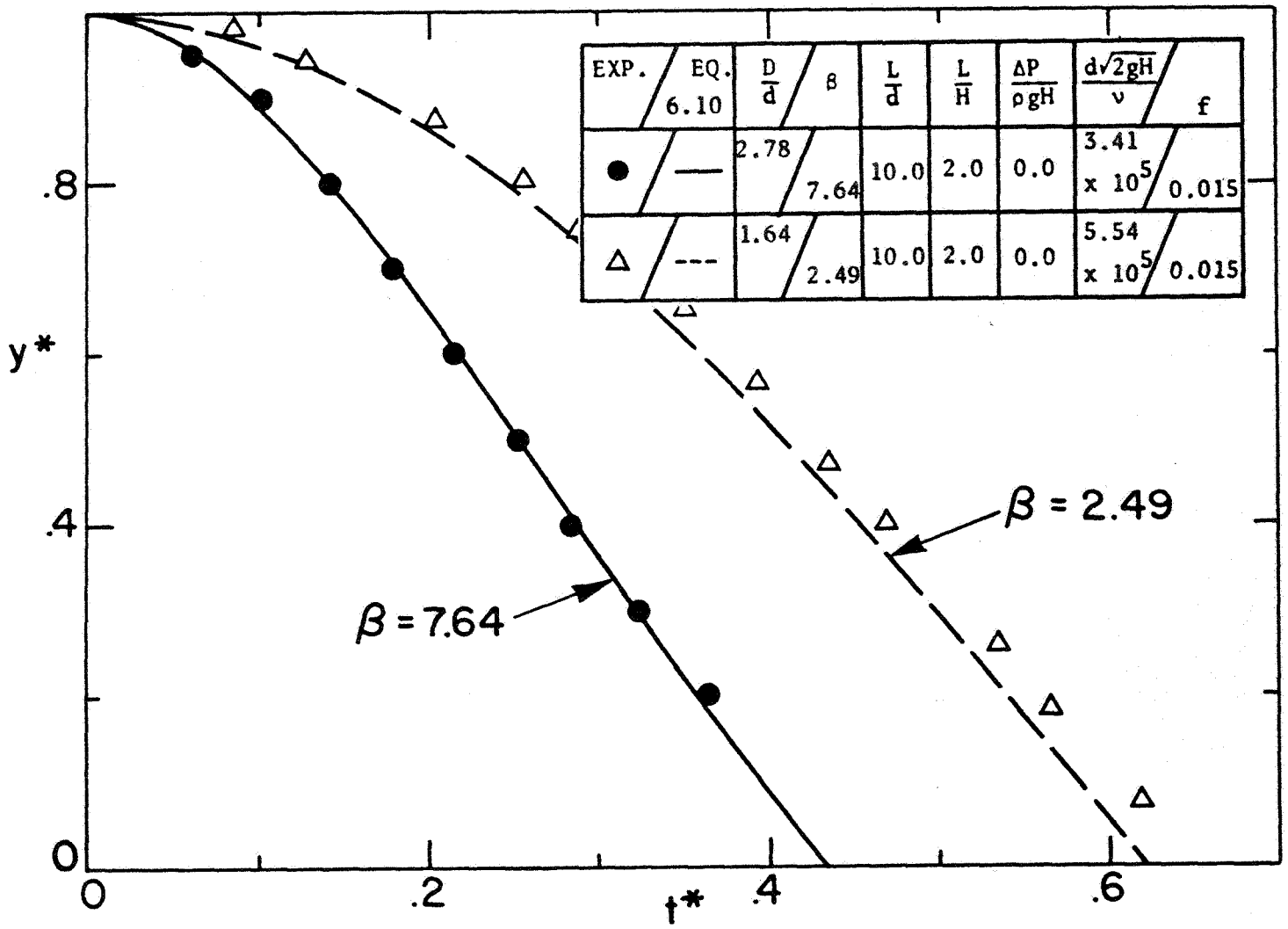

Figure 8.15. Predicted and Measured Results Exhibiting Flow Retardation with Decreasing β (Rounded Entrance)

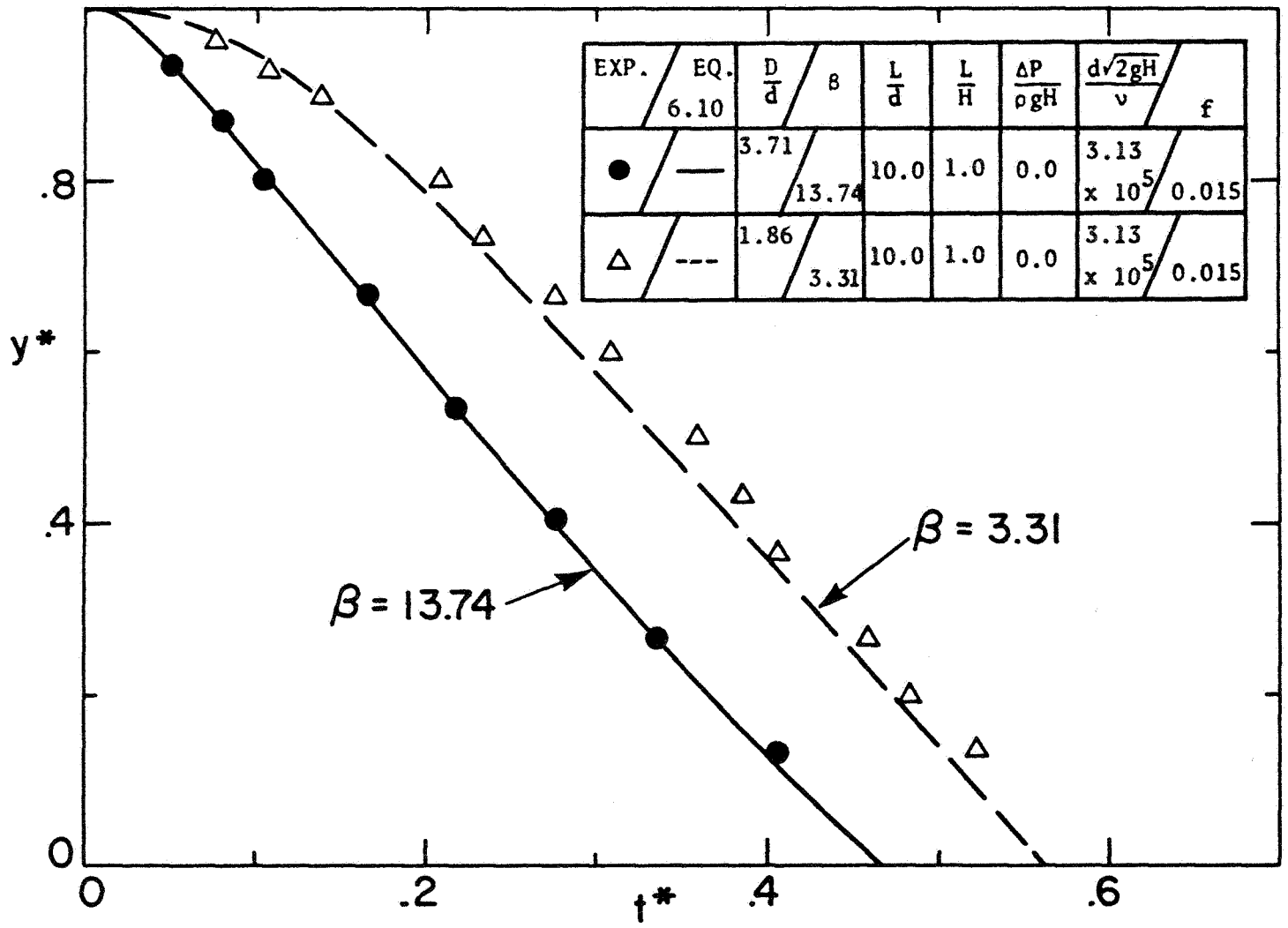

Figure 8.16. Predicted and Measured Results Exhibiting Flow Retardation with Decreasing β (Rounded Entrance)

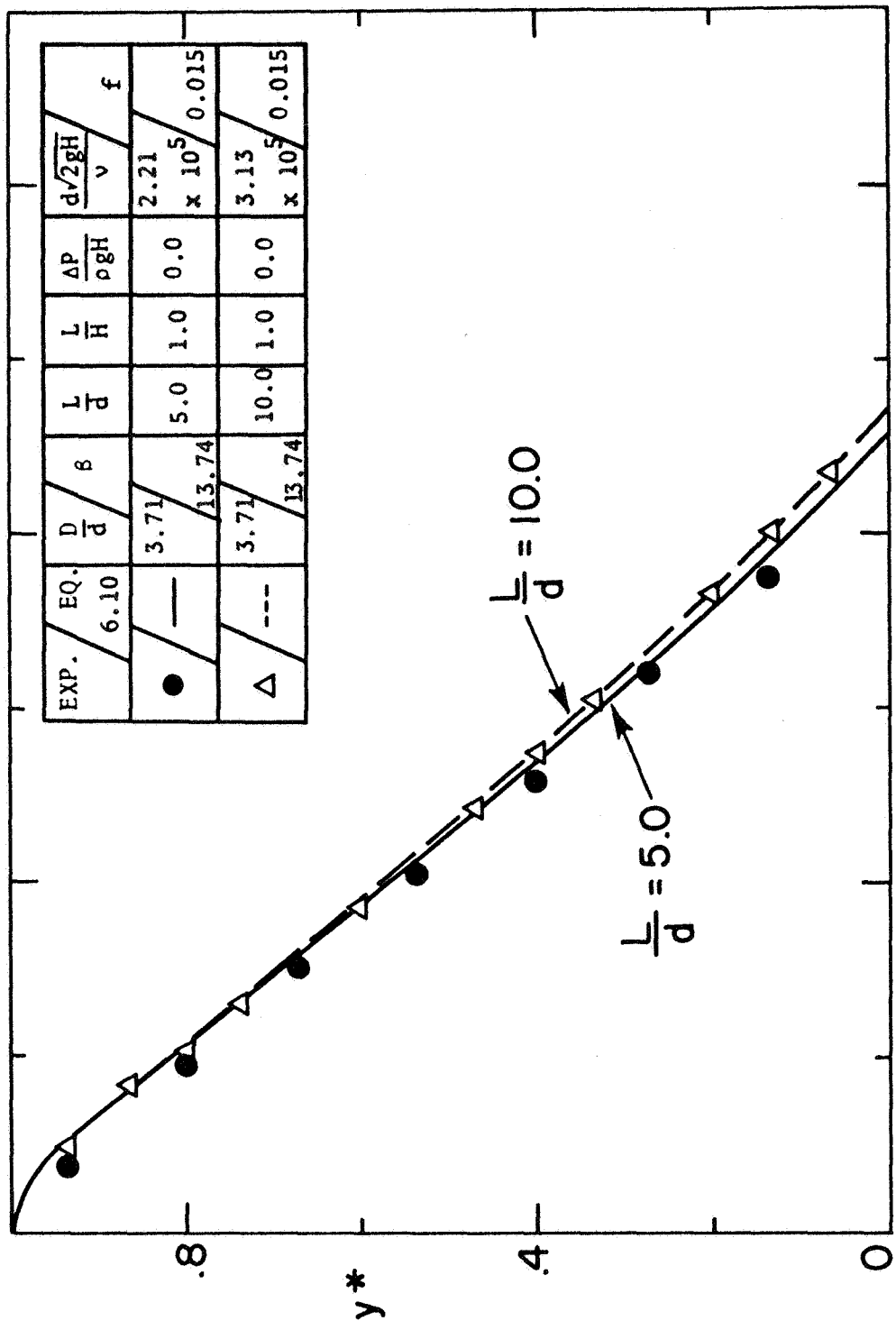

Figure 8.17. Predicted and Measured Results Exhibiting Flow Retardation with Increasing L/d (Rounded Entrance)

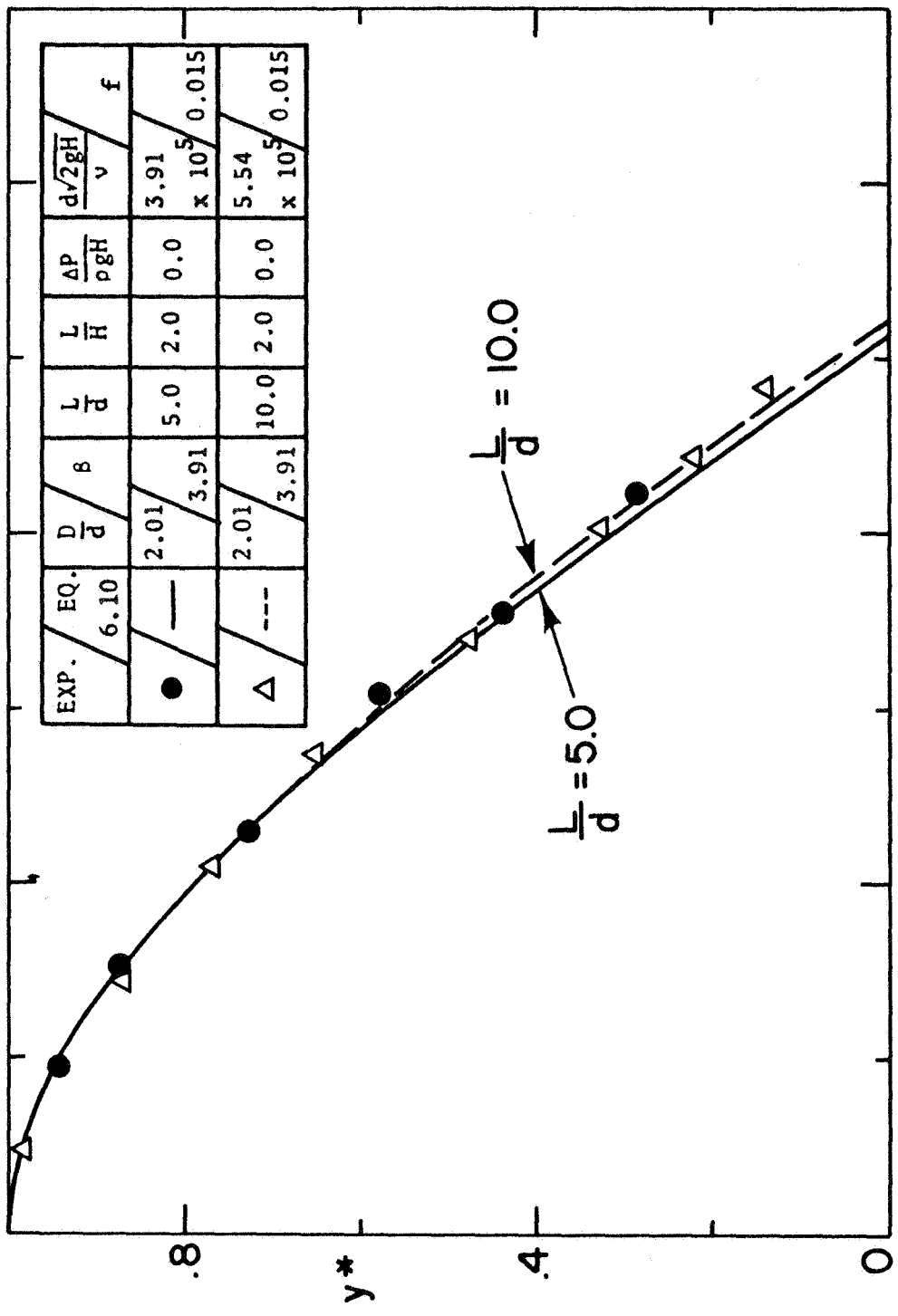

Figure 8.18. Predicted and Measured Results Exhibiting Flow Retardation with Increasing L/d (Rounded Entrance)

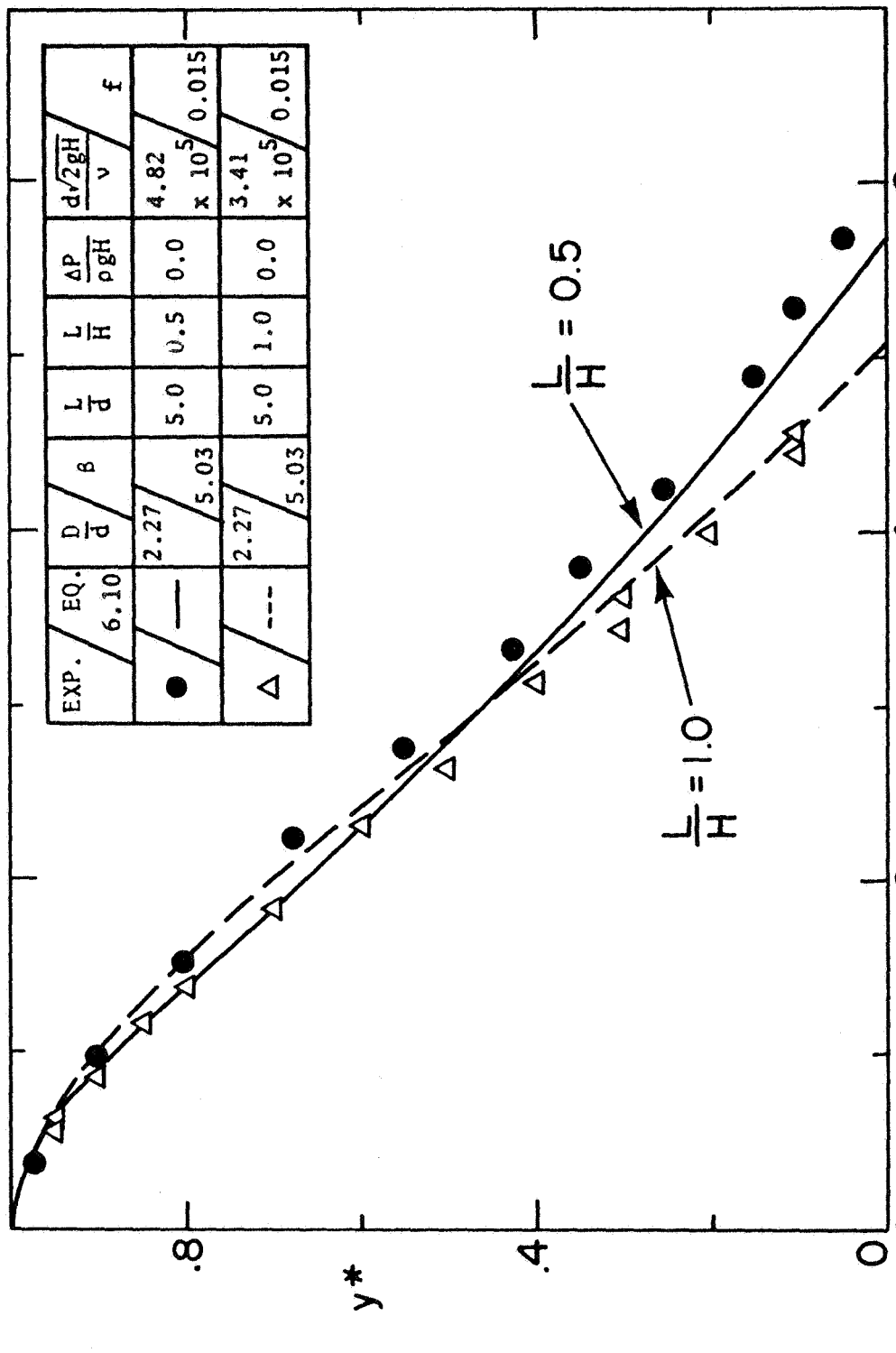

Figure 8.19. Predicted and Measured Results Exhibiting the Influence of L/H (Rounded Entrance)

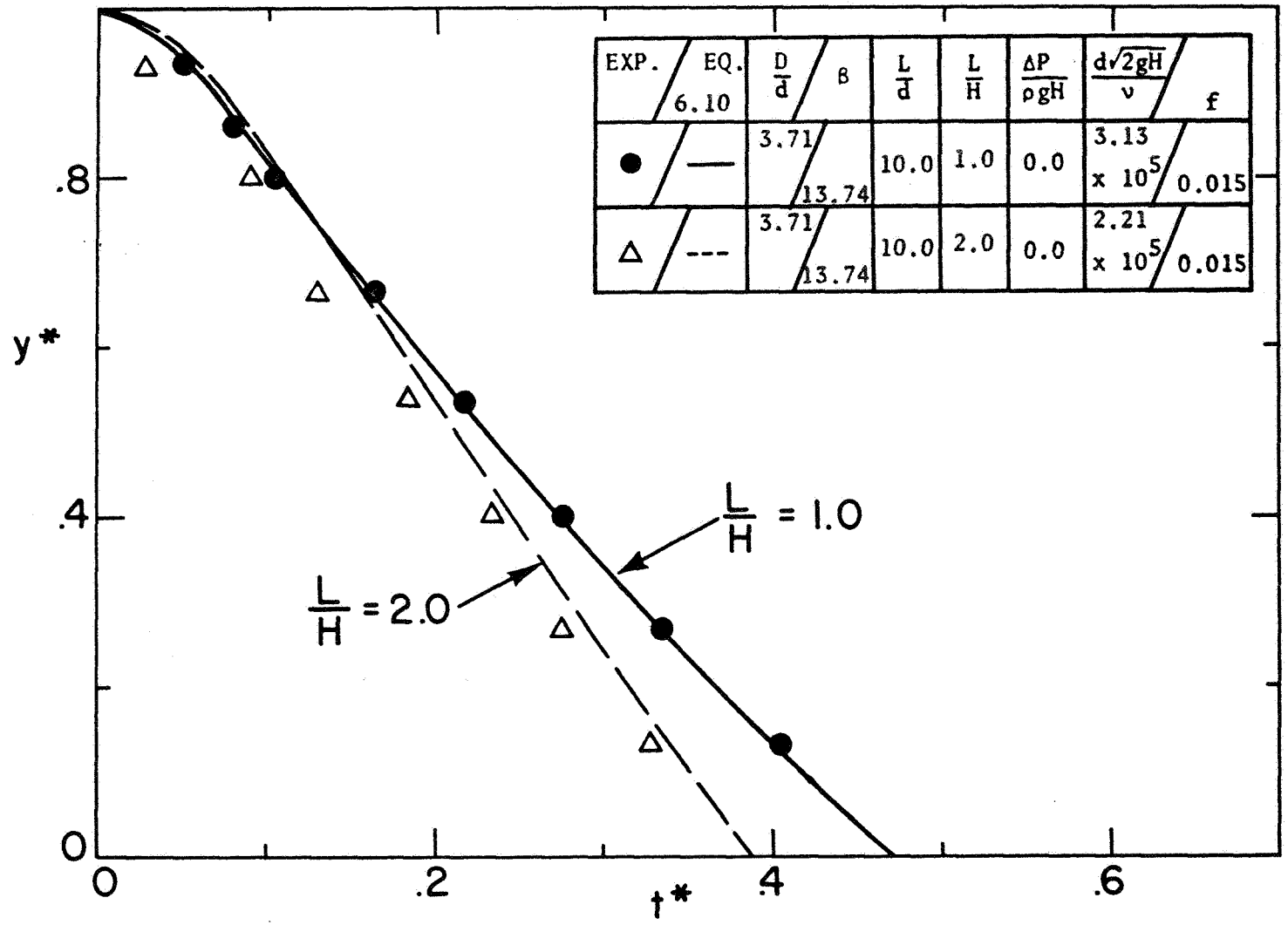

Figure 8.20. Predicted and Measured Results Exhibiting the Influence of L/H (Rounded Entrance)

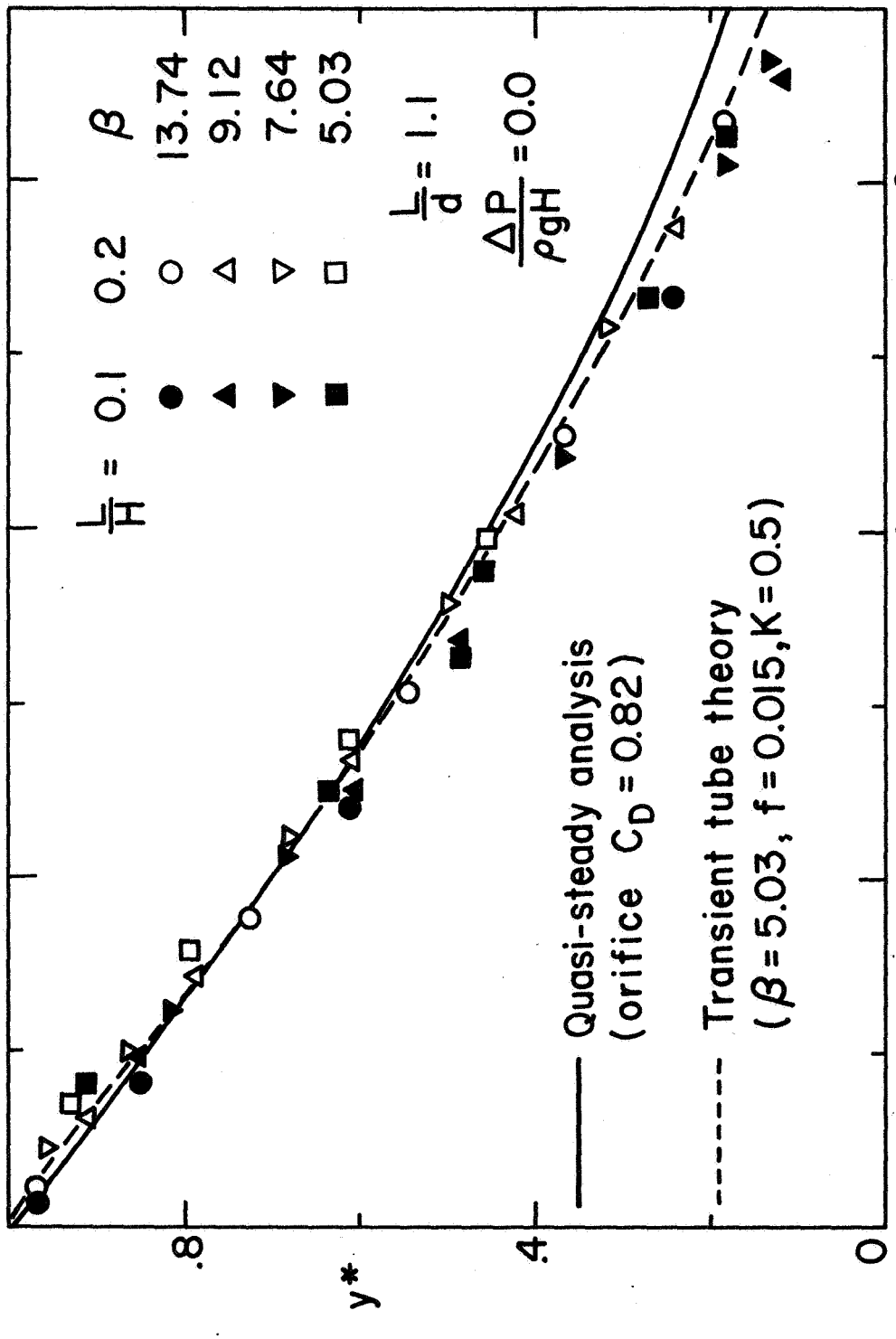

Figure 8.21. Predicted and Measured Results for Various Values of the Parameter β, for Short Tubes (L/d = 1.1, Sharp-Edged Entrance)

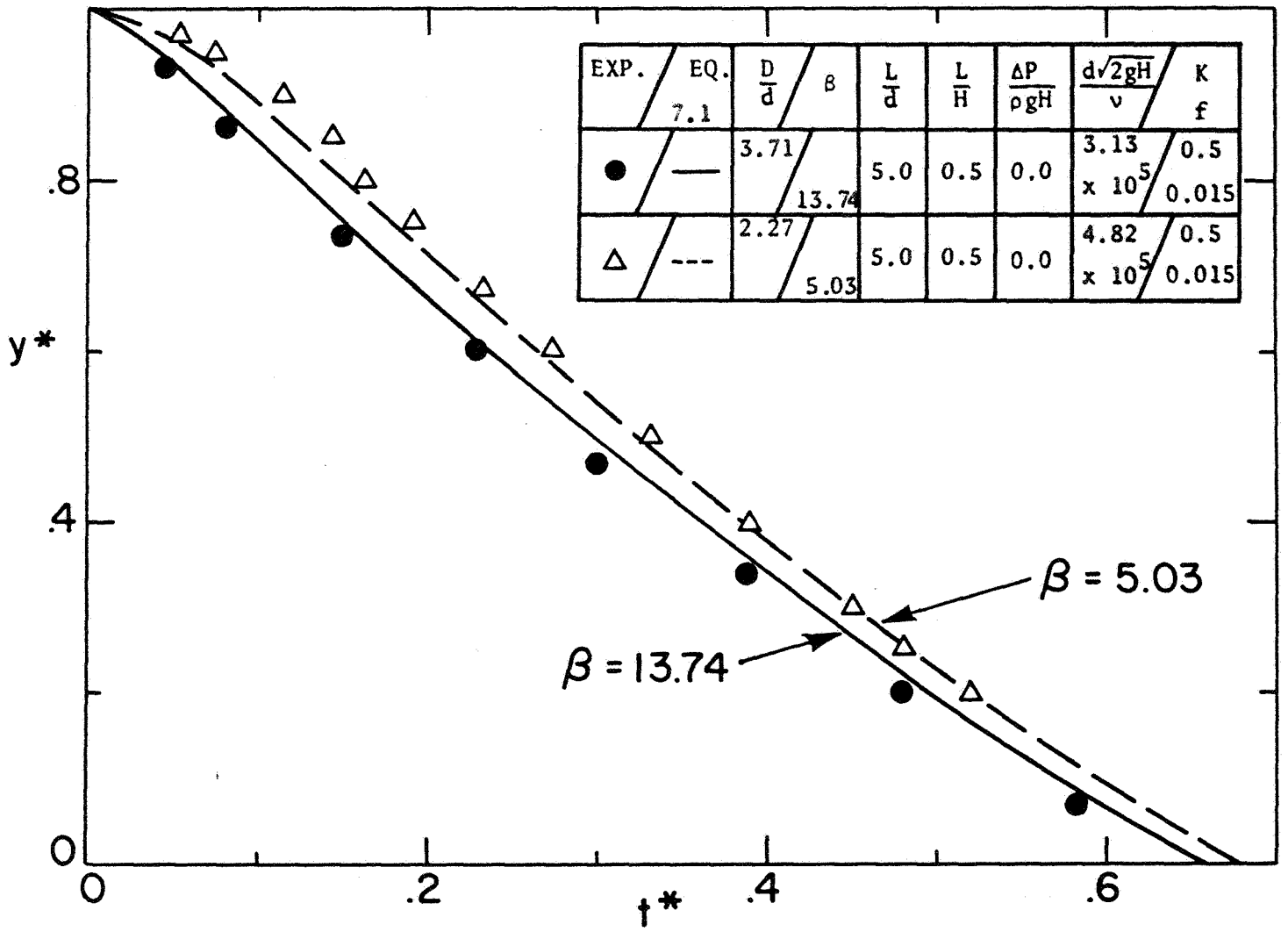

Figure 8.22. Predicted and Measured Results Exhibiting Flow Retardation with Decreasing β (Sharp-Edged Entrance)

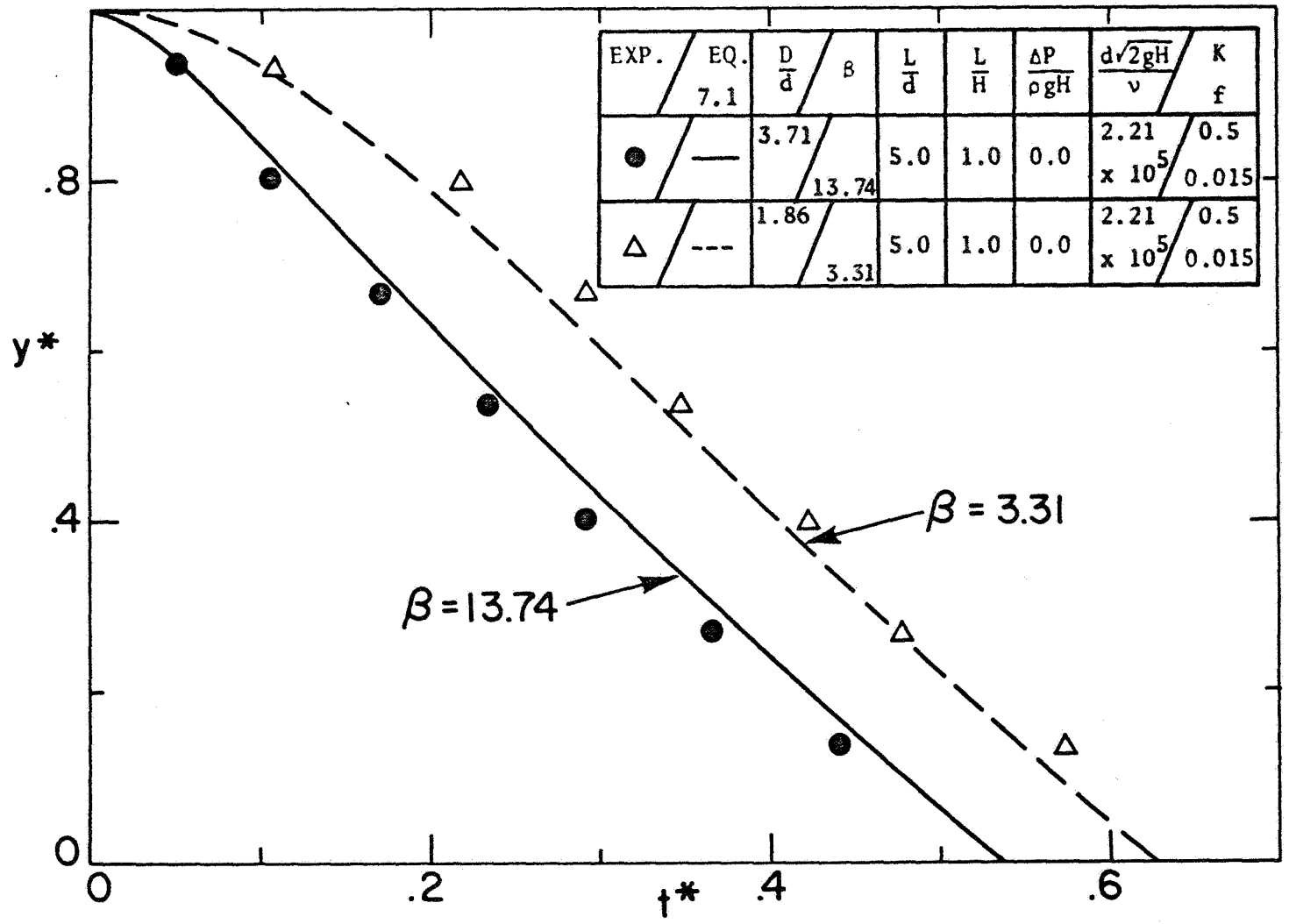

Figure 8.23. Predicted and Measured Results Exhibiting Flow Retardation with Decreasing β (Sharp-Edged Entrance)

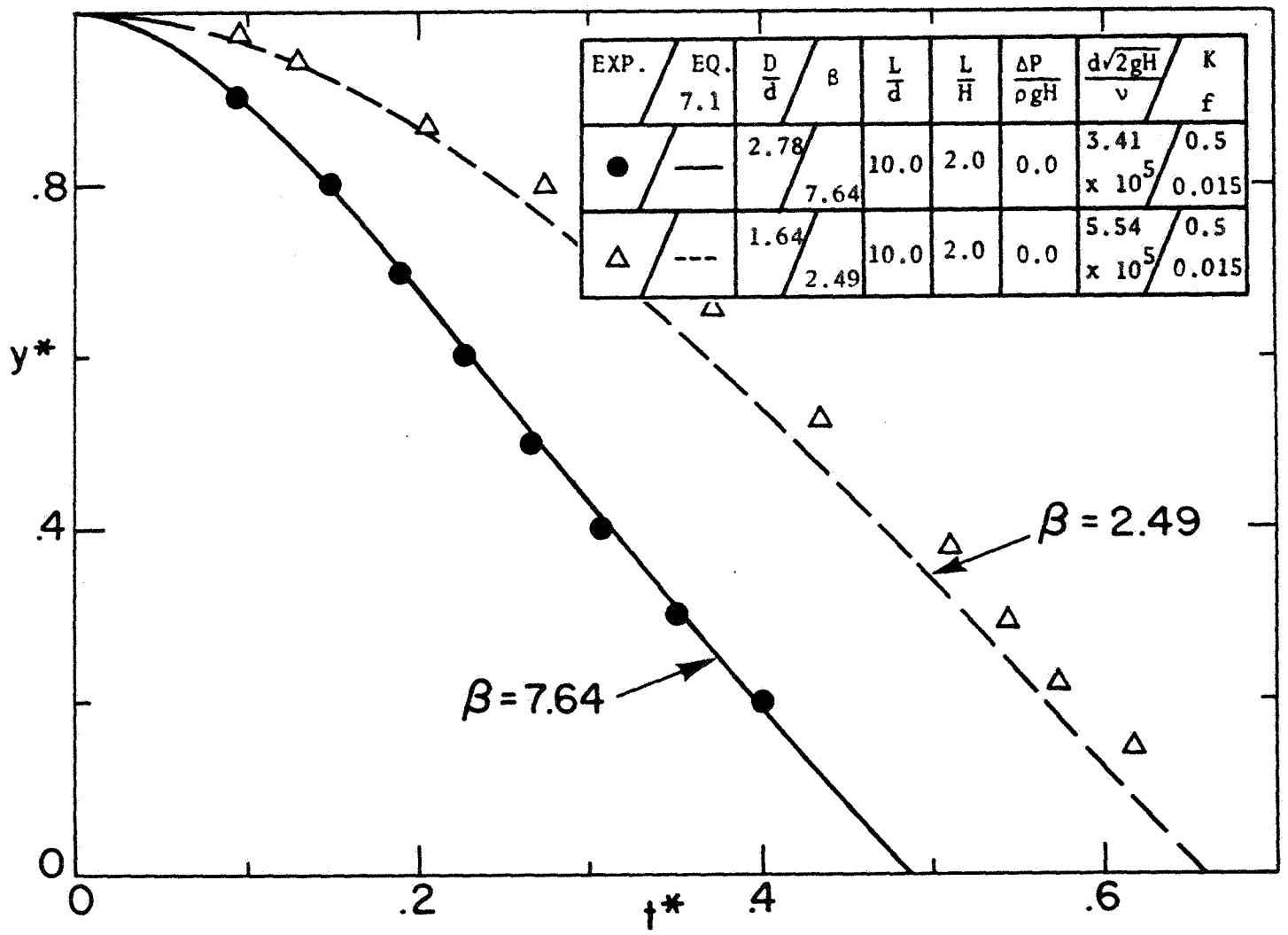

Figure 8.24. Predicted and Measured Results Exhibiting Flow Retardation with Decreasing β (Sharp-Edged Entrance)

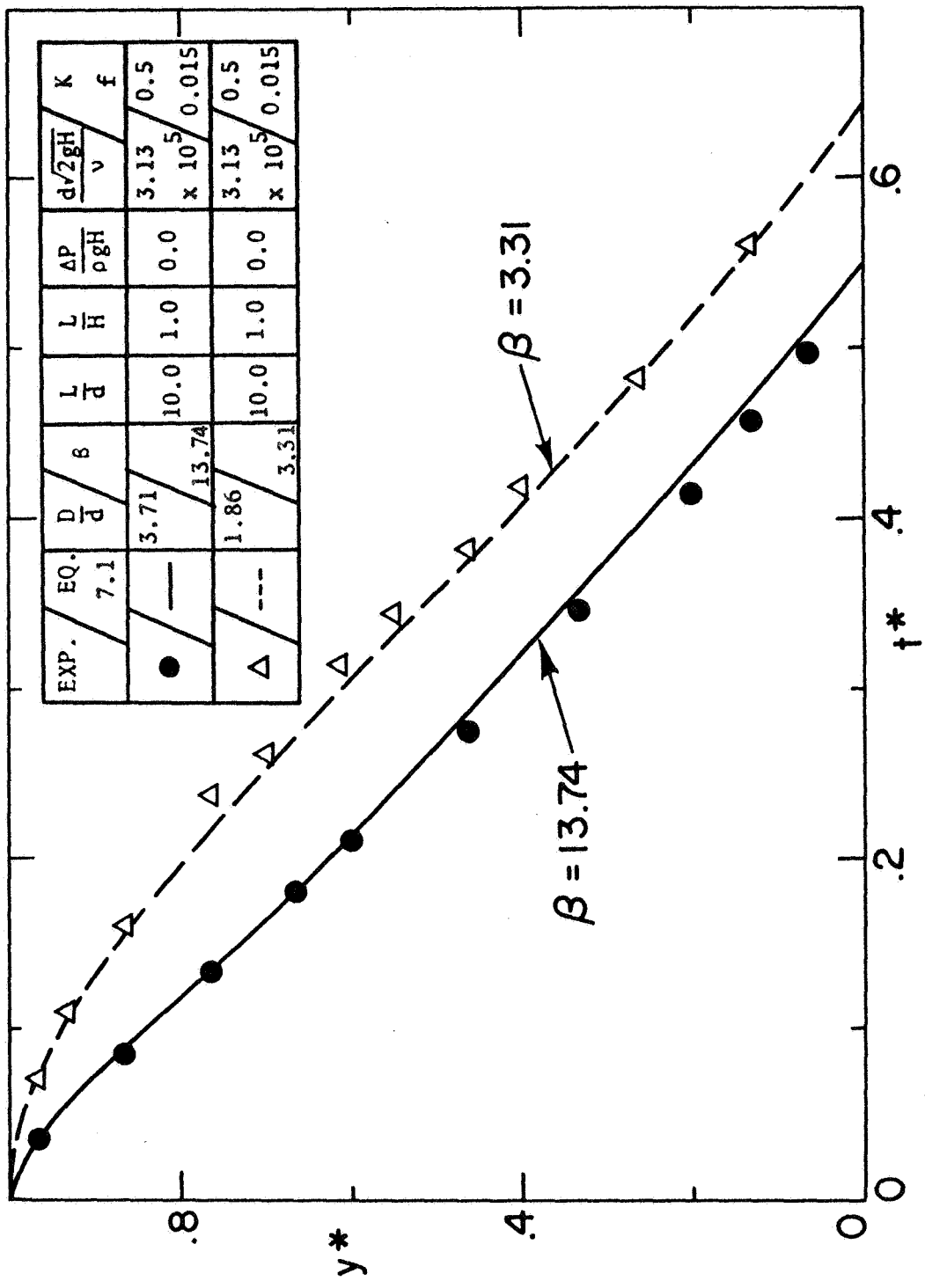

Figure 8.25. Predicted and Measured Results Exhibiting Flow Retardation with Decreasing β (Sharp-Edged Entrance)

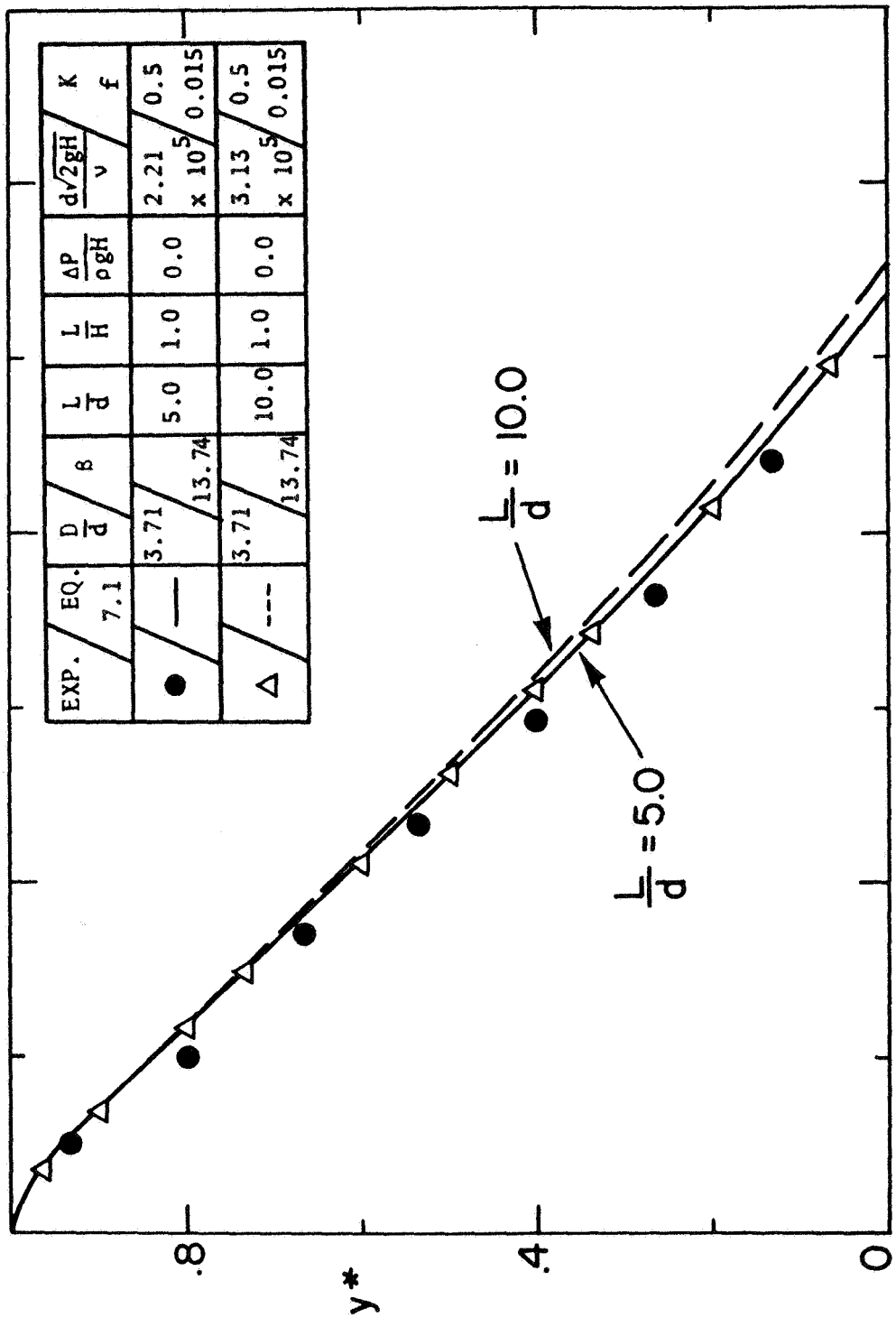

Figure 8.26. Predicted and Measured Results Exhibiting Flow Retardation with Increasing L/d (Sharp Edged Entrance)

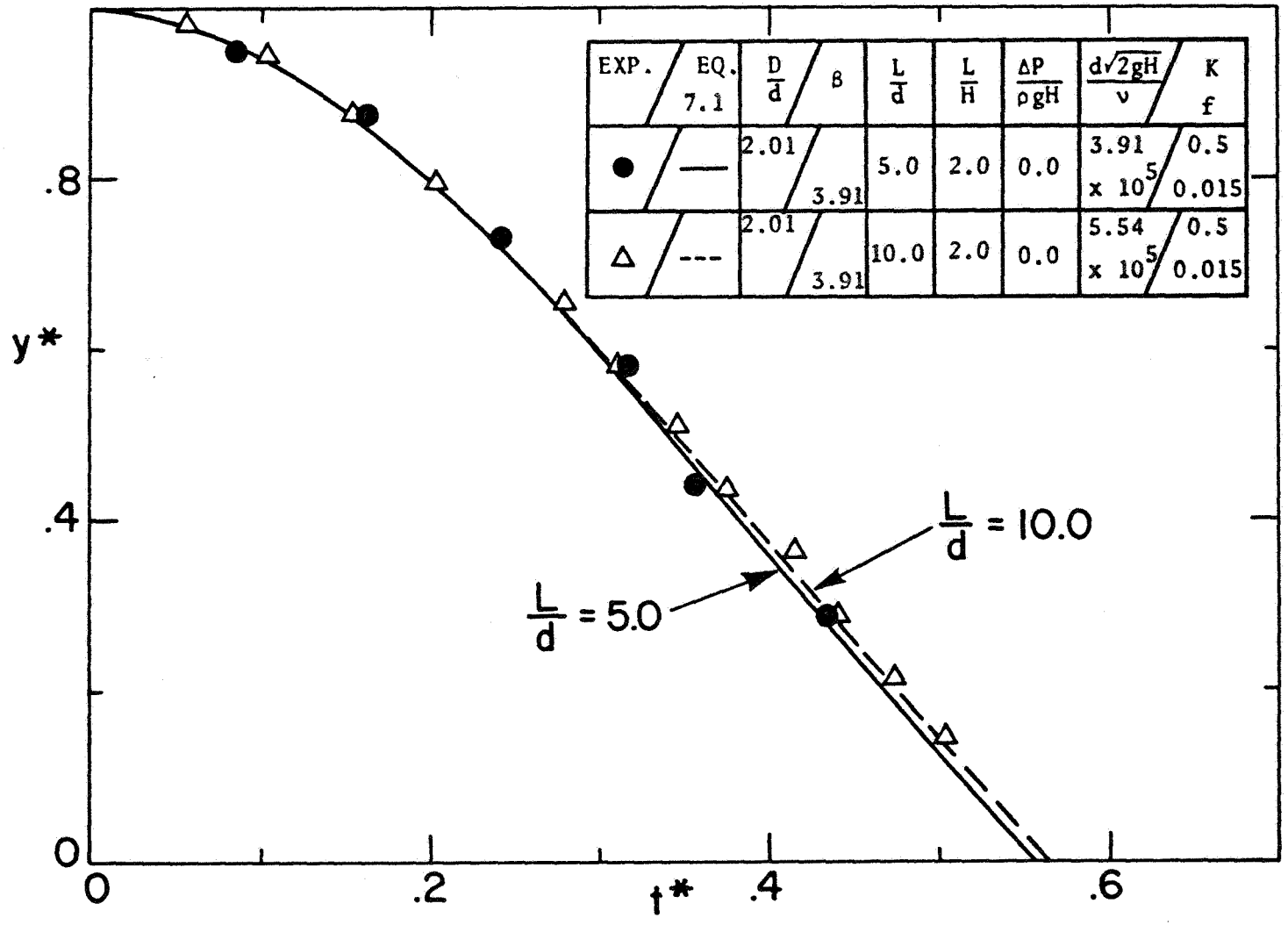

Figure 8.27. Predicted and Measured Results Exhibiting Flow Retardation with Increasing L/d (Sharp Edged Entrance)

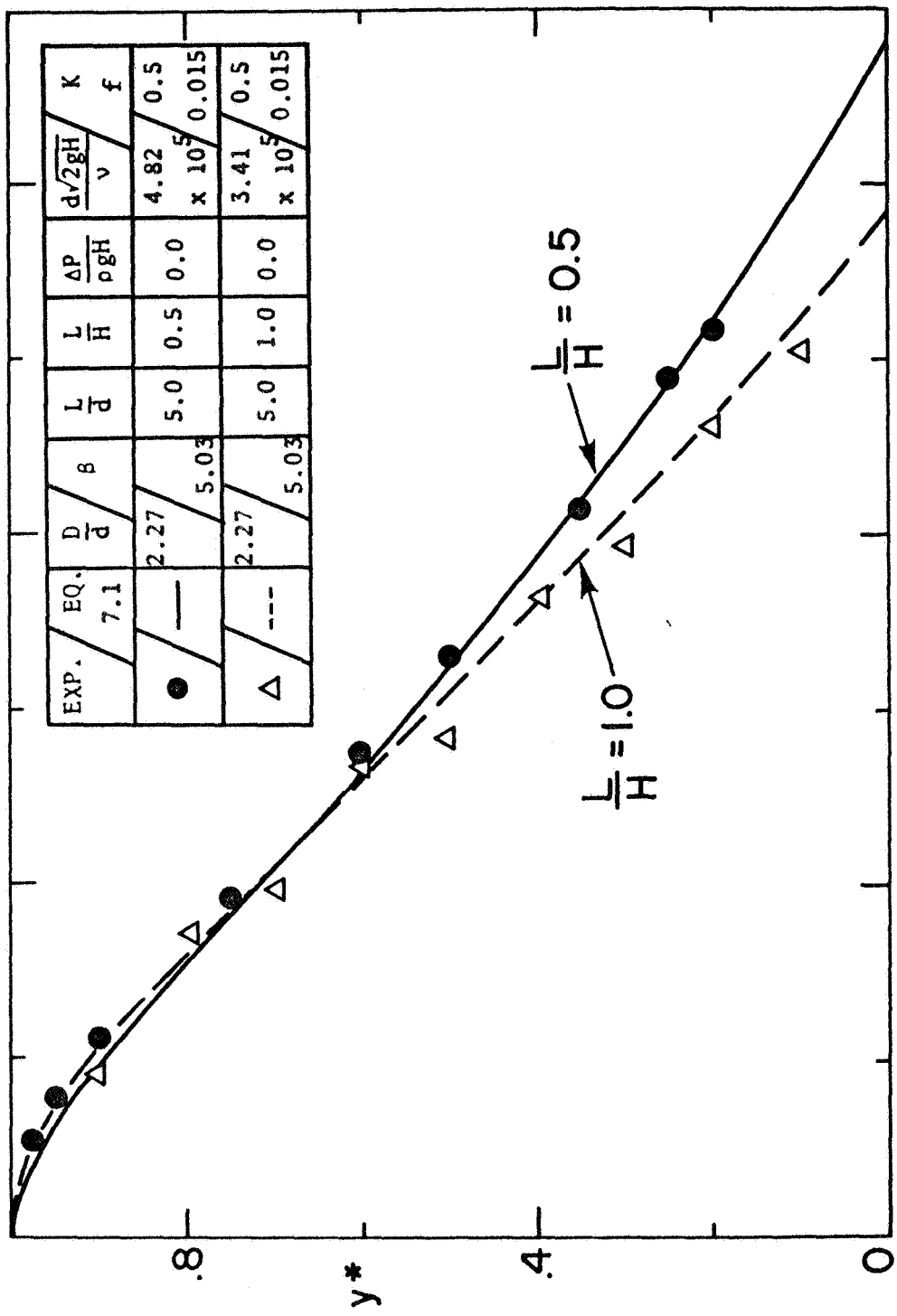

Figure 8.28. Predicted and Measured Results Exhibiting the Influence of L/H (Sharp-Edged Entrance)

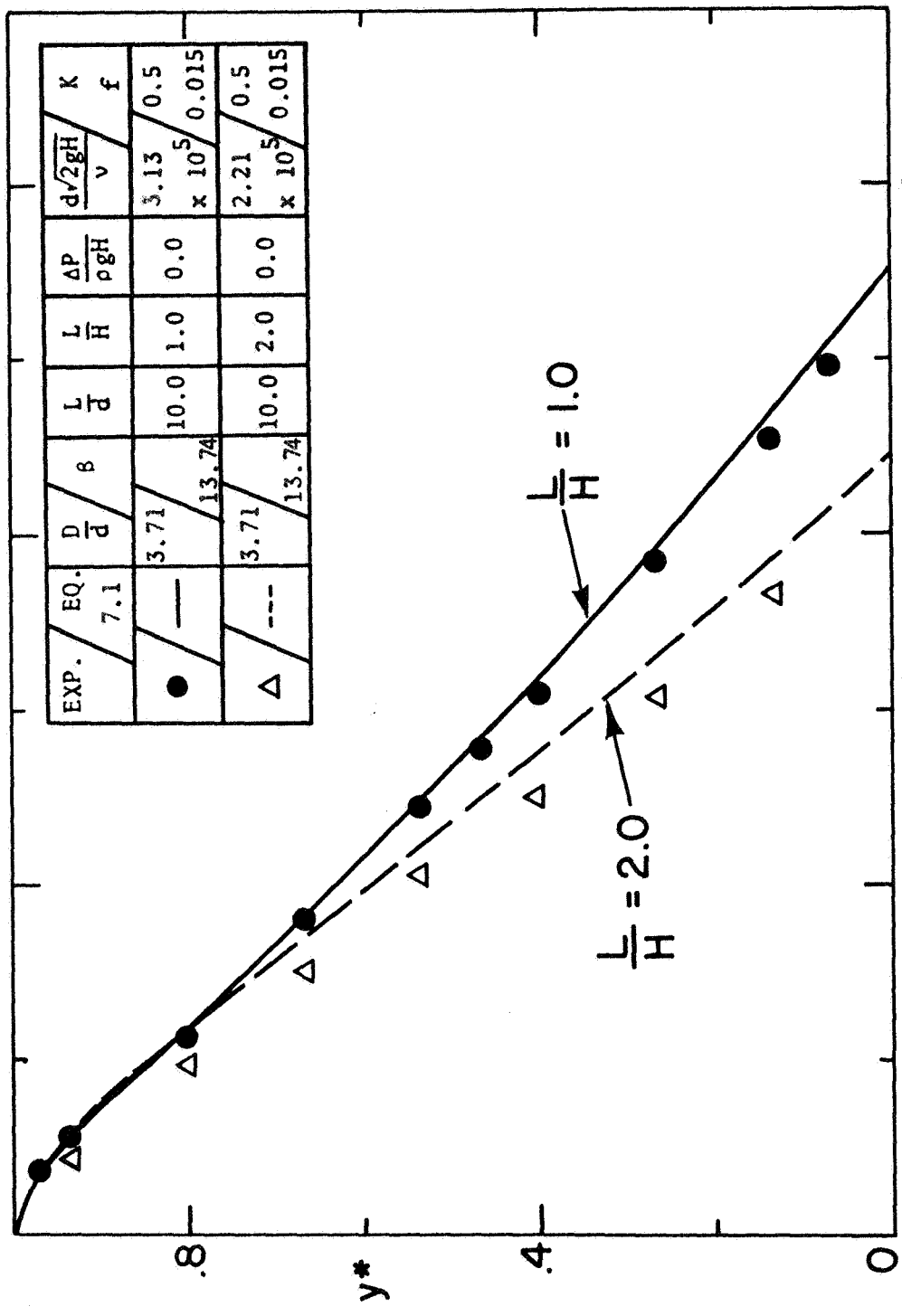

Figure 8.29. Predicted and Measured Results Exhibiting the Influence of L/H (Sharp-Edged Entrance)

CHAPTER 9

SUMMARY AND RECOMMENDATIONS

To summarize the results for the case of single-phase liquid discharge from containers, it can be said that both the instantaneous dimensionless liquid height, $y^* = \frac{y}{H}$, and the instantaneous dimensionless mass flow rate, $\dot{m}^* = \frac{\dot{m}}{\rho\,(\frac{\pi D^2}{4})\,\frac{1}{\beta}\sqrt{2gH}}$, are functions of the parameters $t/(\beta\sqrt{\frac{2H}{g}})$, $\frac{D}{d}$, $\frac{L}{d}$, $\frac{L}{H}$, $\frac{\Delta P/\rho g}{H}$, and $\frac{d\sqrt{2gH}}{\nu}$. Analyses based on one-dimensional flow models yield results consistent with experiments for the two types of discharge investigated, viz. discharge through an orifice and discharge through a tube. Viscous and geometric effects can be accounted for using classical values for C_D, f and K. Thus, the analyses lend support to the scaling procedures developed.

For the case of discharge through an orifice (for which $\frac{L}{d} = \frac{L}{H} \gtrsim 0$):

a. transient effects do not play an important role in the discharge process unless $\beta < 4$;

b. if the thickness of the orifice (L) is zero, the accepted values of C_D give accurate predictions;

c. for $0 < \frac{L}{d} < 1.0$ the value of C_D varies between 0.6 and 0.82;

d. the case of $\frac{L}{d} \geq 1.0$ corresponds to discharge through a tube, and the analysis based on transient discharge through a tube predicts the experimental results accurately.

e. the discharge coefficient C_D may be assumed to remain constant throughout a transient run when $\frac{d\sqrt{2gH}}{\nu} \geq 1000$.

For discharge through a tube:

a. for $\beta > 20$ the quasi-steady flow analysis yields results consistent with experiment, indicating that the inertia of the fluid in the tube can be neglected;

b. for $4 \leq \beta \leq 20$ transient conditions have a pronounced effect on the discharge process. In this range of β-values the inertia of the fluid in the tube should be taken into account; as β is decreased the fluid is retarded in the sense that the mass flow rate, non-dimensionalized according to equation (5.3), decreases and the total dimensionless discharge time increases instead of remaining constant as in the case of quasi-steady flow:

c. for short tubes ($\frac{L}{d} \ll 1$), transient effects are negligible; however the discharge is faster than that predicted by orifice flow equations due to the fact that the head is larger ($\frac{L}{H} \neq 0$);

d. increasing the ratio $\frac{L}{d}$ retards the flow;

e. increasing $\frac{L}{H}$ and $\frac{\Delta P/\rho g}{H}$ accelerates the discharge process;

f. the effect of the parameter $\frac{d\sqrt{2gH}}{\nu}$ is not very pronounced for discharge through smooth tubes (for values above 10^5) and can be taken into account by using the values of friction factors given in the Moody chart; the friction factor f may be assumed to remain constant throughout a transient run over most typical ranges of $\frac{d\sqrt{2gH}}{\nu}$;

g. entrance losses can be accounted for in a conventional manner by assuming the entrance loss coefficient K = 0 for rounded entrances and K = 0.5 for sharp-edged entrances.

It is concluded that the average mass flow rate tends to increase with decreasing β, though not proportionately. The rate of increase decreases with decreasing β. As is to be expected, smooth tubes with rounded entrances are very much better for obtaining larger mass flow rates for a given pressure head than rough tubes and tubes with sharp-edged entrances. Further, rounded entrances delay the onset of cavitation.

Some of the problems which need further investigation are listed below.

1. The single most important problem encountered in the experimental investigation was that of measuring the instantaneous liquid height in the container. When the actual discharge times are about 1 second or more, a closed circuit stop-action TV system is satisfactory and convenient for recording and fast read out of data. For low β values and/or pressurized discharge the times are much shorter (in case of scale model testing) and use of the present TV system would lead to large inaccuracies. Also, high speed photography is time consuming and expensive. Therefore, it would be desirable to develop a method of measuring the instantaneous liquid level perhaps by means of pressure measurements in the container using fast response transducers and recorders. Rouse and Abul-Fetouh (Ref. 16) found that for flow through an orifice the pressure in the container is relatively unaffected (beyond $\frac{y}{d} = 1.0$) by the acceleration near the discharge entrance. This finding may be useful in locating the transducer for pressure measurements.
2. It would be desirable to conduct an experimental investigation of pressurized discharge. Here again the problems relate mostly

to experimental technique. Plexiglass containers may prove hazarduous from a safety viewpoint; hence visual observation techniques may not be so readily employed. Resort to the pressure measurement technique described above may be the most appropriate. A quick acting gate valve should be designed so that it can be operated by an automatic opening device instead of by manual manipulation. This should be coupled to the equipment recording the height of liquid, so that the time of initiation of discharge ($t = 0$) can be accurately determined. Attention should be devoted to keeping the ullage pressure (P_1) in the container constant during rapid discharge.

3. The effect of having multiple outlets, some of which may not be vertical, should be studied. Proper scaling techniques, which depend on the geometry and spacing of the outlets should be developed. The analysis presented in this report can be easily extended to the case of discharge through non-vertical tubes. In this case the gravity force in equation (6.8) should be modified to read $\rho g L a (\cos\theta)$, where θ is the angle of inclination of the discharge tube to the vertical.
4. Scaling of two-phase flows should be studied in order that scaled test results may be truly applicable to large liquid propellant rocket systems using cryogenic propellants and oxydizers. Experiments with liquid nitrogen might prove very fruitful in this endeavor.
5. Measurements of pressure distributions and velocity profiles should be obtained to provide a better knowledge of the flow development and the associated losses under transient discharge conditions.

LIST OF REFERENCES

1. S. S. Penner:
"Similarity Analysis for Chemical Reactors and the Scaling of Liquid Fuel Rocket Engines," CALTECH, JPL TR No. 8, Nov. 1954.

2. H. Rouse and S. Ince:
"History of Hydraulics," Iowa Inst. of Hydraulic Research, State University of Iowa, 1957.

3. V. L. Streeter:
"Fluid Mechanics," Chapters 3, 5, and 9, McGraw-Hill Book Co., Inc., New York, N.Y., 2nd Ed., 1958.

4. R. M. Sabersky and A. J. Acosta:
"Fluid Flow, A First Course in Fluid Mechanics," Chapter 3, Macmillan Co., New York, N.Y., 1964.

5. J. Allen:
"Scale Models in Hydraulic Engineering," Longmans, Green & Co., London, 1947.

6. P. W. Bridgman:
"Dimensional Analysis," Chapter IV, Yale University Press, New Haven, 1931.

7. L. I. Sedov:
"Similarity and Dimensional Methods in Mechanics," Chapter 2, Academic Press, New York, N.Y., 1959.

8. R. C. Pankhurst and D. W. Holder:
"Wind-Tunnel Technique," Chapter 9, Sir Isaac Pitman & Sons, Ltd., 1952.

9. A. Pope:
"Wind-Tunnel Testing," Chapter 7, John Wiley & Sons, Inc., New York, N.Y., 2nd Ed., 1954.

10. L. J. Flanigan and A. A. Putnam:
"The Uses of Fluid Dynamic Modeling Techniques," Battelle Technical Review 13, No. 2, pp. 2-7, Feb. 1966.

11. A. A. Ezra:
"Scaling Laws and Similitude Requirements for Valid Scale Model Work," A Paper presented at a colloquium on "Use of Models and Scaling in Shock and Vibrations," ASME Winter Annual Meeting, Philadelphia, Pa., Nov. 19, 1963, pp. 57-64.

12. W. H. Roudebush and D. A. Mandell:
"Analytical Investigation of Some Important Parameters in the Pressurized Liquid Hydrogen Tank Outflow Problem," in "Proceedings of the Conference on Propellant Tank Pressurization and Stratification," 1, pp. 2-27. George C. Marshall Space Flight Center, Huntsville, Alabama. Jan. 1965.

13. M. E. Nein and J. F. Thompson,Jr.:
"Experimental and Analytical Studies of Cryogenic Propellant Tank Pressurization," In "Proceedings of the Conference on Propellant Tank Pressurization and Stratification," 1, pp. 29-54. George C. Marshall Space Flight Center, Huntsville, Alabama. Jan. 1965.

14. J. A. Clark:
"A Review of Pressurization, Stratification and Interfacial Phenomena," Paper S-1, Presented at 1964 Cryogenic Engineering Conference, Philadelphia, Pa. (International Advances in Cryogenic Engineering 10, pt. 2, pp. 259-283, Plenum Press, New York, N.Y., 1965.)

15. P. Fischer:
"Ähnlichkeitsbedingungen für Strömungsvorgänge mit gleichzeitigem Warmeübergang," ZAMM 43, pp. T122-125, Sonderheft 1963.

16. H. Rouse and A. Abul-Fetouh:
"Characteristics of Irrotational Flow through Axially Symmetric Orifices", Journal of Applied Mechanics, Vol. 17, No. 4, pp. 421-426, Dec. 1950.

17. M. A. Saad and D. A. Oliver:
"Linearized Time Dependent Free Surface Flow in Rectangular and Cylindrical Tanks," Proceedings of the 1964 Heat Transfer and Fluid Mechanics Institute, held at Univ. of California Berkeley, pp. 81-99, June 10, 11, 12, 1964.

18. B. T. Lubin and G. S. Springer:
"The Formation of Dip on the Surface of a Liquid Draining from a Tank," Journal of Fluid Mechanics, Vol. 29, Part 2, pp. 385-390, 1967.

19. L. Schiller:
"Die Entwicklung der laminaren Geschwindigkeitsverteilung und ihre Bedeutung für Zähigkeitsmessungen", Zeitschrift für Angewandte Mathematik und Mechanik, Vol. 2, No. 2. pp. 96-106, 1922.

20. H. Latzko:
"Heat Transfer in a Liquid or Gas Stream," NACA TM No. 1068, Oct. 1944. Translated from German "Der Warmeubergang an einen turbulenten Flussigkeits oder Gasstrom", ZAMM, Vol. 1, No. 4, pp. 268-290, Aug. 1921.

21. L. Prandtl and O. G. Tietjens:
"Applied Hydro- and Aeromechanics," Dover Publications, Inc., New York, N.Y.

22. P. Szymanski:
"Sur l'ecoulement non permanent du fluide visqueux dans le tuyau," Proceedings of the 3rd International Congress of Applied Mechanics, Stockholm, Vol. 1, pp. 249-254, 1930.

23. W. Kaufmann:
"Fluid Mechanics", McGraw Hill Co. Inc., New York, N.Y., 1963.

24. R. B. Bird, W. E. Stewart and E. N. Lightfoot:
"Transport Phenomena", John Wiley & Sons, Inc., New York, N.Y., 1960.

25. E. R. F. Winter, R. J. Schoenhals et al.:
"Improved Fluid Dynamics Similarity, Analysis and Verification," First Annual Report, June 29, 1965-June 28, 1966, School of Mechanical Engineering, Purdue University, Lafayette, Indiana, NASA Contract NAS 8-20222.

26. E. R. F. Winter and R. J. Schoenhals:
"A Similarity Study of Gravity and Pressure Driven Discharge of Liquids from Propellant Tanks," American Astronautical Society, Proceedings of Southeastern Symposium on Missiles and Aerospace Vehicles Sciences, Huntsville, Alabama, Dec. 5, 6, 7, 1966, Vol. I., pp. 48-1 to 48-12.

27. J. Sestak, J. Jezek and M. Jirsak:
"Unsteady Discharge of Ideal Fluids from Vertical Constant Cross-Section Reservoirs," Zeitschrift für angewandte Mathematik und Physik, Vol. 18, Fasc. 1, pp. 78-85, January 1967.

28. W. H. McAdams:
"Heat Transmission", 3rd Ed., pp. 130-133, McGraw-Hill Book Co., Inc., New York, N.Y., 1954.

29. "Handbook of Mathematical Functions" AMS 55, Edited by M. Abramowitz and I. A. Stegun, U.S. Department of Commerce, National Bureau of Standards.

30. H. E. Soper:
"The Numerical Evaluation of the Incomplete B-Function or the Integral

$$\int_0^x x^{(p-1)} (1-x)^{q-1} dx$$

for Ranges of x between 0 and 1," Tracts for Computers, No. VII, p. 23, Cambridge University Press, London, 1921.

31. J. K. Vennard:
"Elementary Fluid Mechanics", pp. 300-308, John Wiley and Sons, Inc., New York.

32. H. Rouse:
"Fluid Mechanics for Hydraulic Engineers," pp. 258-261, Dover Publications Inc., New York, N.Y. 1961.

33. H. Schlichting:
"Boundary Layer Theory," McGraw Hill Book Co., Inc., New York 1960, 4th Ed., p. 503.

34. H. L. Langhaar:
"Steady Flow in the Transition Length of a Straight Tube," Journal of Applied Mechanics, Vol. 9, No. 2, pp. A55-A58, 1942.

35. R. G. Deissler:
"Analysis of Turbulent Heat Transfer and Flow in the Entrance Regions of Smooth Passages," NACA TN No. 3016, Oct. 1953.

36. W. F. Weiland and W. H. Lowdermilk:
"Measurements of Heat-Transfer and Friction Coefficients for Air Flowing in a Tube of Length-Diameter Ratio of 15 at High Surface Temperatures", NACA RM No. E53E04, July 1953

37. R. W. Powell:
"An Elementary Text in Hydraulics and Fluid Mechanics," p. 75, Macmillan, New York, 1951.

APPENDIX A

DIMENSIONAL ANALYSIS OF LIQUID DISCHARGE

For the discharge of a liquid from a container through a tube, the instantaneous liquid height is given by (see equation 3.1a):

$$y = y\ (t,\ D,\ d,\ L,\ H,\ \Delta P,\ g,\ \rho,\ \nu) \qquad (A1)$$

The variables are listed below, along with their dimensions in terms of mass (M), length (L) and time (T).

SYMBOL	VARIABLE	DIMENSIONS
t	time elapsed from initiation of discharge	T
y	liquid height in container at time t	L
D	container diameter	L
d	diameter of discharge	L
L	discharge tube length	L
H	initial height of the liquid in container	L
ΔP	external pressure drop	$ML^{-1}\ T^{-2}$
g	effective gravitational acceleration	$L\ T^{-2}$
ρ	density of liquid	$M\ L^{-3}$
ν	kinematic viscosity of liquid	$L^2\ T^{-1}$

The variables ρ, g, and H are chosen as repeated variables (Ref. 28). These are combined with each of the other variables separately to form dimensionless groups. The following table gives the exponents for the dimensions of M, L, and T, for each of these groups

Dimensionless Group	Dimensions M	L	T
$y\ \rho^a\ g^b\ H^c$	a	-3a +b +c +1	-2b
$t\ \rho^a\ g^b\ H^c$	a	-3a +b +c	-2b +1
$D\ \rho^a\ g^b\ H^c$	a	-3a +b +c +1	-2b
$d\ \rho^a\ g^b\ H^c$	a	-3a +b +c +1	-2b
$L\ \rho^a\ g^b\ H^c$	a	-3a +b +c +1	-2b
$\Delta P\ \rho^a\ g^b\ H^c$	a +1	-3a +b +c -1	-2b -2
$\nu\ \rho^a\ g^b\ H^c$	a	-3a +b +c +2	-2b -1

In order to obtain dimensionless groups in the left hand column, the M, L, and T exponents in each row must simultaneously be zero. For example, the first row gives rise to the following:

Simultaneous Equations	Solutions
a = 0	a = 0
-3a +b +c +1 = 0	b = 0
-2b = 0	c = -1

The dimensionless parameter associated with the first row becomes $\frac{y}{H}$. The dimensionless parameters associated with the other quantities can be obtained similarly.

Thus the various π-factors can be written as $\pi_1 = \frac{y}{H}$, $\pi_2 = \frac{t}{\sqrt{H/g}}$, $\pi_3 = \frac{D}{H}$, $\pi_4 = \frac{d}{H}$, $\pi_5 = \frac{L}{H}$, $\pi_6 = \frac{\Delta P}{\rho g H}$, $\pi_7 = \frac{\nu}{H\sqrt{gH}}$. These π-factors can be

combined to form others, still maintaining the same number of independent dimensionless parameters. For instance π_3 and π_4 can be altered to form two other π factors.

$$\pi_3' = \frac{\pi_3}{\pi_4} = \frac{D}{d} \quad \text{and} \quad \pi_4 = \frac{d}{H}$$

Similarly π_4 and π_7 can be transformed to yield $\pi_4' = \frac{L}{d}$ and $\pi_7' = \frac{d\sqrt{gH}}{\nu}$. For convenience of physical interpretation numerical constants are introduced. π_2 is multiplied by $\frac{1}{\beta}$ where

$$\beta = \sqrt{\left(\frac{A}{a}\right)^2 - 1} = \sqrt{\left(\frac{D}{d}\right)^4 - 1}$$

since this parameter arises naturally in a quasi-steady analysis using Bernoulli's equation (equation 5.1). The final result is written as

$$\frac{Y}{H} = F\left(\frac{t}{\beta\sqrt{\frac{2H}{g}}}, \frac{\Delta P/\rho g}{H}, \frac{d\sqrt{2gH}}{\nu}, \frac{L}{H}, \frac{D}{d}, \frac{L}{d}\right) \tag{A2}$$

In an analogous manner equation (3.1b) can be reduced to yield the dimensionless mass flow rate as

$$\frac{\dot{m}}{\rho\left(\frac{\pi D^4}{4}\right)\frac{1}{\beta}\sqrt{2gH}} = G\left(\frac{t}{\beta\sqrt{\frac{2H}{g}}}, \frac{\Delta P/\rho g}{H}, \frac{d\sqrt{2gH}}{\nu}, \frac{L}{H}, \frac{D}{d}, \frac{L}{d}\right) \tag{A3}$$

APPENDIX B

QUASI-STEADY FLOW THROUGH AN ORIFICE IN THE ABSENCE OF VISCOUS EFFECTS FOR ZERO PRESSURE DROP

Figure 5.1 illustrates the system for this analysis. Here it is assumed that the velocity of the fluid is constant over any cross-section. Also, the surface of the fluid is assumed to be horizontal at all times. The discharge mass flow rate $\dot{m}$ is given $\rho a V_2$, and continuity requires that

$$\rho A V_1 = \rho a V_2 \tag{B1}$$

where V_1 and V_2 are the fluid velocities at locations 1 and 2 respectively. For the conditions indicated in Table 5.1, Bernoulli's equation applies. Thus,

$$P_1 + \rho\, g\, y + \frac{1}{2}\rho V_1^2 = P_2 + \frac{1}{2}\rho V_2^2 \tag{B2}$$

For the coordinate system shown, $V_1 = -\frac{dy}{dt}$ and $V_2 = -\frac{A}{a}\frac{dy}{dt}$. Since $P_1 = P_2$, equation (B2) becomes

$$\rho\, g\, y + \frac{1}{2}\rho\left(-\frac{dy}{dt}\right)^2 = \frac{1}{2}\rho\left(-\frac{A}{a}\frac{dy}{dt}\right)^2 \tag{B3}$$

Solving for $\frac{dy}{dt}$ gives

$$\frac{dy}{dt} = -\frac{1}{\beta}\sqrt{2gy} \tag{B4}$$

where $\beta^2 = [(\frac{A}{a})^2 - 1]$, a parameter depending only on the geometry of the system. Note that the negative sign appears because y decreases as t increases. Integration of equation (B4) yields

$$\int_o^t dt = -\frac{\beta}{\sqrt{2g}} \int_H^y \frac{dy}{\sqrt{y}} . \tag{B5}$$

Finally,

$$t = \beta\left[\sqrt{\frac{2H}{g}} - \sqrt{\frac{2y}{g}}\right] \tag{B6}$$

which relates the instantaneous height of liquid to time after initiation of discharge. Equation (B6) can be rewritten as

$$\frac{y}{H} = \left[1 - (\frac{1}{\beta}) \frac{t}{\sqrt{\frac{2H}{g}}}\right]^2 \tag{B7}$$

which shows that the instantaneous height is related to time parabolically. Also, this result implies that the total discharge time is $\beta\sqrt{\frac{2H}{g}}$. These results are represented graphically in Figure 5.2.

The instantaneous rate of discharge is $\rho A (-\frac{dy}{dt})$ where $\frac{dy}{dt}$ is given by equation (B4). Thus,

$$\dot{m} = \frac{\rho A}{\beta} \sqrt{2gy} \tag{B8}$$

But from equation (B6)

$$\sqrt{2gy} = \sqrt{2gH} - \frac{gt}{\beta} \tag{B9}$$

Therefore, equation (B8) becomes

$$\dot{m} = \frac{\rho A}{\beta}\left[\sqrt{2gH} - \frac{gt}{\beta}\right] . \qquad \text{(B10)}$$

Rearrangement of this equation provides the result in dimensionless form, which is

$$\frac{\dot{m}}{\rho\left(\frac{\pi D^2}{4}\right)\frac{1}{\beta}\sqrt{2gH}} = \left[1 - \frac{1}{\beta}\frac{t}{\sqrt{\frac{2H}{g}}}\right] \qquad \text{(B11)}$$

For systems having fixed geometry, β has a constant value so that

$$\frac{\dot{m}}{\rho\left(\frac{\pi D^2}{4}\right)\frac{1}{\beta}\sqrt{2gH}}$$

is purely a function of $\left[\frac{t}{\sqrt{2H/g}}\right]$ according to equation (B11). This is in agreement with the dimensional analysis result given in equation (3.4b).

A plot of equation (B11) is given in Figure 5.3 which shows that the predicted discharge rate decreases linearly with time. This decrease with time is associated with the drop-off in the hydrostatic head y (which corresponds to the gravitational driving potential) as liquid is removed from the container.

APPENDIX C

LIQUID DISCHARGE THROUGH A TUBE

QUASI-STEADY ANALYSIS

In this section an analysis based on an assumption of quasi-steady flow is presented. Friction and entrance effects will be taken into account. In the earlier presentation of the same problem, (Ref. 25), the effect of the various dimensionless parameters is not readily obvious. In the following analysis, an attempt is made to show explicitly the dependence of the mass flow rate (alternately the instantaneous liquid height) on the various dimensionless parameters. The system configuration and coordinate axes are shown in Figure 1.2. Application of Bernoulli's equation, with the usual nomenclature, yields

$$P_1 + \rho g(y + L) + \frac{1}{2}\rho V_1^2 = P_2 + \frac{1}{2}\rho V_2^2 + h_L \qquad (C1)$$

where h_L is a "loss of head" associated with friction and entrance effects, and is given by

$$h_L = \text{Friction loss} + \text{Entrance Loss}$$

$$= f \cdot \frac{L}{d} \cdot \frac{1}{2}\rho V_2^2 + K \cdot \frac{1}{2}\rho V_2^2 \qquad (C2)$$

In equation (C2) f is the Darcy-Weisbach friction factor and K is the entrance loss coefficient. K for a sharp entrance tube is about 0.5 over a wide range of conditions while f is dependent on the Reynolds

number in the tube and can be obtained from the Moody Chart (Ref. 3).

By continuity $V_2 = \frac{A}{a} V_1 = (\frac{A}{a})\ (-\frac{dy}{dt})$. Substitution of this and equation (C2) in equation (C1) yields

$$P_1 + \rho g(y + L) + \frac{1}{2}\rho(\frac{dy}{dt})^2$$

$$P_2 + \frac{1}{2}\rho(\frac{A}{a} \cdot \frac{dy}{dt})^2\ [1 + f \cdot \frac{L}{d} + K] \qquad \text{(C3)}$$

Rearranging terms and dividing through by $(\frac{1}{2}\rho)$ makes it possible to rewrite equation (C3) as

$$(\frac{A}{a})^2\ [1 + f \cdot \frac{L}{d} + K - (\frac{a}{A})^2]\ (\frac{dy}{dt})^2 - 2gy$$

$$= 2\ [\frac{(P_1-P_2)}{\rho} + gL] \qquad \text{(C4)}$$

Substitution of $y^* = \frac{y}{H}$ and $t^* = \frac{1}{\beta}\frac{t}{\sqrt{2H/g}}$ yields

$$[\beta^2 + (\frac{A}{a})^2 \cdot (f\frac{L}{d} + K)] \cdot \frac{1}{\beta^2} \cdot \frac{gH}{2}\ (\frac{dy^*}{dt^*})^2 - 2gHy^*$$

$$= 2\ [\frac{(P_1-P_2)}{\rho} + gL] \qquad \text{(C5a)}$$

Division throughout by $(\frac{gH}{2\beta^2})$ brings equation (C5a) into dimensionless form. This can be written as

$$[\beta^2 + (\frac{A}{a})^2 \cdot (f \cdot \frac{L}{d} + K)]\ (\frac{dy^*}{dt^*})^2 - 4\beta^2 y^*$$

$$= 4\beta^2\ [(\frac{(P_1-P_2)}{\rho gH}) + \frac{L}{H}] \qquad \text{(C5b)}$$

To obtain the dimensionless height as a function of dimensionless time this equation is solved with the initial condition that at $t^* = 0$,

$y^* = 1$.

It can be seen from the last equation that the instantaneous dimensionless height of the liquid (alternately the dimensionless mass flow rate) is dependent on the six dimensionless parameters obtained by the dimensional analysis. For convenience equation (C5b) can be written as

$$C_1 \left(\frac{dy^*}{dt^*}\right)^2 - C_2\, y^* = C_3 \tag{C5c}$$

where

$$C_1 = \left[\beta^2 + \left(\frac{A}{a}\right)^2 \cdot \left(f\,\frac{L}{d} + K\right)\right]$$

$$C_2 = 4\beta^2 \tag{C5d}$$

$$C_3 = 4\beta^2 \left[\frac{(P_1 - P_2)}{\rho g H} + \frac{L}{H}\right]$$

Since y^* decreases with increasing t^*, equation (C5c) yields

$$\frac{dy^*}{dt^*} = -\left(\frac{C_2 y^* + C_3}{C_1}\right)^{\frac{1}{2}} \tag{C6}$$

equation (C6) can be integrated with the above mentioned initial condition to give

$$\frac{2}{C_2}\left[\sqrt{C_2 + C_3} - \sqrt{C_2 y^* + C_3}\,\right] = \frac{1}{\sqrt{C_1}}\, t^* \tag{C7a}$$

Finally equation (C7a) is rewritten as

$$y^* = 1 - \left(\frac{C_2 + C_3}{C_1}\right)^{\frac{1}{2}} t^* + \frac{C_2}{4C_1}\, t^{*2} \tag{C7b}$$

For the case of negligible viscous and contraction effects equation (C7b) reduces to

$$y^* = 1 - 2\left(1 + \frac{P_1 - P_2}{\rho g H} + \frac{L}{H}\right)^{\frac{1}{2}} t^* + t^{*2} \qquad \text{(C7c)}$$

indicating that the dimensionless height of liquid is independent of the parameter β.

The dimensionless mass flow rate is given by

$$\dot{m}^* = \frac{\dot{m}}{\rho \left(\frac{\pi D^2}{4}\right) \frac{1}{\beta} \sqrt{2gH}} = \frac{\beta}{\sqrt{2gH}} \left(-\frac{dy}{dt}\right) = -\frac{1}{2} \frac{dy^*}{dt^*} \qquad \text{(C8a)}$$

Hence from equation (C7b)

$$\dot{m}^* = \frac{1}{2}\left(\frac{C_2 + C_3}{C_1}\right)^{\frac{1}{2}} - \frac{C_2}{4C_1} t^* \qquad \text{(C8b)}$$

which indicates that the mass flow rate decreases linearly with time.

APPENDIX D

A PROGRAM FOR CALCULATING DIMENSIONLESS LIQUID HEIGHT AND DIMENSIONLESS MASS FLOW RATE AS FUNCTIONS OF DIMENSIONLESS TIME FOR DISCHARGE THROUGH AN ORIFICE

```
15016,MULUKUTLA,T200,CM50000,P5.
RUN(S).
LGO.
7
      PROGRAM MAIN(INPUT,OUTPUT,PUNCH,TAPE5=INPUT,TAPE6=OUTPUT,TAPE7=PUN
     1CH)
C
C  ***************************************************************************
C
C  THIS PROGRAM CALCULATES THE THEORITICAL VALUES OF YSTAR VS. TSTAR
C  BASED ON TRANSIENT DISCHARGE ANALYSIS, FOR A GIVEN SET OF
C  EXPERIMENTAL  CONDITIONS.  FOR THE DISCHARGE THROUGH AN ORIFICE
C                             ----------------------------------
C
C  ***************************************************************************
C
C  CLEAR ARRAYS
      DIMENSION YBAR (50), TBAR (50) ,EMBAR (50)
C
C
C
  100 READ (5,30) MONTH, DAY, YEAR, RUN
   30 FORMAT ( 61X, A3, A3, A2, 7X, A4)
C
      IF (ECF, 5) 99, 9
C
C  READ IN VALUES FOR CONTAINER DIAMETER, DISCHARGE TUBE DIAMETER (IN INCHES)
C  AND THE DISCHARGE COEFFICIENT.
    9 READ (5,1) D1, D2, CD
    1 FORMAT (3F10.3)
C
C  CALCULATION OF EXPERIMENTAL CONSTANTS.
C
      A1BYA2 = (D1/D2)**2
      Q = (A1BYA2)**2
      BETA =  SQRT (Q-1.)
      ALFA = BETA ** 2
      CONS = -(CD)*(SQRT((4.*ALFA)/(ALFA-1.)))
      WRITE (6,200)
  200 FORMAT (1H1, 37X, 51H THEORITICAL CURVE FOR DISCHARGE THROUGH AN
     1ORIFICE//)
      WRITE (6,201)
  201 FORMAT (34X, 56H TRANSIENT DISCHARGE ANALYSIS WITH DISCHARGE COEF
     1FICIENT////)
      WRITE (6,31) RUN, MONTH,  DAY, YEAR
   31 FORMAT (45X, 10HRUN NO. = , A4, 5X, 6HDATE  , A3, A3, A2)
      WRITE (6,32)
```

```
   32  FORMAT (45X,6H------,4X,4H----, 5X, 14H----  --------///)
       WRITE (6,202) D1, A1BYA2
  202  FORMAT (10X, 34HTANK DIAMETER                    D = , F8.3,5H  IN.,
     1 10X, 40HAREA RATIO                              = , F8.3)
       WRITE (6,203) D2, BETA
  203  FORMAT (10X, 34HDISCHARGE DIAMETER                 = ,F8.3, 5H  IN.,
     1 10X,40HBETA                                    = ,F8.3)
       WRITE (6, 204)      CD
  204  FORMAT (67X, 40HDISCHARGE COEFFICIENT                    = , F8.3///
     1/)
       WRITE (6,83)
   83  FORMAT (30X,13HDIMENSIONLESS,15X,13HDIMENSIONLESS,15X, 13HDIMENSI
     1ONLESS)
       WRITE (6,84)
   84  FORMAT (34X,4HTIME,24X,6HHEIGHT,18X,14HMASS FLOW RATE//)
       Z1 = 0.5 / (ALFA - 1.)
       Z2 = SQRT ( Z1 / (2.*ALFA))
       Z3 = Z2 / CD
       CALL BETAAB (Z1, 0.5, BETAXY)
       TBAR (1) = 0.0
       YBAR (1) = 1.0
       EMBAR (1) = 0.0
       WRITE (6,1007)  TBAR (1), YBAR (1),EMBAR (1)
       DO 1003 N = 1,25
       IF (N-10) 1004, 1004, 1005
 1004  YBAR (N+1) = YBAR (N) - 0.02
       GO TO 1006
 1005  YBAR (N+1) = YBAR (N) - 0.05
 1006  VY = YBAR (N+1)
       EX = (VY) ** (ALFA - 1.)
       CALL  INCBET (Z1, 0.5, EX, BETXAB)
       TBAR (N+1) = Z3 * (BETAXY - BETXAB)
       EMBAR (N+1) =-(0.5)*CONS*(SQRT(YBAR(N+1) - (YBAR(N+1)**ALFA)))
       WRITE (6,1007)  TBAR (N+1), YBAR (N+1) , EMBAR (N+1)
 1003  CONTINUE
 1007  FORMAT (30X,F10.3,18X,F10.4,18X,F10.4)
       WRITE (6, 2000) Z1, Z2, Z3, BETAXY
 2000  FORMAT (//// 3F10.6, 5X, E15.6)
       GO TO 100
   99  STOP
       END
       SUBROUTINE  INCBET ( P, Q, X, BETXPQ )
C
C  THIS PROGRAM COMPUTES INCOMPLETE BETA FUNCTIONS USING SOPER APPROXIMATION.
C  (SEE TRACTS FOR COMPUTERS NO.7, PAGE 23)
C
       A = (X**P) / ((P+1.) * (P+2.))
       B1 = 2.0 / P
       B2 = -1.0
       B3 = (4.0) * ((1.0 - (0.5*X)) ** (Q-1.0))
       B4 = P * ((1.0-X) ** (Q-1.0))
       B = B1 + B2 + B3 + B4
       BETXPQ = A * B
       RETURN
       END
       SUBROUTINE  BETAAB ( A, B,  BETA)
C
C  THIS SUBROUTINE COMPUTES COMPLETE BETA FUNCTIONS.
C  FOR GIVEN VALUES OF A AND B
C
C  REMEMBER  BETA (A,B) = BETA (B,A)
```

```
C
      A1 = GAMMA (A)
      B1 = GAMMA (B)
      C = A+B
      C1 = GAMMA (C)
      BETA   = (A1 * B1) / C1
      RETURN
      END
     FUNCTION GAMMA(X)                                                  GAM00001
C
C  THIS IS SHARE PROGRAM NO. 3155.
C
   75 FORMAT(66H GAMMA FUNCTION OF A NEGATIVE INTEGER, OR OF ZERO, IS NOGAM00002
     1T DEFINED.)                                                       GAM00003
    5 IF(X) 10,80,15                                                    GAM00004
   10 N=-X                                                              GAM00005
      EN=-N-1                                                           GAM00006
      V=X-EN                                                            GAM00007
      IF(V-1.) 20,80,20                                                 GAM00008
   15 N=X                                                               GAM00009
      EN=N                                                              GAM00010
      V=X-EN                                                            GAM00011
   20 GAMMA=1.+V*(.422784337+V*(.4118402518+V*(.08157821878+V*          GAM00012
     1(.07423790761+V*(-.0002109074673+V*(.01097369584+V*(-.002466747981GAM00013
     2+V*(.001539768105-V*(.0003442342046-V*.0000677105711))))))))))    GAM00014
      IF(EN-2.) 37,25,30                                                GAM00015
   25 RETURN                                                            GAM00016
   30 N=N-1                                                             GAM00017
      DO 35 I=2,N                                                       GAM00018
      FI=I                                                              GAM00019
   35 GAMMA=GAMMA*(FI+V)                                                GAM00020
      RETURN                                                            GAM00021
   37 N=2.-EN                                                           GAM00022
      DO 40 I=1,N                                                       GAM00023
      FI=2-I                                                            GAM00024
   40 GAMMA=GAMMA/(FI+V)                                                GAM00025
      RETURN                                                            GAM00026
   80  WRITE (6, 75)                                                    GAM00027
       RETURN                                                           GAM00028
      END                                                               GAM00029
7
7
```

APPENDIX E

A PROGRAM FOR REDUCING EXPERIMENTAL DATA AND FITTING A THEORETICAL CURVE BY FOURTH-ORDER RUNGE-KUTTA METHOD FOR DISCHARGE THROUGH A TUBE

```
$ID   15016*2*10*0*MULUKUTLA*
$EXECUTE        IBJOB
$IBJOB
$IBFTC MAIN     NODECK
C*****************************************************************************
C  THIS PROGRAM REDUCES THE EXPERIMENTAL DATA TO A NON-DIMENSIONAL FORM AND
C  CALCULATES THE THEORITICAL CURVE FOR THE GIVEN SET OF EXPERIMENTAL CONDITIONS
C  FOR DISCHARGE OF A CONTAINER THROUGH A TUBE.
C  ------------------------------------------
C*****************************************************************************
C
C  CLEAR ARRAYS
       DIMENSION TRAW (50), Y (50), TSEC (50), TSTAR (50), YSTAR (50)
       DIMENSION TTHEO (3050),YTHEO (3050), EMTHEO (3050)
  100  READ (5,30) MONTH, DAY, YEAR, RUN
   30  FORMAT ( 61X, A3, A3, A2, 7X, A4)
C  READ IN VALUES FOR CONTAINER DIAMETER, DISCHARGE TUBE DIAMETER, LENGTH OF
C  TUBE, AND INITIAL HEIGHT OF LIQUID.  ALL DIMENSIONS SHOULD BE IN INCHES.
       READ (5,1) D1, D2, EL, EH
    1  FORMAT (4F10.3)
C  READ IN FRICTION FACTOR. ENTRANCE LOSS COEFFICIENT, TANK PRESSURE AND THE
C  DISCHARGE PRESSURE.  PRESSURES SHOULD BE IN  PSIA.
       READ (5,2) CD, ENTLOS, P1, P2
    2  FORMAT (4F10.3)
C  READ IN  NDATA EXPERIMENTAL POINTS, WITH TRAW (I) AS CLOCK TIME IN SECS.
C  AND Y (I) THE INSTANTANEOUS HEIGHT IN INCHES FROM THE BOTTOM OF THE TANK
       READ (5,3)  NDATA, (TRAW (I), Y (I), I = 1, NDATA)
    3  FORMAT ( I2 / (2F10.3))
C  CALCULATION OF EXPERIMENTAL CONSTANTS.
       G = 32.2
       DP = (P1-P2)
       A1BYA2 = (D1/D2)**2
       Q = (A1BYA2)**2
       BETA =  SQRT (Q-1.)
       ELBYEH = EL/EH
       ELBYD = EL/D2
C  ASSUMED WATER AS THE WORKING FLUID.
       RHOG = 62.4
       EHFEET = EH/12.
       DPBYRO = (144./RHOG) * (DP/EHFEET)
       TIMCON = SQRT (G/(2.*EHFEET))/ BETA
C  REDUCE EXPERIMENTAL POINTS TO THE DIMENSIONLESS FORM.
       DO 10 K = 1,NDATA
       TSEC (K) = TRAW (K) - TRAW (1)
       TSTAR (K) = TIMCON * TSEC (K)
       YSTAR (K) = Y (K) / EH
   10  CONTINUE
```

```
C  CALCUALATICN OF EXPERIMENTAL VALUES ENDS HERE
C  OUTPUT OF EXPERIMENTAL VALUES
      WRITE (6,200)
  200 FORMAT (1H1, 48X, 25HREDUCED EXPERIMENTAL DATA)
      WRITE (6,201)
  201 FORMAT (49X, 25H-------------------------////)
      WRITE (6,31) RUN, MONTH,  DAY, YEAR
   31 FORMAT (45X, 10HRUN NO. = , A4, 5X, 6HDATE  , A3, A3, A2)
      WRITE (6,32)
   32 FORMAT (45X,6H------,4X,4H----, 5X, 14H----  --------///)
      WRITE (6,202) DI, A1BYA2
  202 FORMAT (10X, 34HTANK DIAMETER                    D = , F8.3,5H  IN.,
     1 10X, 40HAREA RATIO                              = , F8.3)
      WRITE (6,203) D2, BETA
  203 FORMAT (10X, 34HDISCHARGE DIAMETER                 = ,F8.3, 5H  IN.,
     1 10X,40HBETA                                    = ,F8.3)
      WRITE (6,204) EL, ELBYD
  204 FORMAT (10X, 34HDISCHARGE TUBE LENGTH            L = ,F8.3, 5H  IN.,
     1  10X, 40HLENGTH OF TUBE / DIAMETER              = ,F8.3)
      WRITE (6,205) EH, ELBYEH
  205 FORMAT (10X, 34HINITIAL HEIGHT OF LIQUID         H = , F8.3, 5H  IN.
     1 , 10X, 40HLENGTH OF TUBE / INITIAL HEIGHT       = , F8.3)
      WRITE (6,206) P1, DPBYRO
  206 FORMAT (10X, 34HTANK PRESSURE                      = , F8.3,6H  PSIA
     1 , 9X, 40HPRESSURE DIFFERENCE / RHO.G.H          = , F8.3)
      WRITE (6,207) P2, CD
  207 FORMAT (10X, 34HDISCHARGE PRESSURE                 = ,F8.3, 6H  PSIA
     1 ,  9X, 40HFRICTION FACTOR                       = , F8.3)
       WRITE (6,208) ENTLOS
  208 FORMAT (67X, 40HENTRANCE LOSS COEFFICIENT            K = ,F8.3//
     1 ////)
      WRITE (6,209)
  209 FORMAT (30X,4HTIME,11X,13HLIQUID HEIGHT,7X,13HDIMENSIONLESS,
     1 7X,13HDIMENSIONLESS)
      WRITE (6,210)
  210 FORMAT (30X,4HSEC.,15X,6HINCHES,15X,4HTIME,15X,6HHEIGHT///)
      WRITE (6,211) (TSEC (L), Y (L), TSTAR (L), YSTAR (L), L=1,NDATA)
  211 FORMAT (24X, F10.2, 10X, F10.1, 10X, F10.3, 10X, F10.3)
C
C  START CALCULATION OF THEORITICAL VALUES
C
      P = (BETA)**2
      C1 = ELBYEH
      C2 = - 0.5 * ((P/A1BYA2) + ((CD* ELBYD + ENTLOS ) * A1BYA2 ))
      C3 = (2.*P)/(A1BYA2)
      C4 = - (2. * P/A1BYA2) * (ELBYEH + DPBYRO)
      CALL RUNKUT (C1, C2. C3, C4, TTHEO, YTHEO, EMTHEO, J)
C
C  OUTPUT OF THEORITICAL VALUES
      WRITE (6,80)
   80 FORMAT (1H1////46X,37HSOLUTION OF THE DIFFERENTIAL EQUATION)
      WRITE (6,81)
   81 FORMAT (47X, 37H-------------------------------------////)
      WRITE (6,39) RUN, MONTH,  DAY, YEAR
   39 FORMAT (48X, 10HRUN NO. = , A4, 5X, 6HDATE  , A3, A3, A2)
      WRITE (6,82)
   82 FORMAT (48X,6H------,4X,4H----, 5X, 14H----  --------///)
      WRITE (6,83)
   83 FORMAT (30X,13HDIMENSIONLESS,15X,13HDIMENSIONLESS,15X, 13HDIMENSI
     1ONLESS)
      WRITE (6,84)
```

```
   84  FORMAT (34X,4HTIME,24X,6HHEIGHT,18X,14HMASS FLOW RATE//)
       WRITE (6,85) (TTHEO (N), YTHEO (N), EMTHEO (N), N = 1, 200, 10)
   85  FORMAT (30X,F10.2,18X,F10.4,18X,F10.4)
       IF (J-200) 300, 300,310
  310  WRITE (6,86) (TTHEO (N), YTHEO (N) , EMTHEO (N), N = 201, J, 50)
   86  FORMAT (30X,F10.2,18X,F10.4,18X,F10.4)
  300  WRITE (6,706) C1, C2, C3, C4
  706  FORMAT (///4F10.3)
       GO TO 100
       END
$IBFTC RUNK    NODECK
       SUBROUTINE RUNKUT (C1,C2,C3,C4,T,Y,EM, J)
C
C  IN THIS PROGRAM Y IS NONDIMENSIONALISED W.R.T. THE INITIAL LIQUID
C  HEIGHT  CAPITAL H
C  ALSO BETA IS USED TO NONDIMENSIONALISE TIME T
C
       DIMENSION T(3050), Y(3050), V(3050), EM(3050)
       T(1) = 0.0
       Y(1) = 1.0
       V(1) = 0.0
       EH = 0.001
       I = 0
   52  IF (I-3000) 51,50,50
   51  I = I + 1
       EX = T(I)
       VY = Y(I)
       U = V(I)
       D1Y = FYUT (EX,VY, U, C1, C2, C3, C4, EH)
       D1U = GYUT (EX,VY, U, C1, C2, C3, C4, EH)
       D2Y = FYUT ((EX+0.5*EH),(VY+0.5*D1Y),(U+0.5*D1U),C1,C2,C3,C4,EH)
       D2U = GYUT ((EX+0.5*EH),(VY+0.5*D1Y),(U+0.5*D1U),C1,C2,C3,C4,EH)
       D3Y = FYUT ((EX+0.5*EH),(VY+0.5*D2Y),(U+0.5*D2U),C1,C2,C3,C4,EH)
       D3U = GYUT ((EX+0.5*EH),(VY+0.5*D2Y),(U+0.5*D2U),C1,C2,C3,C4,EH)
       D4Y = FYUT ((EX+EH),(VY+D3Y),(U+D3U), C1,C2,C3,C4,EH)
       D4U = GYUT ((EX+EH),(VY+D3Y),(U+D3U), C1,C2,C3,C4,EH)
       DY = (1./6.) * (D1Y+(2.*D2Y)+(2.*D3Y)+D4Y)
       DV = (1./6.) * (D1U +(2.*D2U)+(2.*D3U)+ D4U)
       Y(I+1)= Y(I) +DY
       V(I+1) = V(I) + DV
       T(I+1) = T(I) + EH
       AMOD = Y (I+1)
       IF (AMOD - 0.01 ) 50,50,52
   50  J = I + 1
       DO 70 M = 1,J,10
       EM(M) = -(0.5*V(M))
   70  CONTINUE
       RETURN
       END
$IBFTC FUNC    NODECK
       FUNCTION FYUT (EA,EB,EC,ED,EE,EF,EG,EK)
       FYUT = EC * EK
       RETURN
       END
$IBFTC GUNC    NODECK
       FUNCTION GYUT (A,B,C,D,E,F,G,H)
       A1 =  E * (C**2)
       A2 = F * B
       GYUT =((G - A1 - A2 )* H)/ D
       RETURN
       END
```